THE MICROSTRUCTURE AND YIELDING BEHAVIOUR OF SOME TITANIUM STEELS

by

Gillian Margaret Smith

Newnham College, Cambridge

A dissertation submitted for the
Degree of Doctor of Philosophy
in the University of Cambridge,
February 1984

PREFACE

The following dissertation, which is submitted for the degree of Doctor of Philosophy in the University of Cambridge, describes work carried out in the Department of Metallurgy and Materials Science under the supervision of Professor R W K Honeycombe between October 1978 and September 1981. The contents of this dissertation are, to the best of my knowledge, original except where reference has been made to the work of others. The dissertation is the result of my own work and includes nothing which is the outcome of work done in collaboration. No part of this dissertation has already been, or is currently being, submitted for any other degree, diploma or qualification at any other University. It is less than 60 000 words in length.

Gillian M. Smith

G M Smith

February 1984

ACKNOWLEDGEMENTS

I should like to express my thanks to Professor R W K Honeycombe for the provision of laboratory facilities and for his helpful advice and encouragement during the course of this work. I am also very grateful to my friends and colleagues, and to the assistant staff of the laboratory, for the benefit of their experience and for many valuable discussions. In particular I would like to thank Dr H K D Bhadeshia, Dr P R Howell, Mr J Leader, Dr A R Waugh and Dr S A Waugh.

I am grateful to the Science Research Council for the financial support of the work and for the provision of a maintenance grant.

THE MICROSTRUCTURE AND YIELDING BEHAVIOUR OF SOME TITANIUM STEELS

by G M Smith

SUMMARY

The microstructure and room temperature tensile yielding behaviour of a series of steels containing up to 0.1 wt% carbon and 0.5 wt% titanium have been investigated. The majority of the work concerns microstructures comprising ferrite and dispersions of fine titanium carbide particles formed by the isothermal decomposition of austenite between 800° and 650°C.

At the higher temperatures, transformation took place solely by diffusional growth in several modes to produce an equiaxed grain structure. Both diffusional and displacive transformation mechanisms operated at the lower temperatures giving rise to a less uniform structure. Evidence for these mechanisms is provided by i) the ferrite grain morphologies, after both partial and complete transformation; ii) the distribution of the discrete titanium carbides which were mainly formed by interphase precipitation; and iii) the dislocation densities, quantified using transmission electron microscopy. The total elastic lattice microstrain was measured by X-ray line broadening. The interactions between the strain fields of dislocations, the semi-coherent precipitates and the interstitial atoms are considered with respect to dislocation retention and dislocation behaviour during deformation. Atom probe microanalysis was employed to analyse the fine carbides and to investigate the nature of the carbide/matrix interfaces.

Discontinuous yielding occurred only in those steels with a carbon content surplus to the stoichiometric requirements for titanium carbide formation. Additionally, however, it was influenced by the heat treatment employed. Only those specimnes transformed at the highest temperature, 800°C, exhibited discontinuous yielding in the as-transformed state but yield points were displayed for all the microstructures after a 100°C strain-ageing treatment. The many factors which could be affecting yielding behaviour, including the carbon distribution, residual stresses and grain size are considered. The conclusion is reached that the principal cause for the masking of discontinuous yielding as the transformation temperature was lowered was the increasing inhomogeneity of microstructure particularly on a local scale.

TABLE OF CONTENTS

CHAPTER ONE

GENERAL INTRODUCTION

Steels which exploit the strengthening derived from just small additions of strong carbide-formers are being employed in increasing quantities. Through careful control of the composition and thermo-mechanical processing, these high-strength low-alloy (HSLA) steels achieve their strength principally from stable dispersions of fine niobium, vanadium and titanium carbides and from ferrite grain refinement.

To approach an understanding of the complex relationships between the microstructure and mechanical properties, these alloy systems have been the subject of much recent study. The nature and origin of the carbide dispersions have been explored using model ternary systems, in particular those producing the larger volume fractions of precipitates such as chromium and vanadium carbides. Such steels have also been employed to analyse the strength contributions of the precipitate dispersions.

In addition to the absolute strength level attained, an important mechanical property with regard to the finished product and to the manufacturing process is the nature of the yielding behaviour. A gradual monotonic change in the slope of the load-extension curve as the material begins to deform plastically is termed continuous yielding behaviour; when the load-extension curve displays a plateau and sometimes a drop in load at the onset of plastic deformation this is termed discontinuous yielding, and the material is said to exhibit a yield point.

In the majority of situations discontinuous yielding is undesirable. For example, discontinuous yielding raises the forming loads for pipe steels without producing the benefit of any increase in the yield strength of the finished, expanded pipe. It can also produce unsightly stretcher strains in pressed sheet.

The incidence and magnitude of discontinuous yielding behaviour is found to depend on both the composition and thermomechanical history of the steel. The occurrence of the phenomenon has been extensively studied, but the most detailed work on iron alloys has been performed on simple iron-carbon alloys, principally those with very low carbon contents and in the annealed condition. Numerous studies have also been carried out on commercial HSLA steels but usually these have been prepared by normal manufacturing regimes involving a series of continuous cooling and deformation treatments thus making the development of the microstructures difficult to ascertain.

The work described in this dissertation was undertaken to investigate relationships between heat treatment, microstructure and yielding behaviour using a series of simplified low alloy steels modelled on commercial HSLA steels but containing only a single species of alloy carbide. Titanium was selected as the principal microalloying addition, having affinities for carbon and nitrogen intermediate between those of vanadium and niobium thus compromising between the conflicting desires for a high volume fraction of fine precipitates and a high precipitate stability. For the principal investigations, isothermal heat treatment conditions were selected for the austenite decomposition reactions, with the aim of simplifying the characterisation of transformation mechanisms and the resultant microstructures.

Following the literature review comprising Chapter Two, Chapter Three

reports on the microstructural examinations of the titanium steels. In particular the development of the ferrite and titanium carbide morpologies at different transformation temperatures are discussed. Chapter Four is concerned with the strength and yielding behaviour of the alloys as a function of the transformation temperature, and compares the behaviour of different alloy compositions. The microstructural characteristics are examined in more detail in the next two chapters: Chapter Five deals with dislocation density measurements, and considers the origins of the dislocations and their interactions with the precipitate dispersions; Chapter Six contains the results of high resolution compositional analysis of the precipitates, the matrix and the particle/matrix interfaces. The final chapter of experimental work, Chapter Seven, reports a series of exploratory investigations on the effects of annealing, reaustenitisation, recrystallisation and continuous cooling heat treatments on the microstructures and the corresponding yielding behaviour.

Discussion specific to each set of results is included in the relevant chapters. Then in Chapter Eight, all the experimental findings are considered together in an expanded, general discussion.

CHAPTER TWO

LITERATURE REVIEW

2.1 Introduction

In the first part of this chapter factors which influence the formation of fine dispersions of stable precipitates in steels are reviewed. The solubilities of alloy compounds are compared, and the mechanisms of precipitation and austenite decomposition are surveyed with particular reference to the role played by titanium additions.

Attention is then turned to yielding behaviour. The occurrence of discontinuous yielding and the mechanisms which have been proposed for general application and more specifically in relation to titanium steels are outlined.

2.2 The design of high strength low alloy steels

The precise control of the composition and thermomechanical treatments of high strength low alloy (HSLA) and microalloyed steels enables a range of superior material properties to be achieved with only small quantities of alloying additions. This is accomplished principally through the alteration of the transformation characteristics, the creation of fine dispersions of alloy precipitates and inclusion control. The development and specific qualities of such steels are documented, for example, by Baker (1978); Embury, Evenson & Filipovic (1977); Pickering (1977); Gladman, Dulieu & McIvor (1977); and Baird & Preston (1973). The crystal chemistry and occurrence of carbides and nitrides in steels

have been reviewed by Jack & Jack (1973).

The three principal elements used for dispersion strengthening are niobium, titanium and vanadium. From the heats of formation of the carbides and nitrides given in Table 2.1 (Shaffer 1968), it is seen that in each case the titanium compounds are the most stable. However, the potential for precipitation strengthening also depends on the difference between the solid solubilities in austenite and ferrite. The volume fraction available is determined by the solubility product of the compound in austenite (Figure 2.2, collected by Aronsson, 1969). The relative magnitudes are

$$VC > TiC > NbC > VN > TiN.$$

Very little data on solubility products in ferrite are available because the values are so low, typically two orders of magnitude smaller than in austenite. Gladman & McIvor (1972) report less than 1 ppm nitrogen in equilibrium with VN, TiN or NbN if the alloying element is present to levels greater than nitride stoichiometry. Leslie & Sober (1967) determined equilibrium carbon and nitrogen levels of less than 2 at.ppm in a steel with excess titanium.

Expressions for solubility products in austenite and ferrite as a function of temperature have been compiled by Jones, Hudd & Kale (1970) partly from experimental data and partly from thermodynamic calculation. These are reproduced in Table 2.3 and provide useful information on relative solubilities. However, the numerical values should be applied with caution to practical situations because true equilibrium is rarely attained.

	$-\Delta H^{o}_{298}$ kJ mol^{-1}		$-\Delta H^{o}_{298}$ kJ mol^{-1}
TiC	184	TiN	336
NbC	141	NbN	247
VC	117	VN	251

Table 2.1: Heats of formation of some alloy carbides and nitrides
(from data compiled by Shaffer, 1968)

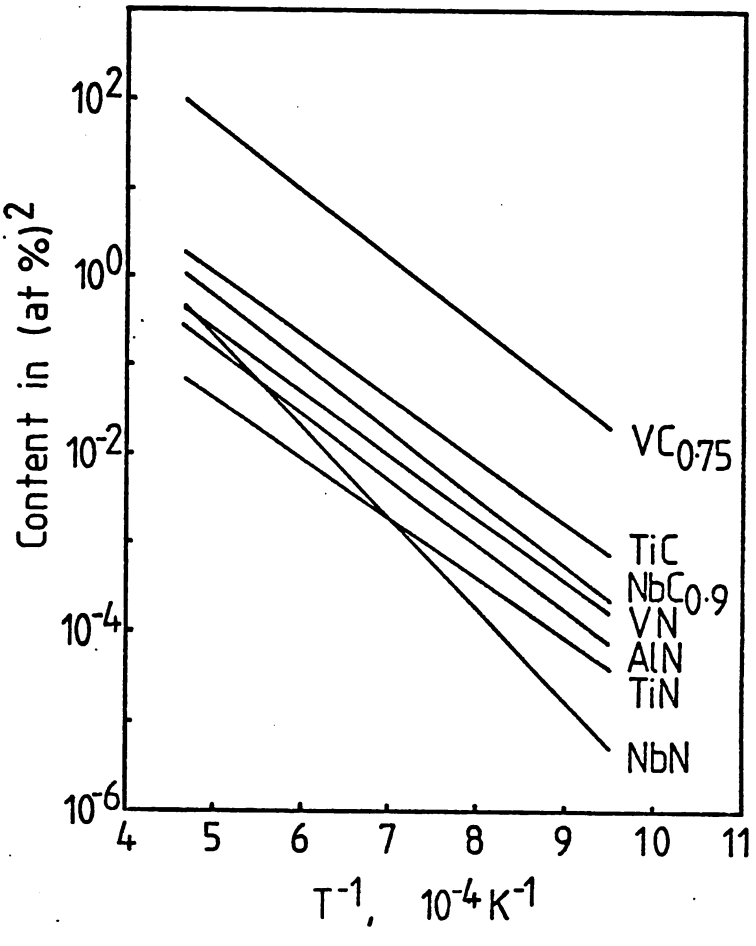

Figure 2.2: Solubility products of carbides and nitrides in austenite as a function of temperature
(from data compiled by Aronsson, 1969)

Solubility in austenite

Precipitate	A	B	Precipitate	A	B
TiC	-7000	2.75	TiN	-20790	7.72
NbC	-7510	2.96	NbN	-10230	4.04
VC	-2940	1.95	VN	- 7070	2.27

Solubility in ferrite

Precipitate	A	B	Precipitate	A	B
TiC	- 7440	3.40	TiN	-20610	8.23
NbC	-10960	5.43	NbN	-12230	4.96
VC	- 5500	3.39	VN	- 7830	2.45

Table 2.3: Solubility equations for carbides and nitrides in austenite and ferrite (from Jones, Hudd & Kale 1970)

Each equation is of the form $\log_{10} K = \frac{A}{T} + B$

where K is the solubility product in weights percent

2.3 The role of titanium

Titanium is added to low alloy steels primarily for dispersion strengthening and for sulphide shape control. Titanium is a strong scavenging element, forming stable oxides, nitrides, carbides and sulphides (Meyer, Heisterkamp & Müschenborn, 1977).

It has been found (e.g. Kiessling & Lange 1966) that titanium oxide and some of the titanium nitride precipitate out in the liquid because they have such high enthalpies of formation: viz 336 kJ per mole for titanium nitride and higher for the oxide, compared with 184 kJ per mole for titanium carbide. Titanium nitride also forms in the austenite and is identifiable as angular, golden-yellow particles. Mixed titanium carbonitrides may also precipitate because the carbide and nitride are isostructural.

Vacancies in the titanium sub-lattice of the NaCl-type titanium carbide structure enable the composition to vary between about $TiC_{0.3}$ to TiC (Storms 1967).

Titanium carbide tends to precipitate out after the oxide, sulphide and nitride because it is the least insoluble. The majority forms as fine dispersions in the ferrite either during the decomposition of the austenite or during the tempering of a quenched structure. Because of the propensity of titanium to form compounds, the volume fraction of dispersed titanium carbide is sensitive to the impurity levels of the steels.

2.4 Titanium carbide solubility

The solubility limit of titanium carbide in austenite has been expressed by Irvine, Pickering & Gladman (1967) as

$$\log_{10} [Ti]_{\gamma} [C]_{\gamma} = \frac{-7000}{T} + 2.75 \qquad \ldots 2.1$$

where $[Ti]_\gamma$, $[C]_\gamma$ are wt% concentrations in austenite.

Using this equation, 1200°C is predicted as the solubility limit for a 0.05C-0.2Ti stoichiometric alloy, and this would correspond to 0.4 vol% carbide.

The volume fraction of titanium carbide precipitated on cooling from the austenitising temperature can be represented on an expanded corner of the Fe-Ti-C ternary phase diagram following the method of Gladman, Dulieu & McIvor (1977) and is shown in Figure 2.4. For a fixed titanium level, all the titanium and carbon will be in solution in the austenite at low carbon levels. The volume fraction of fine TiC precipitates will be limited by the carbon level; when the titanium and carbon are present in the stoichiometric ratio (approximately 4:1 by weight), the precipitate volume fraction is a maximum and remains at this level when the carbon level is increased further - the excess carbon equilibrates with iron carbide. Eventually the solubility limit in the austenite is exceeded and titanium is removed from solution as coarse carbides, decreasing the volume of fine TiC subsequently precipitated. This representation assumes that the levels of titanium and carbon in equilibrium with titanium carbide in the ferrite are negligible.

2.5 The decomposition of austenite

A number of different transformation products can result from the decomposition of austenite in low alloy steels, depending on the transformation temperature and alloy composition. At the higher transformation temperatures diffusional mechanisms dominate producing equiaxed ferrite, whereas at the lowest temperatures shear mechanisms produce martensite. Intermediate morphologies, such as Widmanstätten ferrite and bainite,

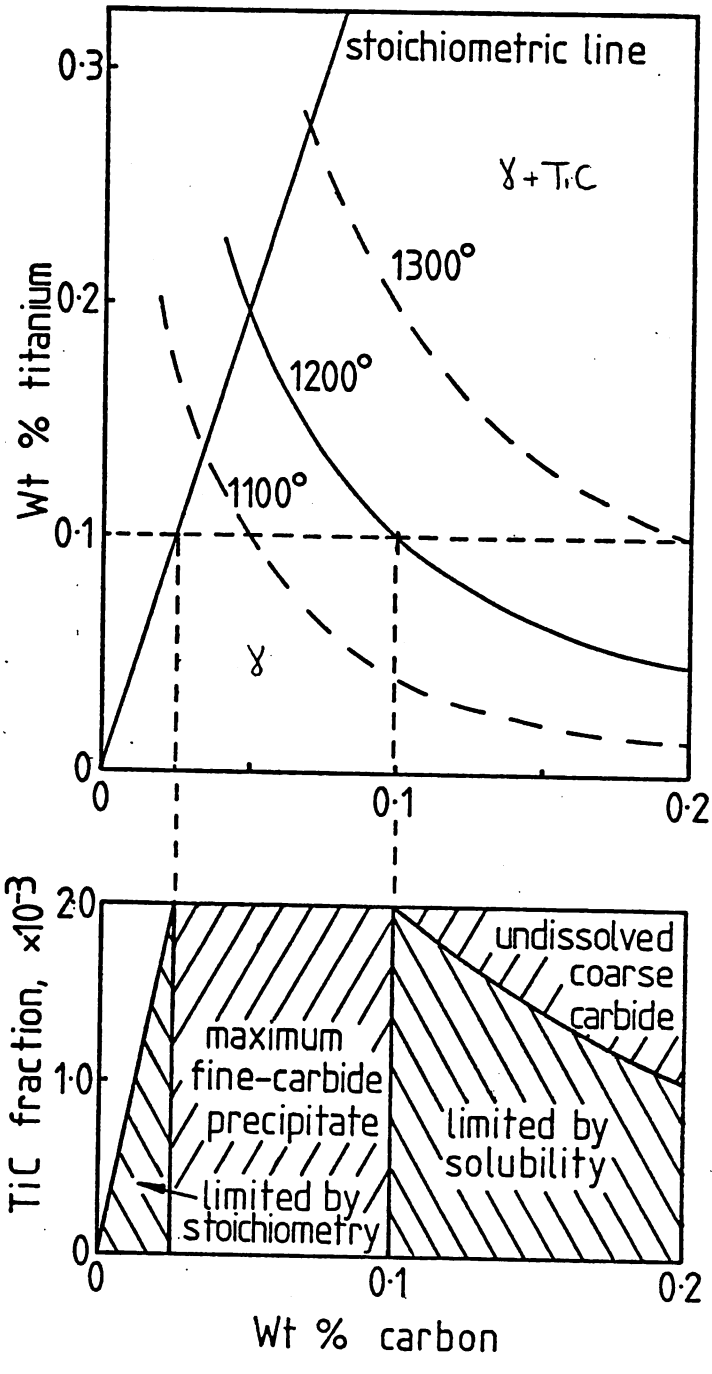

Figure 2.4: Solubility diagram indicating the fraction of fine carbides produced on cooling Fe-Ti-C alloys (from Gladman, Dulieu & McIvor 1977)

develop under conditions between these extremes; the nomenclature, microstructure and transformation mechanisms of these products have been subjects of much debate (e.g. Hehemann, Kinsman & Aaronson 1972; Bhadeshia 1980, 1981; Aaronson 1980).

Ferritic structures generally nucleate on austenite grain boundaries and exhibit an orientation relationship with one or both of the adjacent austenite grains. The normal crystallographic relationship is the Kurdjumov-Sachs (1930) type in which the closest packed planes in the austenite and ferrite are matched:

$$\{111\}_{\gamma} \;//\; \{110\}_{\alpha}$$

$$\langle 110\rangle_{\gamma} \;//\; \langle 111\rangle_{\alpha}$$

At the highest transformation temperatures the grain boundary ferrite allotriomorphs grow by the diffusional movement of the incoherent austenite/ferrite (γ/α) boundaries. When diffusivities become lower at decreased temperatures, the coherent and semi-coherent γ/α interfaces are thought to play a larger part, the boundary movement occurring by the passage of incoherent ledges across the interface. The growth of Widmanstätten ferrite plates has been thought to also occur by a ledge mechanism (e.g. Aaronson 1962; Kinsman, Eichen & Aaronson 1975), but more recently evidence has been provided for a displacive shear mechanism (Bhadeshia 1981). At still lower temperatures, low alloy steels produce an upper bainite in the form of parallel, dislocated laths nucleating directly on the austenite grain boundaries and usually containing interlath carbides.

Bainitic and martensitic products generally have a Kurdjumov-Sachs relationship with the parent austenite and this has been observed directly by Law, Howell & Edmonds (1979) in low alloy vanadium steels containing retained austenite. The Nishiyama-Wassermann relationship (Nishiyama 1934; Wassermann 1933) between austenite and ferritic martensite, viz

$$\{111\}_{\gamma} \;//\; \{110\}_{\alpha}$$

$$\langle 110\rangle_{\gamma} \;//\; \langle 001\rangle_{\alpha}$$

has also been observed, particularly in steels containing manganese or nickel (e.g. Law et al. 1979).

The addition of titanium closes the γ phase field thereby displacing the γ/α transformation to higher temperatures, as depicted in the Fe-Ti-C ternary sections of Figure 2.5 (Goldschmidt 1967). Manganese and nickel additions have a similar effect and their primary use is to retard the transformation reaction: 5 %Mn in a titanium steel has been found to move the position of the ferrite nose on the TTT diagram from 5 s to 30 s (Freeman 1971a).

2.6 Carbide precipitation in ferrite

The large difference in alloy carbide solubility between austenite and ferrite leads either to the precipitation of carbides during transformation or the formation of a supersaturated ferritic product which yields carbide dispersions on tempering. Vanadium, titanium and niobium carbides have a cubic NaCl-type structure and invariably exhibit the Baker-Nutting orientation relationship with the ferrite lattice (Baker & Nutting 1959):

$$\{001\}_{MC} \;//\; \{001\}_{\alpha}$$

$$\langle 100\rangle_{MC} \;//\; \langle 110\rangle_{\alpha}$$

$$\langle 110\rangle_{MC} \;//\; \langle 100\rangle_{\alpha}$$

In quenched and tempered structures, all three crystallographic variants are displayed by the alloy carbides in a single ferritic region; the precipitates nucleate on the dislocation substructure of the martensite and develop as platelets on the {100} ferrite planes at the expense of the first-formed iron carbides (e.g. Tekin & Kelly 1965;

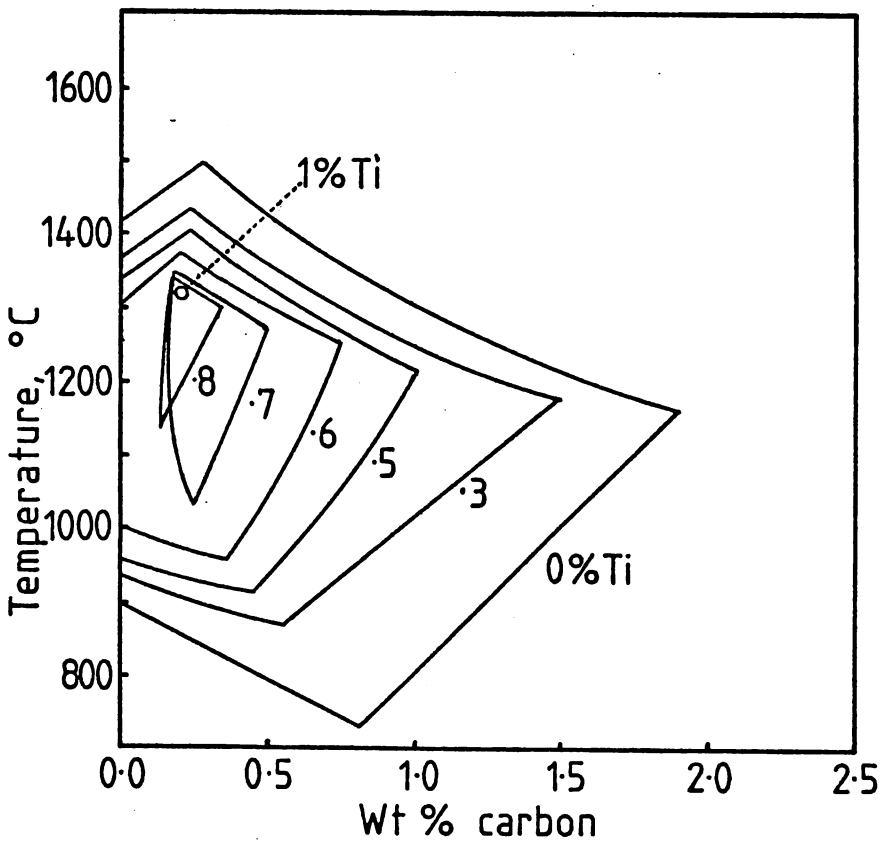

Figure 2.5: Sections through the ternary Fe-Ti-C phase diagram (from Goldschmidt 1967)

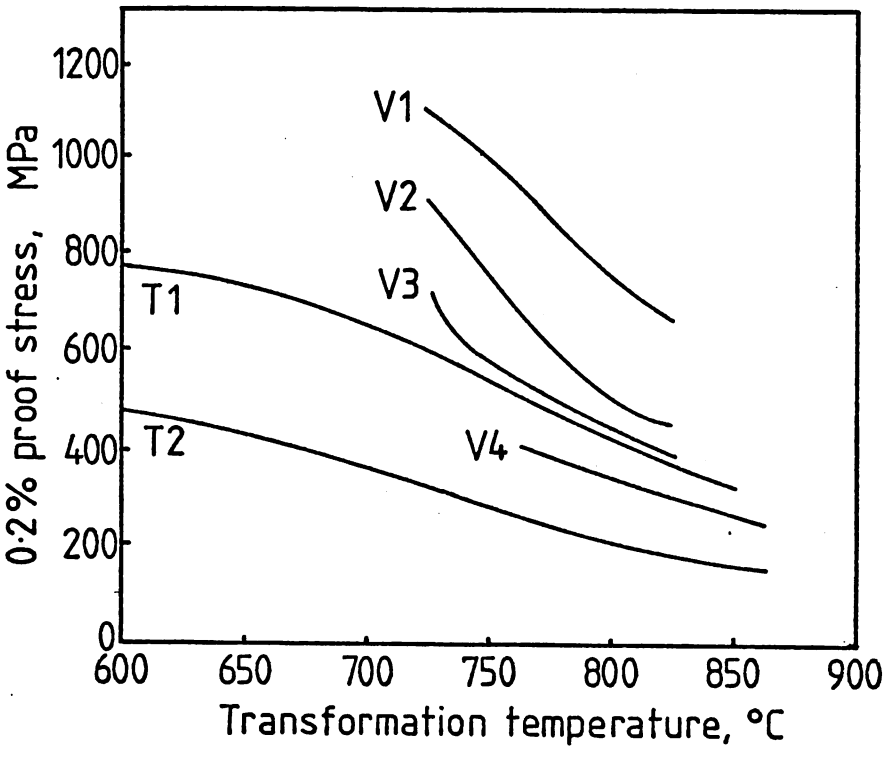

Figure 2.6: Strengths of isothermally transformed titanium and vanadium steels with the following volume fractions of carbides:- T1 = 0.43%, T2 = 0.16%, V1 = 1.23%, V2 = 0.93%, V3 = 0.55%, V4 = 0.23% (from Freeman & Honeycombe 1977)

Speich & Leslie 1972).

Isothermal treatments have been used extensively to study the nature of carbide precipitation during the austenite to ferrite transformation, and reviews of the morphologies found in a wide range of alloy steels have been written, for example, by Honeycombe (1976, 1979). Three types of dispersion can be defined:

i) random precipitation;

ii) fibrous precipitation;

iii) interphase precipitation.

Random precipitation is generally associated with dislocations and several variants of the orientation relation are exhibited in any one ferrite region, because precipitation occurs wholly within the ferrite (Balliger & Honeycombe 1980).

Fibrous and interphase precipitation nucleate at the austenite/ferrite interface and in some systems the two types of precipitation can be found in the same ferrite grain. Fibrous carbides grow normal to the transformation interface (e.g. Ainsley, Cocks & Miller 1979) and tend to form in preference to particulate dispersions when there is a large solute supersaturation or when either alloying additions or a raised temperature decrease the driving force.

The characteristics of interphase precipitation are well documented (e.g. Davenport & Honeycombe 1971). Discrete carbide particles, all in the same orientation, are precipitated in sheets parallel to the γ/α transformation interface. At macroscopically planar, highly coherent γ/α interfaces, the precipitation is thought to be associated with the incoherent, mobile interface ledges (Campbell & Honeycombe 1974). The sheet spacing corresponds to the ledge height and is thus a function of

transformation temperature: the ledge nucleation rate increases as the transformation temperature is lowered and hence the ledge height decreases. To account for interphase precipitation at curved, incoherent γ/α interfaces, Heikkinen (1973) has proposed an interface bowing mechanism and Ricks & Howell (1983) have suggested a "quasi-ledge" mechanism. In each case separation of the interphase precipitates is controlled by the rate of substitutional diffusion within the interface.

Mechanistic studies of interphase precipitation have mainly been performed using steels producing coarse carbide dispersions, for example of chromium carbides. Only a limited number of studies have been made of interphase precipitation in titanium steels. The majority of work on isothermally transformed titanium steels has been performed by Freeman (Freeman 1971a&b; Freeman & Honeycombe 1977).

2.7 Strengthening conferred by titanium carbide dispersions

In terms of the secondary peak hardening of quenched and tempered alloy steels, titanium is a more effective strengthening addition per volume percent of precipitate than vanadium. Data compiled by Haynes & Baker (1981) show strengthening increments of 70 to 90 HV per 0.1 vol% in titanium steels compared with 30 to 50 HV per 0.1 vol% in vanadium steels. The secondary hardening peak of titanium steels occurs at tempering temperatures of approximately 600°C, and because of its very low solubility in ferrite, finely dispersed titanium carbide confers a high resistance to overtempering and recrystallisation (Hornbogen & Minuth 1973; Haynes & Baker 1981)

In isothermally transformed specimens, Freeman (1977) found that the strengthening produced by titanium carbide dispersions varied with volume fraction and heat treatment in a similar manner to vanadium steels, as

shown in Figure 2.6. A detailed analysis by Batte & Honeycombe (1973) of the strength contributed by interphase precipitates in vanadium steels concluded that the strengthening effect of the aligned dispersion is intermediate between that of a lamellar structure and a random dispersion. An empirical relationship between the strength component $\Delta\sigma_\lambda$ and the perpendicular sheet spacing λ was deduced:

$$\Delta\sigma_\lambda = K\lambda^{-0.7} \qquad \ldots 2.2$$

Thus, to obtain the maximum benefit from interphase precipitation a high volume fraction of finely dispersed, stable particles is required and in practice is achieved by the addition of more than one precipitate-forming element.

2.8 Definitions of yielding behaviour

When the stress-strain curve of a material does not show a smooth transition from the elastic to plastic region it is said to exhibit a yield point or discontinuous yielding. Perhaps the most well-known occurrence is in mild steel though in various forms discontinuous yielding is shown in a wide range of materials.

A well-developed yield point in steel shows the stress-strain characteristics displayed in Figure 2.7. Initially the trace is linear whilst the specimen extends elastically. At the upper yield stress the applied stress drops sharply (the yield drop) and may show a minimum before settling at the lower yield stress for as much as several percent strain. This is the Lüders strain when one or more bands of yielded material advance along the gauge length. When the entire gauge length has yielded there may be a small drop in load, caused, it is thought, by local stress interactions when the Lüders bands run together (Brindley & Worthington, 1970; Nilsson, Lagneborg & Sandström, 1975). Further deformation then

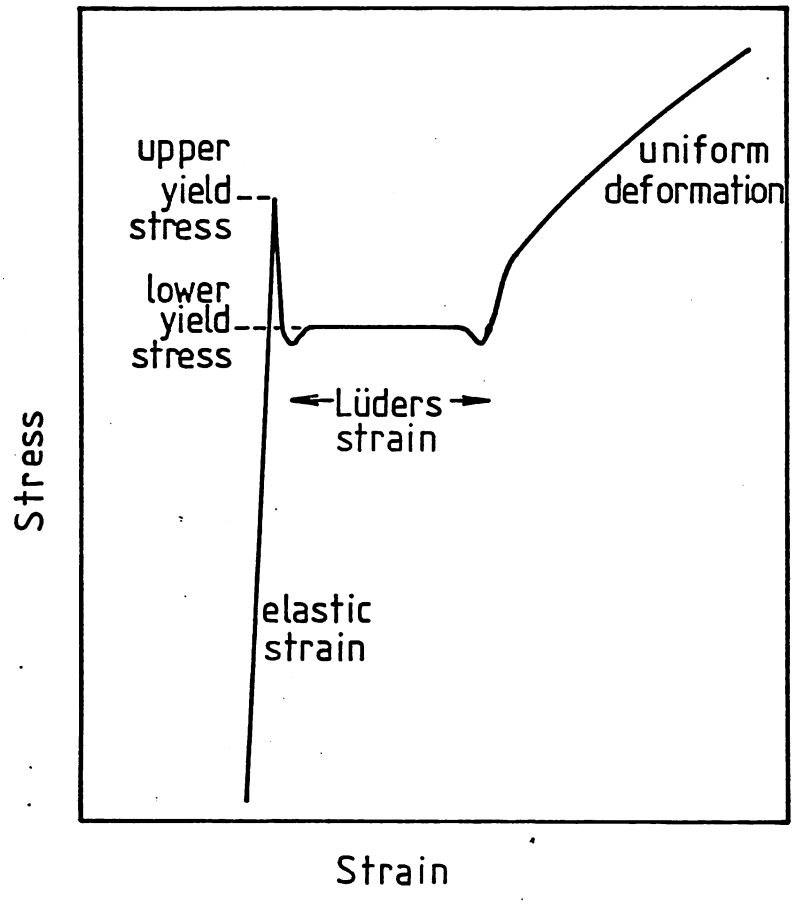

Figure 2.7: Characteristics of a well-developed yield point

proceeds uniformly and the stress-strain curve increases monotonically.

The magnitude of the yield point phenomenon is determined by the material properties and the experimental technique. When the effect becomes less pronounced, the upper yield point becomes rounded and the Lüders strain decreases so that the stress-strain curve exhibits a plateau or merely an inflection at the yield point.

The strain-ageing yield behaviour is demonstrated when a material is further strained after it has been plastically deformed. The initial deformation may be applied either during the production processes or by the pre-straining of a laboratory specimen; the ageing treatment may be time at room temperature or at elevated temperature. On further straining there may be a permanent or temporary increase in flow stress.

2.9 The development of yield point theories

Reviews on yield point phenomena have been written by Hall (1970) and Brindley & Worthington (1970), and specifically on strain-ageing by Baird (1963, 1971) and Balliger & Gladman (1978).

Much of the early work was performed on mild steel for which the magnitude of the yield drop depends on the carbon content. Dalby (1913) suggested that the carbon formed as thin cementite layers along the ferrite grain boundaries and that the yield drop was caused when the films gave way. This theory was discounted because insufficient carbon was available. Interest in the phenomenon increased in the 1940's when the role of dislocations in plastic deformation was appreciated. Cottrell & Bilby (1949) proposed that dislocations were locked by interstitial carbon or nitrogen atoms and that the yield drop was caused when the dislocations broke away from these "atmospheres".

Very low initial densities of mobile dislocations were proposed by

Johnston and Gilman (Johnston & Gilman 1959; Johnston 1962) to explain the yield drops exhibited by lithium fluoride single crystals. Hahn (1962) developed a more general theory with particular reference to the behaviour of iron alloys. The basis of this "dynamic theory of discontinuous yielding" is the Orowan expression relating the parameters of dislocation movement to the applied strain rate:

$$\dot{\epsilon}_p = \alpha b \rho_m v \qquad \ldots 2.3$$

where $\dot{\epsilon}_p$ = applied plastic strain rate

α = an orientation factor

b = Burgers vector

ρ_m = density of mobile dislocations

v = mean dislocation velocity

If there is a low initial density of mobile dislocations, the dislocation velocity v must be high to match the applied strain rate. This is only achievable at high flow stress σ since it is found that

$$v = B\,(\sigma - \sigma_i)^m \qquad \ldots 2.4$$

where B = constant

$(\sigma - \sigma_i)$ = effective stress, the thermal component of σ

σ_i = internal stress, the athermal component of σ, comprising the Hall-Petch term for resistance to grain boundary penetration and friction stresses arising from dislocation structure, precipitates and solute atoms

m = velocity factor for dislocation movement

Once dislocation movement has started, the density of mobile dislocations increases either by unpinning (e.g.from atmospheres) or by multiplication. The dislocation velocity need not then be so high, and

therefore the applied stress to sustain the strain rate drops to the lower yield stress. Hence for a sharp yield drop, Hahn proposed that the following are needed:

i) low initial density of mobile dislocations;

ii) dislocation velocity which must not increase too rapidly with stress; i.e. a low value of m

Typically for pure iron, $m \triangleq 5$ (Michalak 1965)

for mild steel, $m \simeq 35$ (Hahn 1962)

for LiF, $m \triangleq 16$ (Johnston 1962)

iii) rapid dislocation multiplication at yield.

The main weakness in the theory lies in the expression for dislocation velocity which has an empirical basis.

Current explanations for yield point phenomena in steels incorporate the dynamical properties of mobile dislocations with the effects of dislocation locking. Included in the following sections are outlines of some of the recent developments to the theories of yielding behaviour.

2.10 The effects of carbon and nitrogen on yield points in steel

Discontinuous initial and strain-age yielding are absent in simple steels from which both the carbon and nitrogen have been completely removed (e.g. Low & Gensamer 1944), due to the dominance of the Cottrell-Bilby dislocation locking mechanism in discontinuous yielding processes.

However, even at very low interstitial content the yield effects from dislocation locking can be significant. The strain field of an interstitial atom has shear and hydrostatic components (Cottrell & Bilby 1949) resulting in a strong elastic attraction to screw and edge dislocations. For a coverage of one solute atom per atomic plane of dislocation in an annealed mild steel containing typically a dislocation

density of 10^{12} m^{-2} (10^{8} cm^{-2}), a concentration of approximately 10^{-6} wt% of interstitial solute is required. In practice, 0.0001 wt% can give rise to detectable yield effects (Hall 1970).

The ease of unpinning will depend on the degree of segregation of the interstitials and on the testing temperature. If the concentration of segregated atoms is low such as during the early stages of a strain-ageing treatment, or if an elevated test temperature is used, thermal unpinning can occur and the yield effect thus be decreased. For example, the binding energy of dislocation atmospheres is approximately 0.5 eV. Above 300°C thermal energy allows the dislocations to dissociate from the carbon, thereby eliminating the yield point. Under most conditions, however, atmospheres are well developed because of the relatively rapid diffusion of interstitial solute atoms, so yielding is explained in terms of the creation of fresh dislocations rather than unpinning.

Data on the diffusion coefficients and solubilities of carbon and nitrogen in ferrite are presented in Figures 2.8 and 2.9 as functions of temperature. Extrapolation of the iron nitride equilibrium solubility to room temperature implies that only 10^{-4} to 10^{-5} wt%N may remain in solid solution, but this level will not be approached even on very slow cooling. There is also evidence (Cottrell & Leak 1952) that Fe_4N particles can dissolve in the presence of dislocations because of the greater binding energy of nitrogen to the latter.

The solubility of carbon in equilibrium with cementite in iron is calculated to be less than 10^{-6} wt%C at room temperature, at least an order of magnitude lower than nitrogen solubility. However, even when slowly cooled, equilibrium is maintained only down to probably 200°C, corresponding to 0.0001 wt%C, and faster cooling will hold larger concentrations in solid solution especially in the absence of precipitate nuclei (Baird

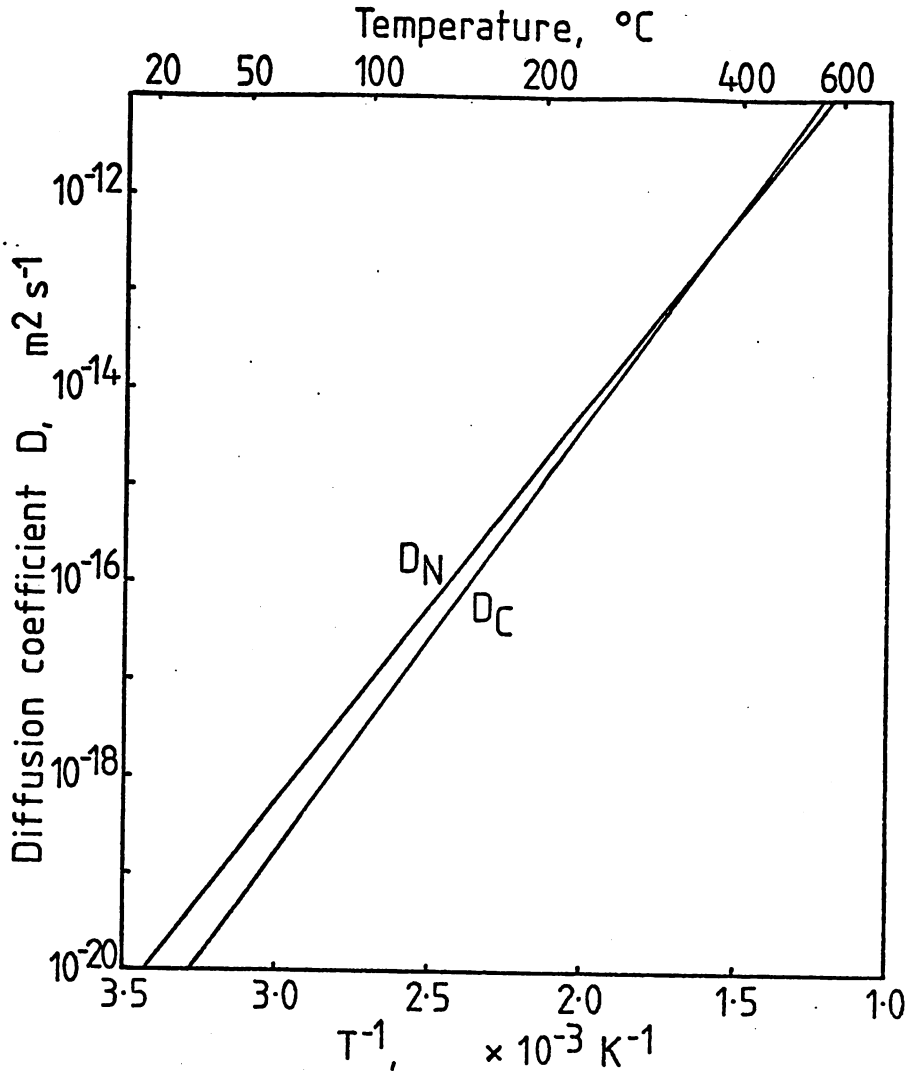

Figure 2.8: Diffusion coefficients of carbon (D_C) and nitrogen (D_N) in iron (Baird 1963)

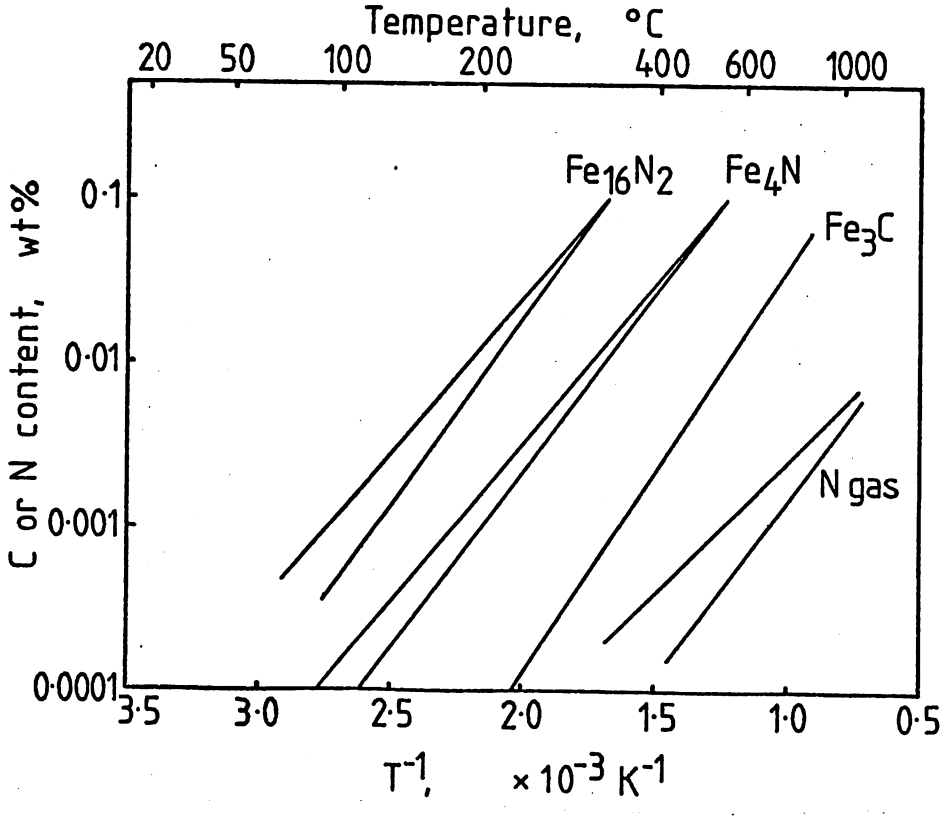

Figure 2.9: Solubilities of carbon and nitrogen in iron (compiled by Baird 1963)

1963). Under subsequent heat treatments carbide clusters and then cementite precipitates may form at dislocation cores.

Once formed, cementite is much less soluble than iron nitride and only begins to dissolve noticeably above 100°C. In consequence of these differences in solubility, initial and strain-age yield effects due to carbon are much more dependent on prior heat treatment than those due to nitrogen. Moreover, in alloy steels one must consider the effects of carbide- and nitride-forming elements. Furthermore, although the presence of interstitial carbon or nitrogen appears to be necessary for discontinuous yielding in steels, it is not the only requirement.

2.11 Grain size dependence of yield points

Both upper and lower yield stresses in steels obey a Hall-Petch relationship with grain size, d, of the form

$$\sigma' = \sigma'_f + k_y d^{-\frac{1}{2}} \qquad \ldots 2.5$$

as shown in Figure 2.10 from Hutchison (1963). The friction stress σ'_f and the Hall-Petch factor k_y have different values for the two critical stresses with the result that the magnitude of the yield point effect diminishes as the grain size increases. Furthermore there is an accompanying transition from heterogeneous to homogeneous discontinuous yielding before continuous yielding is exhibited. Heterogeneous behaviour, as defined by Lagneborg & Sandström (1975), is characterised by the passage of sharp Lüders band fronts along the specimen at constant applied stress, and homogeneous behaviour by simultaneous yielding throughout the gauge length. During the transition the Lüders bands become gradually more numerous and more diffuse.

According to Petch (1964) the difference between the upper and lower yield stress is

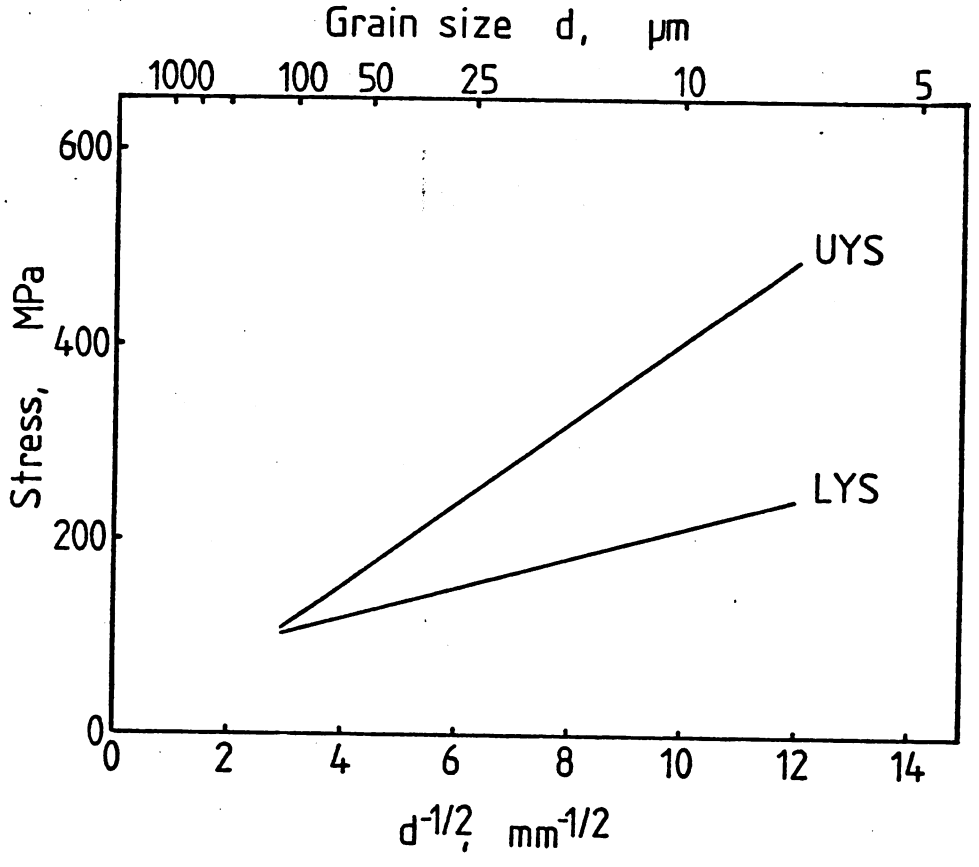

Figure 2.10: Variation of room temperature upper and lower yield stress with grain size (from Hutchison 1963)

$$\Delta\sigma_o \log_{10}\frac{1}{(N_o d^3)}$$

a term which takes account of the velocity effect previously expressed in Equation 2.4. At any instant the fraction of the total volume contributing to the strain rate is Nd^3 where N is the number of yielded grains per unit volume and d the grain size. Consequently $(Nd^3)^{-1}$ is the increase in the dislocation velocity over uniform straining. $\Delta\sigma_o$ is the increase in the effective stress due to a tenfold increase in strain rate. In very fine grained materials the upper yield stress corresponds to the stress at which slip first breaks out through a grain boundary and occurs when N has the value N_o. N_o was found experimentally by Petch to be 10 to 100 grains per mm^3 and to be approximately independent of grain size. Pre-yield microstrain is explained in this model by the creation of plastic nuclei before the upper yield stress is reached. At intermediate grain sizes the stress for grain boundary penetration is lower and the upper yield stress corresponds to the stress when the clusters of yielded grains become large enough to provide plastic strain at the applied strain rate. When $Nd^3 \gg 1$, no yield drop is observed because prior to grain boundary penetration there are sufficient dislocations to provide the strain rate without the stress needing to rise. This condition occurs at grain sizes greater than approximately 100 μm.

Lagneborg & Sandström (1975) have proposed that the difference between the upper and lower yield stresses is principally due to a variation in the Hall-Petch factor k_y rather than the stress-velocity relationship, where k_y is a measure of the ease of dislocation generation. They suggest that initially a high stress is needed either to unlock dislocations or nucleate fresh ones and then to propagate slip across grain boundaries. Once the Lüders band is established, slip penetration can

occur at a lower stress because of dislocation pile-ups in the band.

The microstructural basis of the Hall-Petch relationship itself is not clearly established. Li & Chou (1970) have critically reviewed the many theories proposed. Traditionally it has been explained in terms of stress concentrations due to dislocation pile-ups unpinning dislocation sources at or near grain boundaries. More recently, observations have indicated the need for other mechanisms; there is evidence, for example, that grain boundaries may act as dislocation sources without pile-ups creating stress concentrations. Wilson (1967) and others have suggested that dislocations are nucleated at grain boundary ledges and that the density of such sources in iron can be affected by the segregation of carbon. The grain size relationship would then arise from the difference in grain boundary area.

2.12 Discontinuous yielding in commercial steels

Most HSLA steels contain an excess of carbon with respect to the stoichiometry of the alloy carbides. Consequently they are capable of exhibiting discontinuous yielding behaviour but the occurrence depends on the thermal and mechanical treatments received. Many studies, particularly in recent years, have been made on the microstructural mechanisms which may operate to cause either the elimination or the enhancement of discontinuous yielding in the as-produced material and in the strain-aged condition.

The conventional hot-rolled HSLA steels generally have a polygonal ferrite-pearlite microstructure and exhibit a pronounced initial yield point and yield extension (Rashid 1975). However, if the transformation product is martensite, bainite or acicular ferrite then yield is continuous and is characterised by a low stress at the elastic limit and rapid

work hardening in the early stages of plastic deformation. To investigate these changes in mechanical properties, Boyd (1976) achieved differences in microstructure by altering the cooling rate of a niobium steel containing 1.5 %Mn, and Tither & Lavite (1975) produced similar effects by varying the carbon content and thus the hardenability of a Mo-Nb steel. Continuous yielding in the non-polygonal ferrite microstructures was explained by the combination of high densities of mobile dislocations and residual stresses which had been generated to accommodate the volume expansion and the shear strains involved in the transformation of austenite at lower temperatures. In both studies, discontinuous yielding was developed in the non-polygonal ferrite structures after additional heat treatments at 600°C or higher. The treatment was thought to lower the mobile dislocation density by dislocation recovery and by precipitation on the dislocations.

Owen & Carisella (1976) analyse the yield properties of HSLA steels in terms of the dislocation substructure. In particular they postulate that the primary cause of discontinuous yielding is the elimination of low-stress dislocation sources. They propose that in lath-type structures these sources persist longer in the lath boundaries than in the grain interiors.

The inhomogeneity of the microstructure, non-uniform densities of mobile dislocations and the plastic incompatability of phases with different hardnesses have also been cited (e.g. Speich & Miller 1981; Embury, Evenson & Filipovic 1975) as promoting continuous yielding in non-polygonal ferrites. Butler & Wilson (1963) have proposed that yield points are masked after light temper rolling of low-carbon sheet steel because of the inhomogeneous structure produced rather than the introduction of residual stresses.

Studies of dual-phase steels have identified further variables which can affect yield behaviour. Davies (1979), Morrison (1980) and Hansen & Pradhan (1981) all report the elimination of discontinuous yielding by the presence of martensite in a ferrite matrix. Morrison attributes this behaviour to residual stresses whereas Hansen & Pradhan suggest that mobile dislocations introduced around the martensite islands are the cause. They also show that a fast cooling rate after the martensite formation is additionally required for continuous yielding and suggest that this avoids the pinning of mobile dislocations.

Rashid (1981) and Okamoto & Takahashi (1981) report the presence of metastable retained austenite in the martensite islands of dual-phase steels and propose that continuous yielding is promoted by the high localised stresses generated during the austenite decomposition in the early stages of deformation.

2.13 Discontinuous yielding in titanium steels

In their classic paper of 1940, Edwards, Phillips & Jones showed that of the carbide- and nitride-formers added to steels, titanium is the most effective in removing carbon from solution. A titanium to carbon ratio of approximately 10:1 by weight (2.5:1 atomic ratio) was found by these authors to remove initial and strain-age yield points. It is now agreed that a Ti:(C+N) atomic ratio of 1:1 is sufficient, later investigations by Comstock (1943) and Meyer, Heisterkamp & Müschenborn (1975), for example, having given greater consideration to titanium oxide and nitride formation. In these studies the steels had been cooled moderately slowly in the ferrite region either by furnace cooling or air cooling, thus giving time for precipitation.

Work by Smaill, Keown & Erasmus (1976) and Pussegoda & Erasmus (1977)

on the effects of up to 0.1 %Ti in 0.2C-Mn steels concentrated on the role of nitrogen. The carbon level was well above that for TiC stoichiometry and a 3 h, 100°C strain-ageing treatment was given. When the titanium content was sufficient to combine with all the nitrogen and a pre-ageing treatment at 100°C was given, strain-age yield points were eliminated in rolled material. It was assumed that the pre-ageing treatment precipitated out any carbides still in solid solution after rolling. The majority of all the specimens exhibited initial yield points and the yield extensions were greater at lower titanium contents and at finer grain sizes.

Rashid (1975, 1976) looked at strain-ageing in HSLA steels and found that in as-rolled vanadium and titanium steels, the magnitude of the strain-age yield points was little affected by the ageing time (in the range 3 h to 2 yrs) at room temperature. However at ageing temperatures greater than 100°C the development of strain-age yield points accelerated with increasing time and temperature, suggesting that carbon dissolution was the cause.

In general, initial yield points in such non-ageing steels (i.e. non-ageing at ambient temperature) are attributed to the pinning of existing dislocations but it is not certain which species or precipitate is responsible in each case.

Some workers have deliberately added titanium to experimental alloys with the aim of removing all the oxygen, carbon and nitrogen from solution. Goodenow & Held (1970) used a 0.01C-0.19Ti steel recrystallised at various subcritical temperatures after rolling. At all stages of recovery and recrystallisation tensile yielding was continuous, explained by the complete absence of dislocation pinning by interstitials. Leslie & Sober (1967) used 0.15 %Ti in a nominally pure iron and found discont-

inuous yielding when the recrystallised material was tested at subzero temperatures, and only when the tensile specimens had been machined before rather than after the heat treatment. Only low dislocation densities ($\sim 10^{12}\ m^{-2}$) were measured in the recrystallised material and because of the absence of interstitials, dislocation-dislocation pinning was suggested as a possible reason for the initial yielding behaviour shown by the more dislocated, machined specimens.

CHAPTER THREE

DEVELOPMENT OF MICROSTRUCTURES

3.1 Introduction

This chapter is concerned with the austenite decomposition reaction of two experimental steels alloyed with titanium. Investigations using dilatometry and the quantitative metallography of partially transformed specimens provide details of the reaction kinetics. In particular, the results of isothermal heat treatments at temperatures between 800° and 650°C are analysed. The observed morphology and crystallography of the titanium carbide precipitates and the ferrite are reported, and later in the chapter provide evidence for the transformation mechanisms in operation. The microstructures existing after complete transformation are discussed in relation to transformation temperature and also with respect to the variations observed within individual specimens.

3.2 Experimental method

The principal microstructural investigations were carried out using Alloys 1 and 2. In the course of the studies, several analyses of the alloys were made. The following mean results for the principal alloying elements were obtained

Alloy 1: Fe - 0.070 C - 0.067 Ti

Alloy 2: Fe - 0.073 C - 0.227 Ti

The measured carbon level varied by 0.01 wt% and the titanium level by 0.02 wt% between individual samples of the same alloy. The other

deliberate additions were approximately 0.4 wt% manganese to each to retard the austenite decomposition reaction and 0.03 wt% aluminium to Alloy 2 to remove nitrogen from solution. The full analyses are given in Table A2 of Appendix A.

Alloy 1 was a laboratory-produced 2.5 kg melt and Alloy 2 was received as 12.5 mm plate. The material was prepared and worked to 5 mm and 3 mm diameter rods as described in Appendix A. A standardising solution treatment of 30 mins at 1300°C was then given to remove the microstructural effects of the working operations and to dissolve the precipitates. During the subsequent quench to martensite the titanium alloying additions were retained in solution or as very fine precipitate dispersions.

The nose of the ferrite TTT diagrams occurred at approximately 10 s and thus to approach isothermal conditions before the transformation commenced, cooling from the reaustenitising temperature to the transformation temperature had to be achieved at the maximum heat transfer rate. To compare the cooling rates on transfer from a high temperature furnace to molten salt, molten tin and a fluidised bed, a thermocouple sealed at the centre of a dummy specimen and connected to a rapid response Rikadenki chart recorder was used. The molten tin was found to promote the fastest heat transfer, the rate of which was enhanced by stirring. Temperatures within 5° of the bath temperature were reached in 5 s. This method was selected for isothermal heat treatments of up to 1000 s duration.

To determine the mechanisms and rates of transformation of the alloys, 20 mm lengths of the 3 mm diameter rods were given interrupted isothermal heat treatments. This method was selected in preference to the dilatometry of hollow specimens because the results could be related directly to the heat treatment of tensile specimens. The rods were

reaustenitised in a protective flow of argon for 10 min at 1200°C, a treatment found to be long enough to ensure complete austenite formation and precipitate dissolution without undue grain growth or decarburisation. By this method, austenite grain sizes of approximately 100 μm were attained. The specimens were then plunged into the molten tin maintained within ± 1° of the required transformation temperature, selected between 850° and 550°C. Quenching in iced-brine after pre-selected times preserved the volume fractions transformed. Optical and transmission electron microscopy were used to study the transformation microstructures.

The continuous cooling diagram for Alloy 2 was determined by dilatometry using 15 mm lengths of the 3 mm diameter rods. The cooling rate was varied from a programmed 4° per min to an estimated 30 000°C per min by helium gas quenching. A further specimen was slowly heated at 4° per min allowing the equilibrium transformation temperatures to be determined by comparison with the slowly cooled specimens.

3.3 Transformation kinetics

The volume fractions of ferrite in partially transformed specimens of Alloy 1 were quantified by direct observation of the microstructures and more accurately in Alloy 2 using an image analyser. Thus the TTT diagrams were constructed (Figures 3.1 and 3.2).

For Alloy 2, the nose of the ferrite curve occurred close to 700°C at a time of 10 s. At all temperatures between 850° and 650°C, transformation was complete well before 1000 s. A separate curve was drawn for the bainite reaction; this took place very rapidly at temperatures below 600°C. Because Alloy 1 had a lower titanium content than Alloy 2, at equilibrium there was a higher proportion of cementite present. Consequently the 90% ferrite line, rather than 95%, was used as a guide to

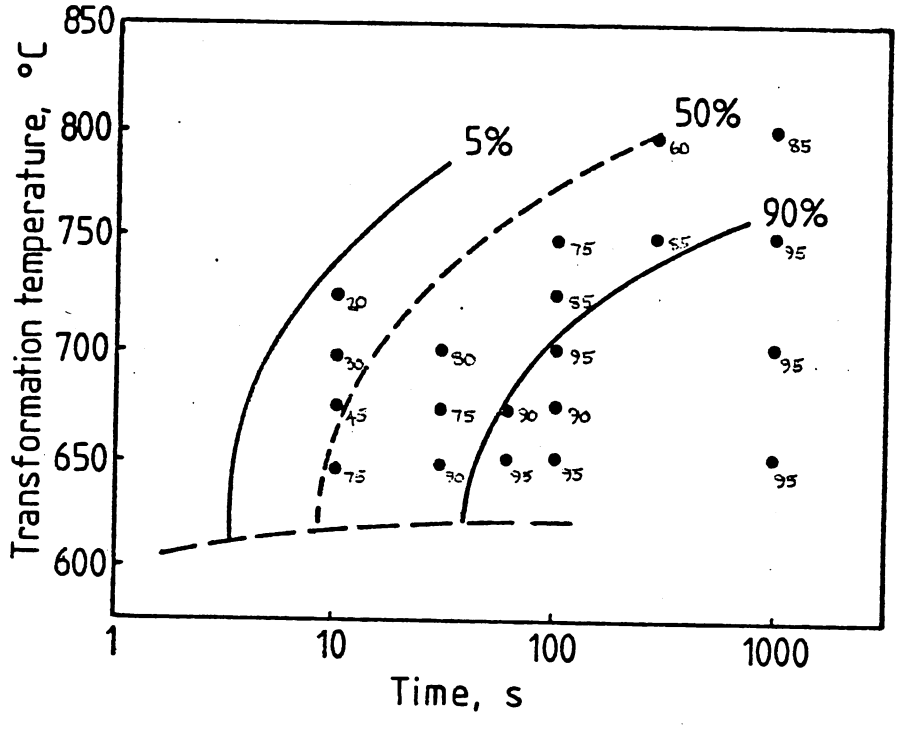

Figure 3.1: Time-temperature-transformation diagram for Alloy 1 (0.07C-0.07Ti)

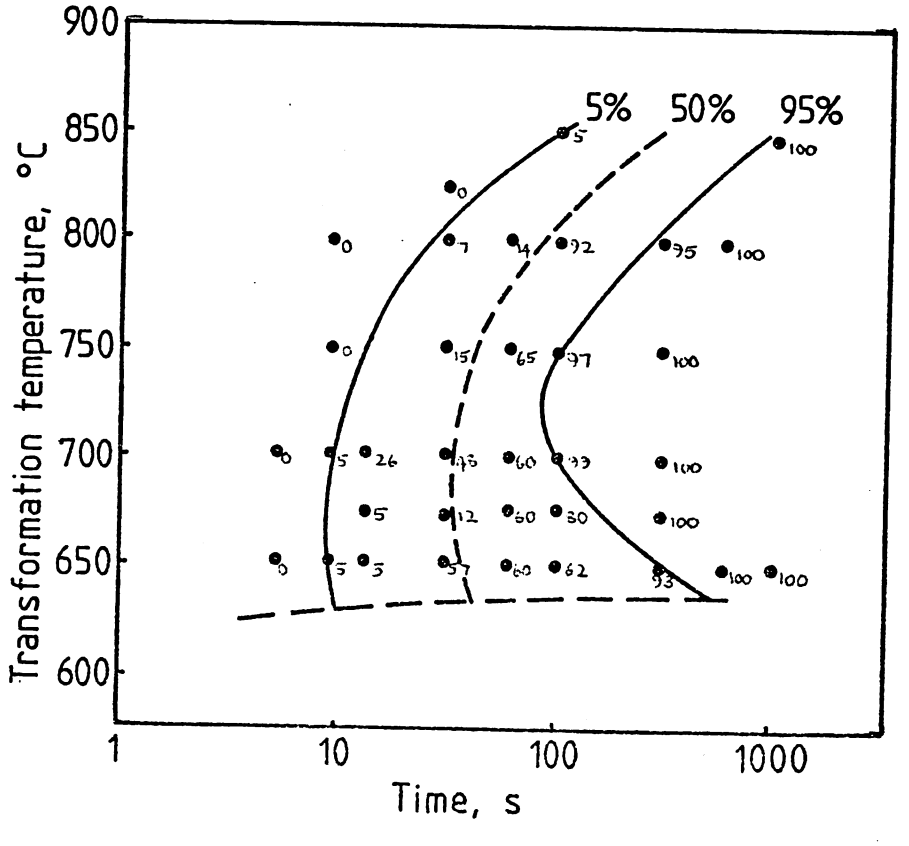

Figure 3.2: Time-temperature-transformation diagram for Alloy 2 (0.07C-0.23Ti)

the reaction termination time in Alloy 1. Compared with Alloy 2 the 5% ferrite nose for Alloy 1 appeared to occur at a shorter time and at a lower temperature, between 650°and 600°C. At 800°C some austenite remained in equilibrium with the ferrite-carbide transformation products in Alloy 1 and subsequently decomposed during cooling.

The continuous cooling diagram for Alloy 2 is presented in Figure 3.3. The austenite/ferrite solvus temperatures were found to be approximately 860°and 900°C.

3.4 As-quenched microstructure

The martensite produced by quenching the austenite is shown in Figures 3.4 and 3.5. Mean linear intercept prior austenite grain sizes of 100 μm and 104 μm were measured for Alloys 1 and 2 respectively.

The transformation product was a lath martensite, with several packets of laths present in each former austenite grain (Figure 3.4). At higher magnifications (Figure 3.5) several lath morphologies were identified: laths of 100 to 200 nm width were arranged in either a regular, parallel fashion (labelled P) or interwoven at different angles (I), and occasional laths up to 1 μm wide were observed (W). In any one packet, most of the laths were misoriented by only a few degrees. All the laths were heavily dislocated and in some, internal twinning (T) was evident.

Figures 3.6a-d are a set of micrographs from a microstructure of martensite (α'), ferrite (α) and retained austenite (γ) produced on quenching Alloy 2 after partial transformation at 650°C. The dark field micrograph (Figure 3.6b), taken using the diffraction spot indicated, shows retained austenite regions, 20 to 50 nm wide. The diffraction pattern analysis (Figure 3.6d) reveals that both the Kurdjumov-Sachs and

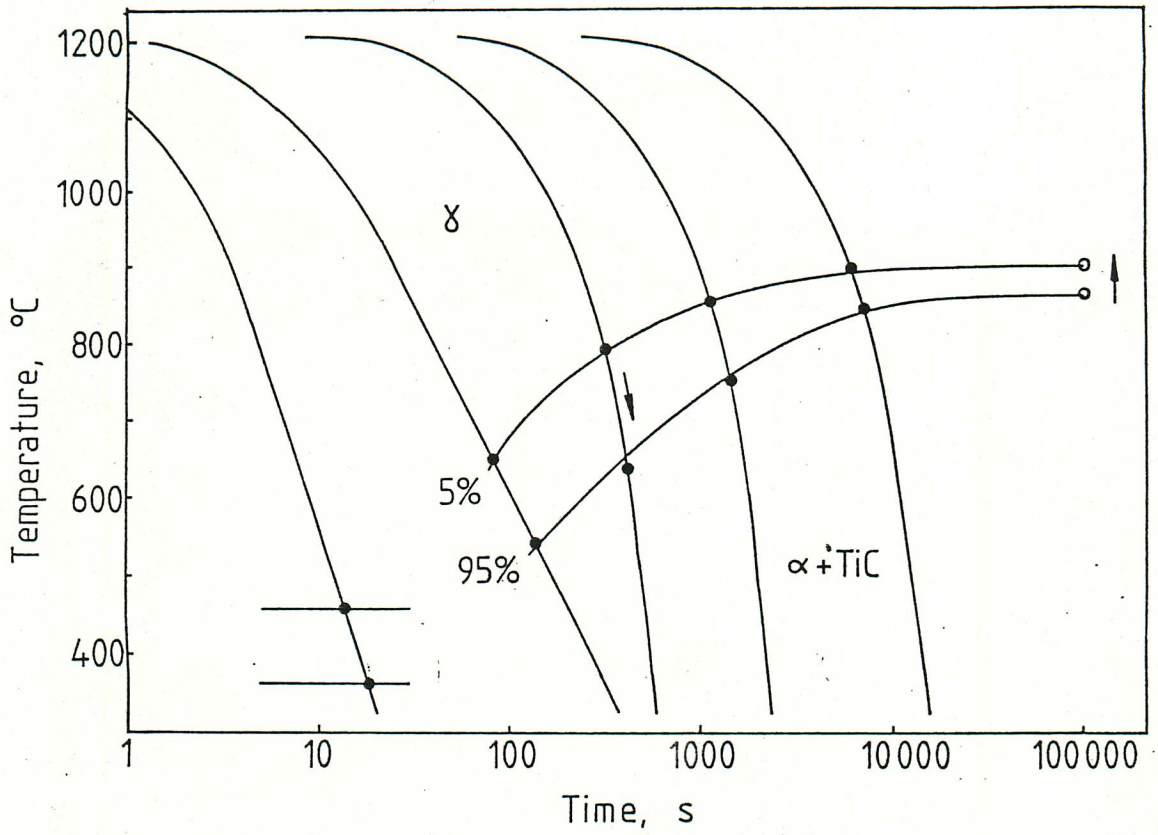

Figure 3.3: Continuous cooling diagram for Alloy 2 determined by dilatometry

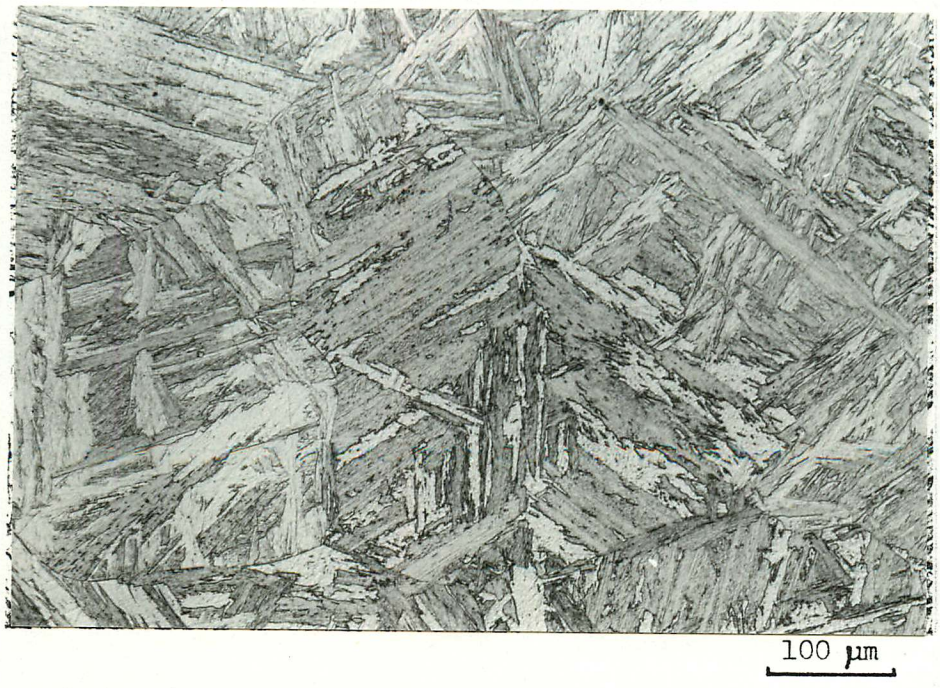

Figure 3.4: Martensite produced in Alloy 2 by iced-brine quench from 1200°C

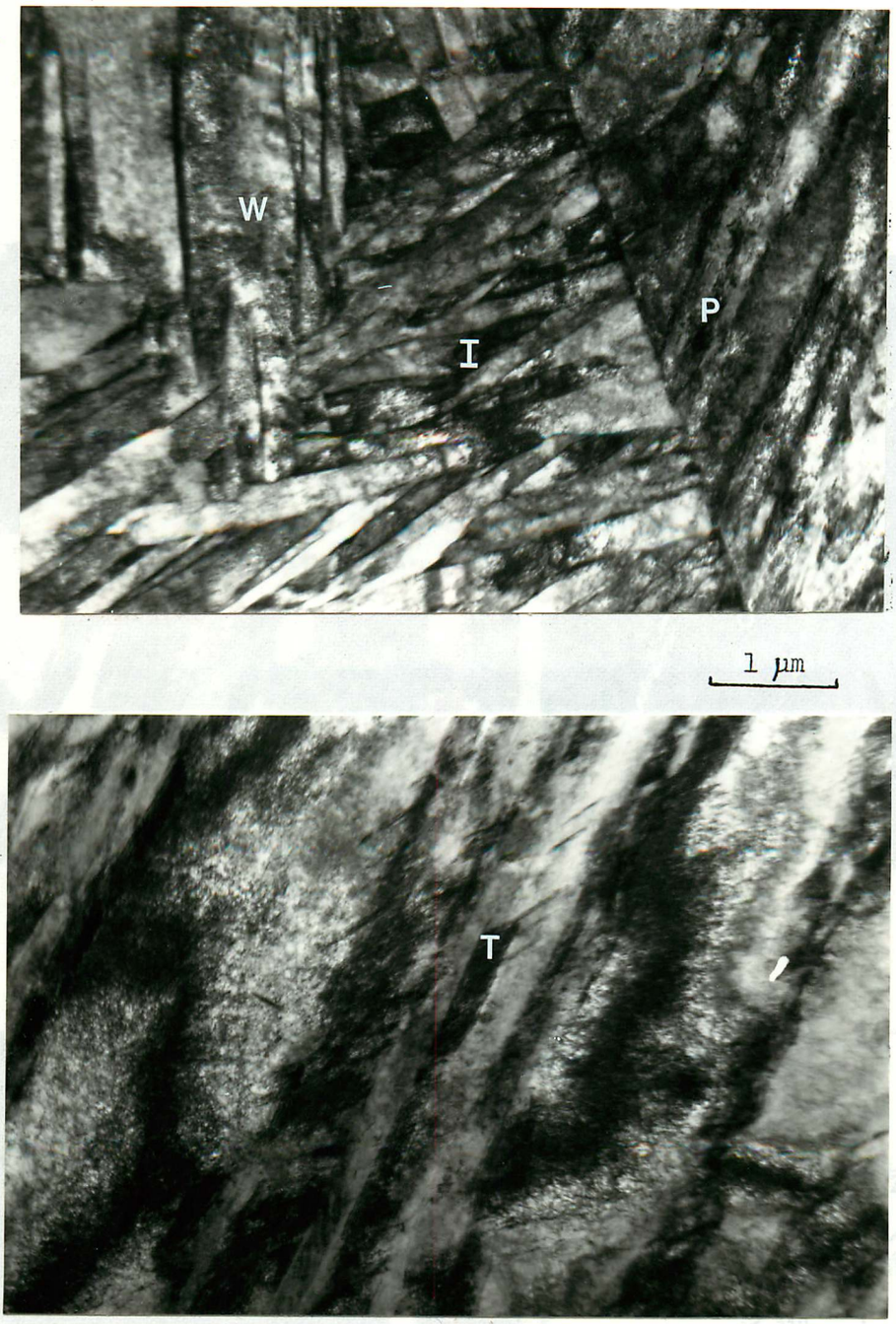

Figure 3.5: Parallel (P) and interwoven (I) laths of martensite with some internal twinning (T); occasional wider laths (W)

Figure 3.6: Martensite, ferrite and retained austenite in Alloy 2 quenched after 30 s at 650°C, showing Kurdjumov-Sachs and Nishiyama-Wassermann relationships

a) Bright field

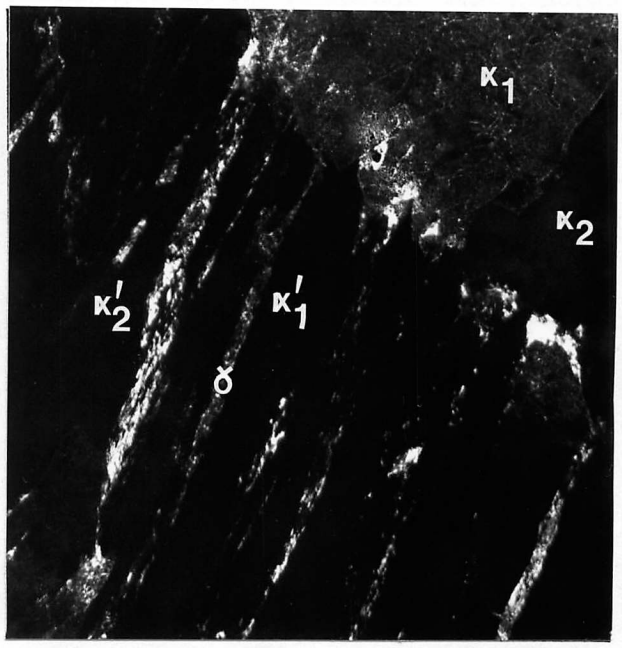

b) Dark field using the spot indicated in c)

0.5 μm

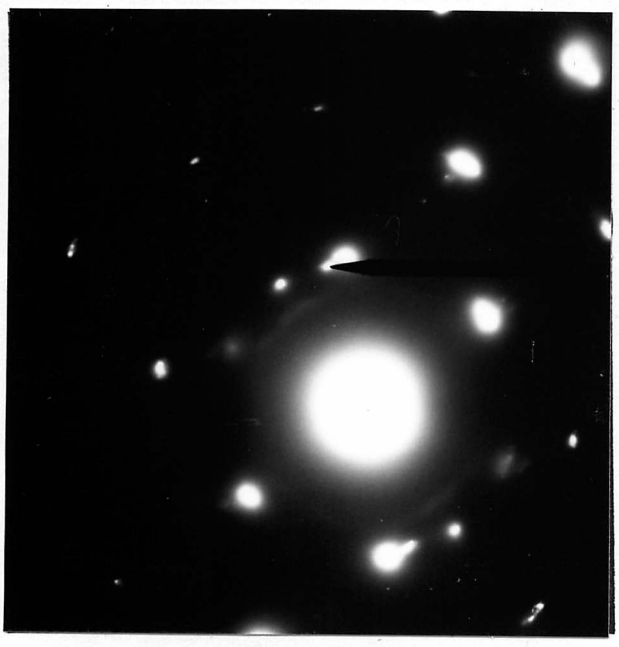

c) Diffraction pattern

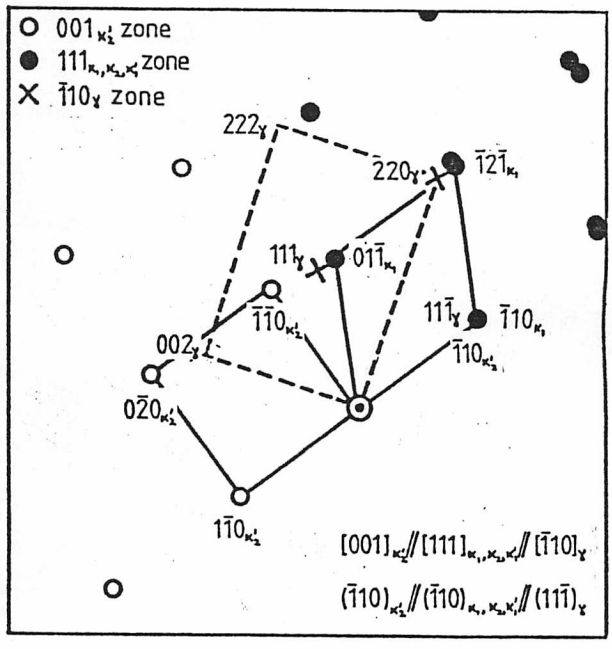

d) Diffraction analysis

Figure 3.6: Martensite, ferrite and retained austenite in Alloy 2 quenched after 30 s at 650°C, showing Kurdjumov-Sachs and Nishiyama-Wassermann relationships

Nishiyama-Wassermann orientation relationships, defined in Section 2.5, existed between the austenite and the martensite or ferrite. The significance of this result is discussed in Section 3.8.

The Nishiyama-Wassermann relationship has been reported in low-alloy vanadium and chromium steels by Law, Howell & Edmonds (1979) and Thomas & Rao (1977) respectively; increasing manganese or nickel content encouraged the transition from the Kurdjumov-Sachs to the Nishiyama-Wassermann relationship.

3.5 Ferrite morphologies formed by isothermal transformation

Alloys 1 and 2 exhibited very similar ferrite growth morphologies. At 850°and 800°C, transformation initiated (Figure 3.7a) by the nucleation of blocky grain boundary ferrite allotriomorphs. Some curved ferrite interfaces were observed (labelled C) but the majority were facetted (F); during subsequent growth (Figure 3.7b) the equiaxed grain morphology and facetted interfaces persisted. There was also possible evidence of sympathetic ferrite nucleation (S) and intragranular nucleation (I).

At lower transformation temperatures there was an increased tendency for the allotriomorphs to grow along the grain boundaries thus delineating the prior austenite grain structure (Figure 3.8). At 650°, the transformation continued by the growth of secondary side-plate or Widmanstätten ferrite from the allotriomorphs into the austenite grain interiors in specific crystallographic directions. The development of this microstructure is shown in Figures 3.9a-d. Transmission electron microscopy revealed that some of the secondary ferrite growth at 650° produced individual elongated grains (Figure 3.10a) whereas some resulted in groups of parallel plates or laths 1 to 2 μm wide, separated by low angle boundaries (Figure 3.10b). In view of the mixture of ferrite grain types

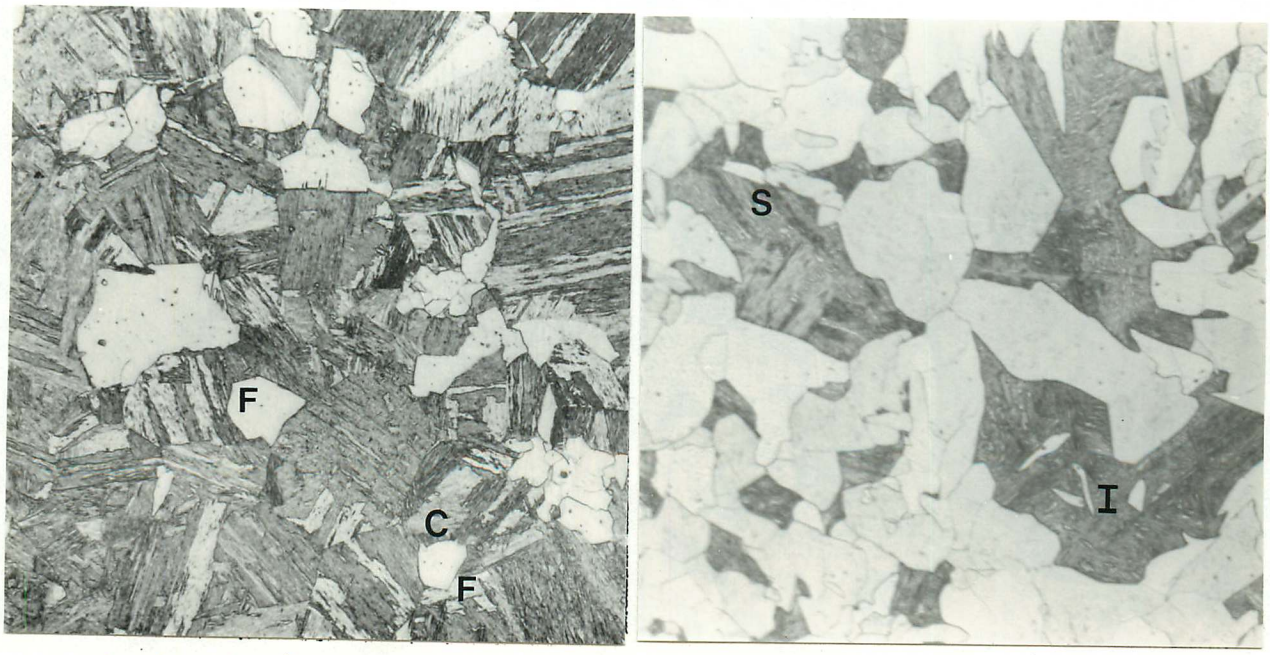

a) 30 s 800°C

b) 300 s 800°C

Figure 3.7: Development of the ferrite microstructure in Alloy 2 at 800°C

100 μm

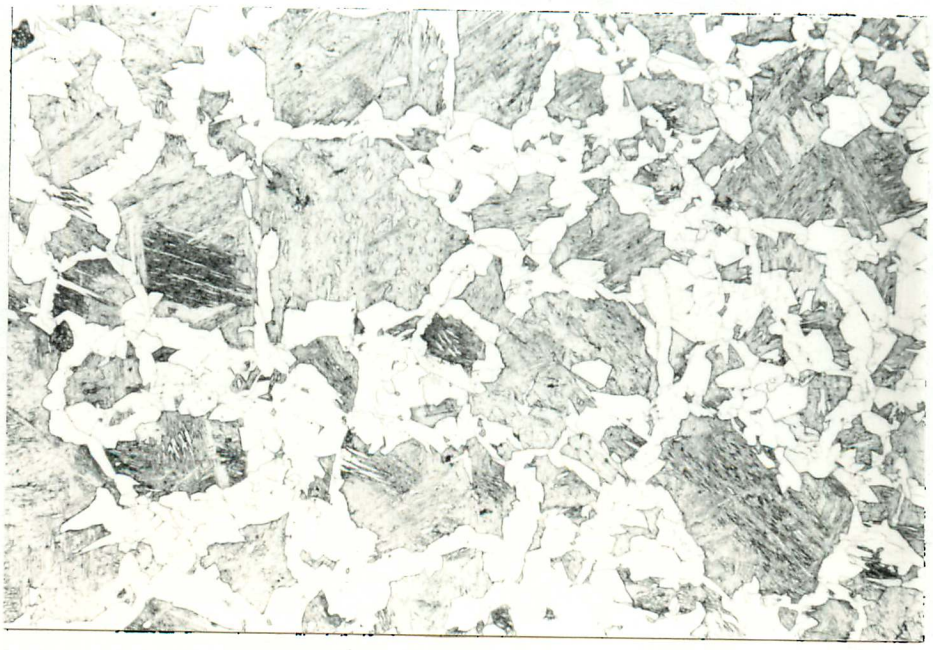

Figure 3.8: Growth of ferrite allotriomorphs along austenite grain boundaries; 10 s 690°C

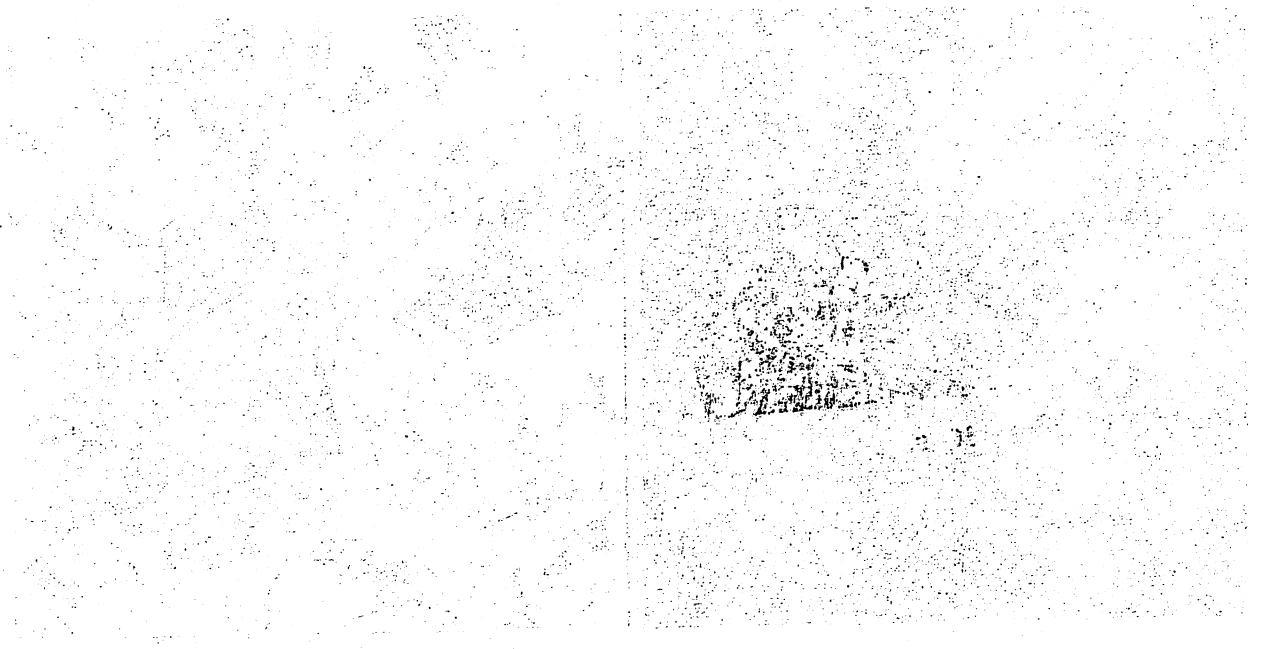

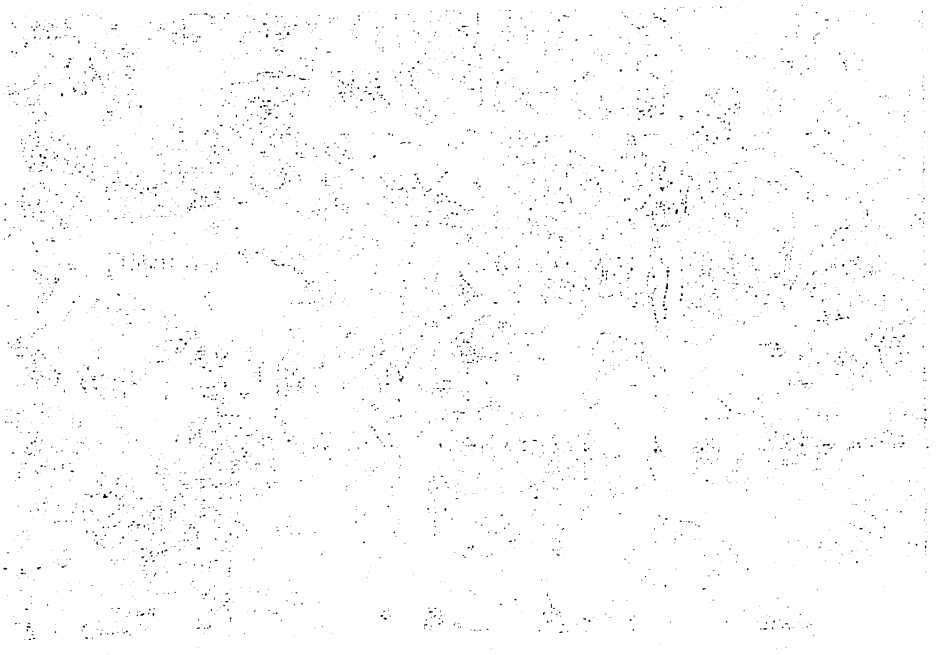

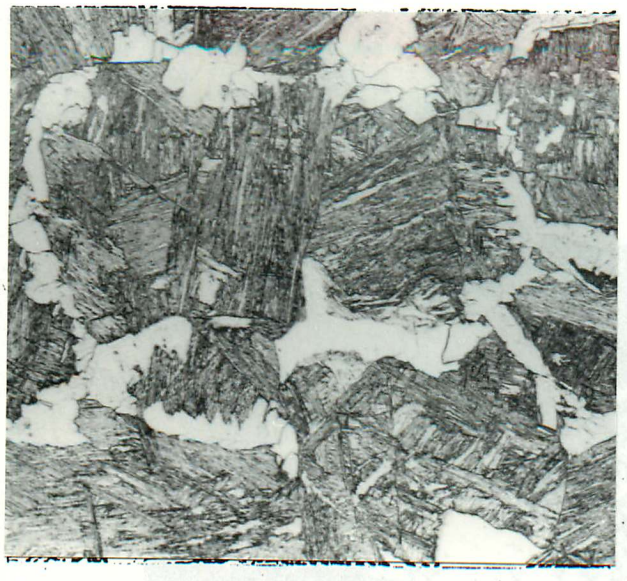

a) 30 s

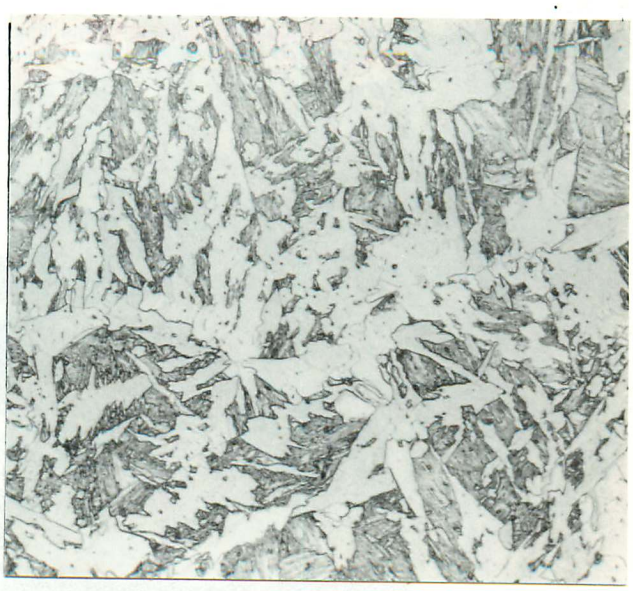

b) 60 s

50 μm

c) 100 s

d) 300 s

Figure 3.9: Ferrite growth at 650°C; Alloy 1

a) individual elongated grain 1 μm

b) group of parallel plates or laths

Figure 3.10: Ferritic structures developed at 650°C; Alloy 2

it was not possible to determine whether the two-dimensional "needles" observed in the latter colonies were sections through laths or plates.

The transition from the equiaxed to the plate morphology occurred at approximately 675°C in both alloys, and over a narrow range of about 25°C; Figures 3.11a-d show the variations in ferrite morphology observed in specimens of Alloy 1 partially transformed at temperatures spanning this transition.

The microstructures of Alloy 1 fully transformed at temperatures between 800° and 650°C are presented in Figure 3.12. At 800° the product was an equiaxed but irregular grain structure with high angle grain boundaries whereas at 650° the microstructure was a mixture of equiaxed grains from the primary allotriomorphs, and regions of high aspect ratio grains from the secondary ferrite growth. The 750° and 700° ferrite structures had intermediate characteristics with the large majority of grains equiaxed. Some austenite remained in equilibrium after transformation at temperatures of 800° and above. The 1000 s isothermal heat treatments given to tensile specimens involved a fast air cool which transformed this remaining austenite to a fine pearlite, resolvable by electron microscope (Figure 3.13). At isothermal transformation temperatures below 600°, the product was a rapidly-formed low-carbon bainitic microstructure (Figure 3.14) consisting almost entirely of parallel, heavily dislocated plates or laths between which carbides were detected.

Figure 3.15 presents the set of fully transformed microstructures for Alloy 2. Because of the lower proportion of cementite, the final ferrite morphologies were less easily identifiable in Alloy 2 than in Alloy 1. A limited investigation by electron and X-ray diffraction did not detect any retained austenite after 1000 s isothermal heat treatments at 650° and

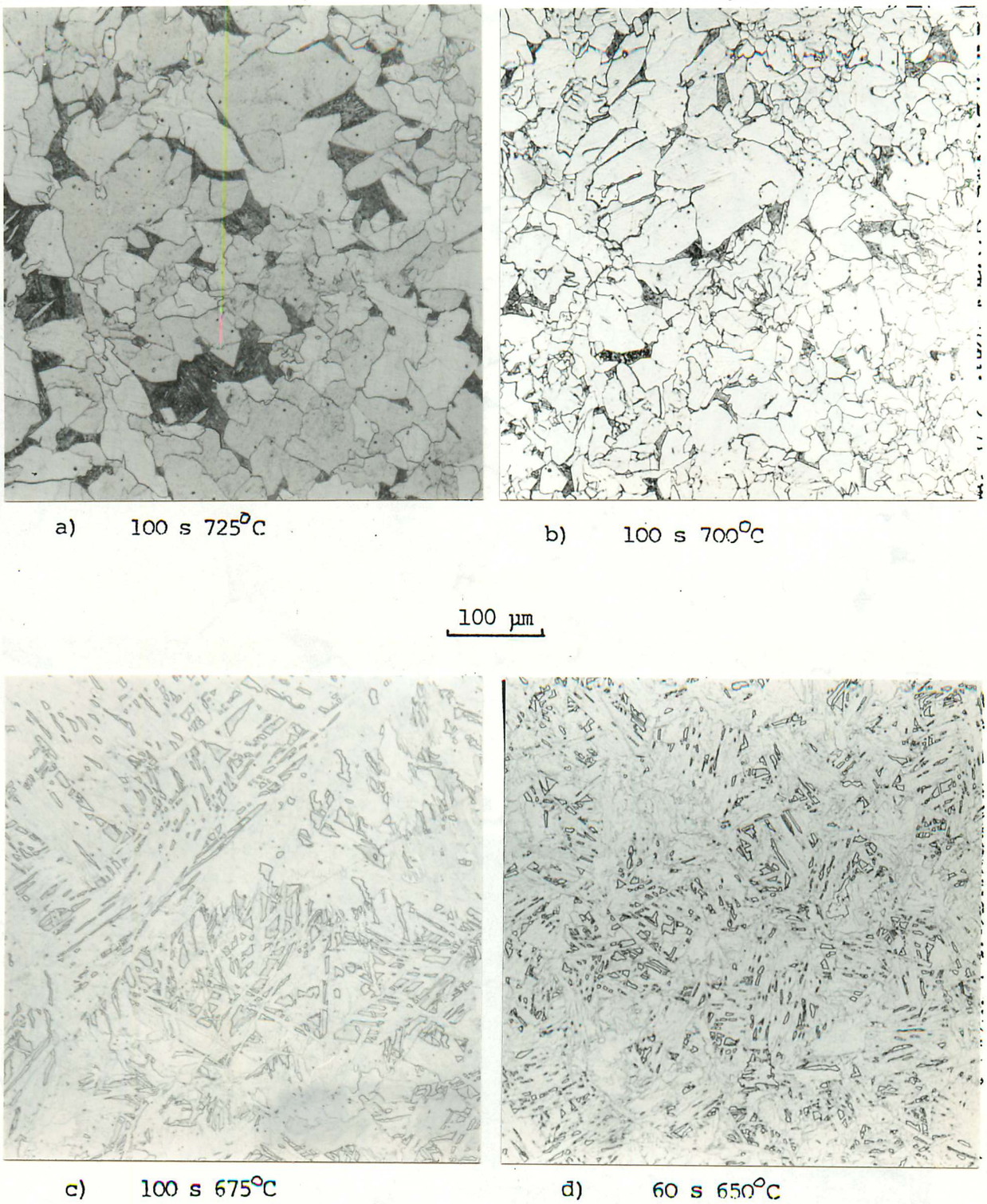

Figure 3.11: Transition in ferrite morphology; Alloy 1

Figure 3.12: Transformed microstructures after 1000 s at temperature; Alloy 1

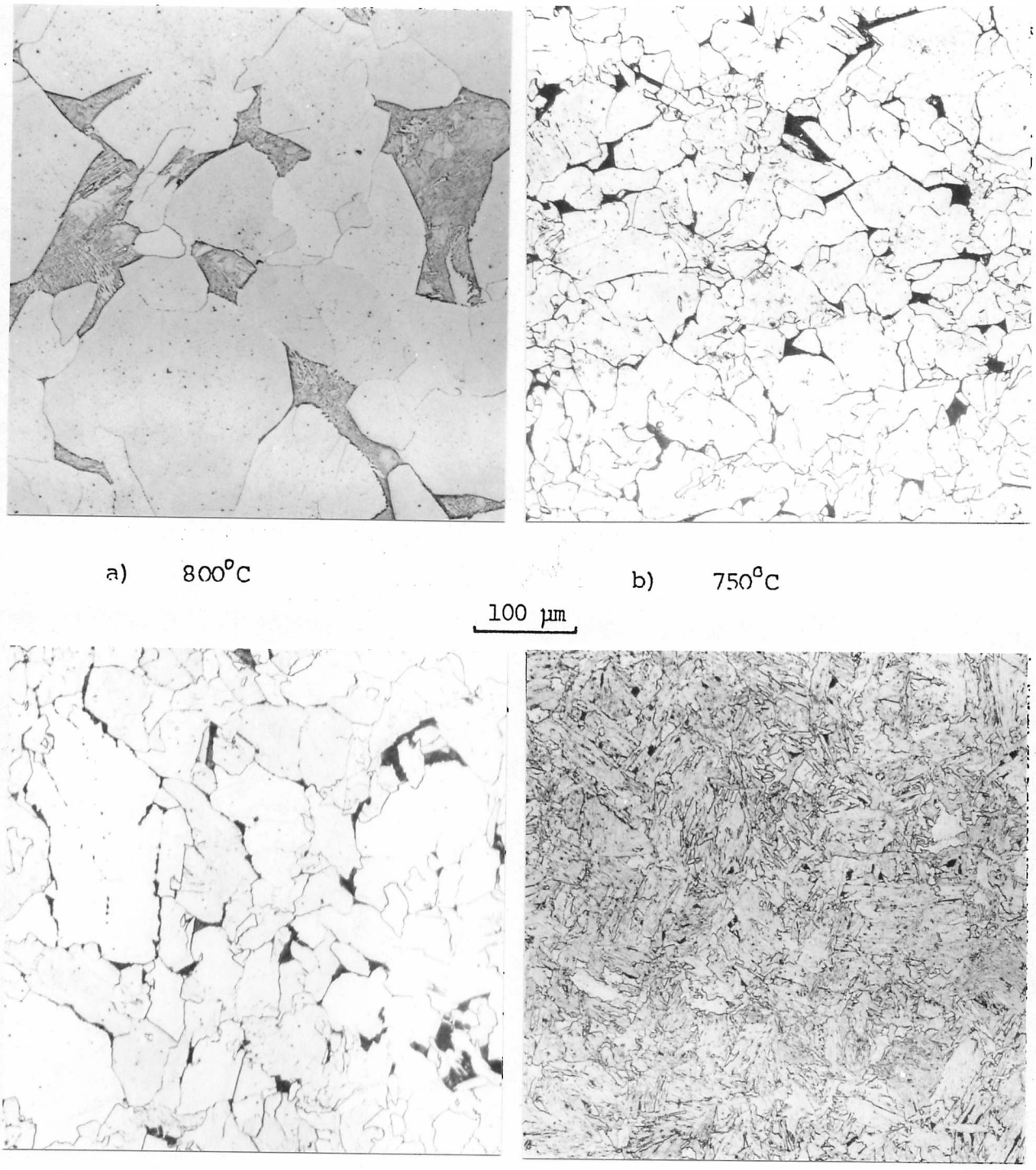

Figure 3.12: Transformed microstructures after 1000 s at temperature; Alloy 1

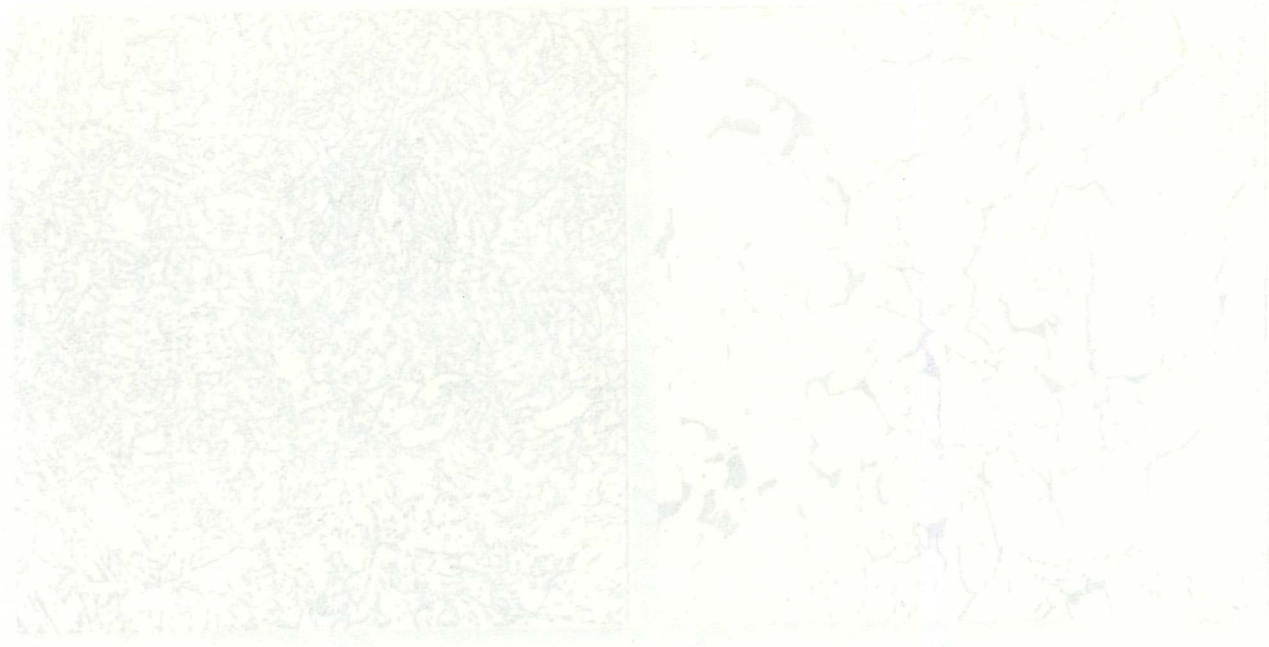

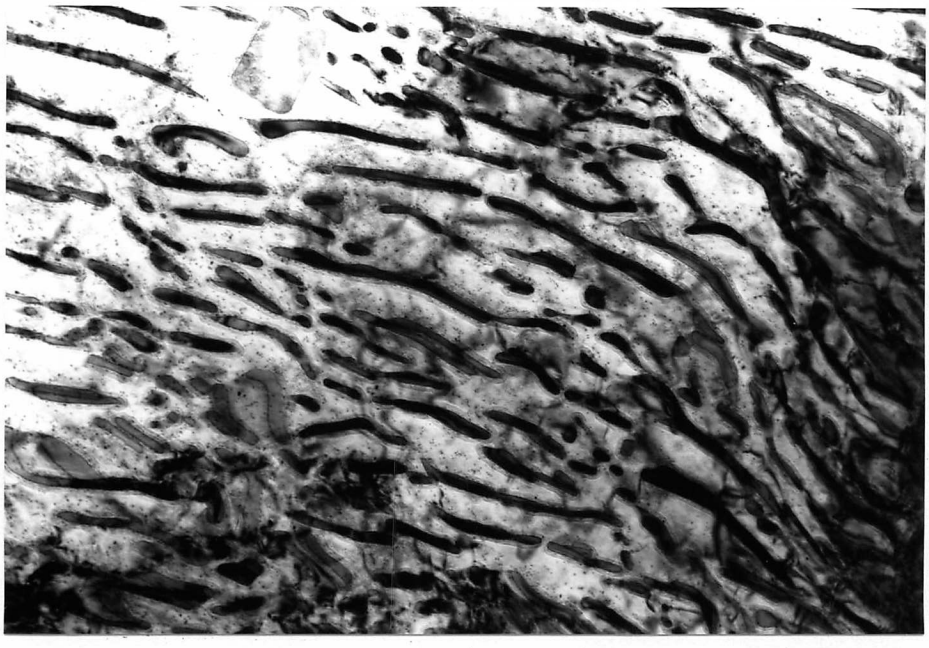

Figure 3.13: Fine pearlite

1 μm

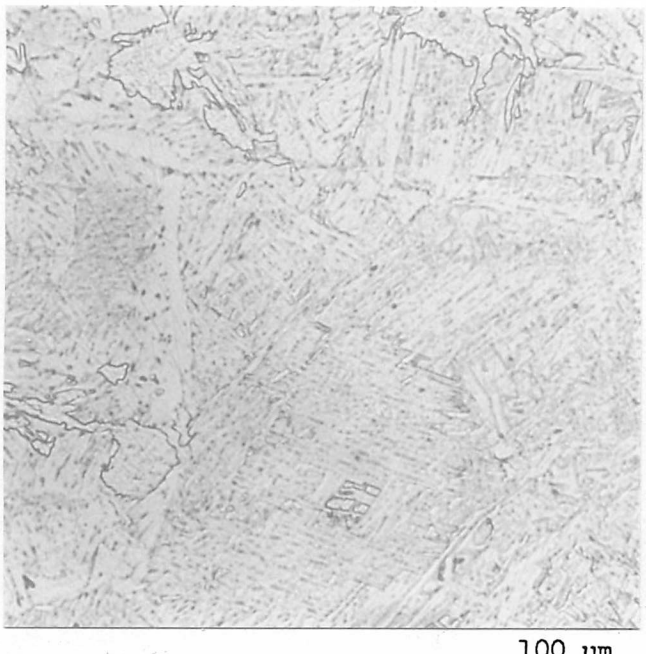

100 μm

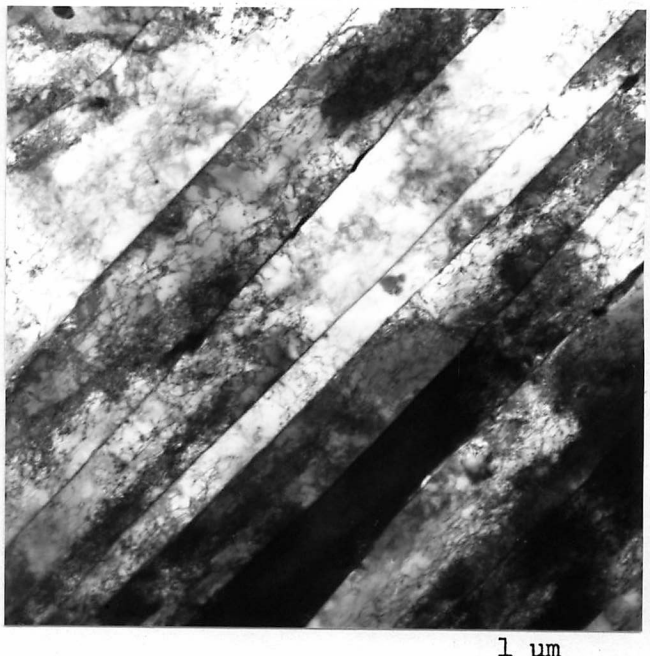

1 μm

Figure 3.14: Bainitic structures
100 s 550°C, Alloy 1

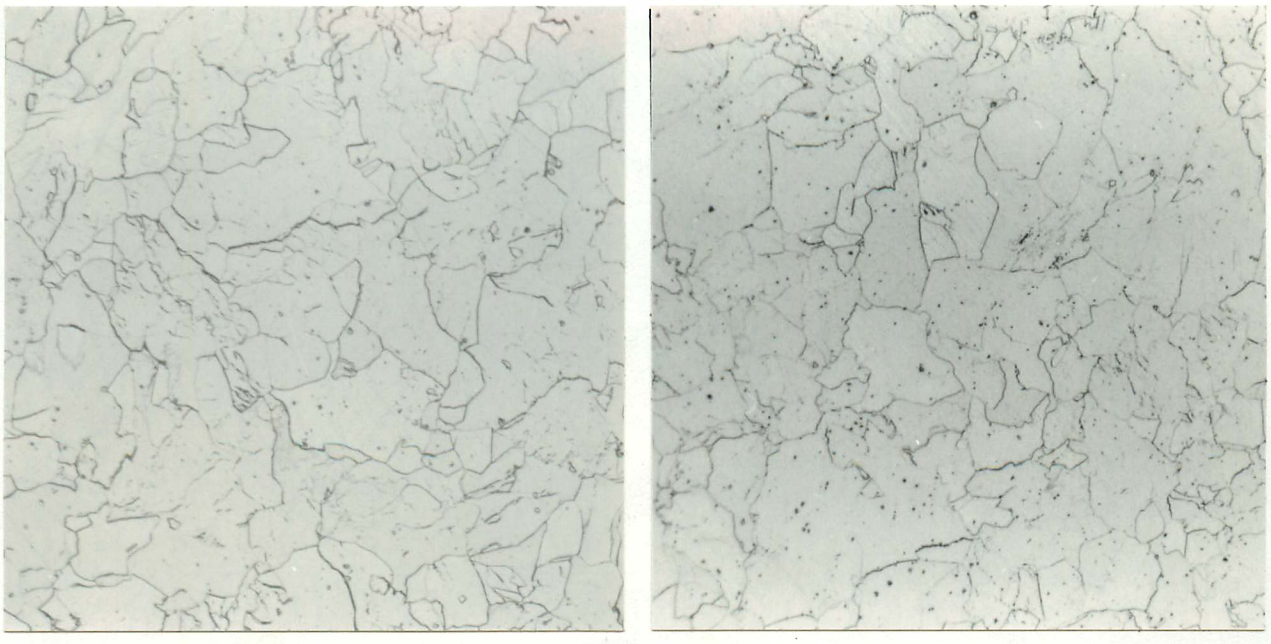

Figure 3.15: Transformed microstructure after 1000 s at temperature; Alloy 2

above.

The mean linear intercept ferrite grain sizes were found to decrease in the range 40 to 25 μm with decreasing transformation temperature between 800° and 700° as shown in Figure 3.16. At 650°C transformation, the grain size was difficult to quantify in Alloy 2 by optical metallography because of the low definition of the interlath boundaries. A value of 21 μm was measured using the high angle boundary intercepts visible on low magnification (x160) micrographs. Using optical micrographs at a magnification of x750 the laths were distinguished more readily and a mean linear intercept of 11 μm was measured. By TEM, projected lath (or plate) widths of 1 to 2 μm were observed. In Alloy 1 the carbides delineated both high and low angle boundaries and a mean linear intercept value of 14 μm was measured using optical micrographs.

3.6 Precipitate dispersions formed by isothermal transformation

Optical microscopy revealed occasional particles up to 5 μm in size in the ferrite. Angular, golden-orange particles were identified as titanium nitrides and grey particles as either oxides, sulphides or mixed compounds such as carbosulphides. No fine dispersions of precipitates could be detected in the ferrite by optical metallography whether the specimen was in the as-polished or in the etched condition.

By employing transmission electron microscopy, fine particulate precipitation was detected in all the specimens of Alloys 1 and 2 transformed at 650°C or above, the scale of the dispersion becoming coarser at the higher transformation temperatures. To ensure that the optimum diffraction conditions were achieved for observing the precipitates, the full range of microscope tilt facilities was employed. All the precipitates exhibited the Baker-Nutting orientation relationship with the

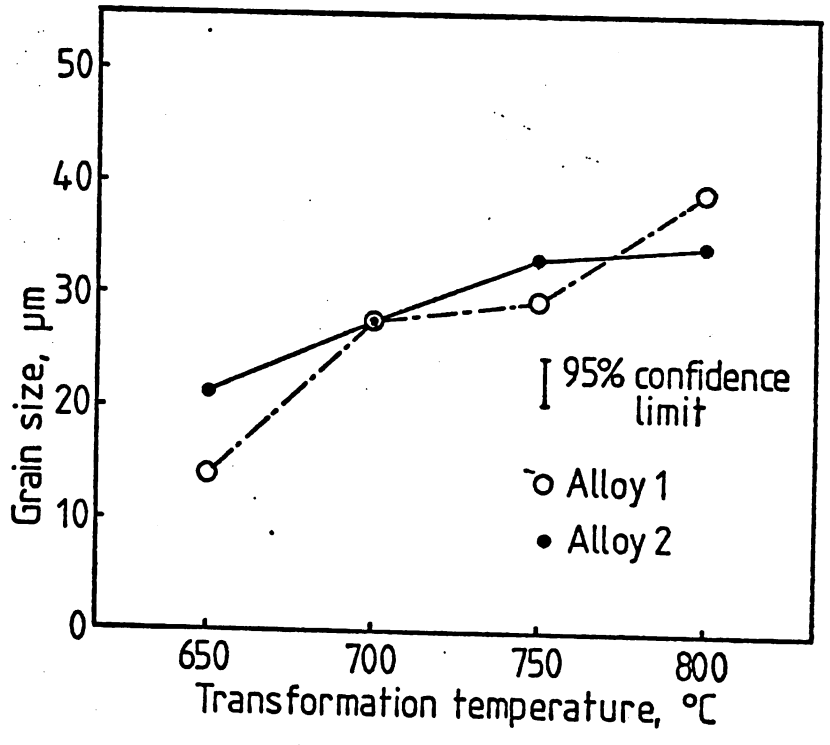

Figure 3.16: Mean linear intercept ferrite grain size after 1000 s isothermal transformation; Alloys 1 and 2

Error bars are 95% confidence limits assuming a uniform grain size, by the method described by Pickering (1976).

ferrite matrix, as described in Section 2.6. From the lattice spacing they were identified as either titanium carbides, nitrides or carbo-nitrides, and in view of the steel compositions and heat treatments the fine precipitates were assumed to be carbides. The verification of this assumption by atom probe microanalysis is reported in Chapter 6.

Parallel sheets of interphase precipitates were frequently observed but were by no means the only precipitate morphology found. The variations between particle dispersions found in nearby areas of Alloy 2 fully transformed after 1000 s at 800°C are illustrated in Figures 3.17 and 3.18. The interphase precipitation shown in Figure 3.17 comprised particles of 5 to 20 nm size and of the same Baker-Nutting variant, arranged in planar sheets. In contrast, the particles shown in Figure 3.18 were primarily in short strings, suggesting that nucleation had occurred on dislocations. Other particles appeared to be randomly distributed in the matrix. Comparison of the bright- and dark-field micrographs of Figure 3.18 reveals that the precipitates were not all in the same orientation; for example, the precipitate reflection employed does not illuminate the particles on the long dislocation in the centre.

Colonies of interphase precipitation exhibiting different variants of the Baker-Nutting relationship could be found within the same ferrite grain: in Figure 3.19, the precipitate-centred dark-field micrographs demonstrate that colonies A and B have different orientations with the matrix. The trace of a prior austenite grain boundary between the two colonies suggests that they were formed at the interfaces of a grain boundary ferrite allotriomorph growing into two adjacent austenite grains.

In general, the sheets of interphase precipitates were planar but occasionally curved sheets were observed (Figure 3.20) at the higher transformation temperatures. The perpendicular intersheet spacings

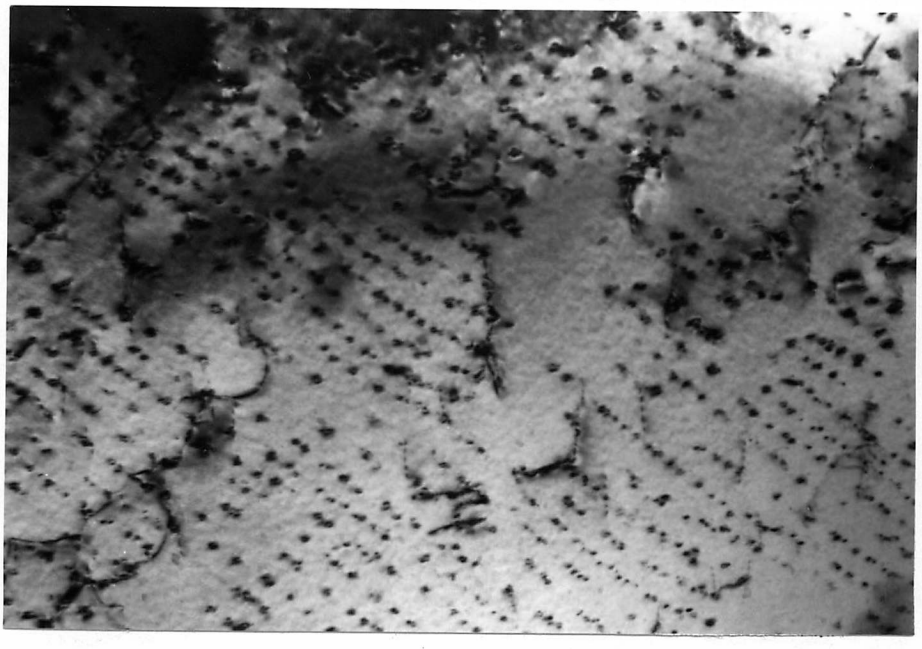

a) Bright field

0.5 μm

b) Precipitate centred dark field

Figure 3.17: 1000 s 800°C; Alloy 2

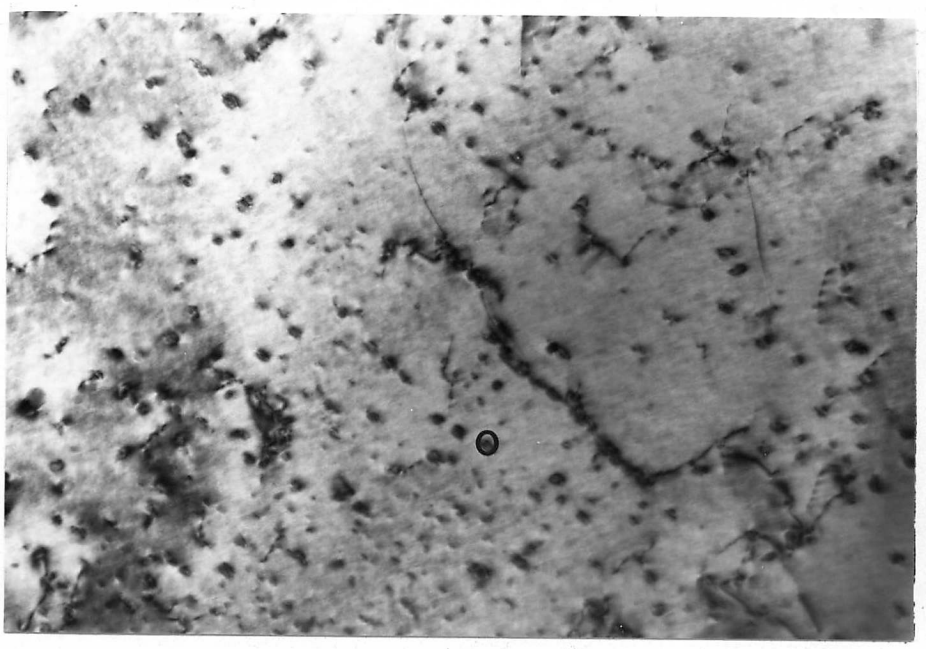

a) Bright field

0.5 μm

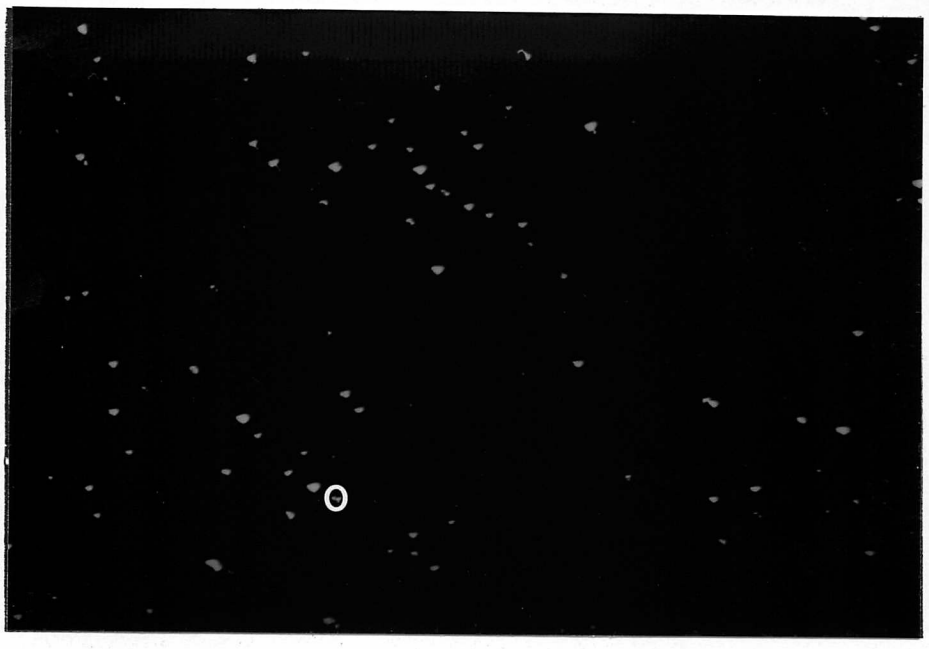

b) Precipitate centred dark field

Figure 3.18: 1000 s 800°C; Alloy 2

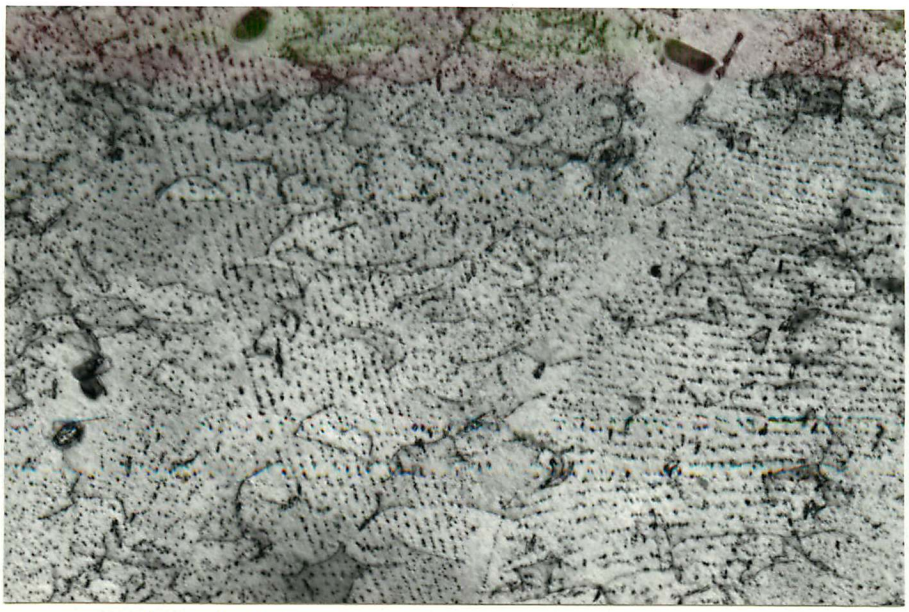

a) Bright field

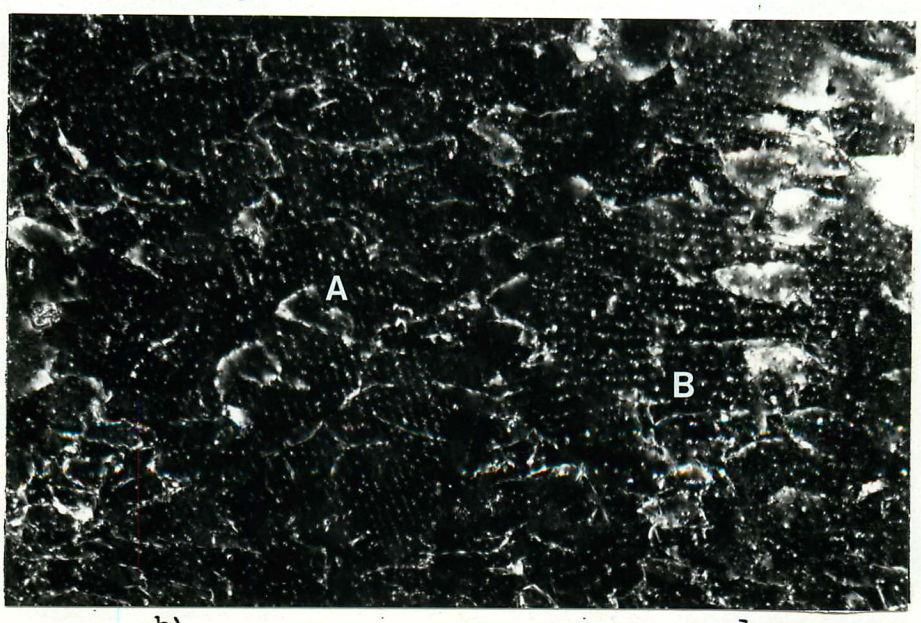

b)

1 μm

c)

b) & c) Dark field using different precipitate diffraction spots

Figure 3.19: Two colonies of titanium carbide precipitates (A and B) in the same ferrite grain 1000 s 800^{O}C; Alloy 2

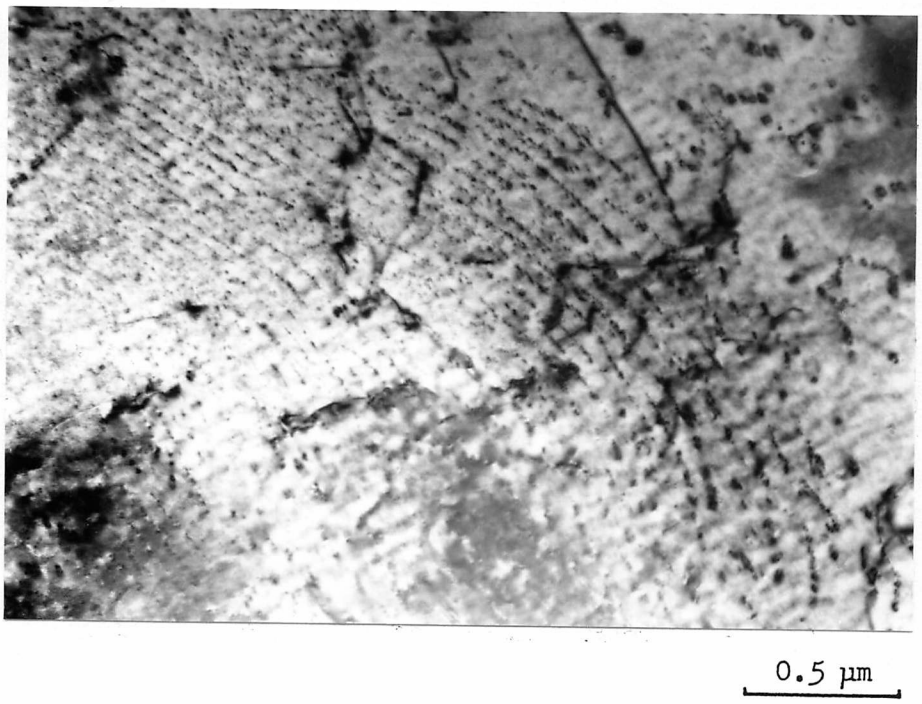

Figure 3.20: Curved sheets of interphase precipitates 1000 s 800°C; Alloy 2

presented for Alloy 2 in Figure 3.21 varied from an average of approximately 40 nm at 650°C to 65 nm at 800°C and 150 nm at 850°C with the most rapid increase in spacing occurring above 750°C. For each transformation temperature the measured intersheet spacings differed between colonies, even after taking into consideration the errors arising from the sheet inclination relative to the foil normal. This range of values is indicated by the standard deviation error bars of Figure 3.21 and is directly evident in the micrograph of Figure 3.19 (and in Figure 5.5).

Precipitates in the platelike grains formed at 650°C were difficult to examine because of the strain contrast from the dislocations, discussed in Chapter 5. An annealing treatment lowered the dislocation density somewhat. Figure 3.22 shows finely spaced interphase precipitates in planar sheets parallel to the axis of an elongated grain. Here, the sheet spacing was less than 40 nm. However, the interphase mode of precipitation was, compared with dislocation precipitation, less common at this lower transformation temperature than at higher temperatures. Precipitation on dislocations was observed at 800° (Figure 3.18a&b) and became more prevalent at lower temperatures. If there was insufficient time for interphase precipitation to form at the advancing interface, the ferrite would become supersaturated in titanium and carbon. Because of the low solubility of titanium carbide, matrix or dislocation precipitation would be likely to occur rapidly whilst the structure was held at the transformation temperature.

The apparently random precipitate dispersions observed in some areas at all the transformation temperatures may arise from sectioning effects in regions of aligned interphase precipitation, from precipitation on dislocations which subsequently moved away or are out of contrast, or could be a real effect from homogeneous nucleation in the matrix.

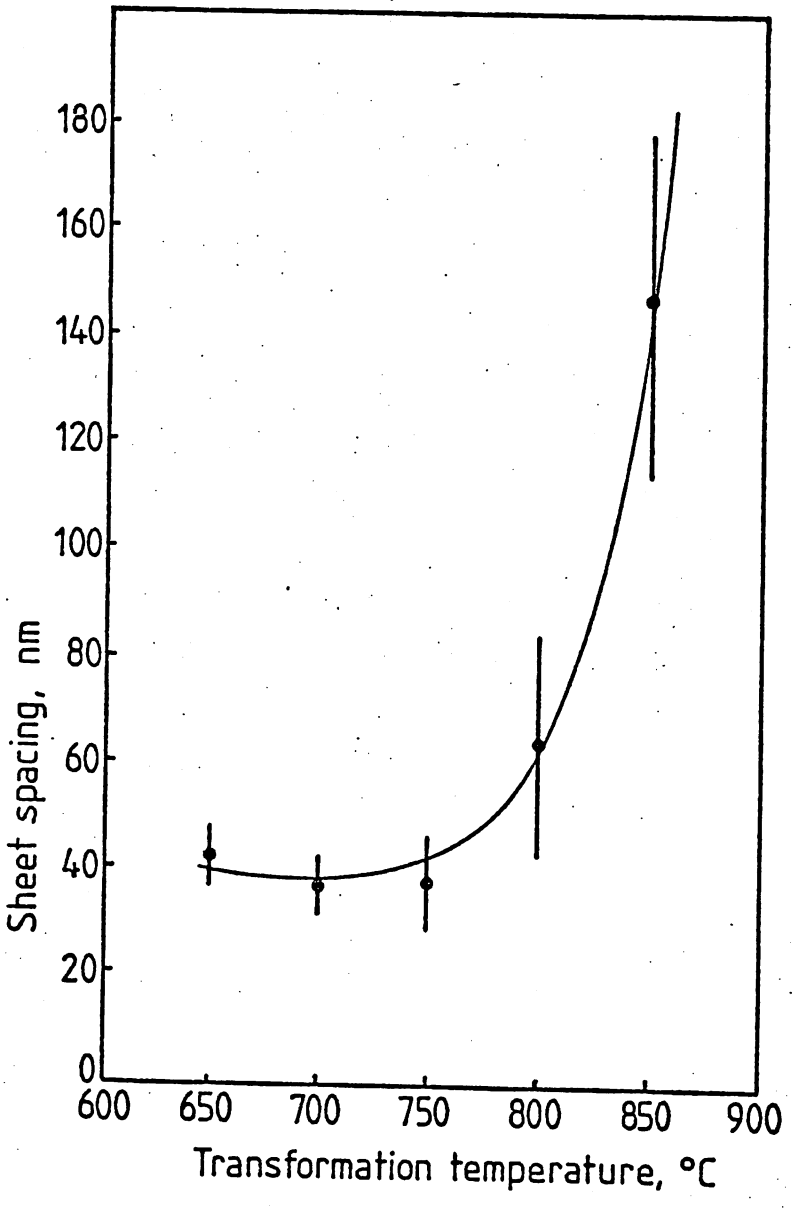

Figure 3.21: Perpendicular sheet spacings

Figure 3.22: Interphase precipitation revealed after isothermal annealing (1000 + 60 000) s 650°C; Alloy 2

The complete absence of fibrous titanium carbide precipitates in the steels reported here can be attributed to a combination of the rapid reaction kinetics and the low precipitate volume fractions. The calculated volume fractions of titanium carbide available, discussed in the next chapter, are 0.11% in Alloy 1 and 0.4% in Alloy 2.

3.7 Precipitate-free regions

Precipitate-free regions may be caused by

i) solute depletion,

ii) solute supersaturation, or

iii) solute partitioning.

Solute depletion would occur in the vicinity of coarse titanium carbide or nitride particles (e.g. Figure 3.19) which had probably precipitated in the austenite. Solute supersaturation would be unlikely to occur except on quenching due to the very low solubility of the titanium compounds in ferrite; however a region could appear to be precipitate-free if a dispersion was so fine as to be undetectable, as might be found in some of the lower temperature microstructures.

Solute partitioning into the austenite during transformation would result in precipitate-free proeutectoid ferrite. Because it is diffusion controlled, such a mechanism would be more likely at high transformation temperatures, as found by Balliger & Honeycombe (1980) in V-C and V-C-N alloy steels. The authors presented discontinuous TTT curves established by high speed dilatometry as supporting evidence for vanadium partitioning and concluded that it does not occur in a V-N steel because of the lower precipitate solubility.

No discontinuities were detected in the TTT curves of the titanium

steels in the present investigation and in view of the faster reaction rate (10 s vs 100 s to 5% transformation) at 800°C and the greater insolubility of titanium carbide than vanadium carbide in ferrite, it is taken that at all temperatures the austenite decomposition reaction to ferrite and titanium carbides occurs almost from the start. In Figure 3.19 the 200 nm wide strip of precipitate-free ferrite between the two carbide colonies may be proeutectoid ferrite. A microanalytical technique would have to be used to determine the composition of such apparently precipitate-free regions to provide more evidence.

3.8 High temperature transformation mechanisms

At high temperatures the ferrite growth occurred by two mechanisms:

i) ledge migration across highly coherent, planar austenite/ferrite interfaces; and

ii) the movement of incoherent, curved interfaces.

The latter growth mode was rarely observed but was found more frequently as the transformation temperature increased. Evidence for the predominance of the ledge mechanism was provided by the high proportion of planar interfaces observed in the partially transformed specimens (e.g. Figure 3.7), and the parallel, planar sheets of interphase precipitation, (e.g. Figures 3.17 to 3.19).

The crystallographic aspects of such diffusional phase transformations have been discussed recently by Howell & Honeycombe (1982). Interfacial energies were shown to provide the major barrier to nucleation and thus interphase boundaries would be expected to adopt configurations of maximum coherence and therefore lowest energy. The authors suggest that with 24 variants of the Kurdjumov-Sachs relationship possible between ferrite and the parent austenite, and the possibility of several degrees of misorientation arising from the atomic mismatch, the majority of inter-

faces would be capable of exhibiting a large degree of coherency. Furthermore, they suggest that ferrite nucleating on an austenite grain boundary adopts the variant which allows an orientation relationship with both austenite grains.

In the microstructures described here, the existence of the Nishiyama-Wassermann relationship (Figure 3.6) in addition to the Kurdjumov-Sachs relationship increases the likelihood of interface coherence.

Although the identification of frequent orientation relationships and planar interfaces implies a high proportion of coherent boundaries, it is appreciated that in isolation this evidence is not conclusive. For example, it is thought possible for a boundary to adopt a planar morphology in the absence of any ferrite/austenite orientation relationship because the surface energy may be minimised; conversely, even if an orientation relationship exists, under certain circumstances the interface can be curved and incoherent. To deduce the transformation mechanisms, other evidence is required such as that provided by precipitate morphologies. Figure 3.23 illustrates the interphase precipitation mechanisms thought to be operating. The coherent or partially coherent interphase boundaries advance by the passage of ledges, shown in Figure 3.23a. The high energy ledges have little or no coherence and therefore greater mobility than the facets. Precipitation occurs on the coherent planar regions of the interface and consequently the ledge mobility is not impaired. Solute diffusion to the precipitates occurs along the phase boundary. The intersheet spacing corresponds to the ledge height and therefore increases at higher temperatures when the driving force for the reaction and hence the rate of ledge nucleation is lower.

On grounds of interfacial energy, incoherent austenite/ferrite inter-

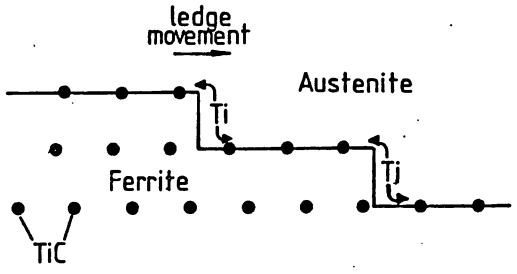

a) Ledge type growth mode at a coherent interface

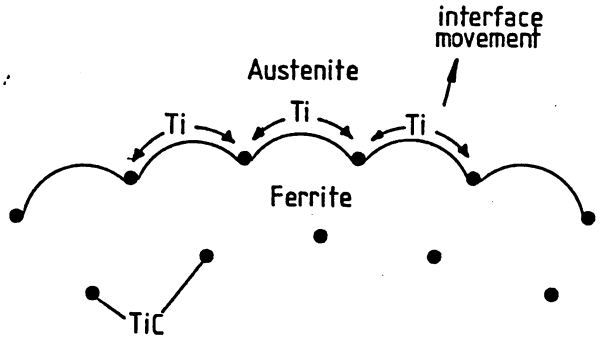

b) Bowing growth mode at an incoherent interface

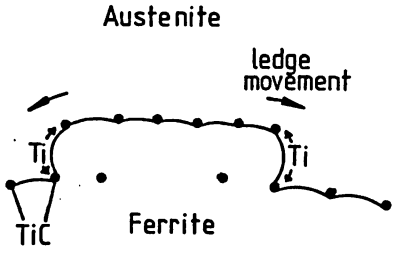

c) Quasi-ledge growth mode at an incoherent interface; widely spaced particles allow bowing, thus providing the sources of ledges

Figure 3.23: Diffusional mechanisms for the austenite decomposition reaction

faces are only expected if the relative orientation of the two phases prevents coherence or partial coherence; Howell & Honeycombe (1982) suggest that this happens rarely, and their proposition is supported experimentally in the present work by the infrequent occurrence of curved boundary morphologies.

Transformation at incoherent interfaces occurs by diffusional atomic rearrangement along the entire boundary. Ricks & Howell (1983) describe two growth mechanisms which may produce arrays of discrete particles at such interfaces. Interphase precipitates nucleated at the incoherent interface may compel the boundary to advance by bowing between them, as illustrated in Figure 3.23b. The interface simultaneously mops up the solute atoms and provides a diffusion path to the growing particles. When the interfacial tension exceeds the pinning force, the interface escapes and the process is repeated. This bowing mechanism can thus account for randomly distributed or curved sheets of interphase precipitates. However, below a critical particle spacing, bowing of the interface will become energetically unfavourable. A "quasi-ledge" mechanism, shown in Figure 3.23c, is then postulated to operate: an interface bulge created between widely spaced precipitates becomes pinned by fresh precipitation and is forced to grow sideways. Again the result can be <u>non-planar</u> sheets of particles. Ricks & Howell have calculated that for the particle spacings found in their isothermally transformed vanadium steels, interface bowing would be rarely possible and that the quasi-ledge mechanism would dominate. The same might be expected for the incoherent austenite/ferrite interfaces in titanium steels.

3.9 Low temperature transformation mechanisms

As the transformation temperature is lowered and approaches the nose of the TTT curve, the increased transformation rate and the decreased solute diffusivity result in the refinement in the size and spacing of the interphase precipitates (Figures 3.17 to 3.22). The absence of curved precipitate sheets at the lower temperatures indicates that the critical particle spacing below which incoherent interface bowing is impossible may have been reached. For vanadium carbide precipitates this critical spacing has been estimated by Howell (1980) to be approximately 20 nm. It is expected to be the same order of magnitude for titanium carbides and therefore in the same range as the dispersions investigated.

The less frequent occurrence of any morphology of interphase precipitation in the 650° microstructures may be a result of a more fundamental change in the transformation mechanism. It is postulated that the highly dislocated, parallel plates (or laths) in this structure, not observed at higher transformation temperatures, were formed by a shear mechanism; whereas the individual, elongated grains were formed by a diffusional ledge mechanism (Aaronsson, 1962). Interphase precipitation would therefore be possible only in the elongated or equiaxed ferrite grains. In the plate-like ferrite, titanium carbide would precipitate finely from supersaturated solid solution.

The colonies of plate-like ferrite in the 650° microstructures were similar to the almost entirely bainitic structures developed in both alloys transformed at 600° and below. However, martensite formation on quenching appeared to be a separate reaction. The martensite start temperature was approximately 450°C and the lath microstructure was on a finer scale and more heavily dislocated than the bainitic ferrite. The

morphologies of both parallel and interwoven martensite laths (Figure 3.5) were similar to the structures observed by Law, Howell & Edmonds (1979) in low alloy vanadium steels.

3.10 Microstructures after complete austenite decomposition

Equiaxed ferrite growth from grain boundary allotriomorphs during transformations at temperatures of 700° and above resulted in equiaxed but irregular grain morphologies in the fully transformed structures (Figures 3.12 and 3.15). It is probable that subsequent polygonisation did not occur because ferrite grain boundary movement would have been severely restricted by the fine dispersions of titanium carbide precipitates.

On a finer scale, variations in ferrite and precipitate morphologies observed from region to region in individual specimens, whatever the transformation temperature will have resulted from the difference in transformation rates at the beginning and end of the transformation and possibly from the temperature gradient which will inevitably be present in the 3 mm diameter sections for the first few seconds in the isothermal medium. The greater inhomogeneity of the substructure and the ferrite grain morphology produced by transformation at 650°C compared with higher temperatures would arise from the overriding effects of both diffusional and shear transformation mechanisms operating in the same specimen.

3.11 Summary

1. The kinetics of austenite decomposition for two titanium steels have been studied using a combination of dilatometry and the metallography of partially transformed specimens. In each alloy, transformation was

very rapid, reaching completion within 1000 s at every temperature of 800°C and below. The reaction products were ferrite, titanium carbide and some cementite.

2. Evidence for the transformation mechanisms was provided by the ferrite morphologies of specimens partially transformed isothermally in the range 850° to 650°C and from the characteristics of the fine titanium carbide dispersions. Ferrite growth occurred predominantly by diffusional ledge mechanisms producing equiaxed and elongated grain structures. In addition, evidence for the diffusional bowing mechanism was found at high transformation temperature and for shearing mechanisms at transformation of 650° and below.

3. Several types of titanium carbide precipitation were identified and their origins discussed: interphase precipitation of straight or curved parallel sheets of particles; dislocation-nucleated precipitation; and apparently random matrix precipitation. Precipitate-free zones were also investigated.

4. After completion of the isothermal austenite decomposition the ferrite grain structures and carbide dispersions were both found to be inhomogeneous, particularly after treatment at 650°C.

CHAPTER FOUR

TENSILE BEHAVIOUR

4.1 Introduction

To complement the studies of the microstructural development, the changes in tensile properties resulting from altering the austenite to ferrite transformation temperature were examined. Alloy compositions containing excesses of titanium relative to titanium carbide stoichiometry were included in these investigations. These were in addition to the two alloys described in the previous chapter which both contained excess carbon.

The role of interstitial atoms in discontinuous yielding behaviour was explored using additional tensile testing regimes. The effects of different cooling rates from the transformation temperature, and the effects of ageing before and after straining are compared. The yielding behaviour after prolonged isothermal annealing treatments is reported and interpreted in terms of the homogeneity and stability of the microstructures. Variance in microhardness measurements is also used to examine microstructural homogeneity.

4.2 Experimental method

The tensile specimens were machined from 5 mm diameter rod before receiving the final isothermal heat treatment. Thus the material was machined in the standardised, martensitic state and the introduction of any machining stresses after the final heat treatment was avoided; Leslie

& Sober (1967) have shown that under certain conditions deformation introduced by machining can eliminate discontinuous yielding in titanium steels. Furthermore the reduction in the specimen mass produced by the machining allowed higher heat transfer rates to be achieved subsequently and hence true isothermal conditions were approached more closely.

The specimens had a 30 mm long, cylindrical gauge length of 10:1 aspect ratio and smoothly tapered shoulders, as shown in Figure 4.1, to minimise stress concentrations. Threaded ends were adopted rather than Hounsfield-type shoulders to reduce the total specimen bulk and to provide a positive location in the load train.

The gauge diameter was machined 0.2 mm oversize to permit the removal of the outer 100 μm layer by electropolishing after the final heat treatment. In this manner, unrepresentative surface microstructures characteristic of surface ferrite nucleation and resulting from any slight decarburisation were removed producing a stress-free surface with a mirror finish.

Investigations by Batte (1970) and Freeman (1971a) have shown that, for the short times involved, there would be no problems from tin attack during transformation. It is not envisaged either that hydrogen ingress would have occurred during electropolishing because the specimen was anodic. Full details of the polishing conditions and the precautions taken during the heat treatment of tensile specimens are given in Appendix A.

For tensile testing a screw driven Mand machine was selected because, of the equipment available, it was found to be the most sensitive to yield points due to its optimum combination of machine hardness and speed of response. Axial alignment was improved by the insertion of spherical bearings in the load train above and below the specimen. In addition to

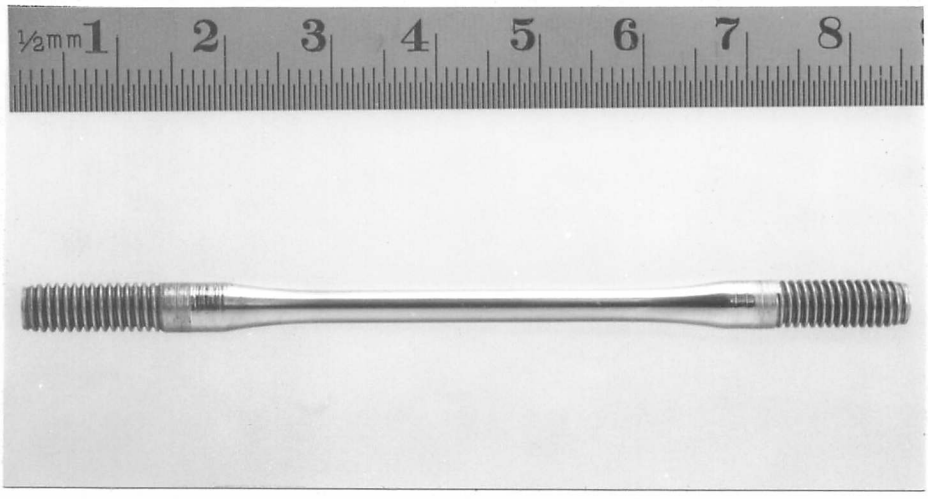

Figure 4.1: Electropolished tensile specimen

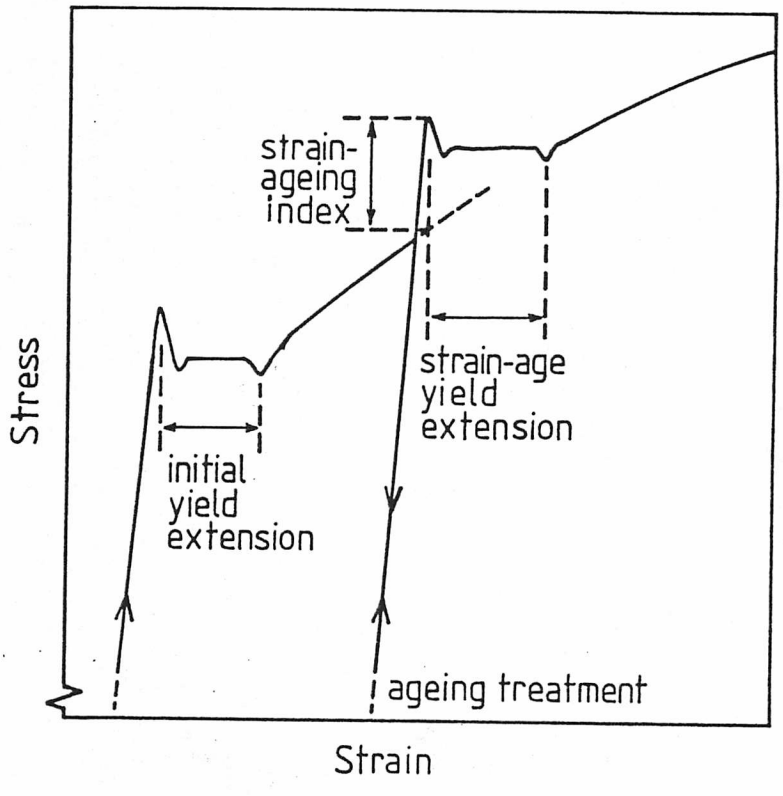

Figure 4.2: Parameters for quantifying yield behaviour

the inbuilt load versus crosshead movement chart recording, simultaneous magnified plots of load versus specimen strain and load versus time were recorded, as described in Appendix A. The graphs provided a stress sensitivity of 0.7 and 1.4 MPa per mm chart for the 5 kN and 10 kN machine load ranges respectively, the precise values depending on the exact specimen diameters. The strain sensitivity was 0.04 % strain per mm chart.

All tensile testing was carried out at a strain rate of $1.4 \times 10^{-4}\ s^{-1}$. For the strain-ageing experiments, samples were pre-strained to approximately 1.5 % elongation and aged in-situ under a constant aligning load of 0.25 kN for 30 min at $100 \pm 2^{\circ}C$ using resistance heating tape. Straining was resumed after cooling for 30 min to room temperature. The prestrain was selected to be greater than any observed initial yield elongations yet less than that associated with the ultimate tensile strength. Thus any strain-age yield elongation was completed before the onset of necking.

The ageing treatment given was such that the work hardening characteristics resulting were similar to those of an uninterrupted test. Following the method of Titchener & Davies (1965) the degree of strain-ageing was quantified by the maximum stress difference ($\Delta\sigma$, the strain-ageing index, depicted in Figure 4.2) measured between the extrapolated initial stress-strain curve and the portion obtained following the ageing treatment. Because it is not possible to define an underlying continuous yielding curve for initial yield points, a quantifying parameter similar to the strain-ageing index cannot be applied. Instead, the yield extension was used as a measure of the yield point magnitude, defined as beginning at the point of deviation from linearity and ending at the minimum in the dip, also shown in Figure 4.2, or, in less well defined cases, when the smooth work hardening curve began.

The yield extensions of the strain-age yield points were also measured. Even for specimens exhibiting discontinuous yielding, the 0.2% proof stress was used as a measure of the yield strength because of the often poorly defined nature of the lower yield stress.

Tensile testing was carried out using the following alloy compositions:

Alloy 1: 0.07 C - 0.07 Ti

Alloy 2: 0.07 C - 0.23 Ti

Alloy 3: 0.10 C - 0.52 Ti

Alloy 4: <0.02 C - 0.38 Ti

Alloys 1 and 2 contained an excess of carbon over the titanium carbide stoichiometric ratio. The other two alloys contained carbon levels below this limit, Alloy 3 by means of an increased titanium level and Alloy 4 by means of a decreased carbon level.

4.3 Strength characteristics

The 0.2 % proof stress, ultimate tensile strength (UTS) and uniform elongation values of the four alloys are presented in Figures 4.3 and 4.4.

In the initial investigations, two specimens were tested for each isothermal heat treatment in the range 800°C to 650°C, one given the standard strain-ageing treatment and the other strained uninterrupted to fracture. Alloys 1 and 2 were tested more extensively in subsequent investigations and these additional results are included in the mean values plotted. Specimens of Alloy 2 transformed to bainite and martensite were tested for comparison. These results are shown in the same figures.

For all four alloys the proof stress and UTS increased as the transformation temperature decreased. The uniform elongation tended to decrease, especially in Alloy 4. For each heat treatment Alloy 2 (0.07C-0.23Ti) was the strongest, exhibiting a proof stress of 302 MPa in

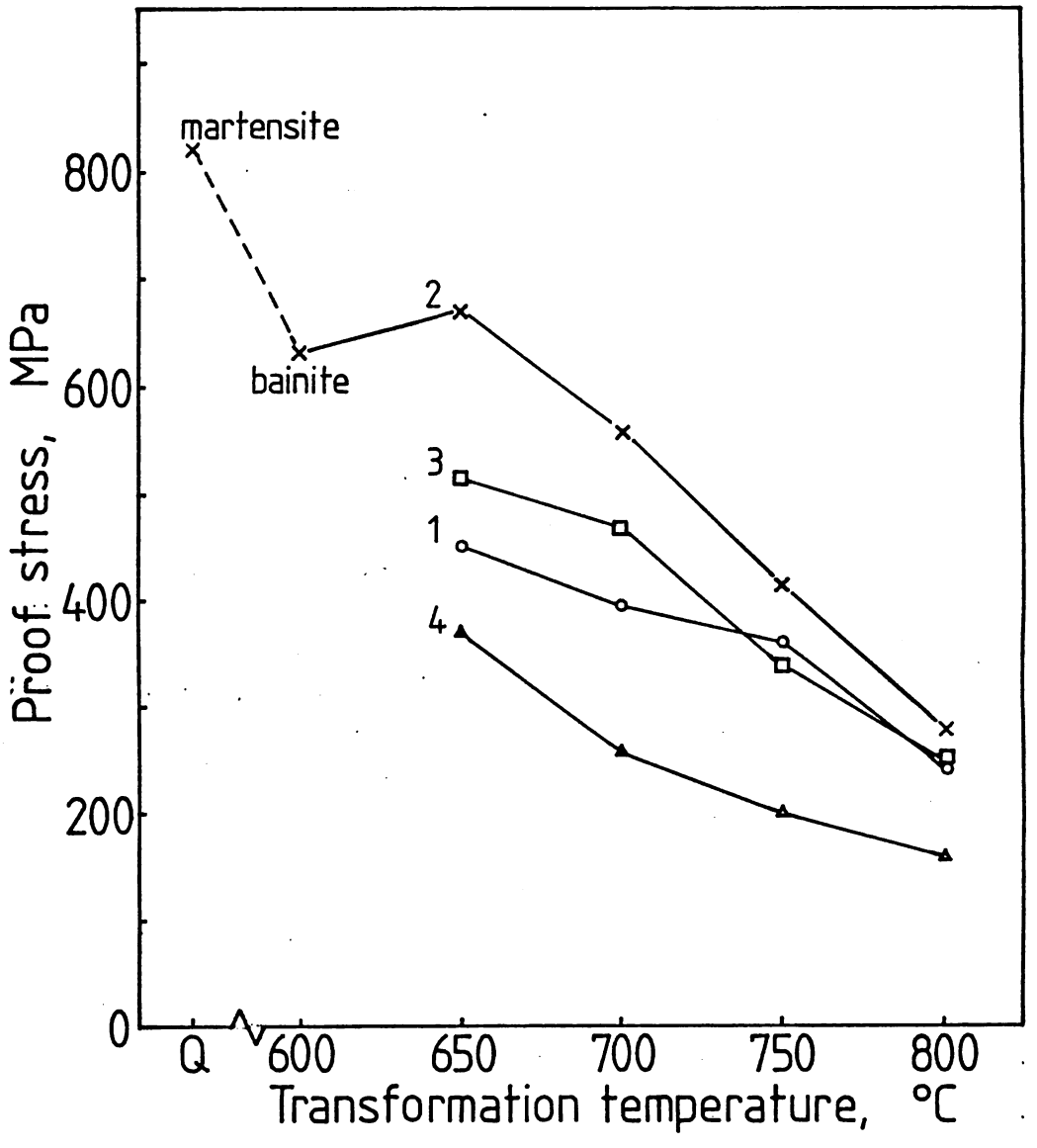

Figure 4.3: 0.2% proof stress variation with isothermal transformation temperature for Alloys 1 to 4

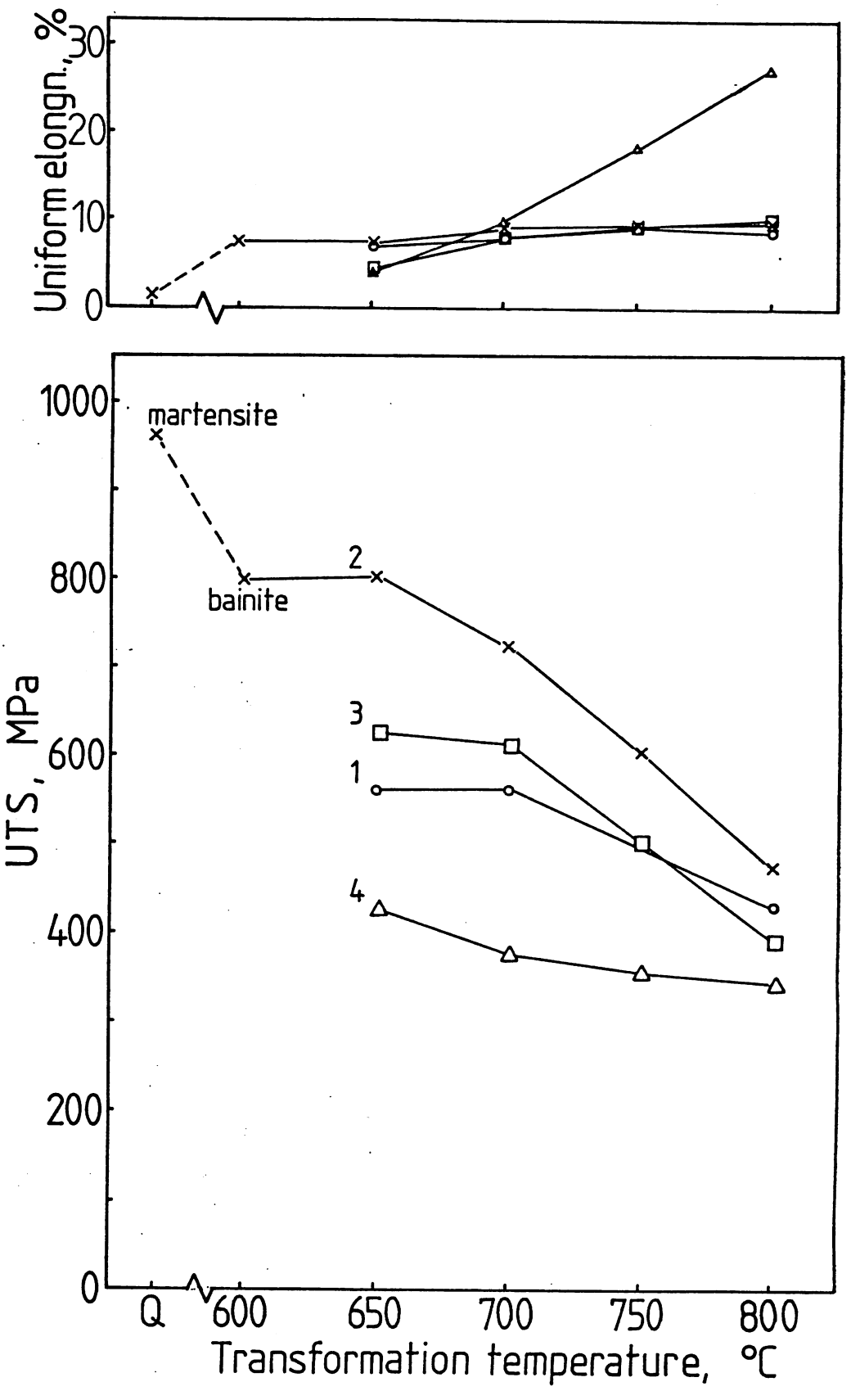

Figure 4.4: Ultimate tensile stress and maximum uniform elongation variations with isothermal transformation temperature for Alloys 1 to 4

the 800° structure and 672 MPa in the 650° structure, and Alloy 4 (<0.02C-0.38Ti) was the weakest with proof stresses of 162 MPa and 370 MPa respectively. Alloy 1 (0.07C-0.07Ti) and Alloy 3 (0.10C-0.52Ti) had similar, intermediate strengths.

The principal microstructural contributions to the yield strength of steels are:

i) inherent matrix strength, σ_o ;

ii) solid solution strengthening, $\Delta\sigma_s = \sum_i k_i c_i$;

iii) precipitation hardening, $\Delta\sigma_p$;

iv) grain size, $\Delta\sigma_g = k_y d^{-1/2}$; and

v) dislocation strengthening, $\Delta\sigma_d = k_d \rho^{1/2}$.

where c_i = concentration of solute element i; d = grain size; ρ = dislocation density; and k_i, k_y and k_d are the corresponding constants.

These strength components are generally assumed to be independent and additive (e.g. Pickering & Gladman 1963):

$$\sigma_y = \sigma_o + \Delta\sigma_s + \Delta\sigma_p + k_y d^{-1/2} + k_d \rho^{1/2} \qquad \ldots 4.1$$

The solid solution strengthening conferred by substitutional titanium is approximately 40 MPa per wt% and 34 MPa per wt% for manganese (derived from the data of Leslie, 1972). In Table 4.5 the excess titanium or carbon contents over the titanium carbide stoichiometric level for the four alloys examined are given. Assuming that all the titanium nitride and titanium carbide are out of solution, it is thus calculated that dissolved manganese and titanium can each contribute a maximum of only 15 MPa to the strength.

Considerable strengthening from the excess carbon in Alloys 1 and 2 would be possible on the basis of the 5000 MPa per wt% of interstitial

Alloy	C	Ti	Mn	N	Ti in TiN	Ti in TiC	vol% TiC	excess C	excess Ti	Ti/C *
1	0.070	0.067	0.34	0.003	0.010	0.057	0.11	0.056	0	0.81
2	0.073	0.227	0.40	0.007	0 +	0.227	0.45	0.016	0	3.11
3	0.10	0.52	0.36	<0.005	<0.017	0.40	0.8	0	0.10 to 0.12	5.03 to 5.20
4	<0.02	0.38	0.27	0.006	0.021	<0.08	<0.16	0	0.28 to 0.36	>17.95

+ Nitrogen removed by aluminium
* Titanium to carbon ratio after allowing for titanium nitride formation

Table 4.5: Calculated distribution of alloying elements in wt%

carbon or nitrogen quoted, for example, by Baker (1978) but only if the carbon were retained in solution. The 0.02 %C excess in Alloy 2 would confer 100 MPa. This strength increment from the interstitials is thought to arise from a combination of dislocation pinning by the segregated atoms, and interactions between the strain fields of dislocation and matrix interstitial atoms. In practice some of the carbon, particularly in Alloy 1, precipitated as cementite in pearlite (Figure 3.13) and more would precipitate very finely as intermediate iron carbides during cooling.

The strength contributions from interphase precipitate dispersions were found by Batte (1970) to be complex functions of the precipitate volume fraction and the scale and nature of the dispersion. The maximum volume fractions of titanium carbide (Table 4.5) were calculated to be 0.11 %, 0.45 % and 0.8 % for Alloys 1, 2 and 3 respectively but the quantity precipitated finely into the ferrite depends on the solubility at the austenitising temperature: at 1200°C the maximum solubility is 0.4 vol% (corresponding to 0.2 wt%Ti, Figure 2.4). Consequently after transformation, Alloys 2 and 3 each contained approximately 0.4 vol% of fine carbides, independent of the temperature of transformation. The remainder was present as coarse carbides, precipitated from the austenite, which would make an insignificant strength contribution.

The decreasing scale of the fine carbide dispersions as the transformation temperature was lowered would result in a greater precipitation strengthening contribution, as described by Equation 2.2 (Batte 1970). However, in view of the inhomogeneity of the precipitate dispersions observed in the titanium steels quantification of the precipitation strengthening component was not considered justified.

The Hall-Petch grain size expression (Equation 2.5), using the

generally accepted value of 0.7 $MNm^{-3/2}$ (Hall, 1970) for the constant k_y, predicts strength contributions of 110 and 140 MPa for ferrite grain sizes of 40 and 25 μm respectively, the range measured in Alloys 1 to 4 (Figure 3.16). However, the non-polygonal nature of the microstructures, especially at the lower transformation temperatures, may necessitate modification of the relationship; when there are high and low angle grain boundaries and elongated grains, the relevant effective grain size to be used in the expression cannot easily be defined.

The increases in dislocation density, ρ, noted with decreasing transformation temperature have a strengthening effect proportional to $\rho^{1/2}$. Using the data of Keh & Weissmann (1963) for k_d, the dislocation contribution to strengthening is calculated to range from 15.6 MPa to 1560 MPa over the dislocation density range of 10^{12} to 10^{16} m^{-2} (10^{8} to 10^{12} cm^{-2}) which are the limits commonly found in steels. In this specific study the mean value of 4×10^{14} m^{-2} for the 650° structure of Alloy 2 would give a strength contribution of ~300 MPa. These dislocation density measurements are reported in detail in Chapter 5.

Thus the increases in proof stress produced in Alloys 1, 2 and 3 on lowering the isothermal transformation temperature resulted from the combination of finer precipitate dispersions, finer grain size and increased dislocation strengthening.

Alloy 4 (0.38Ti) was the weakest of the four alloys because it contained a negligible precipitate volume fraction. The marked increase in proof stress, from 160 MPa at 900° to 370 MPa at 650° transformation temperature was therefore due primarily to the accompanying increases in ferrite grain size and dislocation density rather than the precipitate content.

Comparison of the three precipitation strengthened alloys shows that

Alloys 2 and 3, both containing 0.4 vol% of fine carbides, exhibited proof stress and UTS increases of 250 to 300 MPa on lowering the transformation temperature from 800° to 700°. Over the same temperature range Alloy 1, with only 0.11 vol% fine carbide, exhibited a lower strength increase. The differences in strength between Alloys 2 and 3, and the similarities between Alloys 1 and 3 are therefore explained by the combined effects of precipitation strengthening and solution strengthening from excess carbon.

As expected, the martensite produced by quenching Alloy 2 was considerably stronger (proof stress $\simeq$ 813 MPa, compared with $\sim$680 MPa after 650° transformation) and less ductile than the isothermally transformed specimens due to its much finer ferrite grain structure, high dislocation density and high degree of interstitial solution strengthening. However, the bainitic structure produced by transformation at 600° was less strong (proof stress $\sim$ 630 MPa) than the 650° structure. Cementite, present as relatively coarse precipitates between the ferrite plates, would form in preference to titanium carbide in the bainite. This coarser carbide dispersion was assumed to be the reason for the lower strength despite the finer grain structure and higher dislocation density than the 650° specimen.

4.4 Initial yielding behaviour

Examples of the initial portions of the stress-strain curves are presented in Figures 4.6a-d. Initial yielding was continuous, irrespective of transformation temperature in Alloy 3 (0.10C-0.52Ti) and Alloy 4 (<0.02C-0.38Ti). For Alloy 1 (0.07C-0.07Ti) and Alloy 2 (0.07C-0.23Ti) all the 800° treated specimens exhibited discontinuous yielding; for lower transformation temperatures initial yielding was continuous, although sometimes the 750° specimens and occasionally the 700° specimens showed a sharp gradient change in the stress-strain curve at yield (Figure

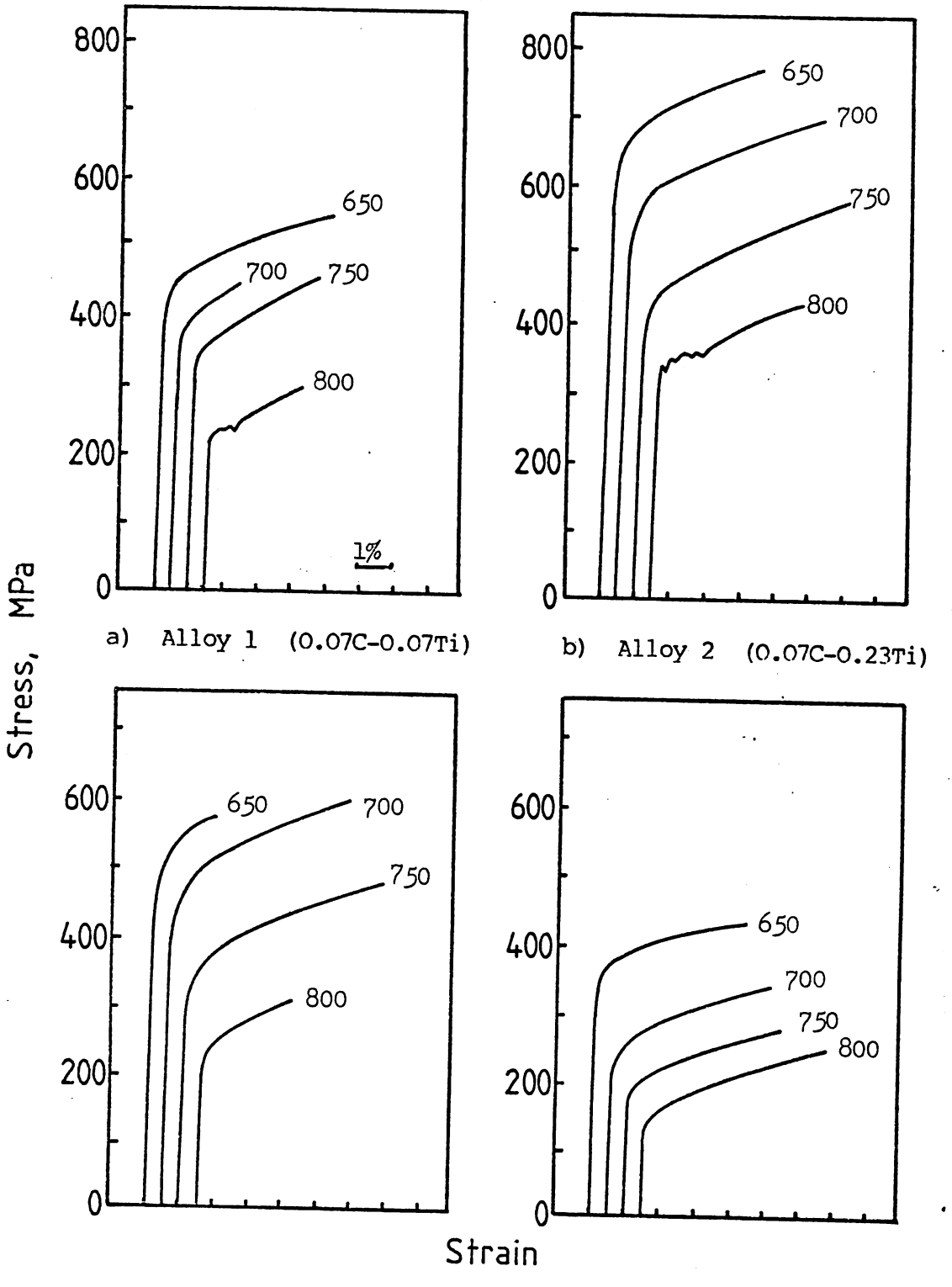

Figure 4.6: Initial yielding behaviour after 1000 s isothermal transformation at the indicated temperatures

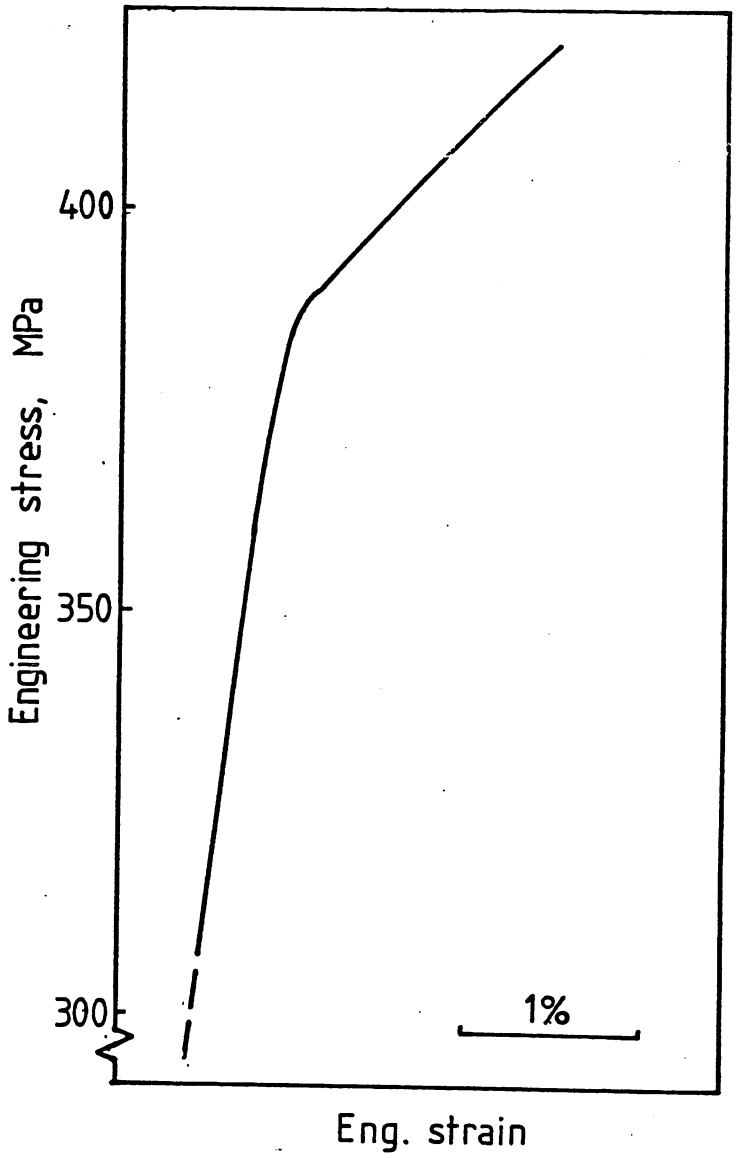

Figure 4.7: Sharp gradient change at initial yield 1000 s 700°C; Alloy 1

4.7). Specimens transformed at 650°C always exhibited smooth, continuous yielding.

The absence of any discontinuous initial yielding in Alloys 3 and 4 appears to correlate with their excesses of titanium relative to the stoichiometric carbide levels. Table 4.5 gives the titanium to carbon ratios by weight for the four alloys. Alloys 2 and 3, which straddle the transition in yielding behaviour, have ratios of 3.1:1 and 5.1:1 respectively. This range spans the generally accepted 4:1 (1:1 atomic) stoichiometric ratio. The atom probe analysis of the titanium carbides in the present investigation, reported in Chapter 6, confirmed this latter value. The yield behaviour of these titanium steels, in relation to their composition, contrasts with that of some vanadium-containing steels given similar isothermal heat treatments by Batte (1970), which exhibited yield points even when there was a large excess of vanadium over vanadium carbide stoichiometry. The probable explanation for this difference in behaviour lies in the higher concentrations of dissolved interstitial species equilibrated with vanadium carbides or nitrides compared with their titanium counterparts.

For those titanium alloys exhibiting discontinuous initial yielding, the absence of the phenomenon at the lower transformation temperature was in accord with the trends exhibited by the vanadium steels of Batte, and was thought likely to be caused either by microstructural effects or by differences in the distribution of solute atoms as discussed in subsequent sections.

The mirror finish of the gauge length enabled surface features to be distinguished but no Lüders bands were observed in any of the specimens exhibiting discontinuous yielding. In each case the deformation appeared to occur uniformly along the gauge length, the phenomenon described by Lagneborg & Sandström (1975) as homogeneous deformation. For initial

yield points exhibited by the 800° specimens of Alloys 1 and 2, the yield extensions were found to vary from 0.5% to 1.2% strain but were insufficiently reproducible to be used as more than a qualitative indication. It was inferred that despite the precautions taken, the method which had to be adopted to achieve the required heat treatments may have caused slight distortion in some of the tensile specimens and hence variation between the stress-strain curves.

The indistinct nature of some of the initial yield points observed may be partly a result of the grain size dependence of yield effects (Section 2.11). The 15 to 40 μm measured grain sizes, d, (Figure 3.16) were close, in terms of $d^{-\frac{1}{2}}$, to the 100 μm limit above which initial yield drops in steels are not displayed. However when considering the change in yielding behaviour with transformation temperature the grain size cannot be the only factor involved because the grain size was found to decrease as the temperature was lowered. On the basis of grain size alone this would have the opposite effect on the yielding behaviour.

Straining the material was envisaged to diminish any local differences in flow stress which may have been causing the absence of yield points. The strain-age yielding behaviour was therefore used to investigate more fully the effects of compositional differences.

4.5 Strain-ageing yield behaviour

Specimens of the four alloys transformed at 650° and 800° were given the 30 min 100°C strain-ageing treatment. The magnified stress-strain curves are presented in Figures 4.8 and 4.9: on reloading after the ageing treatment all the specimens of Alloys 1 and 2 exhibited discontinuous yielding, including those which had shown no yield point during initial yielding.

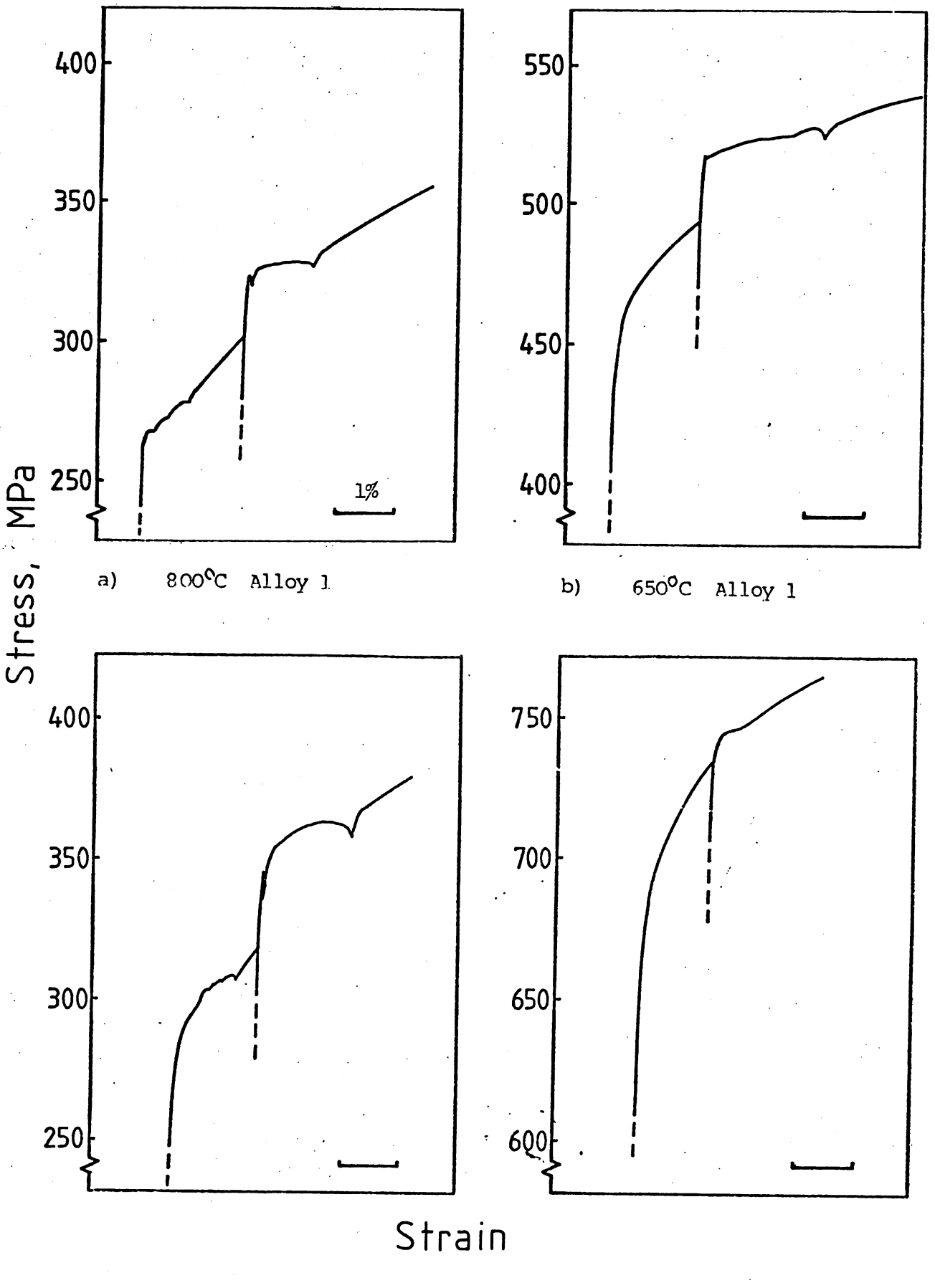

Figure 4.8: Strain-age yielding behaviour of isothermally transformed Alloys 1 and 2

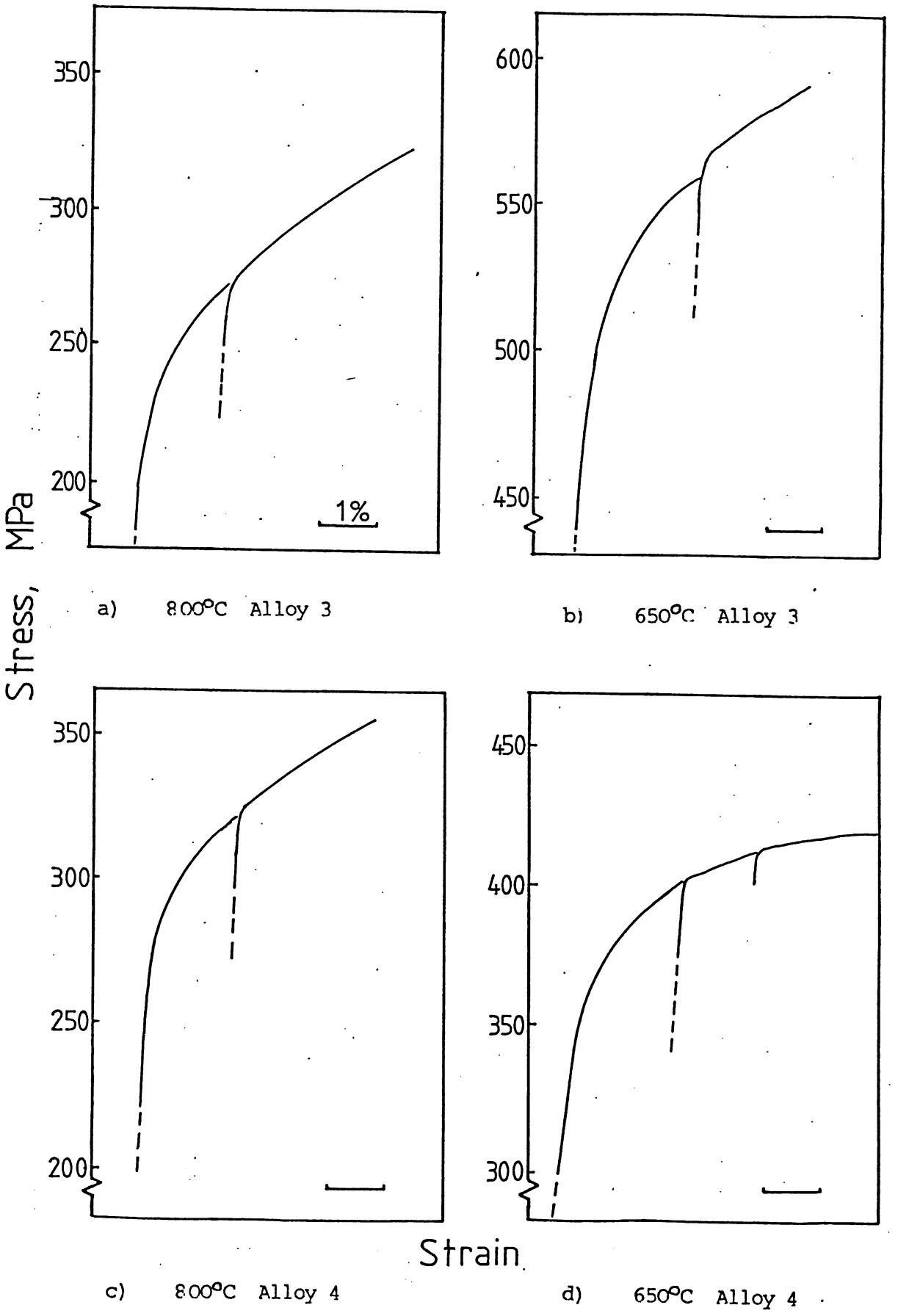

Figure 4.9: Strain-age yielding behaviour of isothermally transformed Alloys 3 and 4

The strain-ageing indices and strain-age yield extensions used to quantify the behaviour of the four alloys are presented in Table 4.10. In each case any stress increase after this ageing treatment was temporary, the stress-strain curves resuming the same behaviour as the uninterrupted curves once strained beyond the strain-age yield extension. Mean values of the index were 24 and 31 MPa for the 800° structures of Alloys 1 and 2 respectively, and 20 and 5 MPa for the 650° structures. None of the specimens of Alloys 3 or 4 exhibited strain-age yield points greater than 1.5 MPa.

4.6 The role of interstitials

The steels in this investigation all contained sufficient titanium to effectively remove all the nitrogen from solution. The residual equilibrium nitrogen levels in austenite, calculated using the data in Table 2.3 are 10^{-6} wt% at 1300°C and would be considerably lower in ferrite. Furthermore, the stability of titanium nitride makes it extremely resistant to dissolution during ageing. Hence any interstitial effects are attributable to the presence of carbon rather than nitrogen.

The absence of strain-age yield points in Alloys 3 and 4 indicated again that carbon contents over the stoichiometric titanium carbide level are a necessary though not the sole requirement for discontinuous yielding. This result is in agreement with the work of Comstock (1943) in his investigation of titanium steels in the normalised and normalised plus annealed conditions, and of Meyer, Heisterkamp & Müschenborn (1977) on cold rolled plus box annealed titanium steels. Titanium thus appears to be a strong enough carbide as well as nitride former to remove all the interstitials from solid solution if present in sufficient quantity.

The carbon excesses of 0.06 % for Alloy 1 and 0.02 % for Alloy 2

Alloy	Composition wt%		Initial yield extension %		Strain-ageing yield extn. %		Strain-ageing index MPa	
	C	Ti	800°	650°	800°	650°	800°	650°
1	0.07	0.07	0.8	0	1.0	1.8	24.0± 7.2	19.6±5.6
2	0.07	0.23	1.1	0	1.7	0.6	30.8±16.4	5.2±4.4
3	0.10	0.52	0	0	0	0	<1.5	<1.5
4	<0.02	0.38	0	0	0	0	<1.5	<1.5

Table 4.10: Strain-ageing behaviour of 800°C and 650°C isothermally transformed specimens

(Table 4.5) would equilibrate as far as possible with cementite but the room temperature equilibrium concentration of less than 10^{-6} wt%C is unlikely to have been approached in view of the relatively fast cooling rate of the specimens to ambient temperature, estimated as 3° - 5°per sec (200° - 300°per min).

To ascertain whether the strain-age yield points were primarily a result of carbon already in solution before any ageing, or a result of the redissolving of cementite at the ageing temperature, a strain-ageing treatment at room temperature was performed. At this temperature precipitated carbon does not dissolve, and to compensate for the reduced mobility of any interstitial carbon atoms, an ageing time of 12 hours was employed. The specimen was of Alloy 1 transformed at 800° and strained 1.5%. A strain-ageing index of 29 MPa, comparable with that recorded after the usual 30 min, 100°C ageing treatment, confirmed the initial presence of interstitial carbon.

The rapid return of small yield points ($\Delta\sigma \simeq 4$ MPa) in Alloys 1 and 2 after 40 s room temperature ageing under full load supported this conclusion. Such yield points arise from stress induced ordering (Wilson & Russell, 1959), and the magnitude is proportional to the dissolved interstitial content. The effect was absent in Alloys 3 and 4.

For the standard strain-ageing treatments the low strain-ageing index (5 MPa) of the 650° structure of Alloy 2 may reflect the combined effects of a high density of segregation sites compared with structures formed at 800°, and a lower concentration of available interstitial carbon atoms compared with Alloy 1.

4.7 Ageing before straining

The appearance of discontinuous yielding in the 800°C specimens indicated that dissolved carbon atoms had sufficient time to segregate to dislocations during cooling and the same would be expected to occur in specimens transformed at all temperatures. If, however, a certain proportion of dislocations remained unlocked (i.e. mobile) in the more heavily dislocated regions of the lower temperature structures, and if this were the sole reason for the absence of an initial yield point in the latter, then a discontinuous yield point should be developed on ageing before straining.

To examine this possibility, a series of specimens of Alloy 1, transformed at 700°C and in the unstrained condition, were given the following ageing treatments: 30 min at 200°C, 30 min at 100°C and six months at ambient temperature. On straining, all the specimens still yielded continuously, indicating that even when one would expect all the dislocations to be immobilised, discontinuous yielding was suppressed.

4.8 Effect of cooling rate from the transformation temperature

The effect of the cooling rate from the transformation temperature was investigated using two specimens of Alloy 2 which had been isothermally transformed at 800°C and strained through initial yield. The specimens were given a series of 1 h annealing treatments at 800°C, each followed by either furnace cooling, water quenching or rapid iced-brine quenching. Quartz encapsulation was used for the heat treatments and to accomplish the two more rapid cooling rates the tubes were crushed before quenching. Immediate tensile straining to approximately 2 % was then given, including a 40 s full load ageing stop, described above, after any yield extension was finished.

The annotated stress-strain curves for the test cycles are given in Figure 4.11. After furnace cooling from 800°C, pronounced initial yield points were exhibited with yield extensions of 1.1 %, 1.8 % and 1.8 %. Water quenching produced either continuous yield or indistinct yield points with yield extensions of 0.6 % and 0.7 %. After iced-brine quenching initial yield in each case was continuous.

The small yield points produced by stress induced ordering showed the opposite trend: furnace cooling resulted in $\Delta\sigma$ of less than 2 MPa; water quenching and iced-brine quenching gave $\Delta\sigma$ of 6 MPa. A standard 100° strain-ageing treatment given to an iced-brine quenched specimen resulted in a large strain-ageing index of 35 MPa.

Comparison of the optical microstructures taken from the gauge length at the end of the cycle of treatments with a specimen taken from the threaded end beforehand showed very little change: grain sizes of 29 μm and 31 μm respectively were measured and both had an irregular but equiaxed grain structure. Moreover, after each cycle, the load at yield returned to approximately the same value.

It was indicated from more detailed annealing investigations, reported in Sections 4.10 and 5.9, that the major effect of the one hour annealing treatment would be to lower the dislocation density developed during deformation. It would have had little effect on the stable titanium carbide dispersion nor on the ferrite grain structure. At 800°C any carbon not combined with titanium would disperse from carbon atmospheres and any cementite precipitates would dissolve. During cooling, carbon atmosphere formation becomes energetically favourable relative to the thermally activated movement of dislocations at temperatures below ~ 300°C. The carbon can then become effective in segregating to and immobilising dislocations.

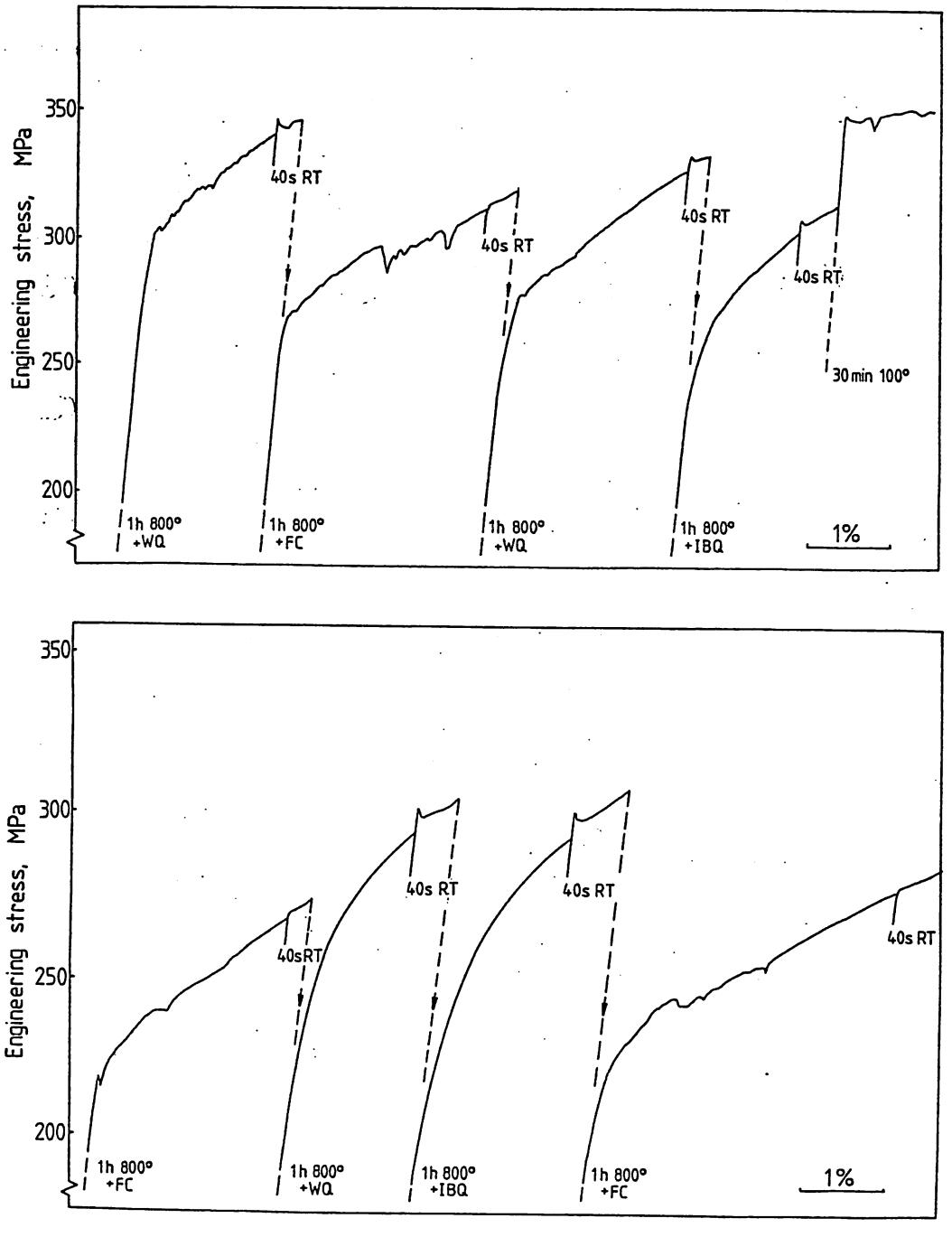

Figure 4.11: Effect of cooling rate from 800°C on yield behaviour

At 300°C carbon diffuses at 200 nm per s. For a dislocation density of $10^{14}\ m^{-2}$ the dislocation separation is of the order of 100 nm. On furnace cooling, therefore, there was ample time for almost complete carbon segregation to dislocations to occur. The absence of stress induced ordering yield points indicates that the carbon was probably present as fine iron carbide precipitates rather than individual interstitial atoms. The precipitates would pin the dislocations and thus cause the initial yield points, but the carbon would not be free to affect subsequent yield points unless redissolved.

After iced-brine quenching the majority of the free carbon would be retained in solid solution. Any carbon which had time to segregate to dislocations would remain as interstitial atoms and would therefore be free to exhibit the large stress induced ordering and 100° strain-ageing yield points observed. The absence of the initial yield point was either caused by the large number of unpinned dislocations, or by residual stresses created during the quench. The latter possibility is considered in the next section.

The restoration of the initial yield point by employing a slightly slower quench rate reflects the sensitivity of yielding behaviour to cooling rate in these steels. It is evident that the air cooling used for the standard tensile specimens was fast enough to retain carbon in solution which then contributed to strain-age yield points; it was not so fast as to remove the initial yield point effects by preventing segregation.

It is unlikely, however, that segregation effects were causing the differences between specimens transformed at different temperatures: all the specimens were deliberately cooled to room temperature at the same rate. It appeared that differences in transformation behaviour were

playing a larger role in determining the initial yielding behaviour.

4.9 Residual stresses

In general residual stresses may be introduced by the combination of differential thermal expansion and transformation strains. Under extreme circumstances, for example in large steel components undergoing rapid temperature changes, residual stresses can be greater than half the yield stress (Thelning, 1975); they may then have a large effect on the yielding behaviour, causing the removal of discontinuous yielding because they have the effect of producing local changes in the flow stress. Long range stresses in such components are relaxed by stress-relief treatments of 1 to 2 hours at temperatures up to 650°C.

This said, however, the heat treatments given to the tensile specimens in the experimental study reported here were far less severe and residual stresses were not envisaged to have been of significant magnitude: in fact two-stage treatments of this nature comprising austenitising followed by isothermal transformation are deliberately used to minimise stresses in production components (ibid). The tensile specimens were made deliberately small and were given isothermal heat treatments such that the microstructure and temperature were at all times approximately uniform throughout the specimen section. There would therefore be few stresses from differential expansion and any local transformation stresses would have had the opportunity to disperse during the time at temperature.

To test this assumption, a simulated stress-relieving treatment of 60 000 s (over 16 h) at 400°C was given to two specimens of Alloy 2 which had been transformed at 650°C: in neither was an initial yield point developed suggesting that other factors were primarily responsible for

suppressing the discontinuous yielding behaviour.

4.10 Time at transformation temperature

It was appreciated that although the specimens had all been held for the same time, 1000 s, at the transformation temperature those specimens at the lower temperatures would have transformed more rapidly; the reaction kinetics were shown on the TTT curves of Figures 3.1 and 3.2. Furthermore within each specimen different regions would have spent longer in the transformed state than others. To investigate the effects the time at temperature had on the yielding behaviour, isothermal annealing treatments were designed: 60 000 s annealing treatments were given to specimens of all four alloys which had been originally transformed by the standard 1000 s treatments at 650°and 800°C. The same temperatures as the initial transformation treatments were selected to minimise the effects on the precipitate dispersions.

Specimens were annealed in both the unstrained and strained (~5%) state. They were treated in the fully prepared (i.e. electropolished) condition, sealed in quartz capsules. Heat treatments were terminated by immersing the unbroken capsules in water, thus producing cooling rates similar to the air cooling employed for the original treatments.

The changes of 0.2% proof stress are plotted in Figure 4.12, with the values for the originally strained and unstrained specimens averaged for each annealing treatment as they were found to be similar. The corresponding optical microstructures displayed in Figures 4.13 and 4.14 show that the ferrite grain structure was little changed by the heat treatment in those alloys (Alloys 1 to 3) containing titanium carbide dispersions. The absence of precipitates in Alloy 4 allowed grain growth to occur and resulted in the greatest lowering of strength.

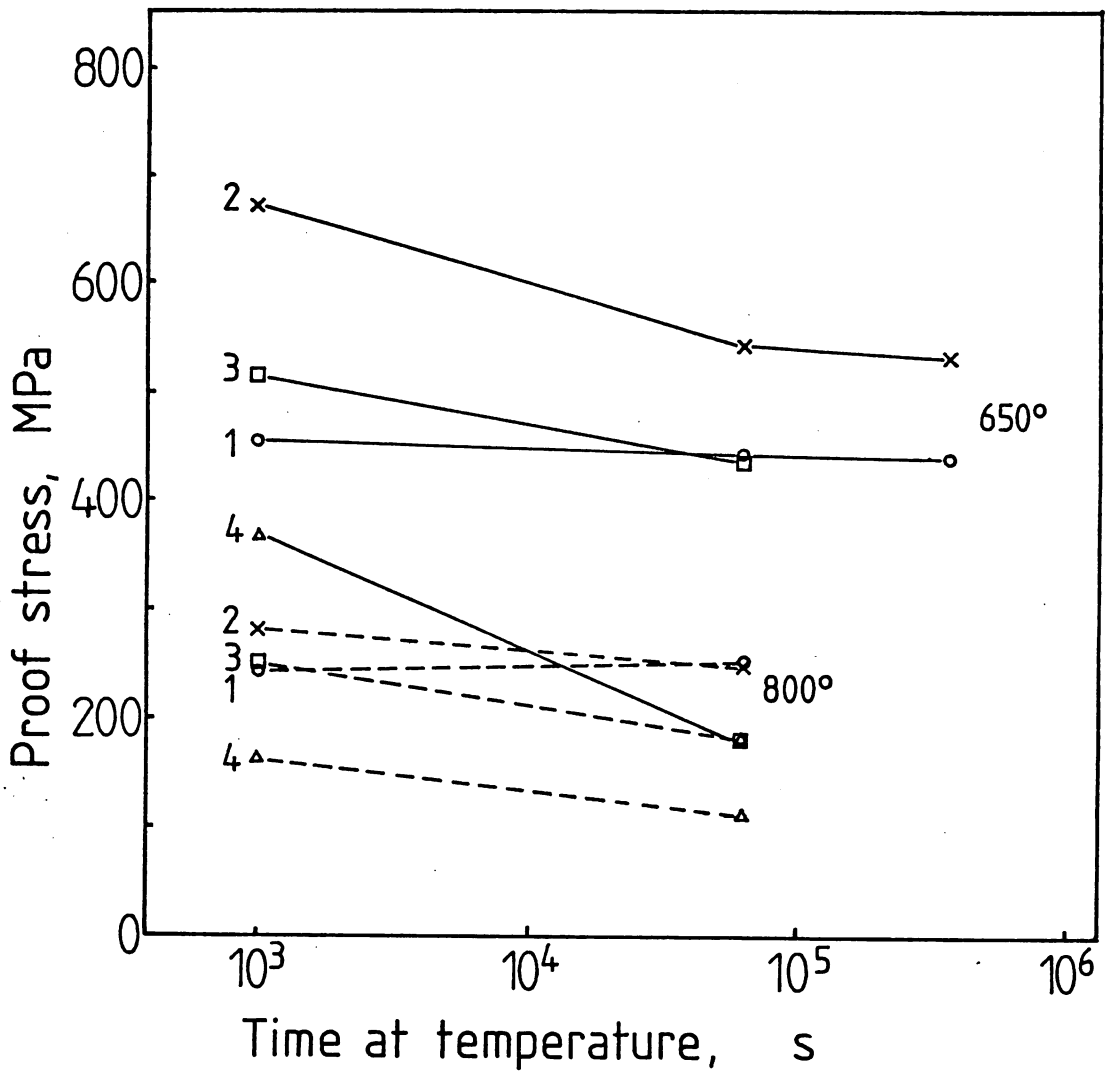

Figure 4.12: 0.2% proof stress variation with isothermal annealing time at 800° and 650°C for Alloys 1 to 4

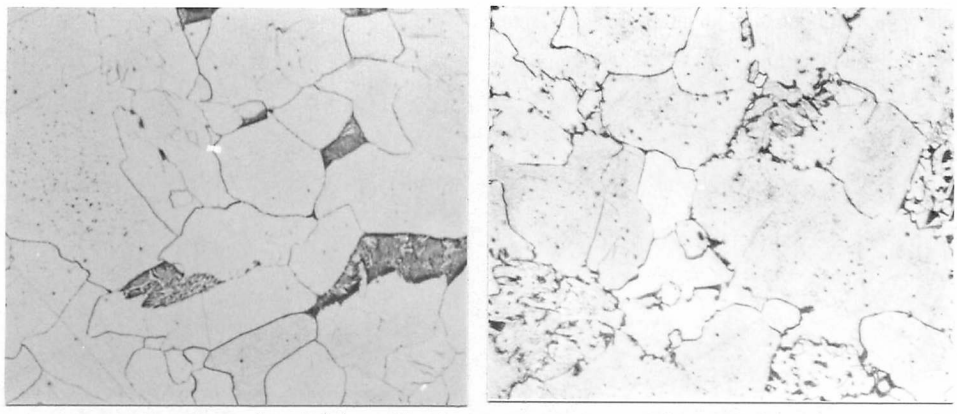

a) Alloy 1 (0.07C - 0.07Ti)

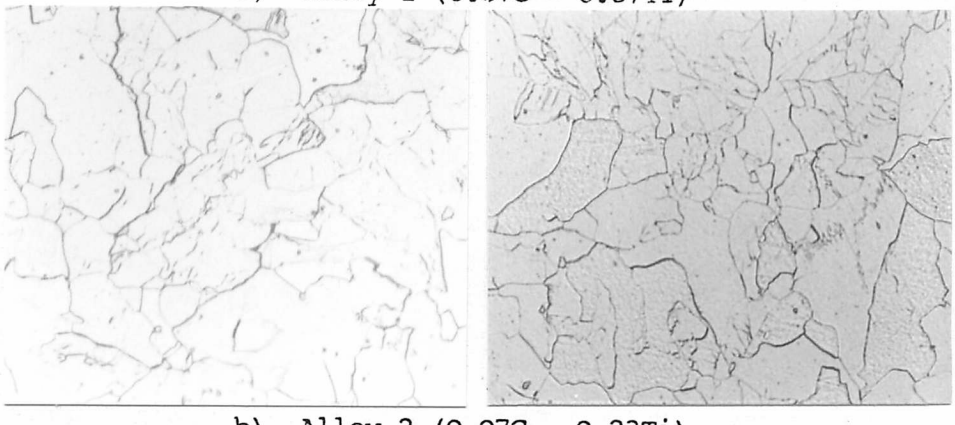

b) Alloy 2 (0.07C - 0.23Ti)

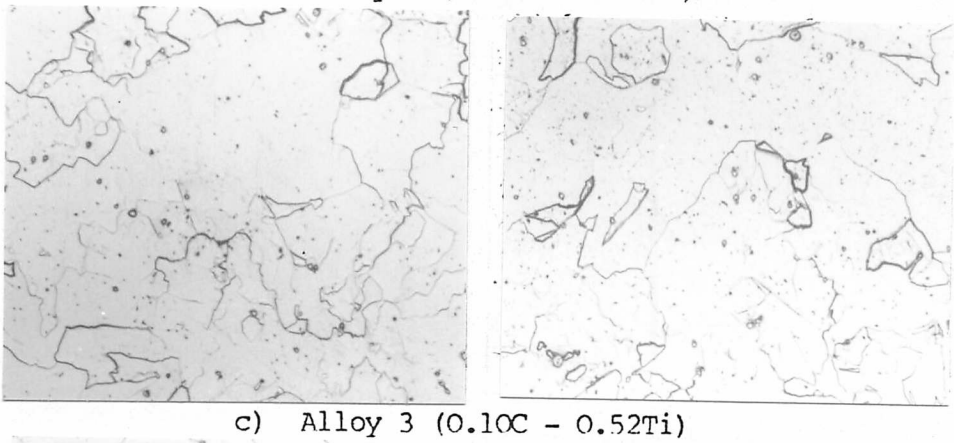

c) Alloy 3 (0.10C - 0.52Ti)

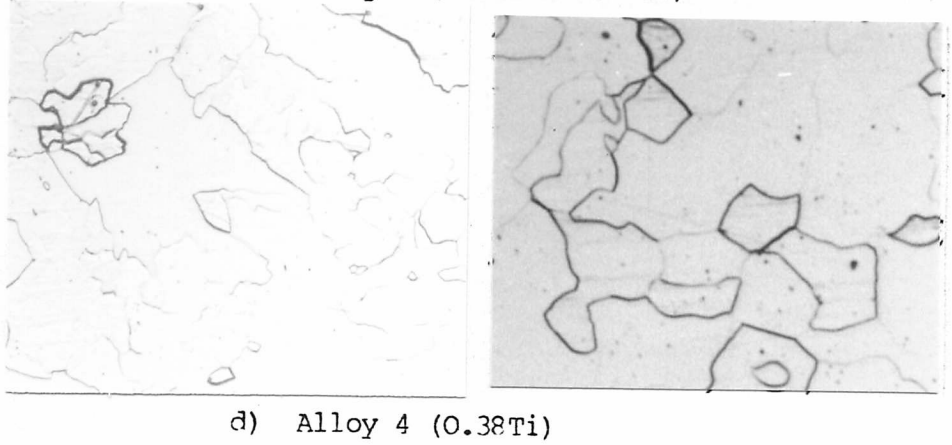

d) Alloy 4 (0.38Ti)

1000 s 800°C

(1000 + 60 000)s 800°C

100 µm

Figure 4.13: Optical microstructures before and after isothermal annealing at 800°C

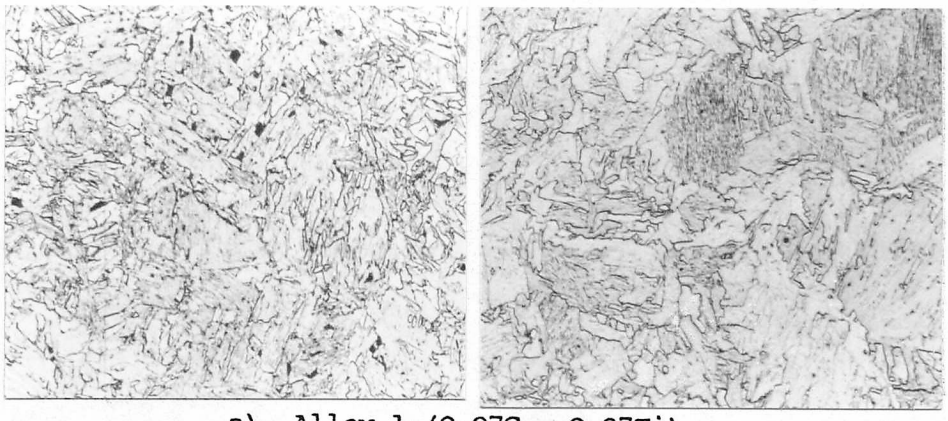

a) Alloy 1 (0.07C - 0.07Ti)

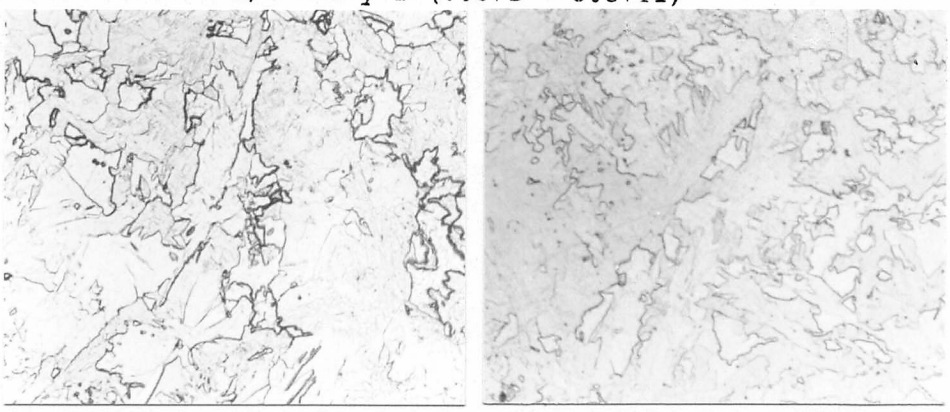

b) Alloy 2 (0.07C - 0.23Ti)

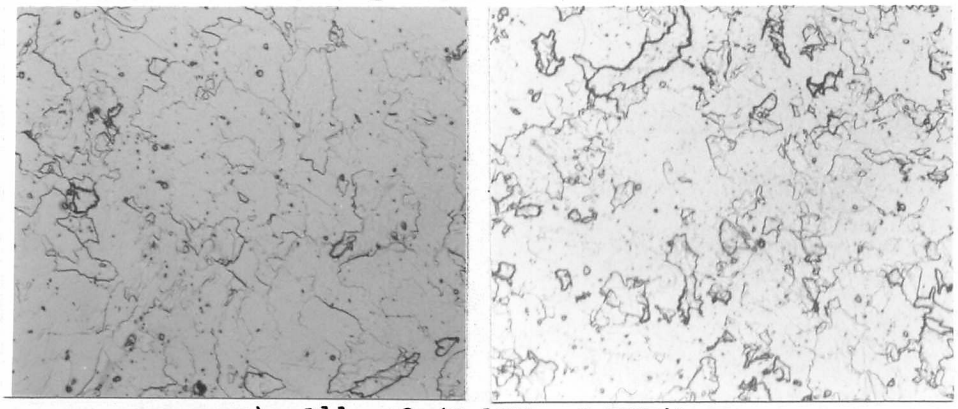

c) Alloy 3 (0.10C - 0.52Ti)

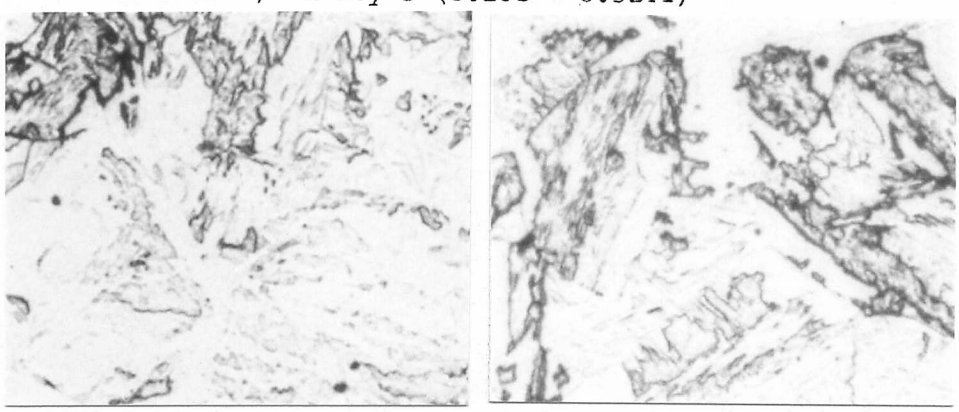

d) Alloy 4 (0.38Ti)

1000 s 650°C (1000 + 60 000)s 650°C

100 μm

Figure 4.14: Optical microstructures before and after isothermal annealing at 650°C

Continuous initial and strain-age yielding behaviour was exhibited by the specimens of Alloys 3 and 4 in all conditions, as before, so attention was concentrated on the other two alloys. The 800° annealed specimens of Alloys 1 and 2 showed discontinuous initial and strain-age yielding behaviour with very similar characteristics to the as-transformed specimens. The greatest difference in behaviour was exhibited by the 650° specimens of Alloys 1 and 2; Figures 4.15 to 4.18 show the progression of stress-strain curves for the initially strained and unstrained specimens. Note the different stress ranges used, enabling the plots to be magnified. In the as-transformed state the initial yield was continuous but after 60 000 s annealing at 650° discontinuous initial yield points began to develop. Additional specimens, both strained and unstrained were therefore isothermally annealed for 360 000 s (100 h) at 650°. There was a further small drop in strength and further development of the initial yield points.

For each series of annealing treatments the development of discontinuous yielding occurred more quickly in the previously strained specimens than the unstrained specimens. There was little difference in the stress levels indicating that the effects of the heat treatment swamped the initial differences in dislocation density: any difference in observed yielding behaviour would be attributable to the improved alignment of the strained specimen.

The interstitial carbon content, as indicated by the magnitude of the strain-ageing index, remained approximately constant throughout. Electron microscopy (Figures 3.22 aand 5.23) revealed that the fine dispersions of titanium carbides were retained after both 650° and 800° treatments, hence

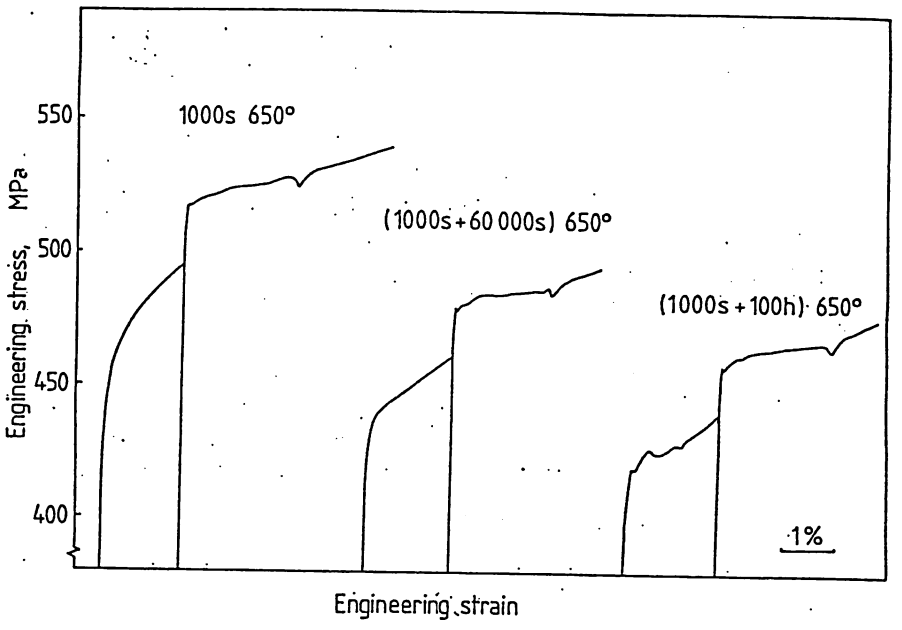

Figure 4.15: Yield behaviour after isothermal annealing unstrained specimens of Alloy 1 at 650°C

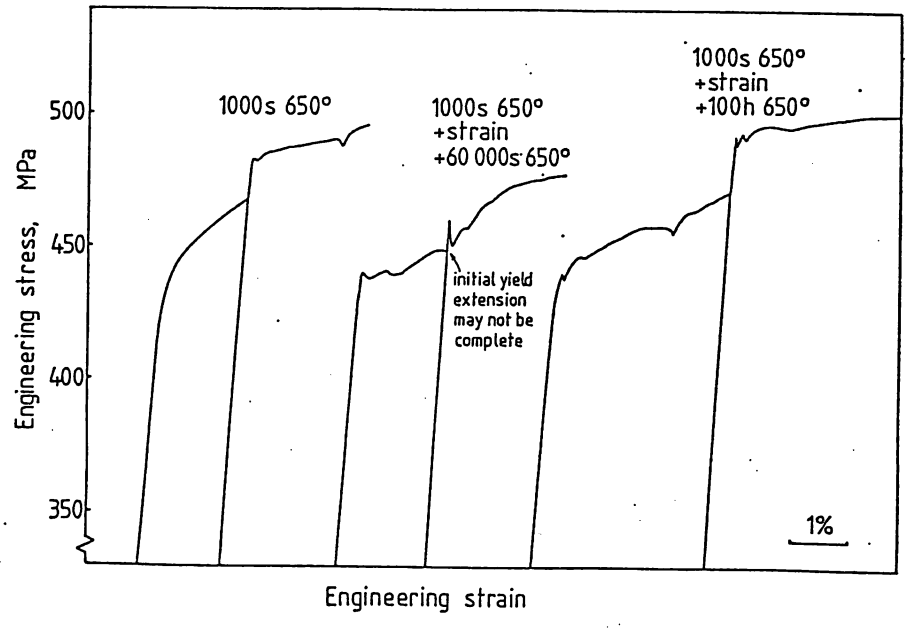

Figure 4.16: Yield behaviour after isothermal annealing initially strained specimens of Alloy 1 at 650°C

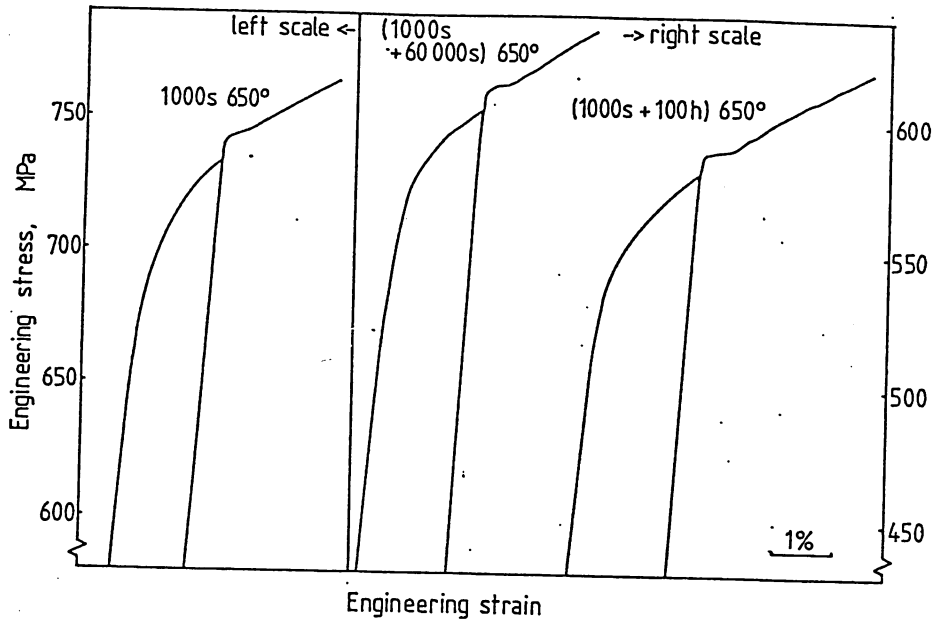

Figure 4.17: Yield behaviour after isothermal annealing unstrained specimens of Alloy 2 at 650°C

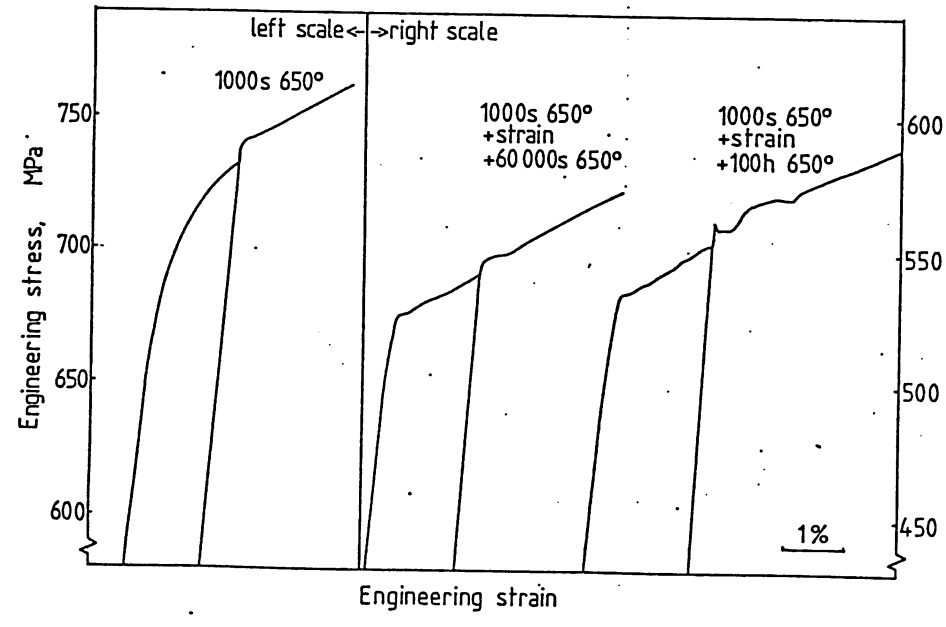

Figure 4.18: Yield behaviour after isothermal annealing initially strained specimens of Alloy 2 at 650°C

demonstrating their resistance to coarsening. There appeared to be some lowering of the dislocation densities particularly from the lathlike grains in the annealed 650° specimens. The effects of these annealing treatments are considered further in the following chapter.

The length of time required for the initial yield elongations to develop suggests that the mechanism involves a larger scale microstructural change than either the diffusion of interstitial atoms or the small adjustments in the dislocation structure which would be required to eliminate any localised stresses. The gradual homogenisation of the microstructure would seem to be a more important factor, and this possibility is considered in the next section. Alternatively, the discontinuous yielding may be promoted by the more thorough pinning of dislocations and the deactivation of dislocation sources by precipitates. All these factors are considered in greater detail in Chapter 8.

4.11 The role of microstructure

Because the observed, macroscopic stress-strain curve is the average deformation behaviour across the specimen cross section, local variations in the yield stress would encourage continuous stress-strain curves even if conditions in individual areas would promote local discontinuous yielding. The inhomogeneities in the precipitate dispersions and ferrite microstructures of the isothermally transformed specimens were therefore thought to be at least partly responsible for the masking of discontinuous initial yielding behaviour.

Microhardness measurements were undertaken to investigate the scale and magnitude of the inhomogeneities. The two samples selected as likely to have the most and least inhomogeneous microstructures were:

i) 1000 s at 650° standard isothermal treatment, as-transformed;

ii) 1000 s at 800° standard isothermal treatment, plus 60 000 s 830° annealing treatment to homogenise (reference sample).

Both were of Alloy 2 (0.07C-0.23Ti). Microhardness indents were made in a regular grid but high angle grain boundaries were avoided.

The results are presented in Table 4.19. For each set of measurements the variance, V, (V = square of the standard deviation) was used to quantify the spread of the indent diameters and the derived hardness values. It is hence a measure of the inhomogeneity, but also includes contributions from measurement errors and the effects of orientation, sectioning and grain boundaries. The variance ratio is used to compare the spreads of two data sets: if the ratio lies outside a given range calculated from the populations of the two samples (Table 4.20), the difference in the spread of results is "significant".

The average microhardnesses of the two samples were 360 and 152 VPN and hence loads of 21 g and 10 g respectively were employed to produce similar indent sizes and thus similar measurement errors. For the 650° sample, there was no significant difference between the spread of results obtained over the whole section and just in the central region, indicating homogeneity on a scale of millimetres between the inside and outside of the sample. Comparison with the annealed, reference sample showed a marginally significant difference in the variance, but with the 650° sample exhibiting the smaller spread of results.

The differences in grain boundary effects as well as in the strength characteristics mean that the results are not completely comparable even though the indent diagonals were very similar. The 10 to 11 μm indents would deform a region of approximately 30 μm diameter which is greater than the grain size of the 650° structure but similar to that of the annealed reference sample. Thus either the microhardness method is

Set	Specimen	Load g	No. indents	Indent diagonal d, μm			Microhardness VPN		
				mean	st.dev	V	mean	st.dev	V
	Transformed 1000 s 650°C								
1	whole section	21	66	10.34	0.33	0.109	357	23	528
2	central region	21	40	10.28	0.34	0.115	362	24	584
3	Annealed, for reference	10	60	11.08	0.43	0.185	152	12	139

Table 4.19 : Results of microhardness survey

	Variance ratio		Population ratio	Range outside which difference in spread is significant (90% confidence)
	Indent diagonals	Micro-hardness		
$V_1 : V_2$	0.95	0.90	66 : 40	0.61 - 1.64
$V_1 : V_3$	0.59	N/A	74 : 60	0.66 - 1.51
$V_2 : V_3$	0.62	N/A	66 : 60	0.65 - 1.53

Table 4.20: Comparison of variances in microhardness results

insufficiently sensitive to detect inhomogeneities on a grain to grain scale, or the inhomogeneities in the 650° structure were primarily present on a scale finer than the grain size.

4.12 Summary

1. The influence of composition on the proof stress and tensile strength levels arises largely through changes to the volume fraction of fine titanium carbide precipitates and the proportion of excess carbon. For each alloy the strength increased with decreasing isothermal transformation temperature due to the refinement of the precipitate dispersions, the refinement of the ferrite grain size and increased dislocation strengthening.

2. Discontinuous initial yielding and strain-age yielding were completely eliminated when the titanium content exceeded that required for titanium carbide stoichiometry.

3. For the isothermal transformation heat treatments given, the cooling rates to room temperature allowed sufficient interstitially dissolved carbon to persist in the ferrite to give rise to strain-age yield extensions in the two alloys with carbon levels above the titanium carbide stoichiometric ratio.

4. Specimens exhibiting strain-age yield extensions did not necessarily show an initial yield point. Transformation at 650°C produced continuous initial yielding whereas the 800°C structures exhibited discontinuous initial yielding.

5. Heat treatments designed to remove any residual stresses did not promote discontinuous yielding in the 650° structures; only after prolonged (up to 100 h) isothermal annealing treatments were initial yield extensions developed.

6. Microstructural inhomogeneities observed in the dislocation and precipitate distributions were suspected as causing the absence of discontinuous initial yielding in the 650° structures, rather than residual stresses or the distribution of interstitial carbon atoms. However such microstructural inhomogeneities were not detectable on a grain to grain scale using microhardness measurements.

CHAPTER FIVE

DISLOCATION POPULATIONS

5.1 Introduction

In this chapter lattice defects present in the isothermally transformed material are investigated. Particular attention is paid to dislocations and the strain fields present from all sources. Consideration is given to the origins of the indigenous dislocation populations arising from different heat treatments and to the development of dislocation arrangements on the deformation of structures containing sheets of interphase precipitates.

Previous work (e.g. Freeman 1971a&b; Freeman & Honeycombe 1977; Balliger & Honeycombe 1980; Haynes & Baker 1981) categorising the microstructure of similar precipitation strengthened microalloyed steels has concentrated principally on the size, spacing and coarsening behaviour of the precipitates and the consequent effect on mechanical properties. The role of dislocations in the coarsening of carbide particles in vanadium and titanium steels has been discussed by Dunlop & Honeycombe (1975) but apart from noting that the dislocation density was higher than that normally seen in annealed microstructures, no quantification of the dislocation populations was made.

Two techniques were selected for the quantitative microstructural investigations reported here:

i) Direct study of lattice defects by transmission electron microscopy, to enable observed dislocation densities to be measured

experimentally and to be related to the local microstructure;

ii) X-ray line broadening to provide information on the degree of total elastic strain in the lattice.

Thus the information obtained by the two methods is complementary. Because the results in each case are sensitive to the techniques of specimen preparation and to the methods of analysing the results, the precise details of the experimental methods employed are given here and in the Appendices.

For each technique all the specimens used had undergone complete isothermal transformation to ferrite and carbides. Subsequent air cooling avoided excessive internal stresses: it was appreciated that although partially transformed structures can provide considerable information about the microstructural development, the rapid quench required can result in the generation of additional dislocations in the ferrite. Such heat treatments were therefore not used in these studies of dislocation populations.

The quantitative dislocation density measurements were confined to specimens isothermally transformed 1000 s at each of 800°, 750°, 700° and 650°C and all were of Alloy 2 (0.07C-0.23Ti). Using TEM, dislocation distributions were characterised and the development of dislocation substructures on room temperature tensile deformation was investigated as a further means of understanding the dislocation-particle interactions. To investigate the thermal stability of the dislocation arrangements formed on transformation, dislocation densities were measured after isothermal annealing.

5.2 Method of TEM dislocation density measurement

The dislocation arrangements observed in thin foils are considered to be equivalent to those existing in bulk material (Hirsch et al. 1977) provided that reasonable precautions are taken during foil preparation to preserve the dislocation structure and that allowances are made for lack of image contrast.

The principal limitations of the TEM method of dislocation density measurement are that only a very small volume of material (typically 3 μm x 3 μm x 250 nm) can be surveyed relative to the size of the specimen, and that only dislocation densities within the range of 10^{12} to 10^{16} m^{-2} (10^{8} to 10^{12} cm^{-2}) are suitable for measurement - dislocation overlap becomes a problem at higher densities and decreased statistical accuracy results at lower densities. In practice all the densities measured fell within this indicated range.

For dislocation density measurement the basic line intersection technique of Staker & Holt (1972) was followed but some modifications and extra precautions were taken to suit the application.

The specimens were taken as discs from the undeformed shoulders of isothermally transformed tensile specimens and they were thinned chemically as this method is thought to be less likely to introduce dislocations than either grinding or spark machining (Hirsch et al. 1977 p56). The discs were then jet polished in the usual way until perforated. The foils were handled with extreme care. Between three and six foils per heat treatment were examined, the greatest number corresponding to the most inhomogeneous microstructure. A 200 kV electron microscope was used in preference to a 100 kV instrument because the greater penetration of the electrons allowed regions up to 350 nm to be examined whilst retaining good image resolution. The main advantages of examining thicker areas are

that

i) The dislocation population is more representative of the bulk material, the effects of both dislocation loss and introduction at free surfaces being diminished; and

ii) A greater number of dislocations is observed per unit foil area, a factor which was particularly important when quantifying the lower densities.

In each region examined, the foil thickness was determined from grain boundary thickness fringes (see Appendix A) with the specimen tilted so that only one of the grains was at the exact Bragg condition.

The dislocation populations in nearby grains were then photographed in bright field with the specimen tilted to image the dislocations close to the extinction contours of low order reflections, usually g=110, for the best resolution. The dislocation densities observed in the micrographs were calculated by the line intersection method (Appendix A). For each heat treatment, between 11 and 17 measurements of dislocation density were obtained, each from a different grain.

The error in each value of observed dislocation density was estimated to be 20%, the principal uncertainty arising from the foil thickness determination. However, a number of factors can cause differences between the observed density and the true value in the bulk specimen. The rotation of dislocations under the influence of surface image forces and the introduction or loss of dislocations during foil preparation will make a minor contribution to this difference. The most significant difference arises from the diffraction conditions rendering some dislocations invisible. The proportions calculated as invisible under different diffraction conditions are presented in Table 5.1. Some authors (e.g. Dingley & McLean 1967) have sought to minimise these problems using

Diffraction conditions	Proportion of $\frac{a}{2}$ <111> Burgers vectors invisible in b.c.c. lattice
Two-beam	
g = 110	0.5
g = 200	0
g = 211	0.25
Multibeam	
111 zone	0.25
001 zone	0
011 zone	0
113 zone	0

Table 5.1: Dislocation invisibility conditions

multibeam conditions but even then, contrast from all the dislocations is not guaranteed. In the present work, two-beam conditions were used and the appropriate invisibilty corrections applied. The corrections assumed

i) All dislocations had Burgers vectors of the type $\underline{b}=\frac{a}{2}\langle 111\rangle$;

ii) The dislocations were randomly distributed both in space and between the four possible variants of the Burgers vector;

iii) All dislocations satisfying the invisibility criterion were completely out of contrast. In practice the residual contrast of some dislocations will have led to their inclusion in the observed dislocation density so the "corrected" value will be an overestimate.

5.3 Method of X-ray strain measurement

X-ray line broadening is an indirect method of examining the strains present in a lattice. Line broadening is caused by the spread in the values of interplanar spacing resulting from local lattice disturbances but noticeable broadening can also be produced when the diffracting crystallites are small. Relative to TEM measurements, X-ray broadening gives results from a much larger volume of material, typically 10 mm x 3 mm x 25 μm and therefore can be used more reliably to show microstructural trends due to changes in heat treatment or deformation. A further advantage is the comparative speed of the technique. The principal drawback of X-ray methods is that it can be difficult to separate the various effects which contribute to line broadening.

Standard textbooks (e.g. Klug & Alexander 1974) describe the theory, techniques and methods of data analysis for X-ray diffractometry.

Longitudinal sections were cut from the shoulders and gauge length of tensile specimens for the investigation of the as-heat treated and plastically strained structures respectively. The flat surfaces were

given a deep chemical polish to remove any non-representative surface layer.

The specimens were mounted in the diffractometer with the long axis normal to the plane of the X-rays. CoK_{α} radiation was used and for each specimen the profile of the 211 diffraction peak was recorded by step scanning. In addition the 110 peaks were plotted for the as-heat treated, isothermally transformed specimens. Under identical diffractometer conditions, a sample of annealed mild steel was used to provide calibration peaks for instrumental broadening.

From each smoothed computer plot of diffracted intensity against angle the background intensity was subtracted and the Rachinger (1948) correction applied to separate the α_1 and α_2 contributions. Both the integral breadth β and the full width at half peak height 2w were then determined for each broadened α_1 peak, enabling the correction for instrumental broadening to be carried out using the method described by Langford (1979), outlined in Appendix B. It was assumed that all broadening in the specimens under investigation arose from lattice distortion because, in general, size broadening is only discernable when the crystallite size is below about 0.5 μm which is much smaller than the grain dimensions reported in Chapter 3. The integral strain breadth ε^2, defined as

$$\varepsilon^2 = \frac{\beta_f^2}{4 \tan^2 \theta} \qquad \ldots 5.1$$

where β_f is the integral breadth of the corrected peak in radians 2θ. ε^2 is used as a direct measure of lattice distortion because it is directly proportional to the stored energy (Williamson & Smallman 1956). The principal sources of error in the X-ray measurements were

i) residual broadening in the calibration specimen;

ii) measuring errors and approximations in data-handling equations; and

iii) instrument misalignment.

The calibration specimen was recrystallised mild steel which had a grain size of 20 μm and an anticipated dislocation density of less than 10^{12} m^{-2} (10^{8} cm^{-2}). The integral breadth resulting from the dislocations would be around 0.0003 (2θ). Greater errors arose from the measurement of the instrumental broadening peaks and the effect on subtraction from the observed profiles, particularly those which were especially narrow. As the numerical route from measured peak parameters to integral breadth was tortuous, the accumulated net errors were evaluated by substitution into a selection of the results. The maximum errors in measured peak width were estimated as $\pm 0.005^{o}$ in 2θ and this resulted in an error of around ± 0.07 in the form factor ϕ (i.e. $\sim$ 10 %) and $\pm 0.006^{o}$ (7 %) in the integral breadth β_{ξ} of the 211 peak of the 800^{o} sample. For broader observed peaks the percentage errors would be smaller. The errors arising from the mathematical assumptions in the equations used were approximately 1%.

The strain fields, assumed to be the principal cause of the line broadening, originate principally from

i) dislocations;

ii) second phase particles; and

iii) grain boundaries.

In deformed single phase materials the major source of strain broadening is the dislocation population, and thus the integral strain breadth ξ^{2} is directly proportional to the dislocation density ρ as a result of the strain energy introduced. The theoretical basis for this relationship is discussed by Williamson & Smallman (1956) and in practice

the generally used expression for dislocated iron is, (Mirkin 1964)

$$\rho \simeq 2 \times 10^{20} \xi^2 \ m^{-2} \qquad \ldots 5.2$$

For each of the X-ray line profiles obtained in the present work, this equivalent dislocation density was calculated and is presented.

5.4 Dislocation distributions after isothermal transformation

For specimens isothermally transformed 1000 s at each of 800°, 750°, 700° and 650°C, the observed and corrected values of TEM dislocation density measurements, as defined in Section 5.2, are presented in Figures 5.2 and 5.3 respectively. It is seen that the lower transformation temperatures, especially 650°C, produced a higher and less uniform density of dislocations than the higher transformation temperatures.

For those specimens transformed at 800°, 750° and 700°C no distinction was made between grain types, each having an essentially equiaxed structure. Dislocation densities were more homogeneous than in the 650° structure, the occasional elongated grains having values similar to the equiaxed grains as shown qualitatively in Figure 5.4. Mean dislocation densities of approximately $0.7 \times 10^{14} m^{-2}$ were calculated from TEM measurements with a possible trend to higher values as the transformation temperature decreased from 800° to 700°C. Figure 5.5 shows a typical region of a specimen transformed at 800°C. The dislocation density is relatively high for an equiaxed ferrite structure and there are many examples of dislocation pinning by the interphase precipitates, some of which are labelled, P. More examples of the microstructures were given in Chapter 3.

In the 650° structure the regions of high dislocation density were found mainly in the platelike ferrite grains, as in Figure 5.6a, where a maximum corrected density of $8.0 \times 10^{14} m^{-2}$ was recorded. Regions of lower

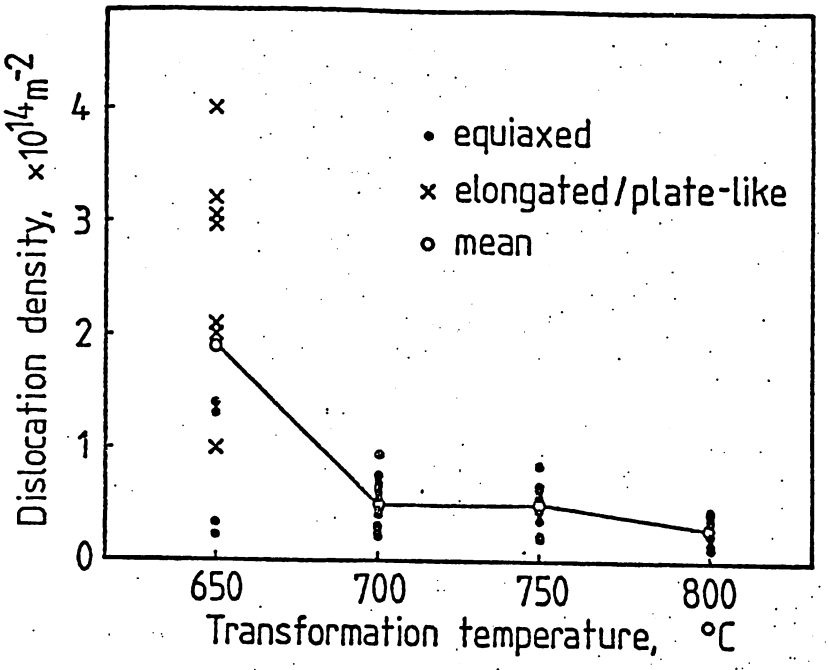

Figure 5.2: Dislocation density as a function of isothermal transformation temperature - TEM observed values

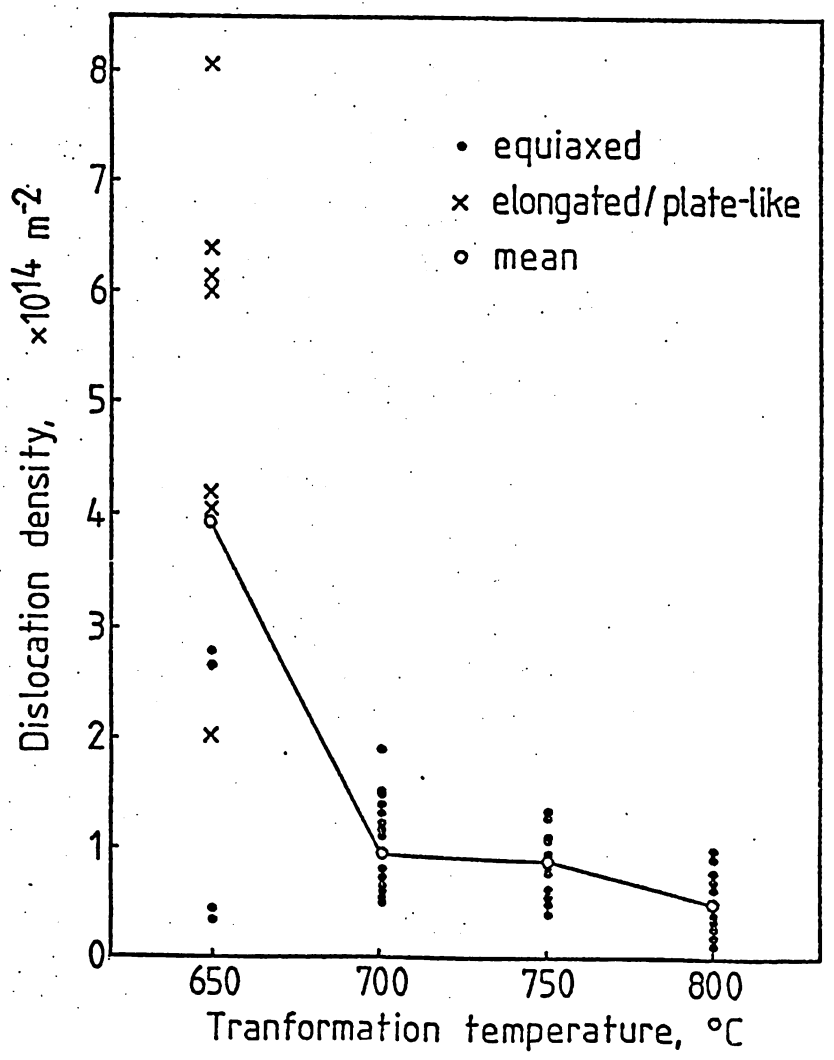

Figure 5.3: Dislocation density as a function of isothermal transformation temperature - corrected for invisibility

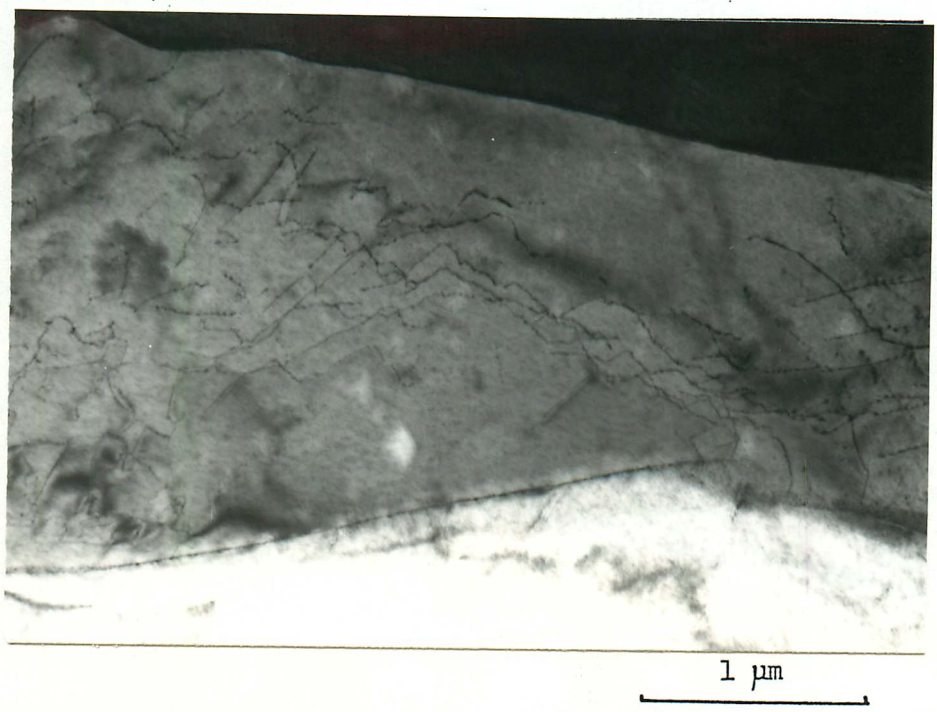

Figure 5.4: Elongated grain, formed at 700°C

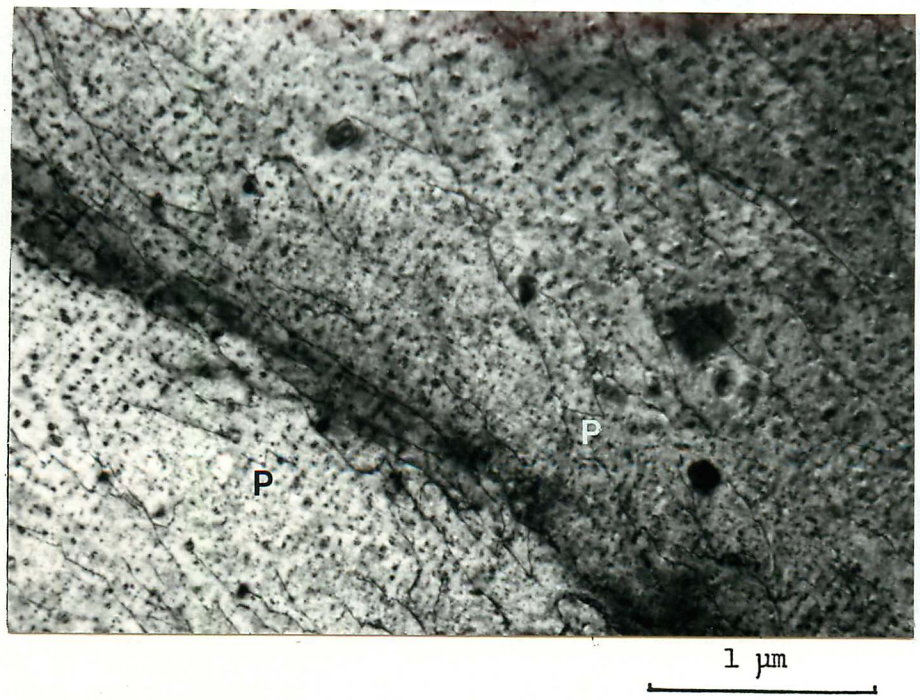

Figure 5.5: Dislocation distribution after isothermal transformation at 800°C
Examples of dislocation-particle interactions are labelled.

a) High dislocation density in laths

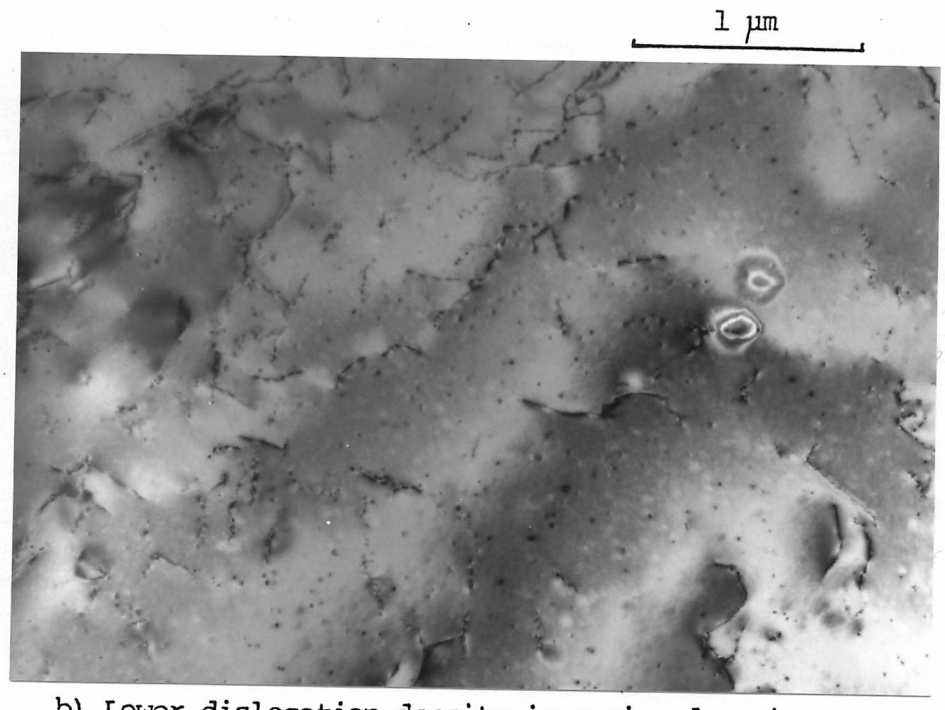

b) Lower dislocation density in equiaxed grain

Figure 5.6: Variation in dislocation density observed after isothermal transformation 1000s 650°C

dislocation density, down to 0.4 x 10^{14} m^{-2} were generally associated with the more equiaxed grains (Figure 5.6b). For measurements made from the 650° structures, plate-like or elongated and equiaxed grains are distinguished in Figures 5.2 and 5.3 by the symbols × and • respectively.

The observed X-ray line profiles for 110 and 211 reflections of the isothermally transformed specimens are shown in Figures 5.7 and 5.8 with the calibration peaks for comparison. The extent of α_1/α_2 overlap is a guide to the degree of broadening. The peak breadth data are presented in Appendix B for the instrumental, observed and specimen diffraction profiles.

The X-ray results show that the strain broadening increased steadily as the transformation temperature decreased. For example the 211 integral breadth β_f was ~0.09 (2θ) for 800° transformation and 0.28 (2θ) for 650°. The corresponding values of integral strain breadth ξ^2 were 0.46 x 10^{-6} and 4.17 x 10^{-6} and these are displayed graphically in Figure 5.9 together with the equivalent dislocation density figures of 0.9 and 8.3 x 10^{14} m^{-2} calculated using Equation 5.2. These latter measurements were approximately twice the corrected dislocation densities measured directly by TEM (Figure 5.3) for all transformation temperatures. On this basis, dislocations were providing half the total of local elastic lattice strain; precipitate strain fields and grain boundaries were providing the remainder.

It is evident that in the isothermally transformed condition all the precipitation strengthened structures studied had average dislocation densities greater than 10^{14} m^{-2} (10^{10} cm^{-2}) which is 2 to 3 orders of magnitude greater than that frequently quoted in mild steel, for example, given similar heat treatments. Furthermore the average dislocation density increased as the transformation temperature decreased, and the

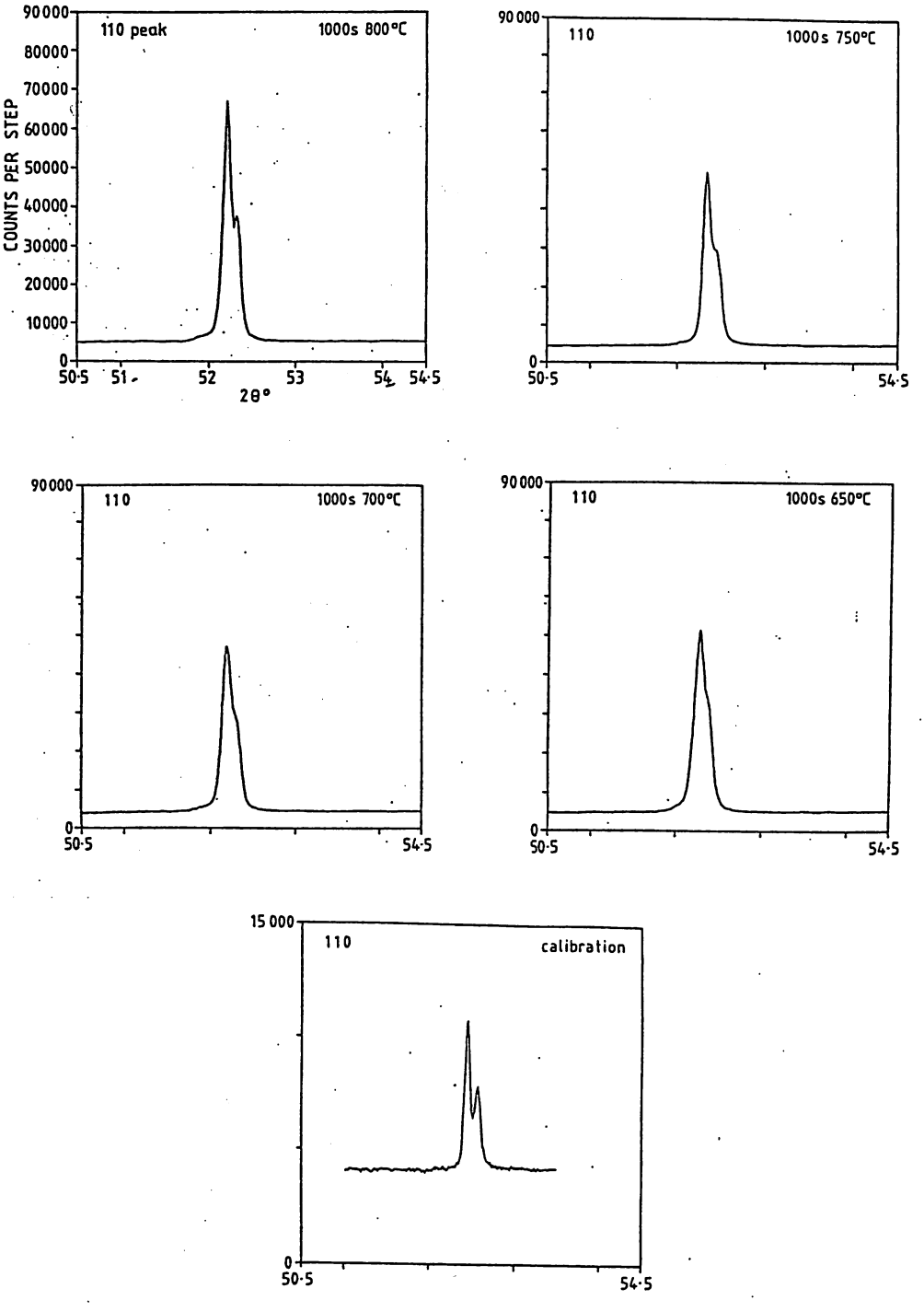

Figure 5.7: 110 X-ray line profiles of isothermally transformed specimens

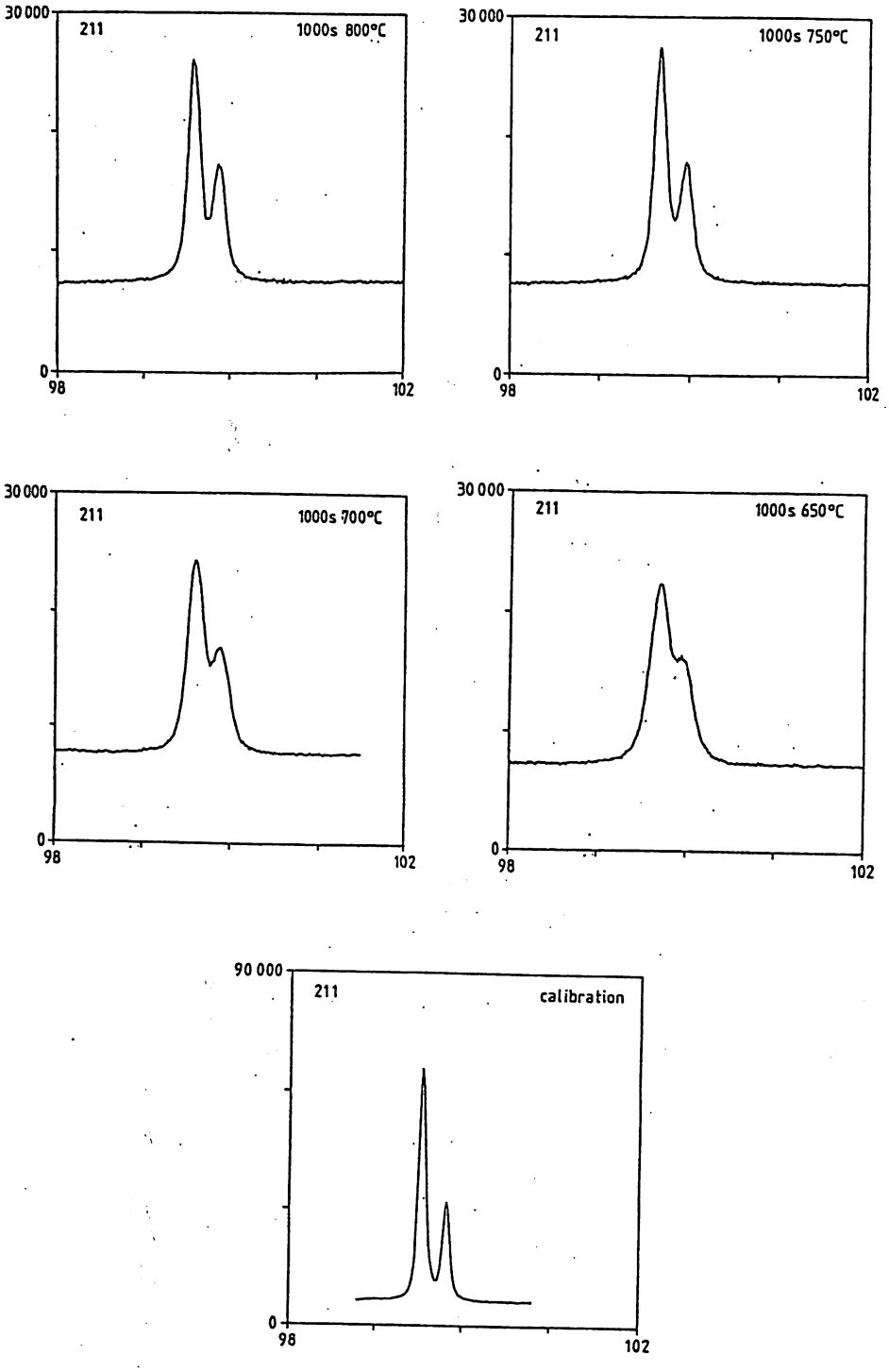

Figure 5.8: 211 X-ray line profiles of isothermally transformed specimens

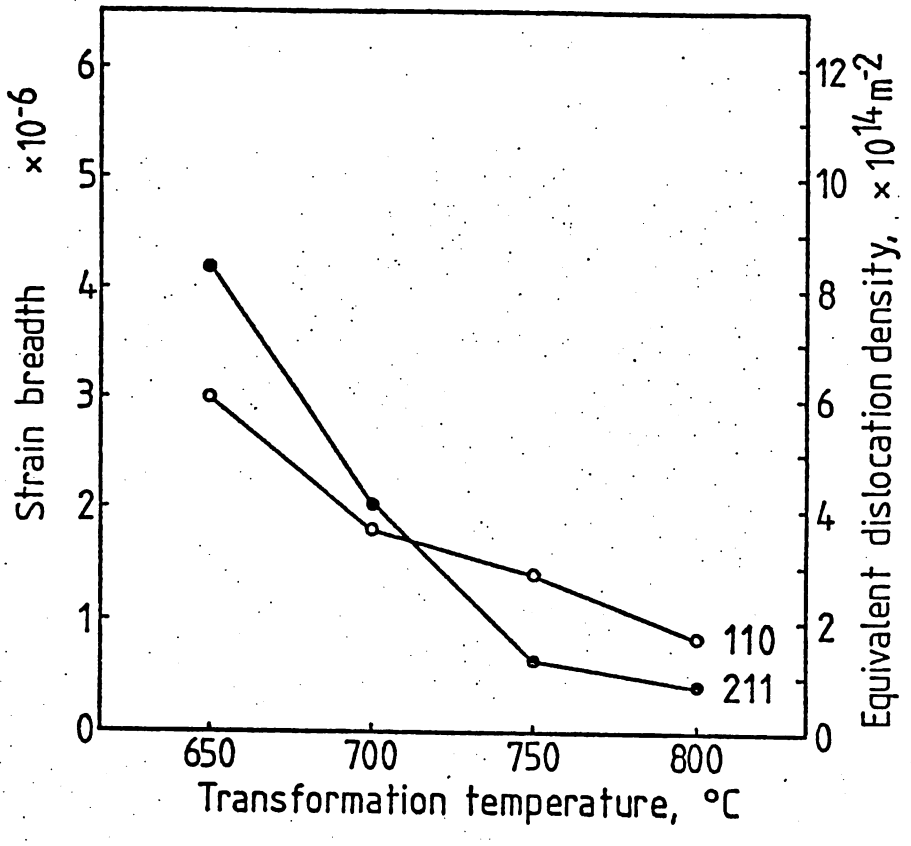

Figure 5.9: Strain breadth as a function of isothermal transformation temperature

distribution became more inhomogeneous. In the next section the origins of these indigenous dislocation populations are discussed.

5.5 Dislocation creation

The major supply of lattice dislocations is provided during the transformation of austenite to a ferritic product and is often attributed to the net volume increase. Dislocations per se cannot alleviate such a volume change because they introduce a small lattice expansion but they provide the plastic distortion needed to preserve grain boundary contiguity. The atomic volumes of ferrite and austenite are given in Figure 5.10 together with the transformation volume expansion. The latter increases with decreasing transformation temperature from 1.49 % at 900° to 1.89 % at 650° and 3.61 % at 20°C (Pearson 1967).

The transformation mechanism is an additional factor to be considered in the interpretation of dislocation density variations, and in Chapter 3 it was seen that ferrite microstructures corresponding to the whole spectrum from purely diffusional growth to shear transformation were found in these steels, but that the modes of transformation were not certain in some of the intermediate products.

The martensitic structure formed on iced-brine quenching (see Section 3.4) had a dislocation density too high to be measured directly by TEM. The X-ray line profile of the fully martensitic specimen exhibited broadening equivalent to a dislocation density of $7.5 \times 10^{15} m^{-2}$, originating chiefly from the shearing mechanism.

On isothermal transformation in the 650° to 900°C range the structures could be classed as intermediate between the extremes outlined above. It could not be established conclusively if the plate-like grains observed grew by a cooperative shear mechanism. However in the 650°

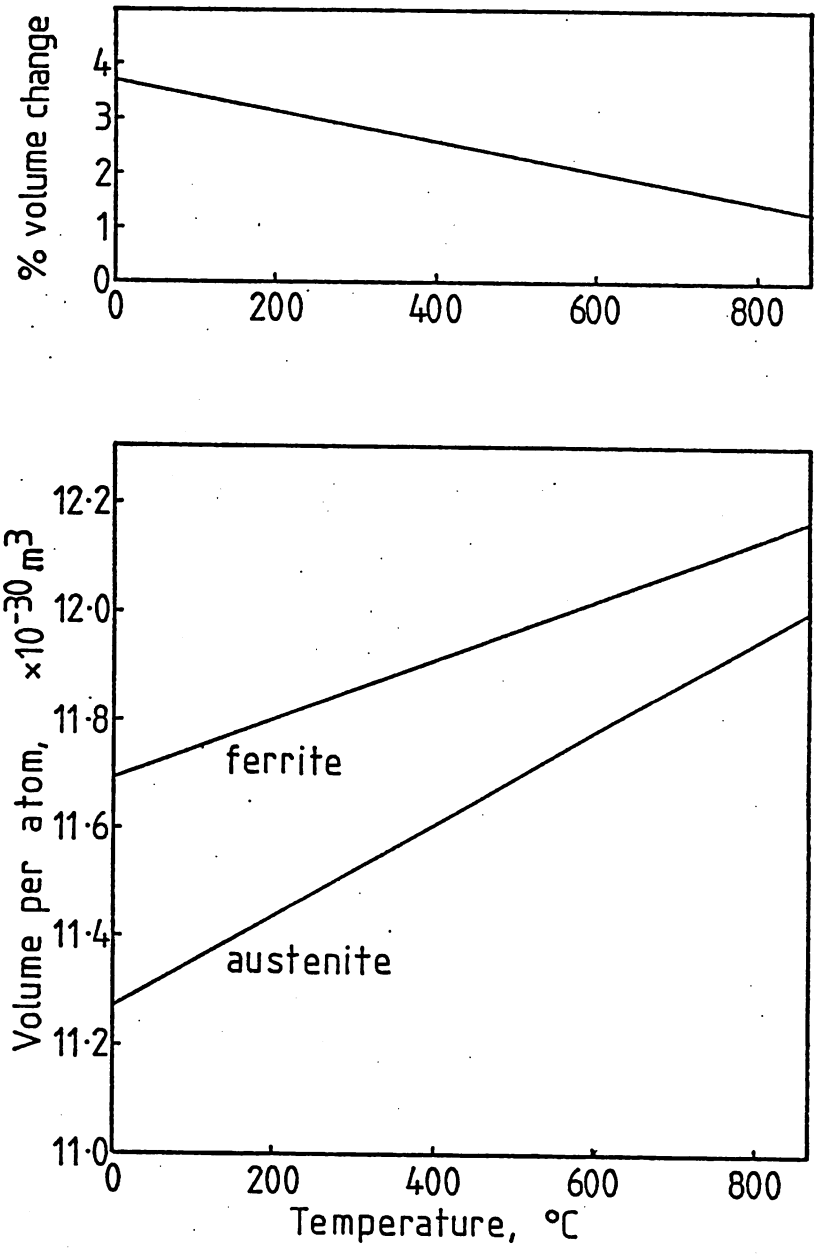

Figure 5.10: Ferrite and austenite atomic volumes and percent volume change on transformation as functions of temperature
(using data from Pearson, 1967)

structures the incidence of dislocation densities higher in the plate-like grains than in the more equiaxed grains (see Figure 5.6) suggests that different transformation mechanisms were operating at the same temperature and that differences in dislocation density were a consequence of mechanism as well as temperature.

Regardless of transformation mechanism it is envisaged that the lattice dislocations were nucleated both at the transformation interface and at grain boundaries when the newly formed ferritic regions impinged. At elevated temperatures when glide and climb are easy, dislocations would be readily attracted to sinks such as grain boundaries or would rearrange to form dislocation networks provided their movement was unimpeded. This would therefore rapidly result in a reduced dislocation density following transformation.

However in a lattice containing precipitate dispersions, the interaction between dislocations and particle strain fields, discussed subsequently, would hinder dislocation movement. Furthermore since the interphase precipitates and the lattice dislocations were generated simultaneously at the transformation front, this dislocation trapping would come into play immediately. Hence the dislocation densities developed during transformation would tend to be preserved.

Note: The lattice dislocations should be distinguished from the dislocation structures accommodating the planar mismatch of the boundaries. The latter are confined to the boundary and are termed intrinsic dislocations or, in the case of a transformation front, transformation dislocations.

5.6 Precipitate strain fields

Strain contrast was observed in bright field TEM around many of the titanium carbide precipitates (Figure 5.11), confirming the presence of strain fields indicated by the X-ray line broadening results. For carbides and nitrides of this type and size, the effect is generally ascribed to coherency mismatch. However, it is evident from the work of Stuart & Ridley (1970) that, regardless of the coherence, a considerable thermal strain can be set up on cooling to ambient temperature due to the relative thermal expansion coefficients of the precipitate and matrix. An examination of the particle coherence is therefore necessary to determine the strain fields present at the transformation temperature.

Calculations on the lattice mismatch and field ion microscope investigations by Freeman (1971a) with Youle have shown that the titanium carbide precipitates retain some degree of coherency in ferrite until they exceed 15 nm diameter which is greater than those in question here. Using the lattice data of Stuart & Ridley it is found that the linear mismatch δ in the $\langle 110 \rangle_{\alpha} // \langle 100 \rangle_{TiC}$ direction on the $\{001\}_{\alpha} // \{001\}_{TiC}$ habit plane of the Baker-Nutting orientation relationship is 5.9% at 800°C and 6.4% at 20°C.

Thus, for the coherent and semi-coherent titanium carbide particles found in these steels there will be coherency strain fields caused by the relative local expansion of the adjacent ferrite matrix, irrespective of temperature, and these strain fields will affect the dislocation-particle interactions.

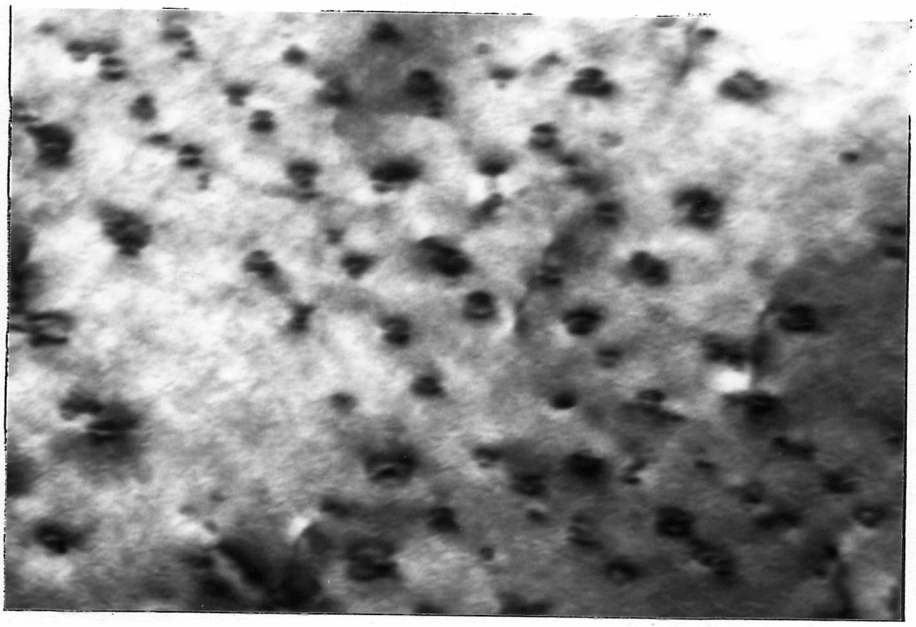

Figure 5.11: Strain contrast surrounding titanium carbide precipitates formed during 800°C transformation

5.7 Dislocation-particle interactions

In general, the interaction forces experienced by dislocations moving through a dispersion of particles may have various origins and recent reviews of the possible mechanisms have been written by Gerold (1979) and Brown & Ham (1971). In the main, these forces are repulsive so an increased applied stress is required for the dislocation both to approach the particles and to pass beyond whether by a cutting or by a bowing mechanism.

Some models, for example the following that of Eshelby (1957) for a spherical coherent particle, depicted in Figure 5.12 show that the interaction force can be attractive. When this is so, the particles are in effect competing for the dislocations against the attraction of dislocation sinks. Figure 5.12a is a vectorial plot of the variation in interaction force with the position of an edge dislocation. An increase in the degree of interface mismatch or a decrease in particle size will also produce increases in the magnitude of the strain-field interaction force. Moreover, the force depends on the sign of the dislocation, as shown in Figure 5.12b and on the dislocation line rigidity.

In the microstructure under consideration here the precise strain-field interactions are more complicated because the particles are non-spherical and the interfacial mismatch varies over the surface of the oriented metal carbides. Qualitatively, however, it is expected that both attractive and repulsive dislocation-particle strain field interactions are present.

Those dislocations attracted to particles may either become trapped close to the interface or, if the particle size is close to the coherency stability limit, the dislocations may interact with the interface causing a partial loss of coherency and a decrease in the attractive interaction

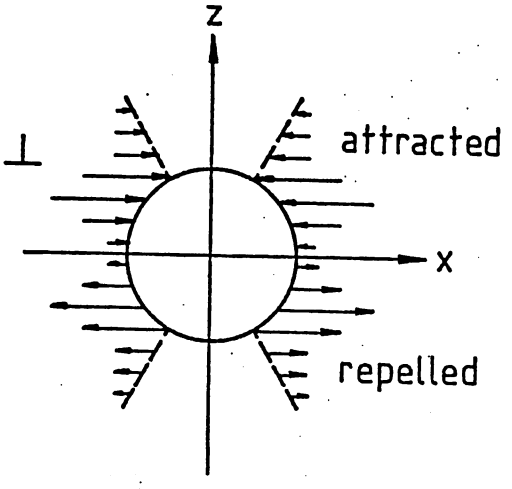

a) Maximum interaction force F on a rigid edge dislocation. The lengths of the arrows mark the values of F for positions of the dislocation contacting either the sphere or the dashed line.

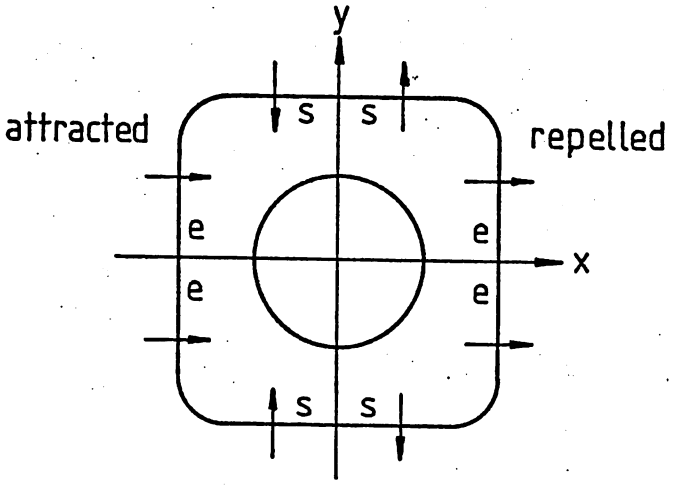

b) The sign of the force F on a dislocation loop for z>0
s = screw, e = edge

Figure 5.12: Interaction force between a dislocation and the coherency strain field of a spherical particle (ϵ>0) (after Gerold 1979).

force. This mechanism was suggested by Dunlop & Honeycombe (1975) in explaining the bimodal coarsening of carbides during long-term ageing. They postulated that dislocation trapping allowed enhanced coarsening by pipe diffusion and that the dislocations escaped when the precipitates became large enough to lose coherency.

Various criteria can be used to determine quantitatively the state of coherency of interfaces. According to Brooks (1952) the stability limit for complete coherency occurs at a size $\frac{3b}{2\delta}$ where $\underline{b}$ is the interfacial dislocation Burgers vector given by the ferrite lattice vector 0.287 nm, and δ is the misfit parameter. On the $(001)_{V,TiC}$ habit plane at 800°C this predicts a value of 6.4 nm in the $[110]_{\alpha}$ direction and 1.2 nm in the $[001]_{\alpha}$ direction. An alternative criterion by Smith (1966) results in critical sizes of half these values. For comparison, the coherency limit determined experimentally by Youle was around 3 nm with semi-coherency found up to 15 nm.

It can therefore be estimated that in the isothermally transformed specimens studied here, containing particle sizes up to approximately 10 nm, all would contain coherency strain fields of some magnitude which would be capable of attracting and trapping dislocations at the transformation temperature despite the ease of climb and cross-slip through thermal activation. The coherency strain fields would contribute to X-ray line broadening, in a similar manner to dislocation strain fields. The effect would be greater for lower transformation temperature structures because of the smaller particle size. It would also be expected that interactions would occur between the coherency strain fields and those of interstitial atoms.

The interactions between dislocations and the titanium carbide precipitates are observed in many of the micrographs presented in this dissertation, particularly in Chapters 3, 5 and 7. In the current chapter, specific examples are labelled in Figure 5.5 illustrating

dislocations zig-zagging from one precipitate to the next, the attraction of the precipitates apparently dominating the dislocation line tension forces.

5.8 Dislocation distributions after deformation

The effects of room temperature tensile deformation on the X-ray line profiles of the 800° and 650° isothermally transformed structures are shown in Figures 5.13 and 5.14. The corresponding increases in strain breadth are displayed graphically in Figure 5.15. The more rapid increase in lattice strain of the 650° structure compared with the 800° structure correlates with the higher work hardening rate of the former.

Micrographs of the 650° structure in Figure 5.16 show that after 5% strain both equiaxed and elongated ferrite grains were heavily dislocated, the dislocations appearing to form clusters and in some areas cell walls (W). Walls of dislocations are more easily seen in the coarser microstructures originating from higher transformation temperatures. Dark field analysis of a specimen transformed at 700°, Figure 5.17, showed that the dislocation walls are associated with the sheets of interphase precipitates, as is indicated qualitatively by the wall separation.

The phenomenon was investigated further in a specimen which had been deliberately slow cooled at 25°C per minute through the transformation range to produce a relatively coarse interphase precipitation. The sheet spacing was between 150 and 300 nm. After 2% room temperature strain, dislocation walls were beginning to form (Figure 5.18). After 7.5% strain, shown in Figure 5.19, the walls have become broader and cross-linking dislocation tangles have been produced.

It is thus evident from the micrographs that the sheets of fine titanium carbide precipitates are acting as obstacles to dislocation

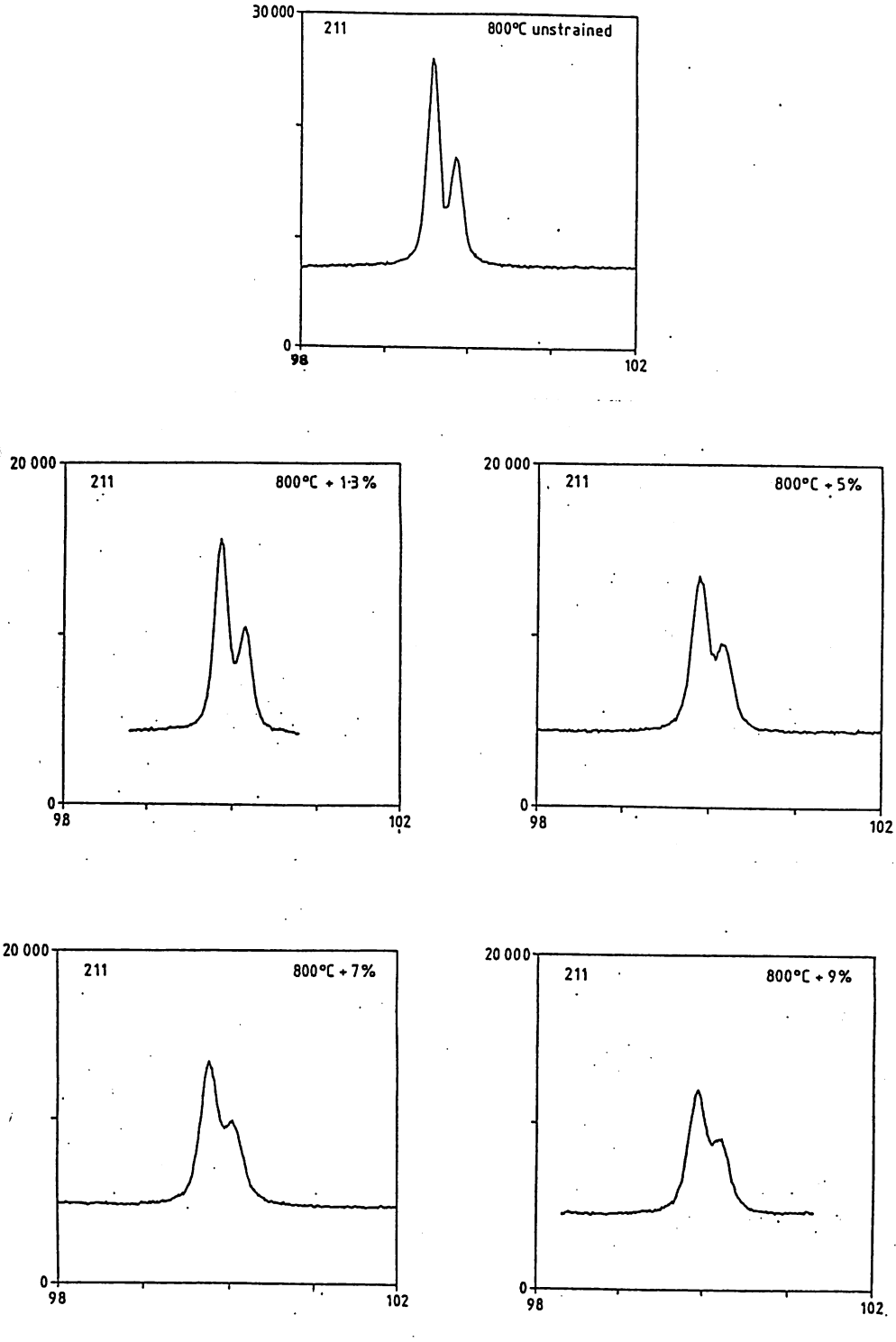

Figure 5.13: Effect of deformation on the X-ray line profile of 800° structure

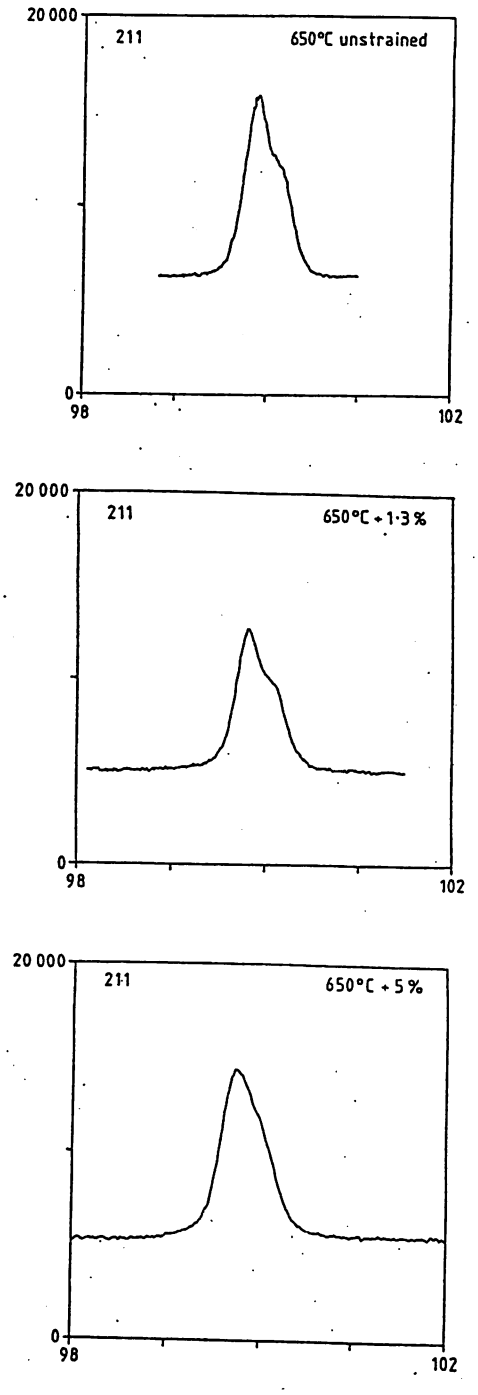

Figure 5.14: Effect of deformation on the X-ray line profile of 650° structure

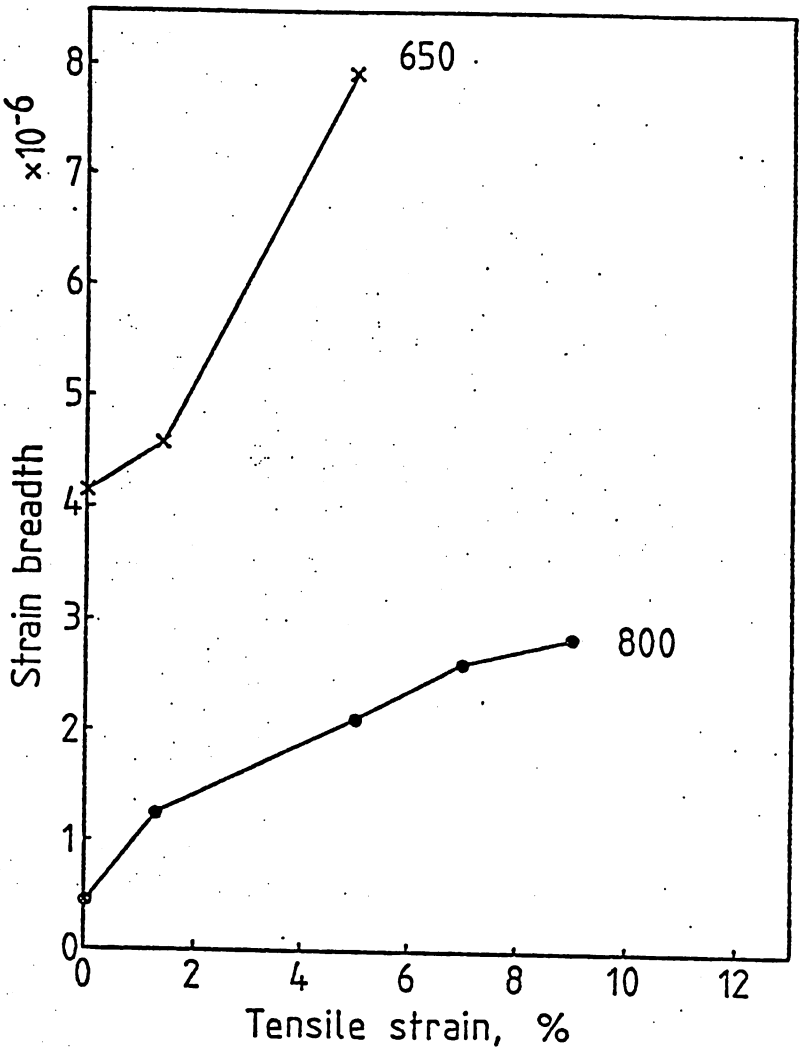

Figure 5.15: Effect of tensile deformation on strain breadth in structures transformed at 800° and 650°C

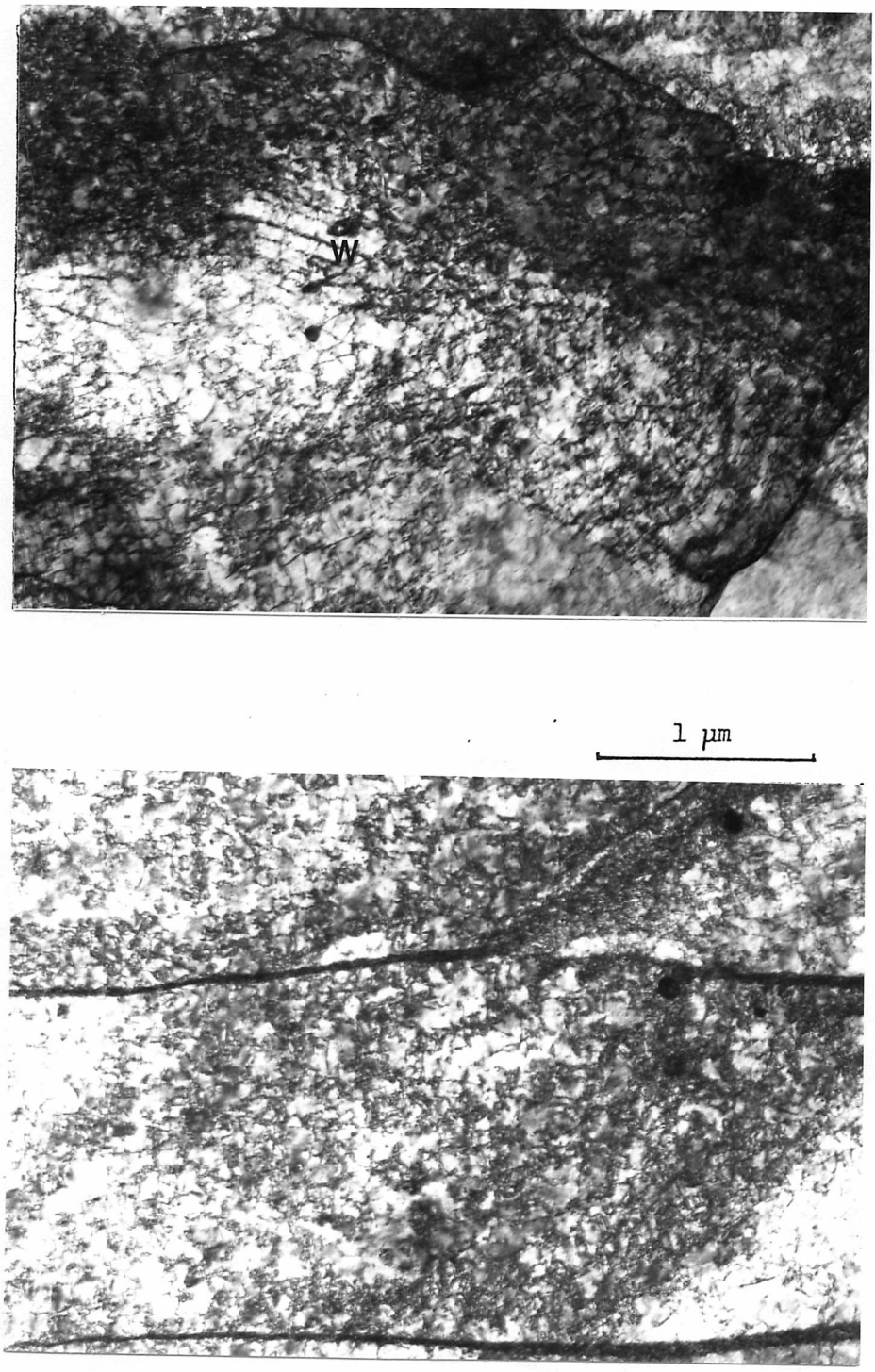

Figure 5.16: Dislocation clusters and walls (W) in 650° structure after 5% strain

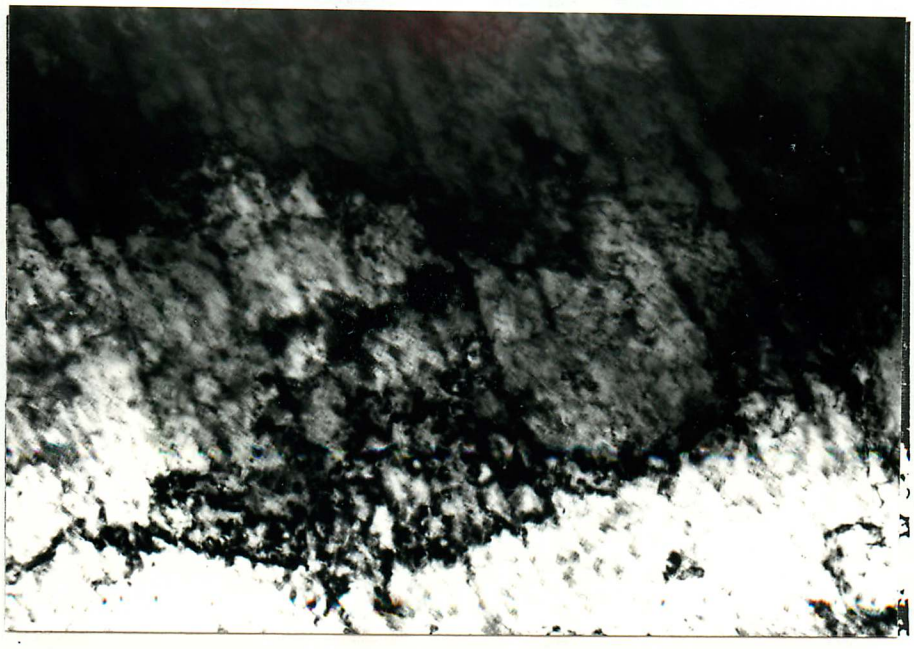

a) Bright field

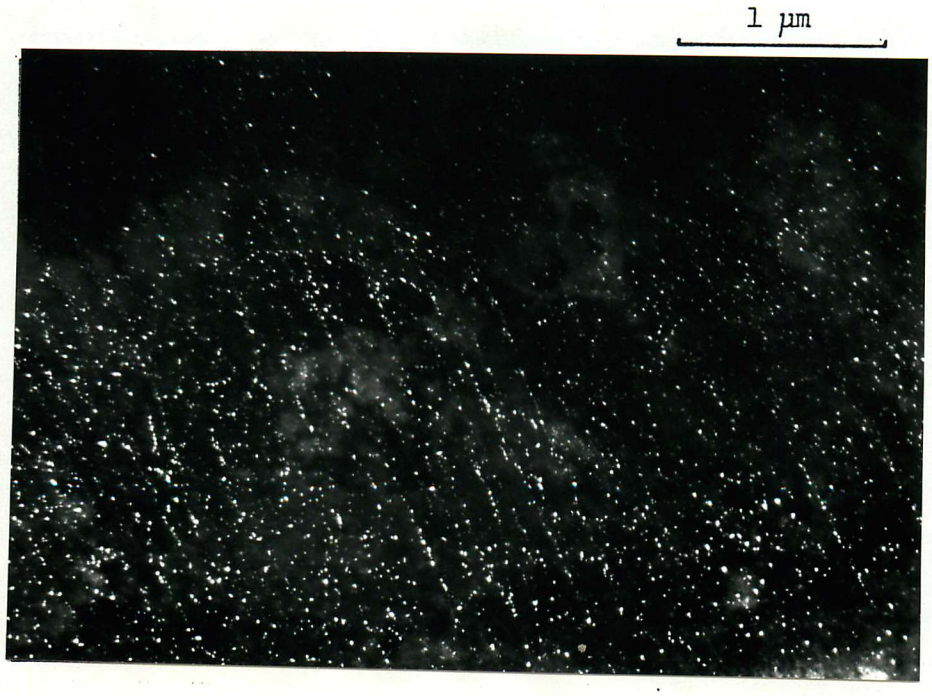

b) Precipitate centred dark field

Figure 5.17: 700° structure after 6% strain

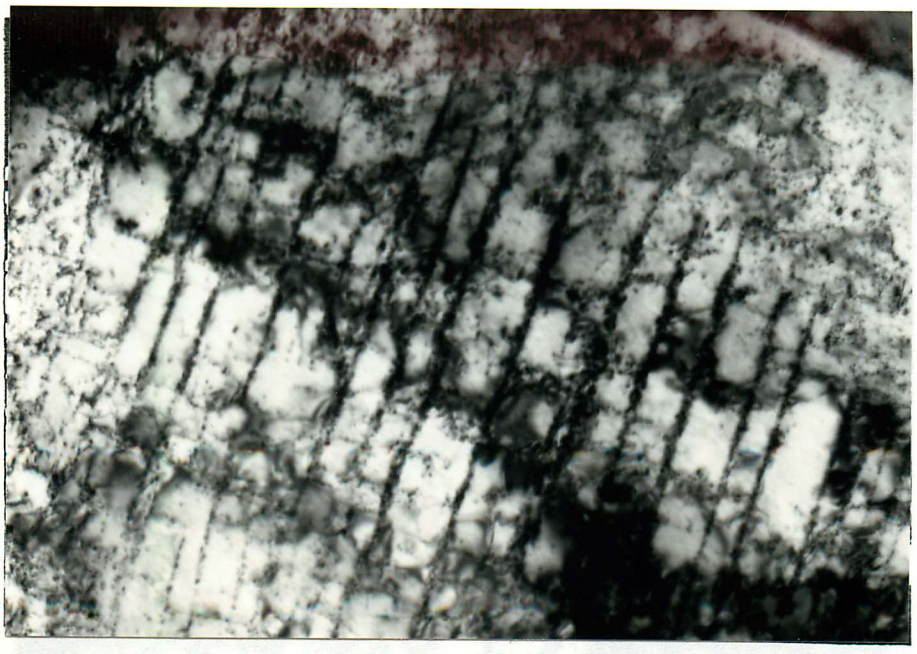

a) Bright field

1 μm

b) Precipitate centred dark field

Figure 5.18: Coarse microstructure produced by slow cooling; strained 2%

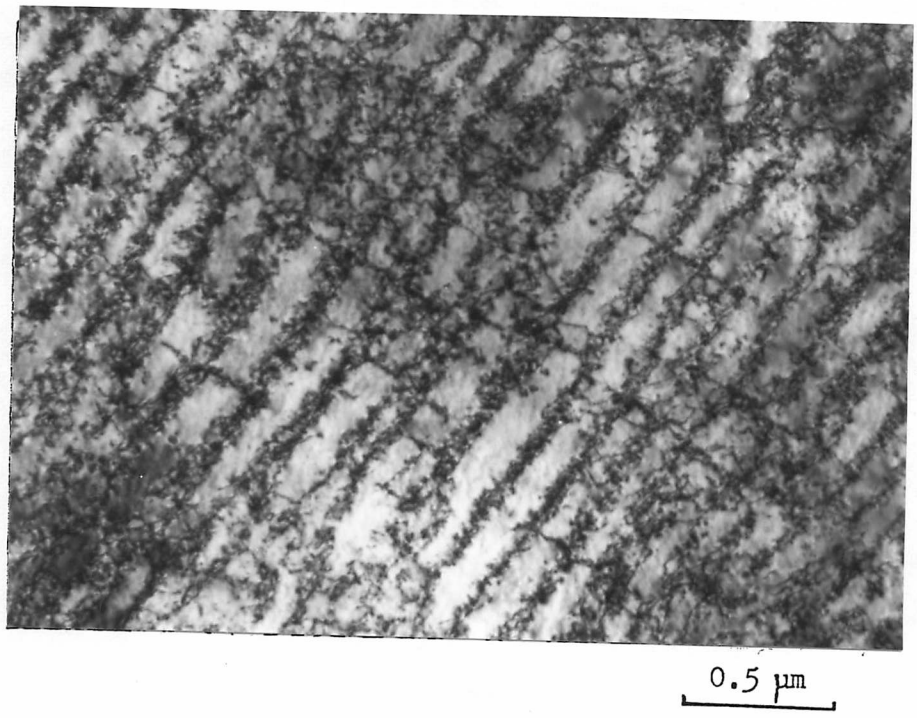

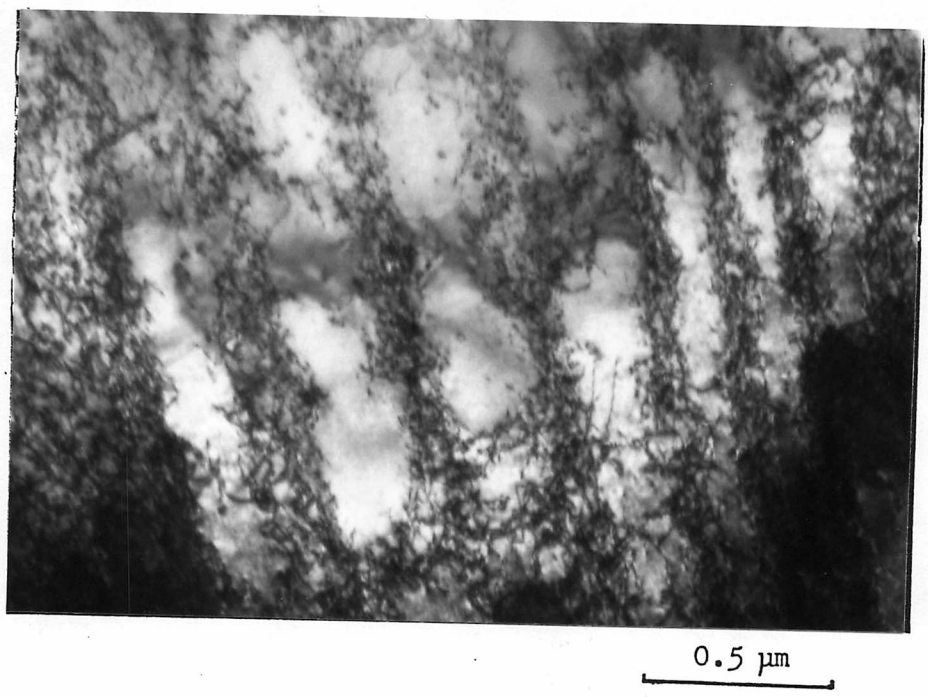

Figure 5.19: Dislocation walls and cells in coarse microstructure; strained 7.5%

motion and dislocations are either pinned by the precipitates or must bypass by a bowing mechanism leaving behind dislocation loops. In all the specimens containing interphase precipitation the sheet morphology was found to be extremely stable to deformation. Even after the 800° structure had been strained 9% to fracture, the parallel sheets were visible, for example in Figure 5.20. This gives further evidence that dislocations are bowing rather than shearing through the particles.

If X-ray and electron microscopy results are compared for the heavily deformed 800° structure, it is found that although a high dislocation density is observed after 9% strain, the X-ray broadening is still less than that for the undeformed 650° structure. This is probably caused by the greater proportion of X-ray broadening contributed by particle strain fields, rather than dislocation strain fields in the lower temperature microstructure arising from the greater coherency and finer particle sizes compared with those in higher temperature microstructures. Furthermore, deformation would tend to reduce coherency strains due to the reaction of dislocation loops with metastable particle interfaces.

5.9 Dislocation distributions after isothermal annealing

In Section 4.10 the effects of 60 000 s isothermal annealing, in addition to the original 1000 s at the transformation temperature, on the microstructure and yielding behaviour were reported.

Electron microscopy revealed that the mixed grain structure was retained in the 650° specimen and furthermore it appeared that the dislocation loss was greater from the platelike grains than from the more equiaxed grains, resulting in a more homogeneous overall dislocation distribution. Figure 5.22, of a platelike grain after annealing permits a comparison with Figure 5.6 of the structure before annealing. A large

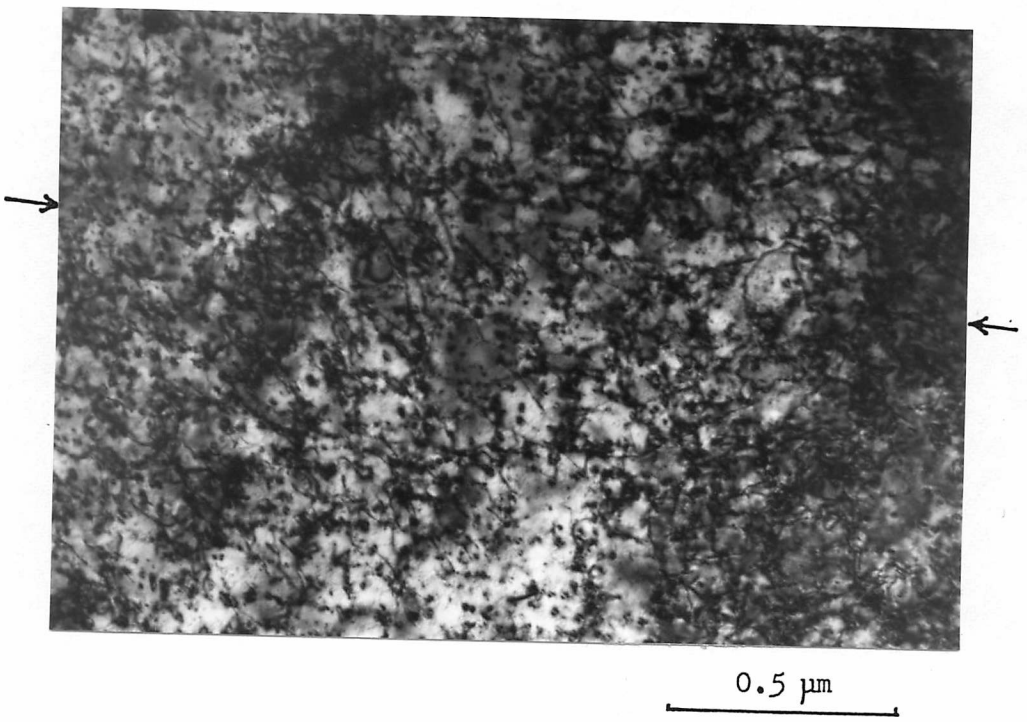

Figure 5.20: Persistence of precipitate sheets in 800° structure; strained 9%

difference remained between the X-ray broadening of the 800° and 650° microstructures after annealing. Figure 5.21 presents the line profiles and Figure 5.22 plots the strain breadths from the data tabulated in Appendix B. Both 800° and 650° structures showed some decrease in strain broadening with the 650° structure exhibiting the larger proportional (and absolute) change. These reductions in strain broadening are taken to be primarily caused by a lowering of the average dislocation density. The contributions from precipitate strain fields and grain boundaries would be expected to remain approximately constant in view of the observed stability of the carbides and of the ferrite grain structure.

Figure 5.23 is a micrograph of the annealed 800° structure. The sheets of interphase precipitation are still evident and a large number of dislocations appear to be pinned within the dispersion. It is therefore envisaged that the trapping mechanisms postulated to be occurring directly after transformation will continue to operate during annealing. Moreover, because of this dislocation retention, the annealed 650° specimen still shows as much line broadening as the as-transformed 700° sample, and the annealed 800° specimen still considerably more than the calibration specimen.

The persistence of line broadening after 60 000 s annealing also lends weight to the argument that dislocation trapping rather than solely the short time (1000 s) at temperature caused the dislocation abundancy in the as-transformed structures.

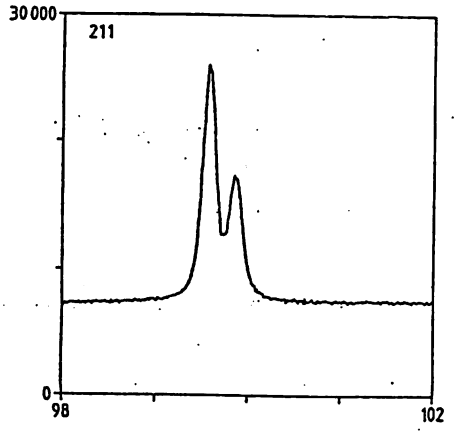

a) 1000 s 800°

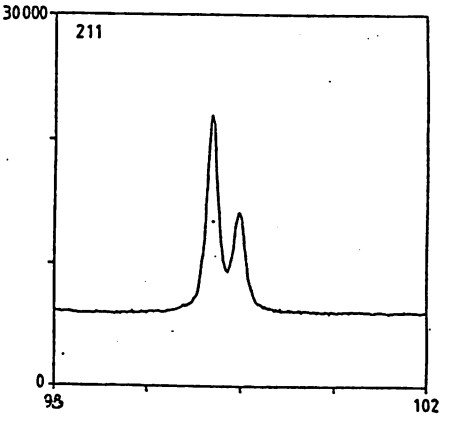

b) (1000 + 60 000) s 800°

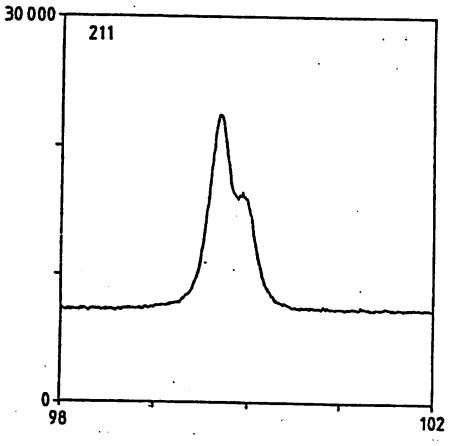

c) 1000 s 650°

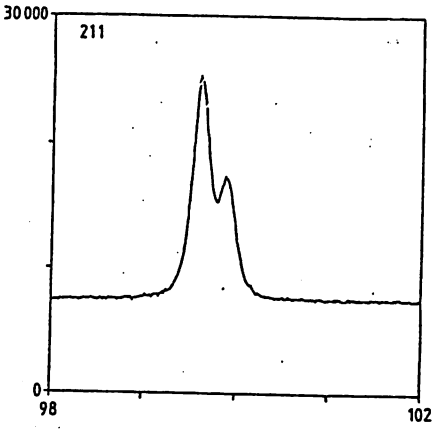

d) (1000 + 60 000) s 650

Figure 5.21: Effect of isothermal annealing on X-ray line profiles

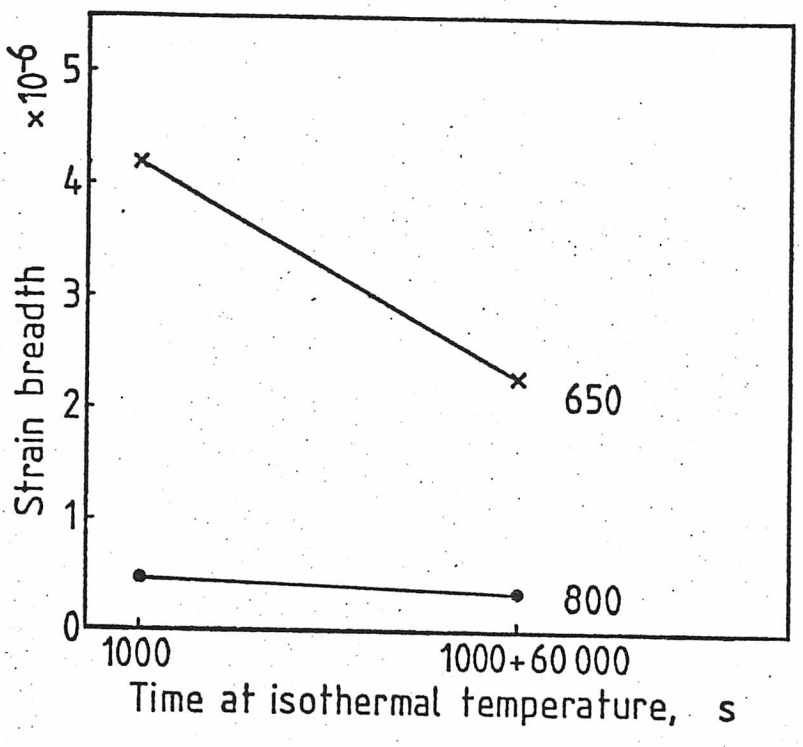

Figure 5.22: Effects of annealing time on strain breadth in structures isothermally transformed at 800° and 650°.

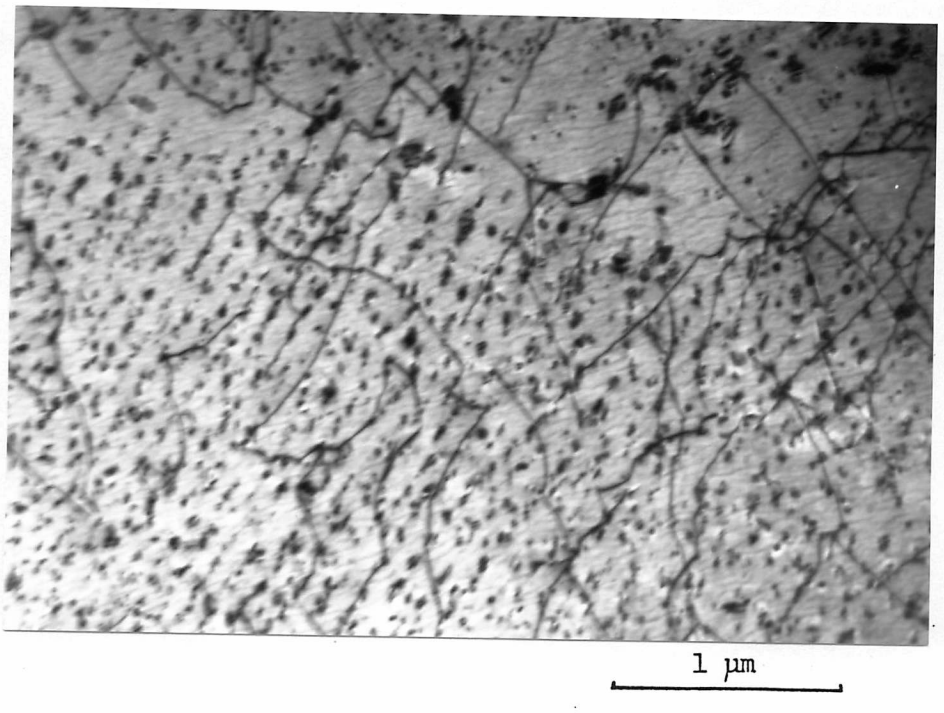

Figure 5.23: Dislocation density remaining in equiaxed after isothermal annealing of 800° structure

5.10 Summary

1. Using transmission electron microscopy, average dislocation densities of greater than 10^{14} m^{-2} were measured in all the isothermally transformed specimens, which is higher than would be found in a simple ferrite after the same heat treatments. The total degree of short range lattice straining, including that contributed by dislocations, was measured by X-ray line broadening.

2. Comparison of microstructures formed at different temperatures in the range 800° to 650°C revealed that at the lowest transformation temperature the average dislocation density was the highest and in addition the dislocation distribution was the most inhomogeneous. Equiaxed grains tended to have lower dislocation densities than platelike grains.

3. The mechanisms of dislocation creation during transformation and the subsequent retention of dislocations in the lattice have been considered. The greater transformation expansion and diminished thermal activation for movement led to higher dislocation densities at lower temperatures. At a given temperature, differences in dislocation density may have resulted from different transformation mechanisms, higher densities arising from mechanisms involving shear.

It is postulated that not only is dislocation movement obstructed by the fine interphase precipitates but that dislocations can be trapped in the lattice by the attractive interaction between the strain fields of dislocations and particles.

4. Theoretical analyses and observations of dislocation behaviour in

lightly deformed material indicate that dislocation bypass occurs by bowing rather than particle shearing. As deformation proceeds, dislocation walls build up around the sheets of interphase precipitates. The walls become broader and link to form dislocation cells of similar size to the interphase sheet spacing. The persistence of the sheet morphology of the precipitates after heavy deformation provides evidence that the particles are not shearing.

5. Isothermal annealing of the undeformed structures slowly lowered the average dislocation densities at each temperature. Considerable differences between the X-ray strain broadening of the 800° and 650°C structures remained.

CHAPTER SIX

DISTRIBUTION OF ELEMENTS

6.1 Introduction

This chapter describes the results of microanalytical work undertaken to investigate the distribution of elements throughout the microstructure of the isothermally transformed specimens. In view of the importance of interstitial solutes in the study of yield behaviour, the techniques of atom-probe microscopy were used to enable compositional variations including carbon and nitrogen to be examined on the fine scale (0.1 to 1.0 nm) of the interphase precipitates.

Several studies of ultra fine precipitation in steels have been made by previous workers using both field ion microscopy (FIM) and atom-probe field ion microscopy: most are mentioned in the recent review paper by Brenner & Miller (1980). Some of the earliest work of relevance was by Schwartz (1968). This included studies of isothermally transformed Fe-2V-0.2C using FIM to measure particle sizes. Atom probe FIM was used by Dunlop & Turner (1975) to examine the composition of mixed vanadium-titanium carbides.

Of particular interest to the present study are the investigations by Youle (1972) and Youle, Ralph, Freeman & Honeycombe (1974) into the ageing behaviour of isothermally transformed Fe-0.5Ti-0.1C. FIM was employed to examine the orientation, size, shape and coherency of the interphase precipitates. The results of Youle and Dunlop & Turner are discussed later in this chapter.

For the present study an imaging atom probe combined with a high mass-resolution energy compensating time-of-flight spectrometer (Waugh & Southon 1979) was employed; The author is grateful to Dr A R Waugh for his assistance with the operation of the instrument.

The interphase precipitate composition, the matrix composition and the composition profile of the precipitate/matrix interface were investigated. In addition, a small number of electron probe X-ray microanalyses were performed using energy dispersive and wavelength dispersive detection systems to investigate the larger 1 to 5 μm particles.

6.2 Experimental method

Field ion specimens were prepared (see Appendix A) from tensile specimens of Alloy 2 (0.07C-0.23Ti) isothermally transformed at both 800° and 700° which had exhibited discontinuous and continuous yielding respectively.

The operation of the atom probe is described in detail in several papers; for example, Andren & Nordren 1979 and Waugh & Southon 1979. For this study the instrument was used in several modes:

i) as a conventional field ion microscope using neon imaging gas to obtain information on the positioning of precipitates in the specimen tip and the crystallographic orientation of the specimen;

ii) as an imaging atom probe where the desorption image, gated for a selected mass-to-charge ratio of the field-evaporated ions, enabled the spatial distribution of a particular species to be observed; and

iii) as a microanalyser, the mass spectrometer providing direct compositional analysis with single ion sensitivity on probing through the specimen.

6.3 Interphase precipitate composition

Using the atom probe with an effective probe hole diameter of approximately 3 nm it was possible to determine the composition of individual precipitates without interference from surrounding matrix atoms. This was especially true for the larger particle sizes, up to 10 nm, found in the specimen transformed at the higher temperature (1000 s 800°). The second advantage in examining larger particles is the greater statistical confidence in interpretation with longer data chains.

Figure 6.1a is a field ion micrograph showing a precipitate in the 800° specimen, oriented on the (200) ferrite pole as indicated in the schematic diagram of Figure 6.1b. The particle was then positioned under the probe hole and about 1500 ions were collected, the entire chain taken from within the particle. The mass-to-charge (m/e) spectrum is given in Figure 6.2. It can be seen that the vast majority of ions were either carbon or titanium, present in approximately equal numbers. A logarithmic scale is used to accentuate any small peaks such as iron.

Identification cannot be completely unambiguous because of the spread of each peak, but a computer program was used to identify the ions individually in the data chain by setting mass-to-charge windows for each element. Discarding the neon imaging-gas count, the compositional analysis was found to be 49 at%Ti, 51 at%C and less than 1 at%Fe. This corresponds to a titanium to carbon atomic ratio of 0.94. The quantity of nitrogen (m/e=14) was negligible compared with carbon. The errors in the titanium and carbon values arising from the choice of window and statistical limitations are estimated to be 5 at%.

Several hundred atoms are removed in random order for each plane of material probed; hence the position of an individual atom in the data chain relative to its neighbours cannot be directly related to its

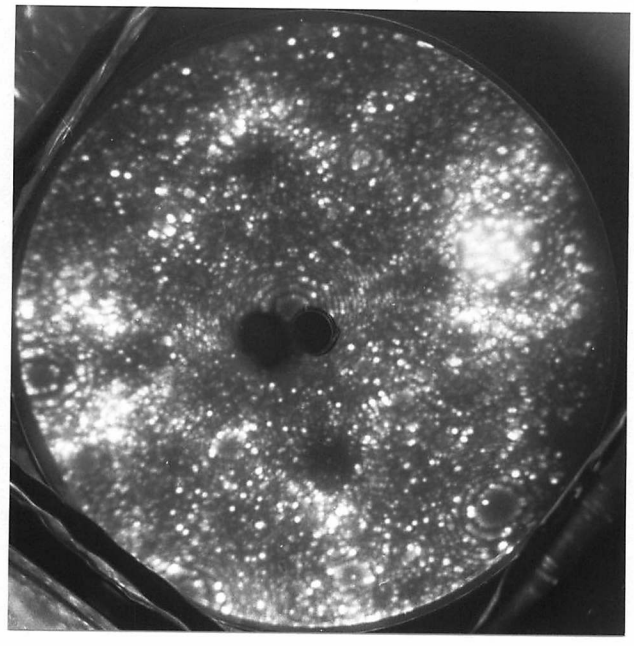

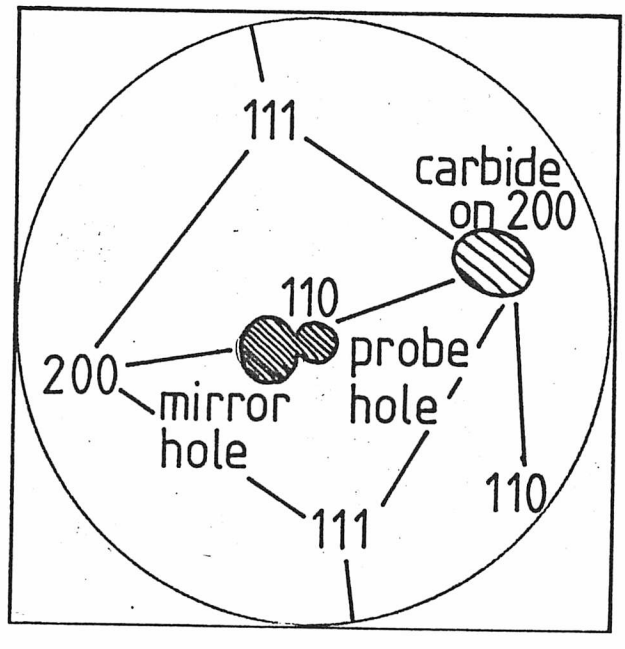

Figure 6.1: Field ion micrograph showing titanium carbide precipitate on (200) ferrite pole; transformed at 800°C

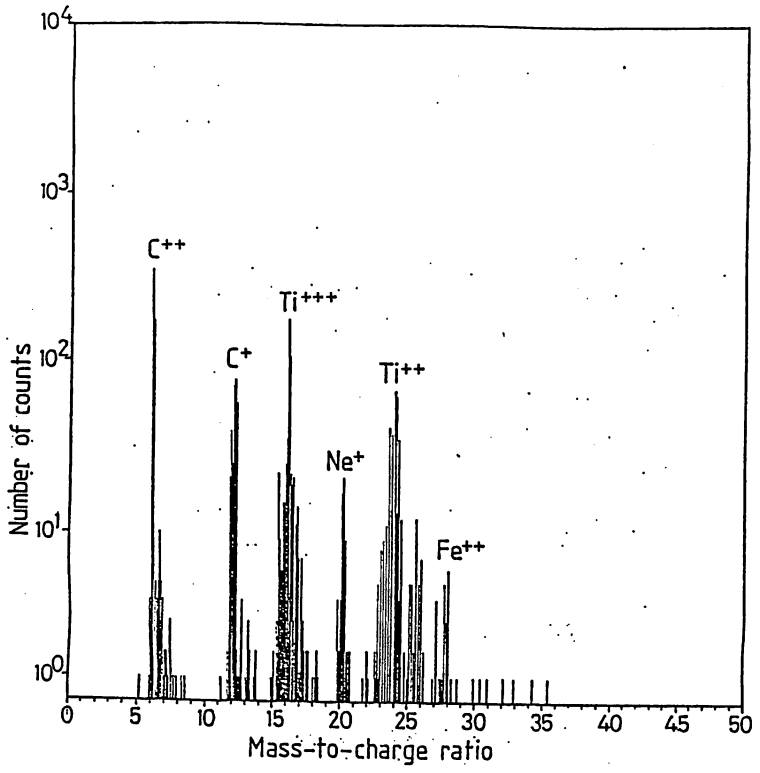

Figure 6.2: Mass-to-charge spectrum of the titanium carbide precipitate of Figure 6.1

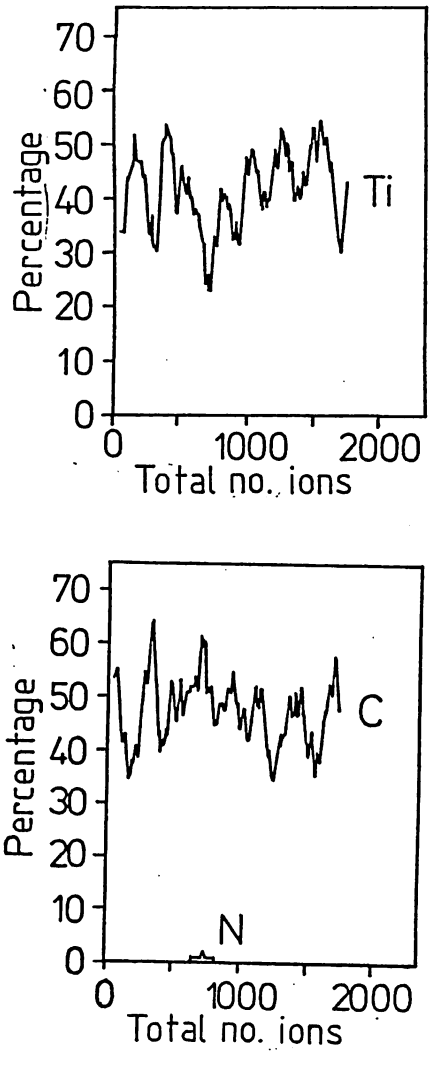

Figure 6.3: Composition profile through the precipitate of Figure 6.1

position in the specimen. A running mean was therefore calculated to obtain a compositional profile (Figure 6.3) taking samples of 100 ions in steps of 10 ions along the data chain. The titanium and carbon levels were found to oscillate in antiphase with a periodicity of approximately 250 ions. This is consistent with the number of ions removed per plane when using a 3 nm probe hole. Since the probing direction was normal to the $(100)_{\alpha}$ planes and the carbide is expected to exhibit a Baker-Nutting orientation relationship with the ferrite, the probing direction through the carbide would be normal to either the $(110)_{TiC}$ or $(100)_{TiC}$ planes. In the NaCl crystal structure both these sets of planes have equal densities of the two species, but as titanium has a greater evaporation energy than carbon it is to be expected that the carbon will tend to be removed first when each new plane is exposed.

The specimen transformed at 700° contained particles of a smaller size, 3 to 5 nm, corresponding to just 2000 to 5000 atoms per particle. The data chains, therefore, could be only short so even if the probe hole did exclude all the matrix atoms, quantitative analysis of such particles would be less accurate. Two particles were analysed and it was found that they contained predominantly titanium and carbon in similar proportions, and negligible nitrogen.

Three sizes of interphase particles were examined by Dunlop & Turner (1975) in their study of mixed vanadium-titanium carbides: $\sim$2.0 nm; 5 to 6 nm; and $\sim$ 20 nm. The largest particles were found to contain just vanadium, titanium and carbon but in the others iron was discovered additionally. In their study, as in the present one, the detection of iron may be attributable to the surrounding matrix.

The metal to carbon ratios obtained by Dunlop & Turner were in the range 1.2 to 1.4, and in the present study of titanium carbide 0.95 ± 0.25.

These are consistent within error with the range $TiC_{0.98}$ to $TiC_{0.3}$ obtained by Storms (1967) in single crystal bulk carbides, corresponding to titanium to carbon ratios of 1.02 to 3.33.

6.4 Matrix composition

Data chains of 5000, 8500 and 10500 ions were collected on probing through the ferrite matrix of the 800° specimen. Figure 6.4 shows the spectrum from the latter data chain. The Mn^{++} peak (m/e = 27.5) cannot be resolved between the Fe^{++} isotopes. As before, the spread of the peaks prevents unambiguous interpretation: it appears that there was no titanium or carbon present. The whole specimen tip was examined for carbon by gating for a C^{++} desorption image but no ions were detected.

Data chains of 1000, 1500 and 1550 ions were collected from the matrix of the 700° specimen. An additional magnetic deflector had produced improved resolution of the spectrum (Figure 6.5) so that it can be stated explicitly that no carbon, nitrogen or titanium were found. Blank carbon desorption images confirmed tha absence of the element. No defects (e.g. dislocations or grain boundaries) were found in any of the matrix examined.

In view of the small volume of matrix probed and the low overall levels of carbon and nitrogen in the alloy, it is not surprising that the defect-free areas of matrix were found to be clean of interstitial elements; even if the carbon had been uniformly distributed, the 0.07 wt% (0.33 at%) would yield only 3 atoms per 1000 which, although low, should be detected reliably by the atom probe.

The high affinity of titanium for carbon, resulting in the formation of titanium carbide removed all the titanium from solid solution and reduced the matrix level of carbon. It is anticipated that any remaining

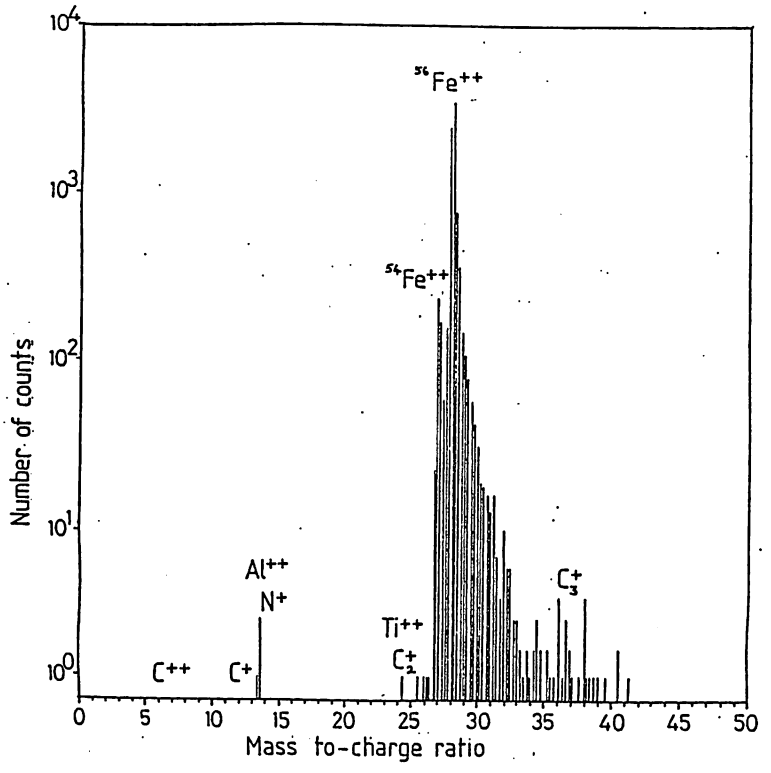

Figure 6.4: Mass-to-charge spectrum of matrix; transformed 800°C

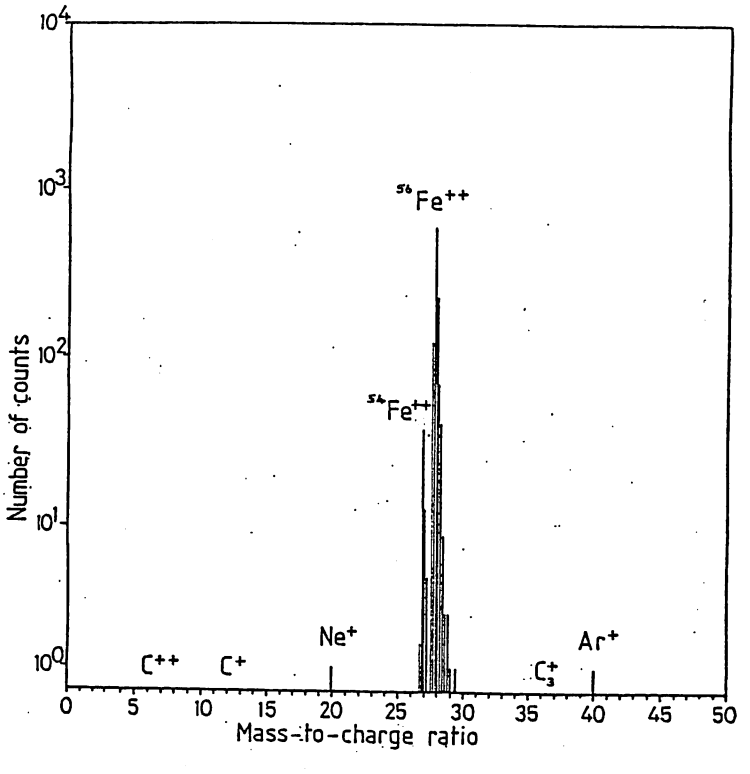

Figure 6.5: Mass-to-charge spectrum of matrix; transformed at 700°C

interstitial atoms would have segregated to lower energy sites such as grain boundaries and dislocations. It was unfortunate from the point of view of examining the distribution of interstitials that during the present atom probe work dislocations were not encountered despite the high dislocation density after deformation.

6.5 Precipitate-matrix interfaces

For the 800° specimen the same particle was examined as described in Section 6.3. 3000 ions were collected on probing from inside the carbide out into the matrix. The composition profile (Figure 6.6) showed the steady decrease in titanium and carbon over a distance of approximately 1000 ions, equivalent to 4 planes, the balance consisting of iron. The carbon persisted into the matrix for a greater distance than did the titanium and it should be mentioned that the effect may be more pronounced than is indicated in the Figure because the two lone titanium ions identified after a total number of approximately 1500 ions both had m/e = 24 which can also correspond to C_2^+. When the numbers of different types of carbon ion collected in the particle bulk are compared with those in the tail beyond the interface (Table 6.7) it is found that whereas most of those in the carbide bulk evaporated singly, those outside were more often detected as multiple ions.

Four carbide-matrix interfaces were probed in the 700° specimen; the composition profile of one is presented in Figure 6.8. In each case carbon was found a further distance into the matrix than titanium and was often detected as multiple ions.

It has been noted by Waugh (1978) that the metal and carbon desorption images of carbides in steel do not coincide, the carbon producing a halo. This effect has been explained by disturbances in the

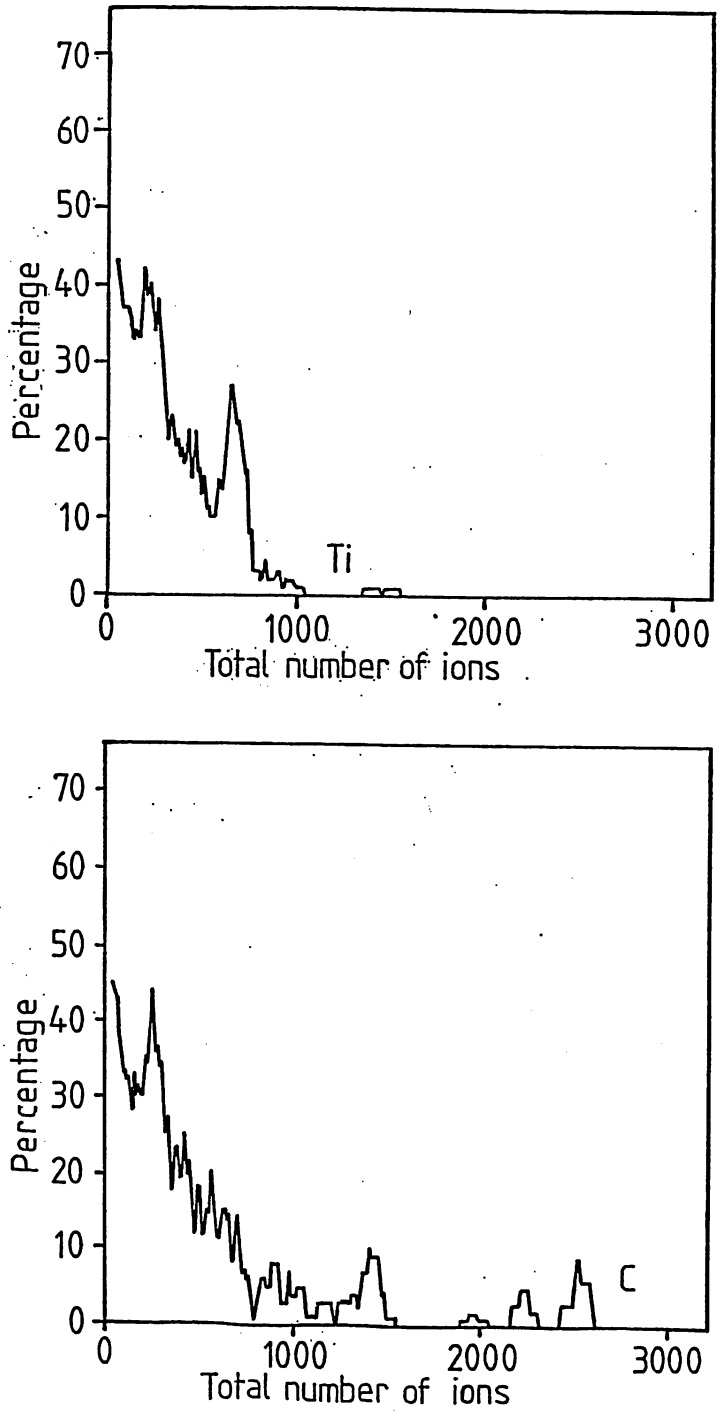

Figure 6.6: Composition profiles across the precipitate-matrix interface; transformed at 800°C

Bulk of carbide

Mass-to-charge ratio, m/e	6	12	18	36
ion species	C^{++}	C^{+}	$3C^{++}$	$3C^{+}$
no. ions detected	558	196	4	1
no. atoms	558	196	12	3
% of total C	72.6	25.5	1.6	0.4

Matrix close to carbide

Mass-to-charge ratio, m/e	6	12	18	36
ion species	C^{++}	C^{+}	$3C^{++}$	$3C^{+}$
no. ions detected	4	1	3	1
no. atoms	4	1	9	3
% of total C	23.5	5.9	52.9	17.6

Table 6.7: Relative proportions of carbon ion species

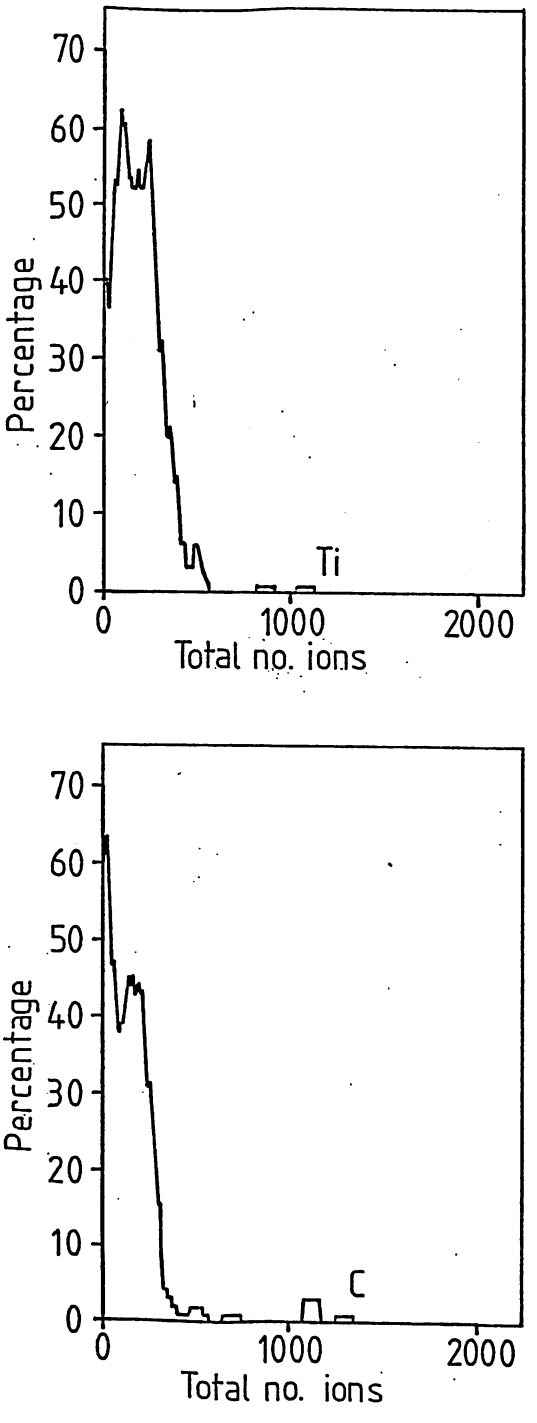

Figure 6.8: Composition profile across the precipitate-matrix interface; transformed at 700°

trajectories of the carbon ions in the strong electric fields around the specimen tip. However when examined here by the technique of quantitative probing, the halo of carbon atoms is still apparent.

The effect could be a consequence of carbon atoms which have migrated across the specimen surface, or from contamination, but in either case one would expect a similar result when examining the matrix alone. This is not so. Hence it is proposed that the carbon halo effect is real.

Transmission electron micrographs (e.g. Figure 5.11) clearly show strain contrast around precipitates formed at 800° C. This observation is consistent with the results of Youle (1972) who found using FIM that titanium carbide particles of < 3 nm were completely coherent, that between 3 and 15 nm they were partially coherent, and that coherency with the matrix was lost at sizes greater than approximately 20 nm. The two specimens in the present study contained interphase carbides in the partially coherent size range. The carbides were therefore surrounded by positive strain fields. Just as interstitial atoms are attracted by the strain fields of dislocations so would they be attracted to these expanded regions of matrix.

It is generally found in atom probe work that carbon atoms in a ferrite matrix are detected as multiple ions whereas those in an ionic compound are collected singly. Detection of the halo atoms as multiple ions therefore lends weight to the argument that they are present in the matrix.

The carbon atom configuration envisaged is similar to that of nitrogen proposed by Ronay (1981) in relation to the early stages of precipitation in nitrided titanium steels: namely that the strain energy barrier for the nucleation of titanium nitride is minimised by its co-precipitation with Fe_4N.

It is appreciated that with the small number of particles examined here, and other factors not possible to consider fully such as

i) the crystallography of the particle-matrix interface;

ii) the thermodynamics involved; and

iii) the possible presence of dislocations pinned by the carbides,

the proposed explanation for the apparent carbon halo can remain only tentative.

6.6 Effect of transformation temperature on local composition

Using the atom probe, no obvious differences could be discerned which could directly explain the differences in yielding behaviour between the specimens transformed at 800°and 700°. The interphase precipitates in the two specimens had similar compositions and structures although they were of a different size and spacing. However, the carbon haloes surrounding the carbides appeared to be more pronounced in the 800° specimen which yielded discontinuously. This could be taken as an indication that there was also more carbon available in the matrix of the specimen for dislocation pinning. In future atom probe work it would be informative to determine whether carbon haloes are present around precipitates when the overall carbon content is below the titanium carbide stoichiometric limit.

6.7 Composition of coarse particles

Angular particles up to 5 μm across were detected by optical and transmission electron microscopy in all the alloys investigated regardless of the heat treatments. The coarse size and spacing of these particles procluded the use of atom probe techniques; electron probe techniques provided adequate spatial resolution (1 to 2 μm) for the brief examination undertaken.

The energy dispersive X-ray microanalysis (EDAX) was performed using TEM foils prepared in the usual way. The eight particles examined, between 0.5 and 2 μm across, were found to have very similar compositions. The spectrum of characteristic X-ray energies of one of the particles is given in Figure 6.9: the elements identified were titanium, sulphur and iron. Elements lighter than sodium cannot be detected by the technique so the carbon and nitrogen levels were unknown. It was assumed that the iron detected was from the matrix. Conversion of the relative intensities to atomic ratios (Table 6.10) showed that in each case there were approximately twice the number of titanium atoms as sulphur atoms in these particles, consistent with the existence of titanium carbosulphide $Ti_4C_2S_2$.

The wavelength dispersive system of a Microscan was employed to analyse for carbon, nitrogen, sulphur and titanium in six particles of approximately 5 μm size. Polished bulk samples were used and care was taken to avoid surface contamination. Figure 6.11a presents line traces across two adjacent particles and Figure 6.11b across a single particle. The peak heights cannot be compared directly as quantitative measures of the composition because the sensitivity of the detector is different for each element. However the distribution of the elements can be seen. There was a tendency for the nitrogen to be concentrated in the centre of the particles and the sulphur at the edges. This is particularly noticeable in Figure 6.11b.

The presence of these coarse particles in quenched as well as isothermally transformed microstructures confirms that they were precipitated into the liquid or austenite. The more stable titanium nitride would precipitate first, thus removing all the nitrogen from solution, and the isostructural sulphide and carbide compounds would

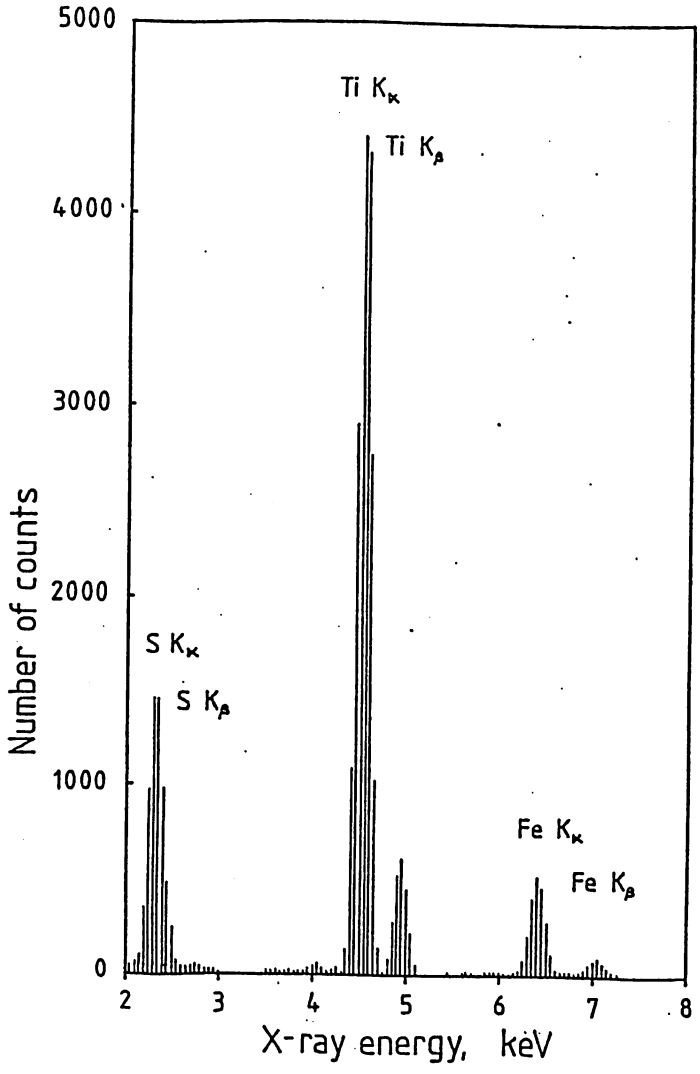

Figure 6.9: Spectral microanalysis of a 1 μm particle

	Ti	S	Fe
normalised intensity	69.5	21.5	9.0
approximate atomic ratio	63	30	7

Table 6.10: Proportions of elements detected (spectrum of Figure 6.9)

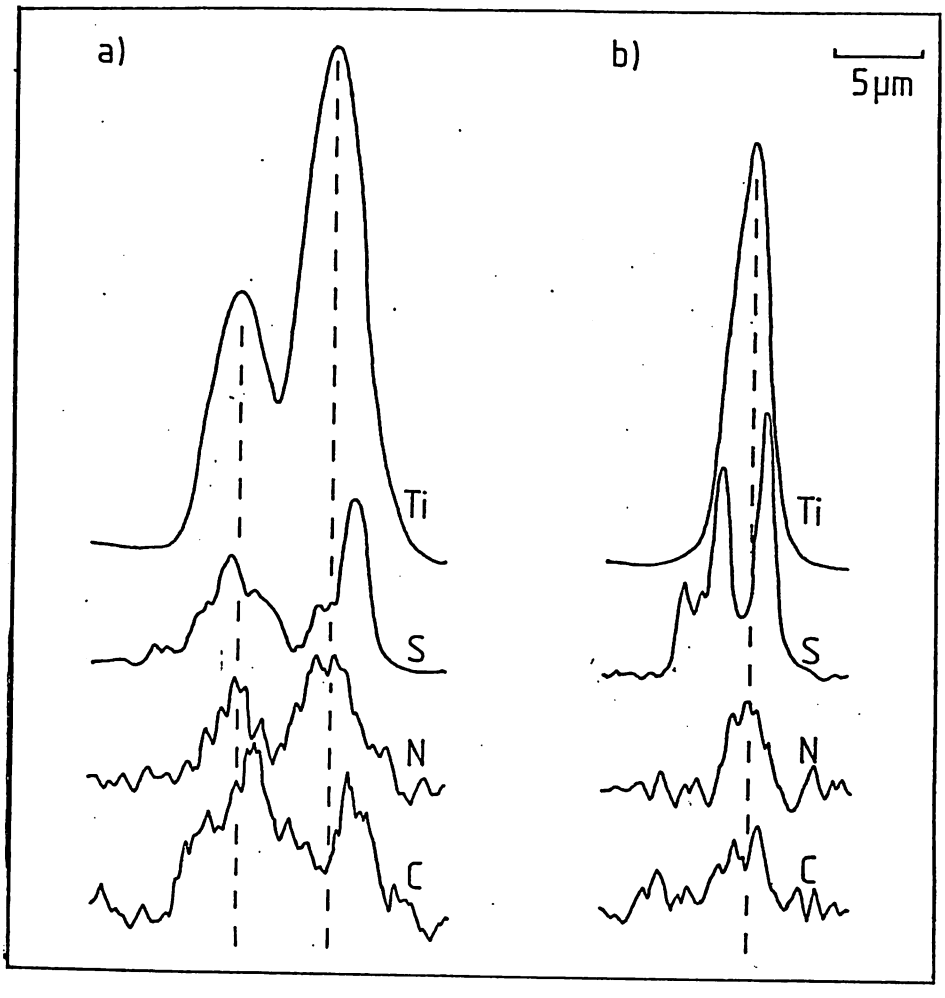

Figure 6.11: Elemental microanalysis of coarse (~5 µm) particles

precipitate subsequently on reaching their solubility limits.

6.8 Summary

1. The high resolution of the atom probe permitted analysis of the fine scale structure with an accuracy not attainable by other techniques. Simultaneously, however, the volume of material which could be examined was limited and the inherent statistical difficulties were encountered.

2. The atom probe studies have confirmed that the interphase precipitates were titanium carbide and contained negligible quantities of nitrogen or iron. The titanium to carbon atomic ratio in the carbides was 0.95±0.25.

3. The volumes of matrix examined were all defect-free. No carbon, nitrogen or titanium were detected in the bulk matrix: it was thought that any free interstitial atoms had segregated to low energy sites and that all the titanium was present in compounds.

4. Carbon ions were detected in the matrix immediately surrounding the titanium carbide precipitates. It is postulated that these carbon haloes are attracted to the strain fields of the precipitates.

5. Energy dispersive and wavelength dispersive X-ray microanalysis techniques have shown particles between 1 and 5 μm in size to be mixed compounds of titanium, nitrogen, sulphur and carbon. The more stable titanium nitride tended to be present in the particle cores.

CHAPTER SEVEN

ADDITIONAL THERMOMECHANICAL TREATMENTS

7.1 Introduction

To explore further the conditions favouring discontinuous yielding, the range of microstructures was broadened; in particular the mechanical and thermal treatments were designed to more closely resemble those encountered in practical situations.

Two regimes of reheating treatment were given, which could serve for example to simulate the changes in microstructure and mechanical behaviour which might be developed in the heat affected zones surrounding a weld. In each case isothermally transformed starting structures were employed and the subsequent treatments were:

i) sub-critical annealing at 830°C, near the boundary of the ferrite phase field. This was intended to achieve maximum modification of the existing microstructure, for example by accelerating precipitate coarsening;

ii) reaustenitisation at 1000°C, just within the austenite phase field, to produce a new ferrite grain structure on cooling.

Annealing treatments, within the ferrite phase field, were also given to heavily deformed specimens with the aim of producing a fully recrystallised ferrite structure. Also examined were a series of specimens which had been continuously cooled from austenite at different

rates.

This chapter considers the development of these microstructures and discusses the changes observed in the initial and strain-ageing yield behaviour.

7.2 Sub-critical annealing

Tensile specimens with the standard 800° and 650°isothermally transformed structures were sealed in quartz capsules and held at 830°C for times up to 60 000 s. The capsules were then water quenched, providing a specimen cooling rate equivalent to an air cool and thus conforming with the cooling rates of other heat treatments.

Figure 7.1 presents the microstructures of Alloy 2 after sub-critical annealing. Figures 7.1a&b show the equaxed ferrite microstructures in the 800° specimen after 330 s and 60 000 s at 830°C. Figure 7.2a shows sheets of interphase precipitation, formed during the 800° transformation, little changed during 330 s at the annealing temperature. After 60 000 s, colonies of regular interphase sheets were no longer found, but strings of larger titanium carbides (e.g. Figure 7.2b) in the grain interiors and on the grain boundaries indicated that diffusion along dislocations (as described by Dunlop & Honeycombe 1975) and within the moving boundaries had aided precipitate coarsening. Figure 7.2b exhibits the angular morphology of these large carbides of up to 200 nm resulting from preferential crystallographic growth. The hardness, plotted in Figure 7.3 as a function of annealing time, decreased slowly in the 800° structure from an initial 166 to 113 HV_{10} after 60 000 s, reflecting the coarsening of the precipitate dispersion.

The ferrite grain morphologies of the 650° specimen, shown in Figures 7.1c&d, retained their jagged appearance after the annealing treatments;

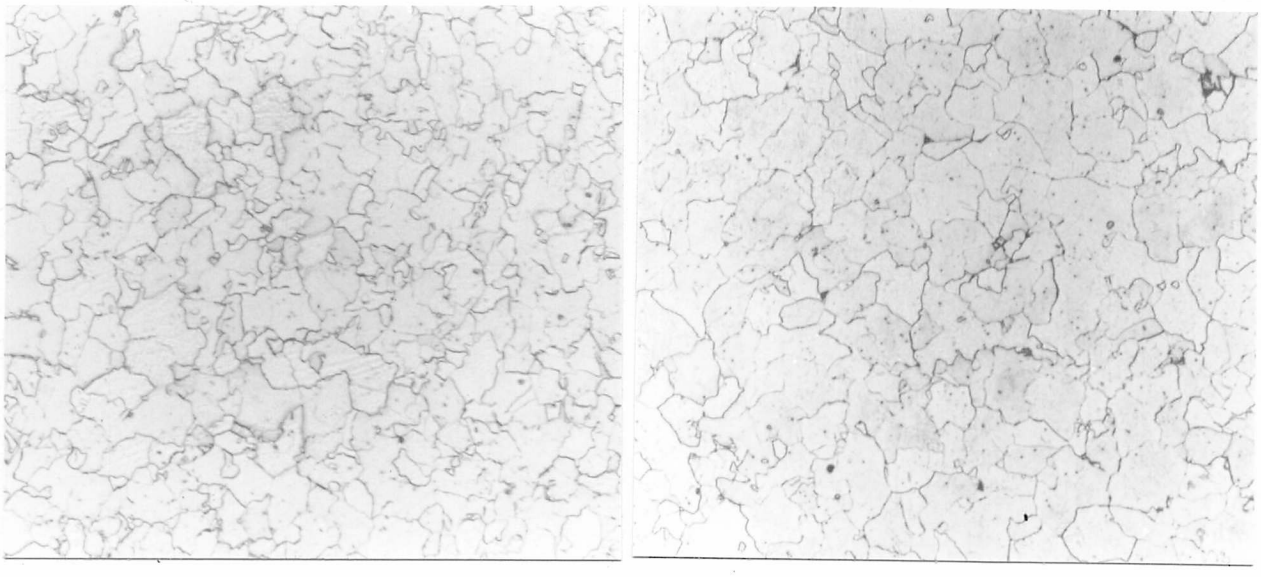

a) 800° structure + 330 s 830°C

b) 800° structure + 60 000 s 830°C

100 µm

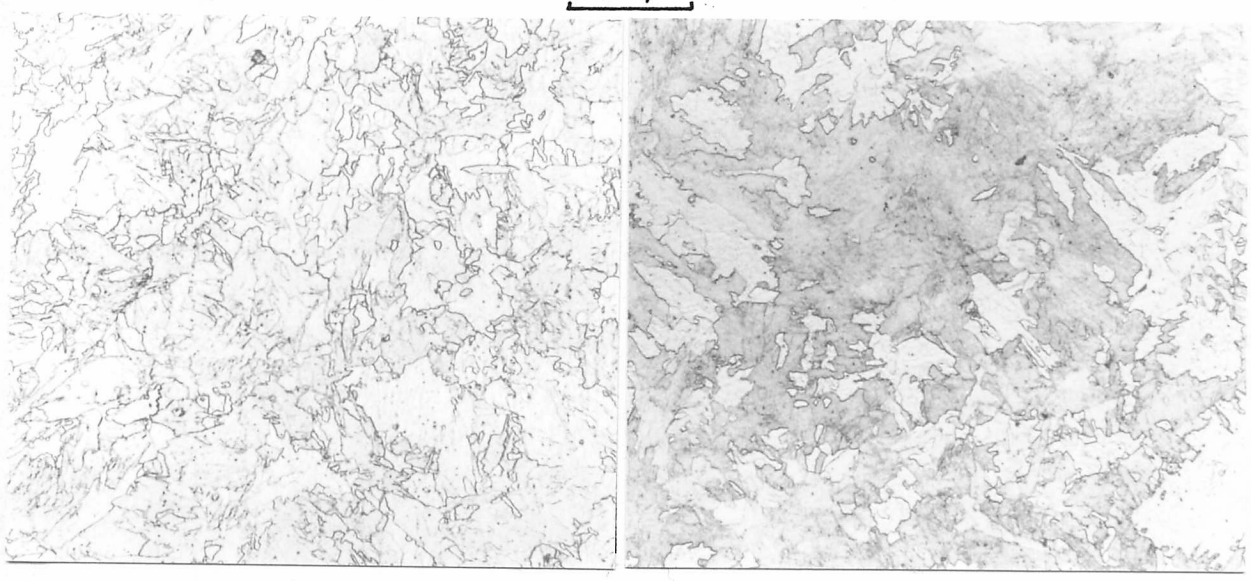

c) 650° structure + 330 s 830°C

d) 650° structure + 60 000 s 830°C

Figure 7.1: Microstructures developed by subcritical annealing
Alloy 2

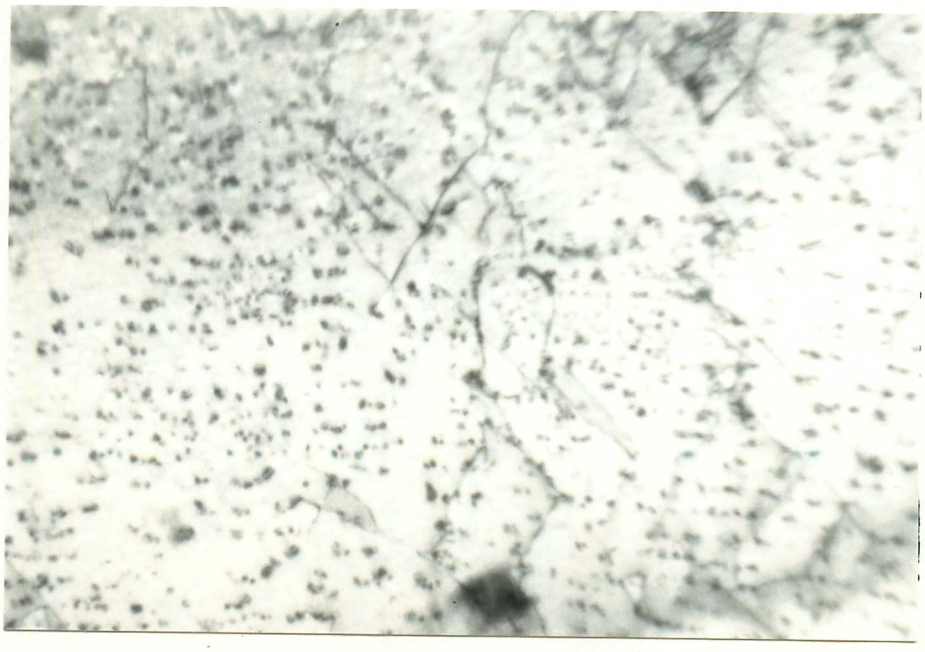

a) + 330 s 830°C
bright field

1 μm

b) + 60 000 s 830°C
precipitate centred
dark field

Figure 7.2: 800° structure, sub-critically annealed

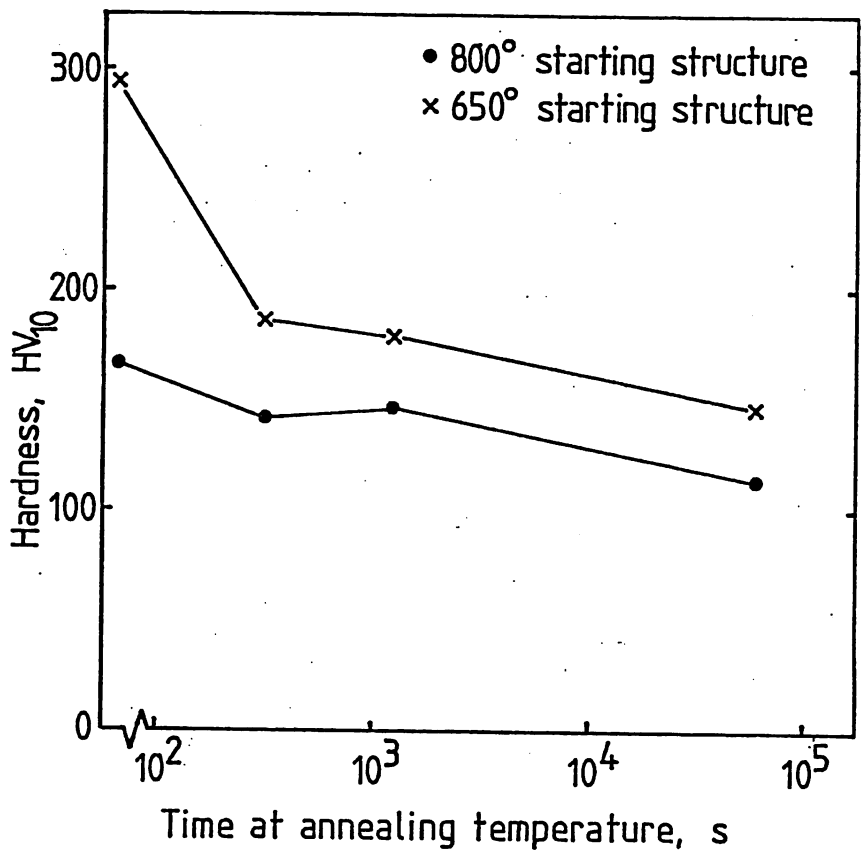

Figure 7.3: Hardness after sub-critical annealing

after 330 s at 830°, dislocated elongated grains remained (Figure 7.4a) but there was evidence (Figure 7.4b) of the preferential growth of small equiaxed grains in which the advancing grain boundaries had left behind precipitate-free regions. This phenomenon was more noticeable after 60 000 s at 830°, as shown in Figure 7.5a. Figure 7.5b illustrates the dislocation arrangements, and titanium carbide coarsening in preferential directions to produce rod-shaped precipitates. These microstructural changes led to a marked decrease in hardness from 294 to 186 HV_{10} after 330 s, and 146 HV_{10} after 60 000 s annealing. However, the hardness was still 30% higher than that of the annealed 800° structure indicating that significant microstructural differences still persisted.

The yielding behaviour of the tensile specimens is presented in Table 7.6: each of the sub-critically annealed specimens of Alloy 2, whether initially transformed at 800° or 650°, exhibited a well-defined initial yield extension of between 1% and 2% strain and a strain-ageing yield extension of similar magnitude. Strain-ageing indices of up to 41 MPa were measured. Large initial yield points were developed in the 650° specimens even after just 330 s at this 830° annealing temperature. This compares with the 100 h, reported in Chapter 4, required to produce a similar effect using <u>isothermal</u> annealing at 650° C. The high temperature sub-critical annealing treatments thus had the effect of accelerating the changes in carbide dispersion and dislocation distribution which had been observed in the isothermally annealed specimens hence accelerating the development of discontinuous yielding.

The 60 000 s annealing treatment at 830° was also given to tensile specimens of Alloys 1,3 and 4 which had been isothermally transformed at 800° and 650°C. Alloys 3 and 4 showed no tendency towards discontinuous initial or strain-age yielding thus indicating that even after holding at

a) elongated grains 1 µm

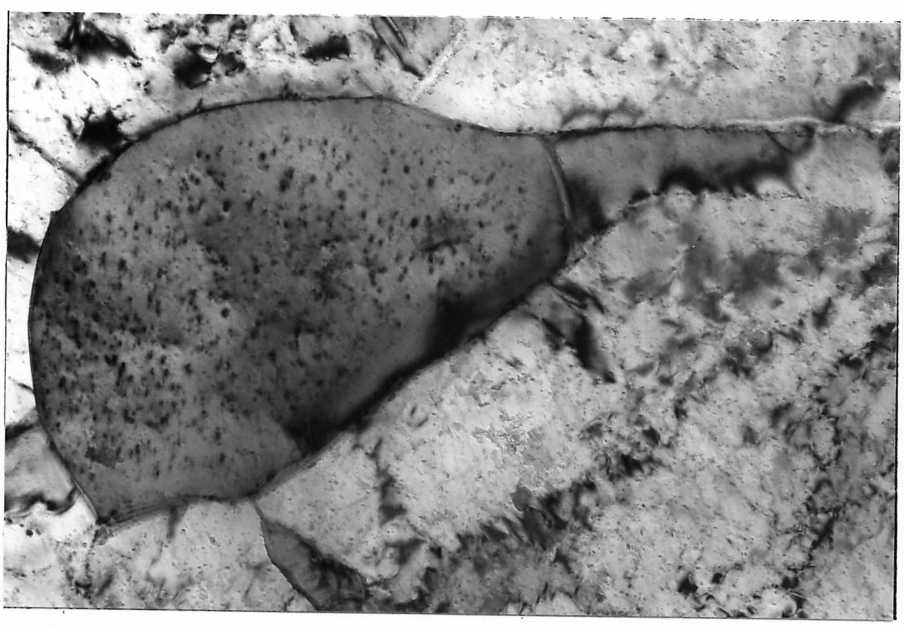

b) equiaxed grain 1 µm

Figure 7.4: 650° structure, sub-critically annealed 330 s 830°

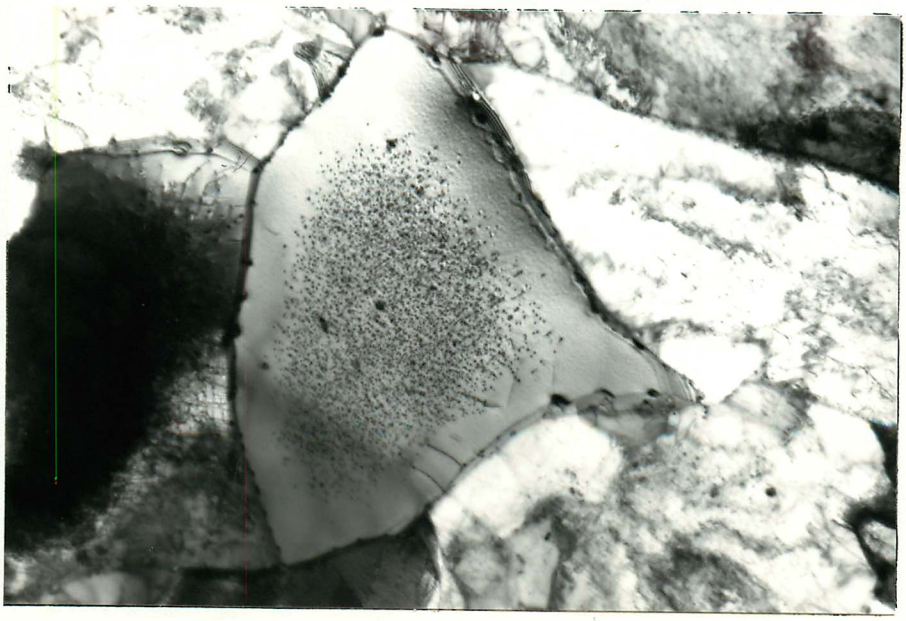

a) precipitate-free behind grain boundaries

1 µm

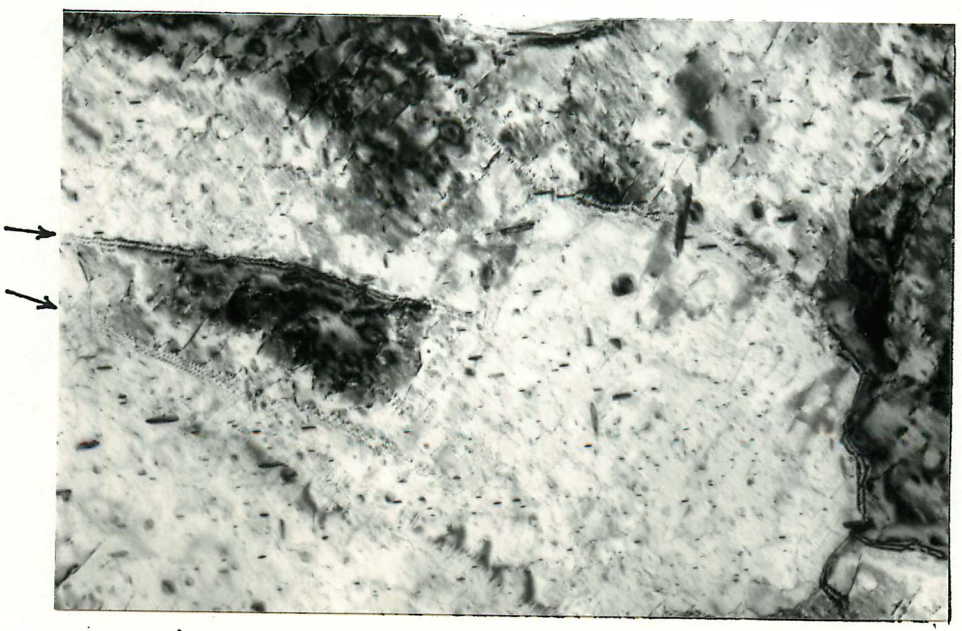

b) sub-grain boundaries and rod shaped precipitates

1 µm

Figure 7.5: 650° structure, sub-critically annealed 60 000 s 830°

		initial yield extension %	strain-ageing yield extension %	strain-ageing index MPa	stress-induced ordering index MPa	HV_{10}
Alloy 2	800° structure	1.1	1.7	31	4	166
	+ 330s 830°	1.9	2.6	27	-	142
	+ 1350s 830°	1.4	1.8	41	4.2	146
	+60000s 830°	1.8	1.6	34	-	113
Alloy 2	650° structure	0	0.6	5	2	294
	+ 330s 830°	1.4	1.7	14	1.5	186
	+ 1250s 830°	1.6	1.4	11	1.5	178
	+60000s 830°	1.4	necked	28	2.1	146
Alloy 1	800° structure	0.8	1.0	24		
	+60000s 830°	0.4	1.5	24	2.9	97
Alloy 1	650° structure	0	1.8	20		
	+60000s 830°	0.8	2.1	25	2.8	126

Table 7.6: Initial and strain-age yielding behaviour after sub-critical annealing

this elevated temperature a negligible concentration of interstitial species went into solution. The yielding behaviour of Alloy 1 showed trends like those of Alloy 2, because both contained excess carbon above TiC stoichiometry. The 650° starting structure exhibited a similar development of discontinuous initial yielding behaviour after the sub-critical annealing treatment, as detailed in Table 7.6.

7.3 Reaustenitisation

Except at temperatures very close to the austenite/ferrite phase field boundary, when the thermodynamic driving force is low, the nucleation rate of the reaustenitisation reaction is generally very fast principally because of the rapid diffusion rates at the elevated temperatures involved. The grain size of the resulting austenite is thus largely controlled by the degree of grain boundary pinning by dispersions of precipitates.

Using Equation 2.1 the equilibrium solubility of titanium carbide in austenite at 1000°C is calculated to be 0.17 vol% compared with the 0.40 vol% at 1200°C. Thus the 0.4 vol% of fine titanium carbides precipitated during the isothermal transformation of Alloy 2 from 1200°C would not all be anticipated to redissolve on reaustenitisation at the lower temperature. Such a heat treatment was therefore utilised to exploit the austenite grain refinement provided by the fine undissolved carbides.

Exploratory experiments were performed using specimens of Alloy 2 isothermally transformed in the standard manner from a 1200°C solution treatment. These were reaustenitised at 1000°C and air cooled to room temperature.

Figure 7.7 shows the optical microstructures resulting from different reaustenitising times and Figure 7.8 those from starting structures

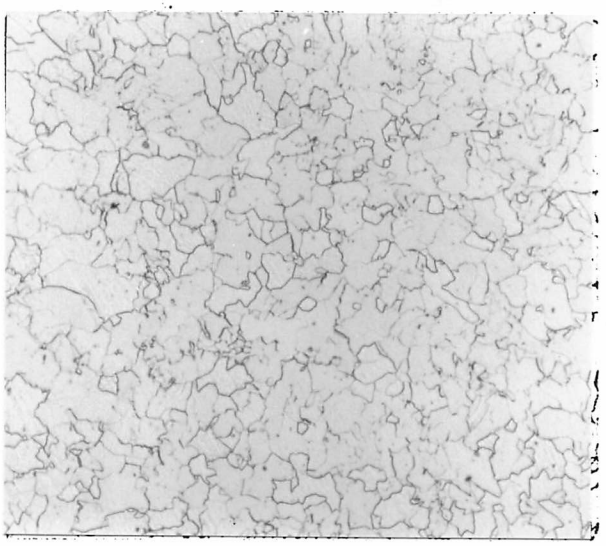

a) 100 s 1000°/ AC

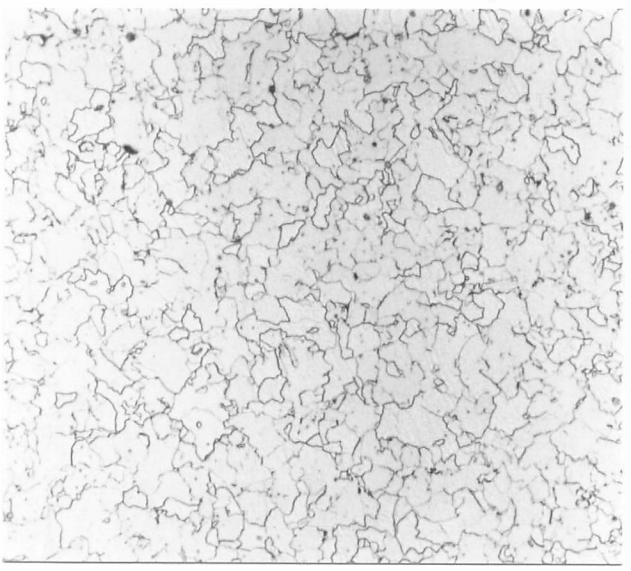

100 μm

b) 300 s 1000°/ AC

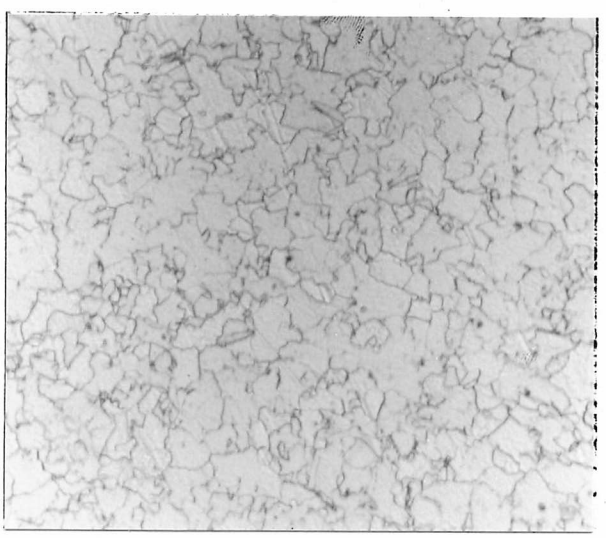

c) 600 s 1000°/ AC

Figure 7.7: Microstructures on reaustenitising for different times after isothermal transformation at 750°, Alloy 2

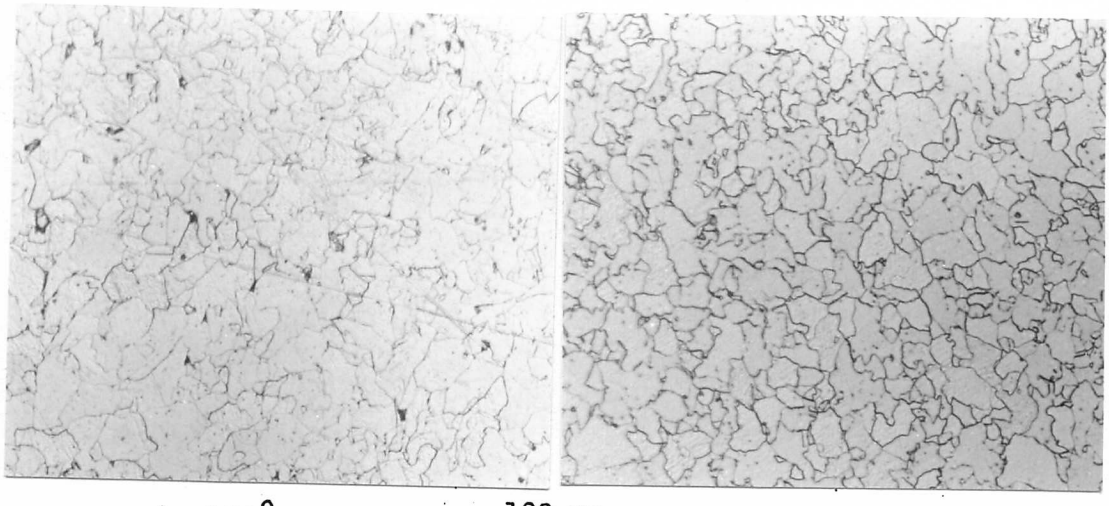

Figure 7.8: Microstructures on reaustenitising 300 s 1000° after isothermal transformation at temperatures indicated, Alloy 2

heat treatment	HV_{10}	grain size µm
750° starting structure + 100s 1000°/AC	151	11
" " " + 300s 1000°/AC	163	11
" " " + 600s 1000°/AC	167	11
800° starting structure + 300s 1000°/AC	148	14
750° " " " " "	151	11
700° " " " " "	147	13
650° " " " " "	158	11

Table 7.9: The effect of reaustenitising and air cooling isothermally transformed specimens, Alloy 2

corresponding to different isothermal transformation temperatures. The grain morphologies developed by these reaustenitisation treatments were all very similar, comprising slightly irregular but equiaxed grains with grain sizes between 11 and 14 μm, as recorded in Table 7.9. The hardnesses were also very similar, varying randomly within the range 147 to 167 HV_{10}.

Electron microscopy, for example Figure 7.10a, revealed high precipitate densities in irregularly shaped grains and dislocation densities of 10^{14} to 10^{15} m^{-2}, similar to those of the original isothermally transformed specimens reported in Chapter 5.

Figure 7.10b shows a colony of uniquely oriented titanium carbides extending across a new ferrite grain boundary, indicating that the particle nuclei had persisted throughout the heat treatment. Remnants of the original interphase precipitate sheet morphology are also seen in the micrograph.

Many of the fine titanium carbides produced during the original isothermal transformation thus remained out of solution during the later reaustenitisation treatment, thereby serving to stabilise the austenite grain structure against grain growth as intended. However the elevated temperature and moving transformation boundaries would have allowed these carbides to coarsen and redistribute, reducing the differences between the precipitate dispersions inherited from the original starting structures.

Another factor contributing to the achievement of the reproducible, fine grained equiaxed ferrite structure desired was the more rapid kinetics of the austenite decomposition reaction during cooling from 1000° compared with 1200°; this arose from a combination of the finer austenite grain size and the lower concentrations of dissolved alloying elements at the lower austenitising temperature.

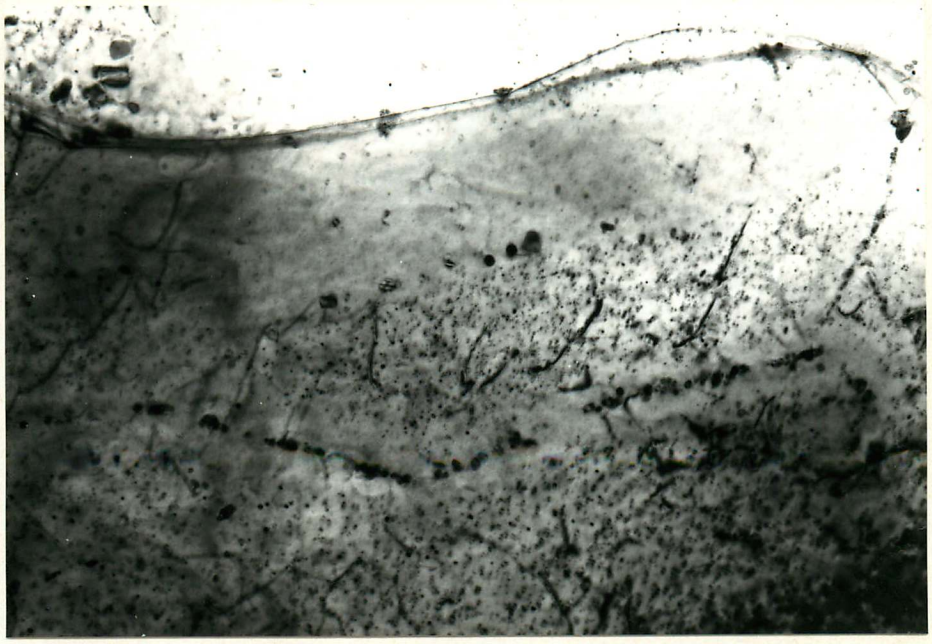

a) Bright field

1 μm

new ferrite grain boundary

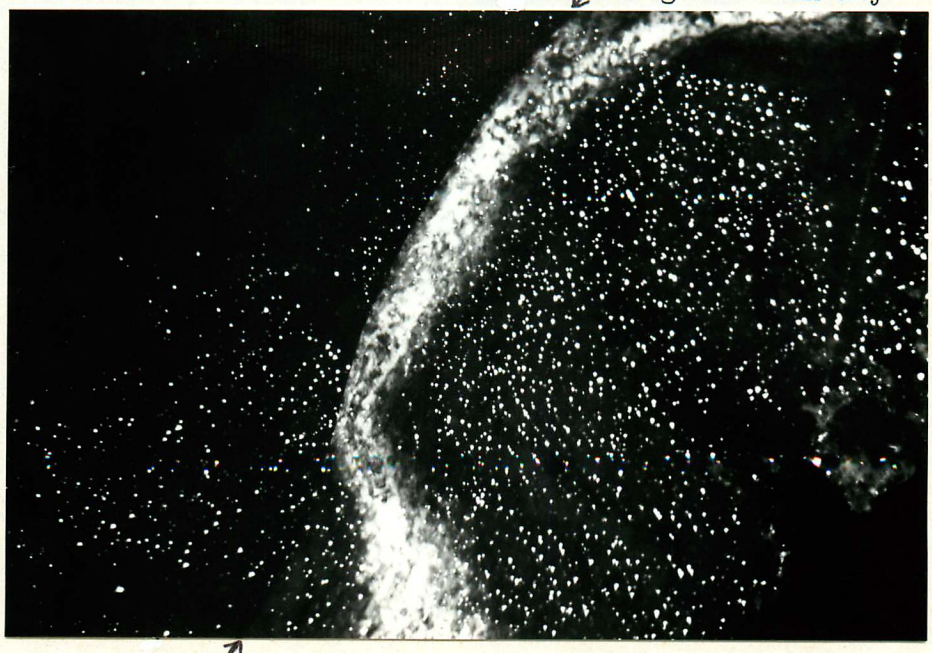

b) Precipitate centred dark field, different area, showing precipitate colony extending across new ferrite grain boundary

Figure 7.10: Isothermally transformed at 650° + 300 s 1000°/ AC

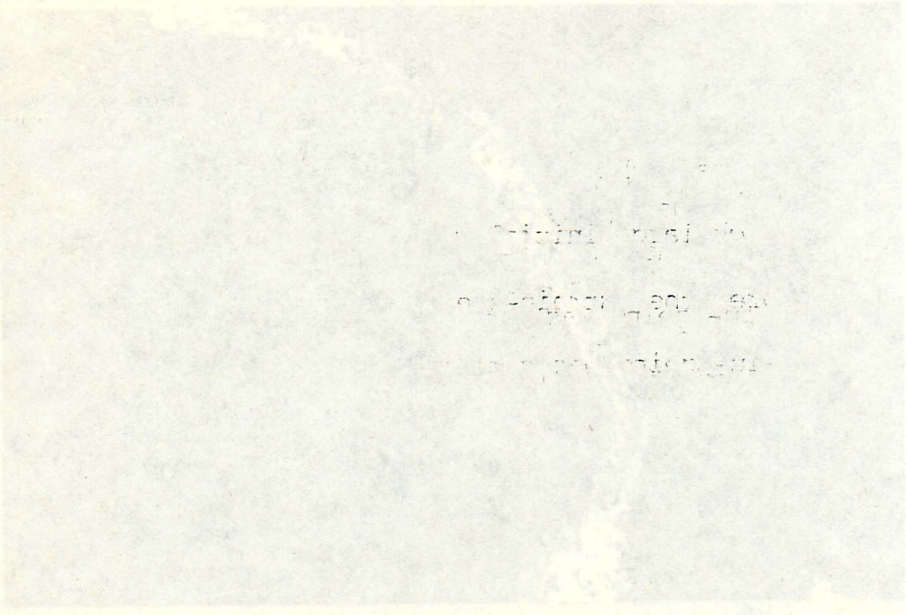

For the tensile tests, the heat treatments of 300 s at 1000° with an air cool were given to five tensile specimens which had been isothermally transformed at 800°, 700° or 650° by the standard method described in Chapter 4. The specimens had been strained by less than 5% in the as-transformed condition prior to this reaustenitising treatment. However it was anticipated that the effects of reaustenitisation would obliterate any microstructural differences caused by the amount of prestrain in the same way that differences arising from the original transformation temperature were negated. Indeed, comparison of the previously strained gauge length and unstrained shoulders after the reaustenitisation treatment indicated no discernable difference between the optical microstructures.

After the reaustenitising heat treatments all the specimens exhibited very large initial yield effects (Table 7.11). The initial yield extensions were between 2.2 and 4.0 %, and were serrated, for example as illustrated in the stress-strain curves of Figure 7.12. Each serration is thought to represent the break-out of an individual yield nucleus.

Because such large initial yield extensions were encountered, the prestrain before the strain-ageing treatments had to be increased to 5% to ensure strain-ageing was performed on uniformly strained specimens. The strain-age yield extensions were also large, each 2.2%, and the strain-ageing indices were 27 and 19 MPa. The strain-age yield extensions were smooth, perhaps because many yield nuclei operated simultaneously.

Stress-induced ordering indices of approximately 1.5 MPa were recorded, indicating that the heat treatment had <u>not</u> resulted in any large increase in the concentration of interstitial species available for dislocation pinning. It therefore seems likely that the occurrence of discontinuous yielding was encouraged by the combination of the refinement of

heat treatment	init. yield extn. %	strain-age yield extn. %	strain-ageing index MPa	stress-ind. ordering index MPa
Reaustenitisation				
800° starting structure + 300s 1000°/ AC	3.1 2.2	2.2 -	27 -	- -
700° starting structure + 300s 1000°/AC	3.8	-	-	-
650° starting structure + 300s 1000°/AC	2.2 4.0	2.2 necked	19 -	1.5 1.5
Deformation and recrystallisation				
62%RA as-deformed	0	-	-	-
62%RA + 1000s 750°	2.3	3.4	44	2

Table 7.11: Yielding behaviour of Alloy 2

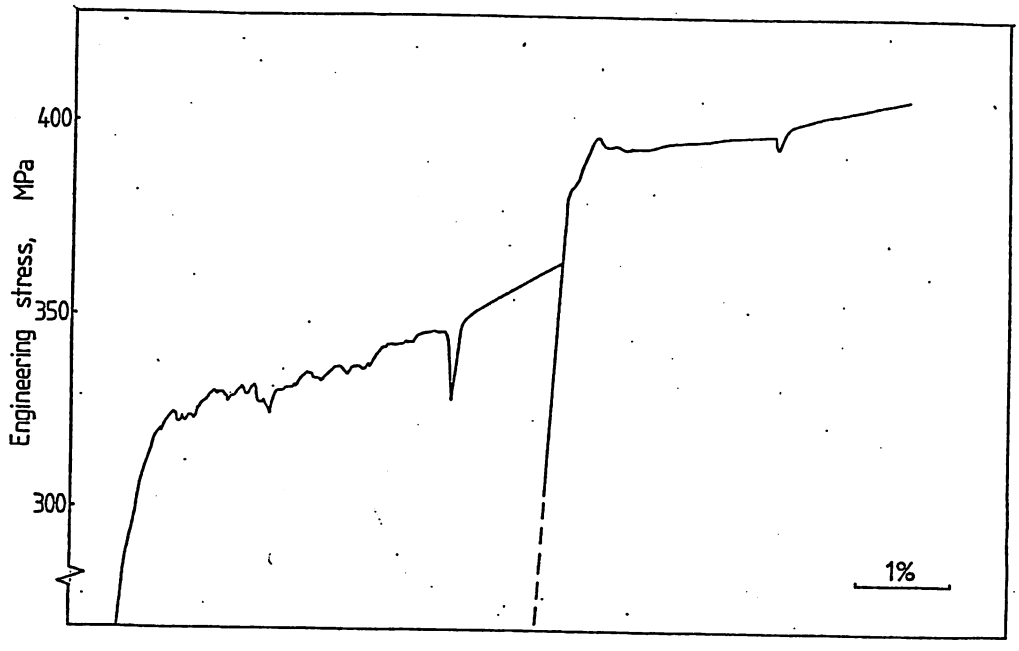

a) 800° structure + 300 s 1000°/ AC

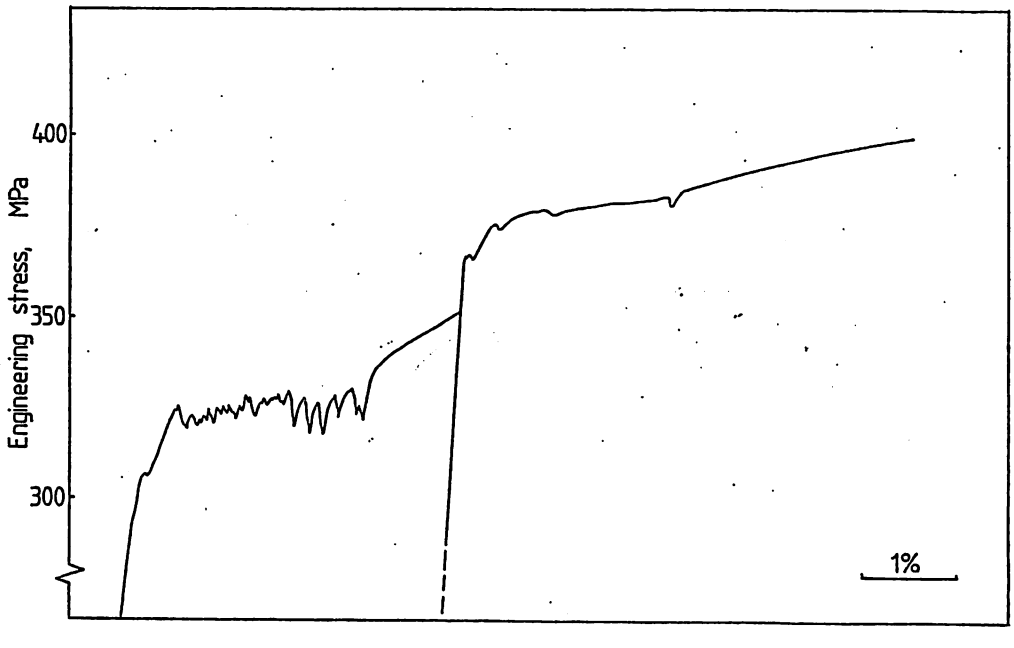

b) 650° structure + 300 s 1000°/ AC

Figure 7.12: Yielding behaviour of reaustenitised and air-cooled specimens, Alloy 2

the ferrite grain size and the uniformity of the grain structure.

7.4 Deformation and recrystallisation

During recovery and recrystallisation processes, the greater the driving force is, the greater is the density of new, strain-free nuclei produced. Thus, because of its high strain energy density a heavily deformed microstructure can be heat treated to produce a fine grained, uniform ferrite structure, provided that grain growth can be controlled.

To this end, tensile specimens were prepared from 5 mm diameter rod of Alloy 2 which had been deformed to 62% reduction in area by a series of cold swageing and drawing operations. The fine grained, deformed ferrite microstructure of the cold worked material is presented in Figure 7.13a. After machining, the specimens were heat treated for 1000 s at 750° in molten tin, producing a polygonal structure of recrystallised ferrite (Figure 7.13b) with a grain size of approximately 10 μm. Grain growth would be restricted by the fine, undissolved titanium carbides.

The tensile results are included in Table 7.11. In the as-deformed state, initial yielding was continuous but after recrystallisation large initial yield extensions of 2.3% strain were exhibited of the form shown in Figure 7.14. Just as for the reaustenitised specimens, the prestrain had to be increased to 5% to ensure uniform strain conditions were reached. The strain-ageing yield behaviour of the recrystallised specimens was pronounced; a strain-ageing yield extension of 3.4% and a strain-ageing index of 44 MPa were recorded.

Once more the initial yield extension was serrated but the strain-age yield extension was smooth, and again the pronounced discontinuous yielding behaviour would appear to be caused by the combined effects of a fine grain size and a uniform, almost strain-free lattice containing few

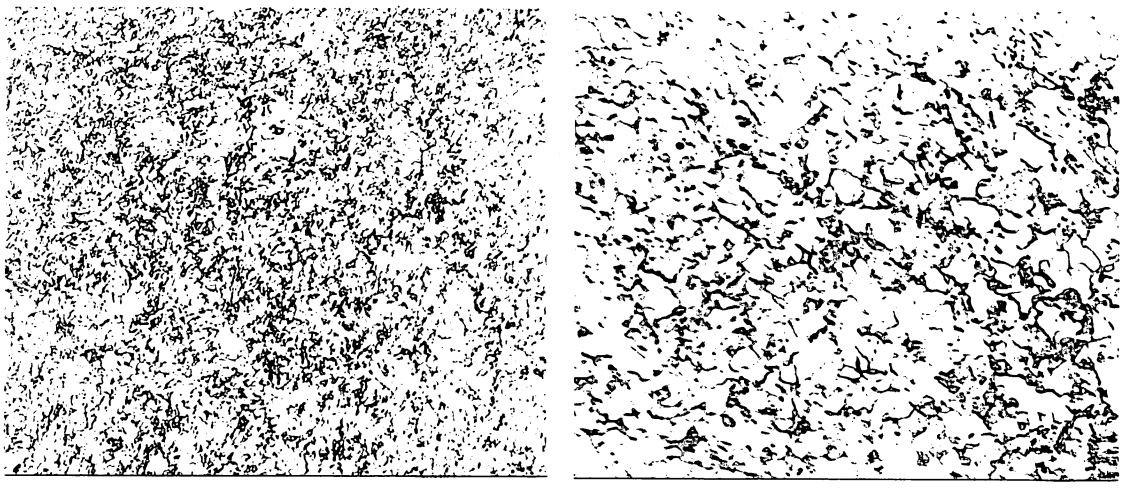

a) as-deformed to 62% reduction in area

100 μm

b) 62%RA + 1000 s 750°C recrystallisation

Figure 7.13: Microstructures developed by deformation and recrystallisation Alloy 2

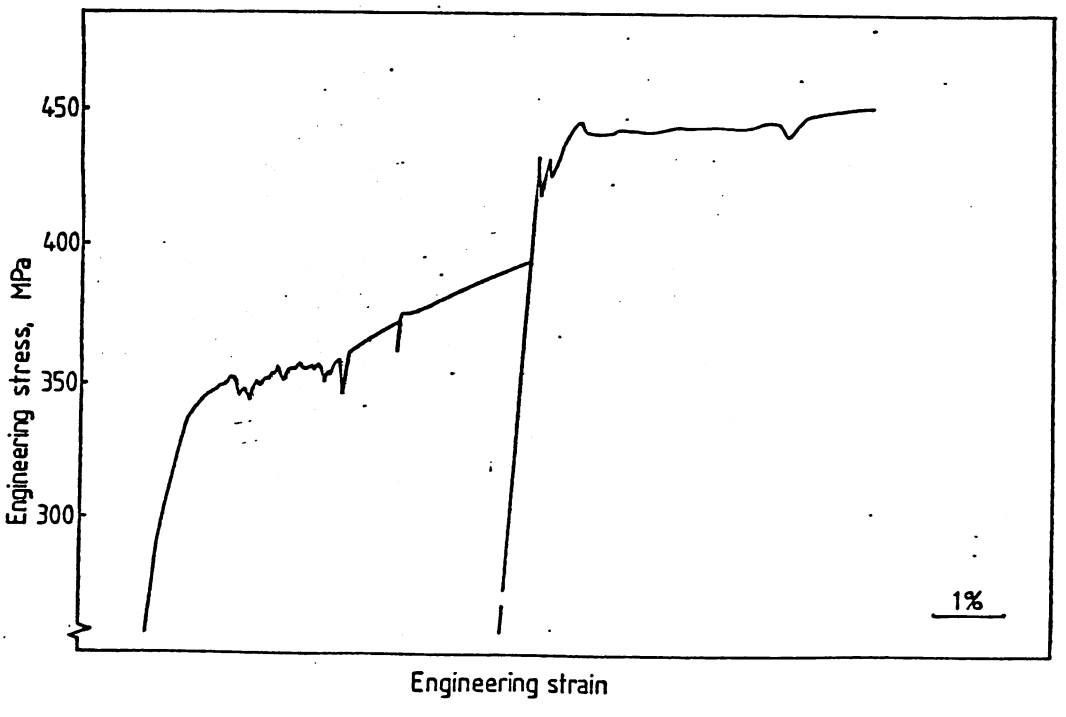

Figure 7.14: Yielding behaviour after deformation and recrystallisation
62%RA + 1000 s 750°C, Alloy 2

dislocations.

7.5 Continuous cooling

Tensile specimens of Alloy 2 in the standardised martensitic condition were reaustenitised for 10 min at 1200° and cooled at one of four rates through the transformation region:

i) 5°C per min by furnace cooling (denoted FC);

ii) 25°C per min by transferring to a furnace at 700° and immediately furnace cooling (700FC);

iii) 400 °C per min by cooling in still air (AC); or

iv) 30 000°C per min by quenching in iced-brine (IBQ).

Quartz encapsulation was employed for the two treatments involving furnace cooling; for the air cooled and iced-brine quenched specimens an argon protective flow was used during reaustenitisation. An iced-brine quench from 1300° was also included. In Figure 7.15 the cooling lines of the tensile specimens are superimposed upon the continuous cooling diagram already presented as Figure 3.3. The microstructures produced are shown in Figure 7.16, and the initial and strain-age yielding characteristics in Table 7.17.

The furnace cooled specimen, transformed progressively between approximately 900° and 750°C had an equiaxed but non-polygonal ferrite microstructure and a proof stress of 286 MPa which is similar to that of specimens isothermally transformed at 800°. However, although titanium carbide dispersions on various scales were identified in this specimen, no sheets of interphase precipitation were found and the similarity in strength with the 800° specimen is probably coincidental. A further difference was that the furnace cooled specimen did not exhibit an initial

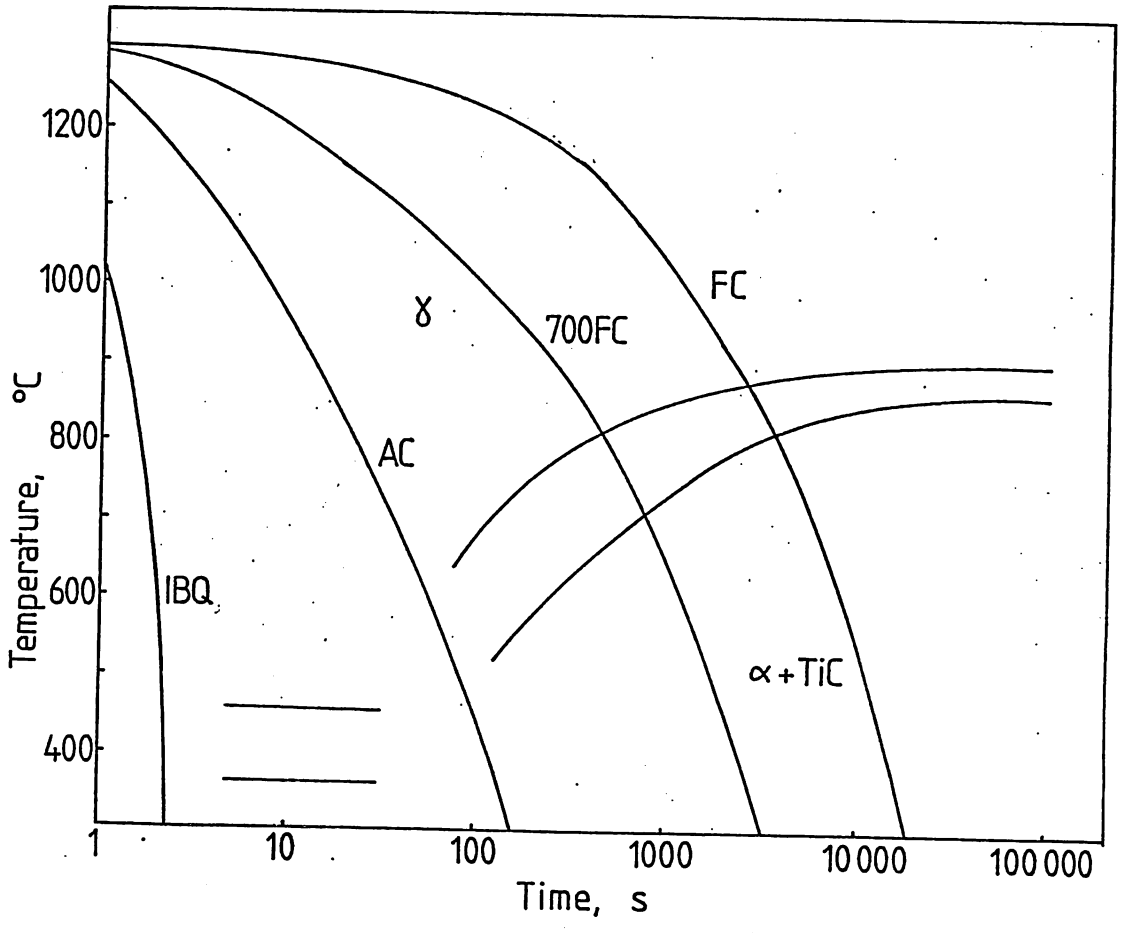

Figure 7.15: CCT diagram (Figure 3.3) with cooling lines of tensile specimens superimposed

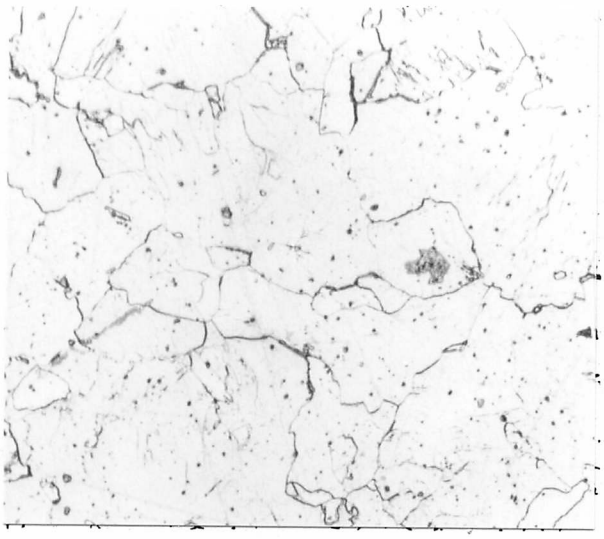

a) 5°C min^{-1}

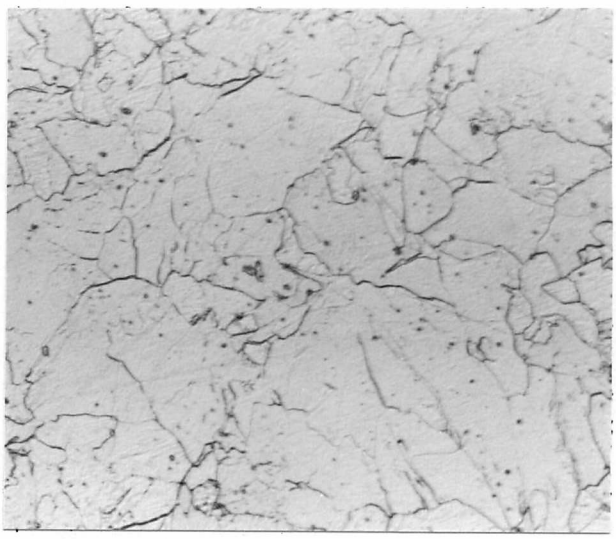

b) 25°C min^{-1}

100 μm

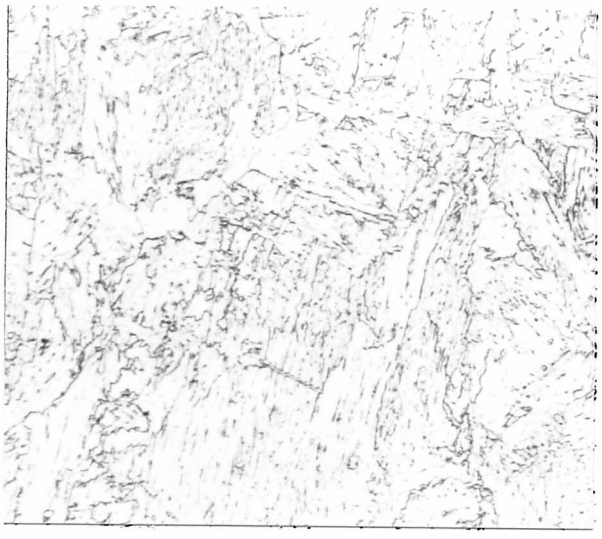

c) 400°C min^{-1}

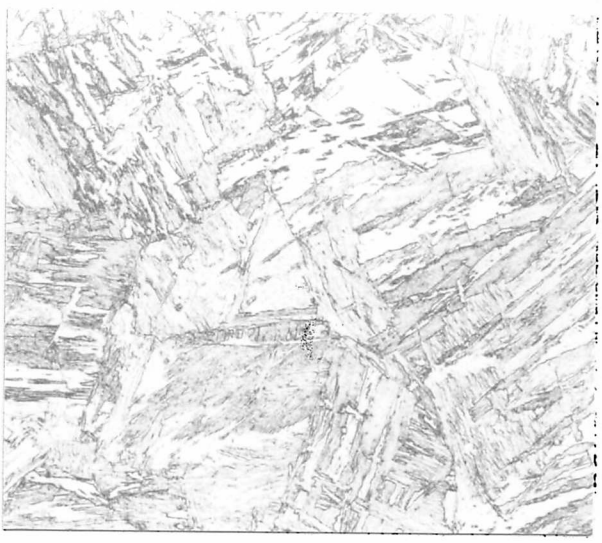

d) 30 000°C min^{-1}

Figure 7.16: Microstructures produced by continuous cooling
Alloy 2

heat treatment	init. yield	0.2% proof stress MPa	strain-age yield extension %	strain-ageing index MPa	stress-ind. ordering index MPa
600s 1300°/FC	0	286	0.72	9.8	<1
600s 1300°/700FC	0	503	0.34	7.0	<1
600s 1300°/AC	0	514	3.06	21	1.4
600s 1200°/AC	0	494	2.13	33	2.9
600s 1300°/IBQ	0	845	-	-	-
600s 1200°/IBQ	0	831	-	-	-
" " "	0	803	-	83 (1.4% prestrain)	
" " "	0	804	>1	62 (0.7% prestrain)	

Table 7.17: Yielding behaviour of continuously cooled specimens

yield point. The formation of a range of different microstructures as the temperature changed during transformation may have been the cause. The stress-induced ordering index of less than 1 MPa and the strain-ageing index of 9.8 MPa indicated that there was much less interstitial carbon available in the furnace cooled specimen than in the 800° specimen. The corresponding indices for the latter were 4 MPa and 31 MPa. Furnace cooling would have allowed the majority of the carbon to be removed from solid solution.

At the second slowest cooling rate, 25°C per min, transformation occurred continuously between 850° and 700°. Interphase and dislocation precipitation of titanium carbides were identified, as shown in Figures 7.18a&b. The observed wide variation in interphase sheet spacing reflected the range of transformation temperature. The regions with the coarsest, 250 nm spacing, used to examine dislocation-particle interactions (Chapter 5), were probably formed at the top of the transformation range. Again there was no evidence of an initial yield point. The proof stress was 503 MPa which is 75% greater than that of the furnace cooled specimen. One must assume that the differences in precipitate dispersions and in the ferrite sub-structure produced by the faster cooling rate and consequent lower transformation temperatures were the cause: the strain-ageing and stress-induced ordering behaviour indicate that the quantity of interstitial carbon remaining were similarly small, and the optical microstructures were similar.

Micrographs of the air cooled specimen such as Figure 7.19a&b show a mixed grain structure comprising dislocated platelike grains interspersed with more equiaxed grains. This is very similar to the microstructure produced by isothermal transformation at 650°C. Likewise, the air cooled specimen exhibited continuous initial yielding behaviour. In contrast,

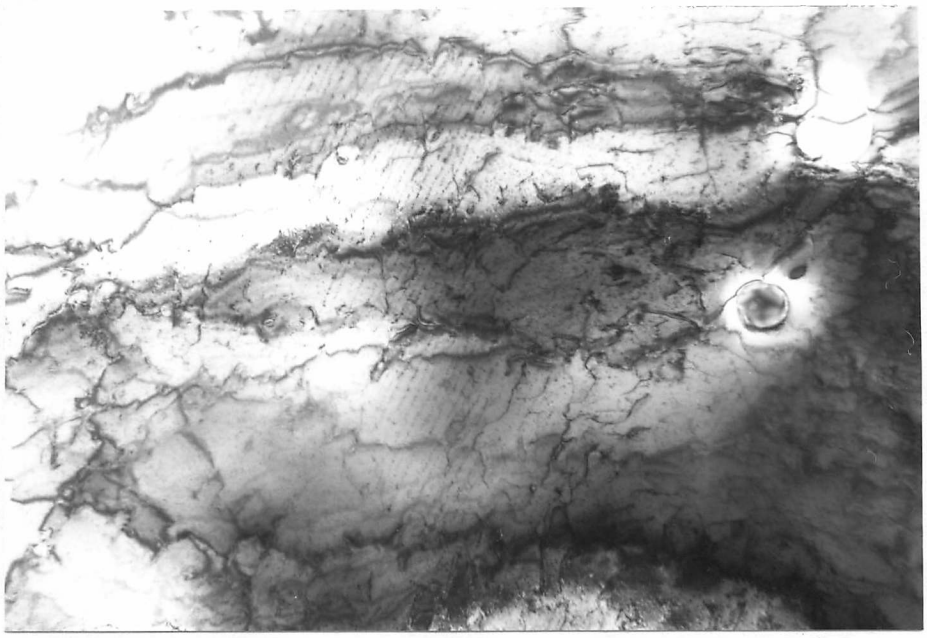

a) bright field

1 μm

b) precipitate centred dark field

Figure 7.18: Dislocation precipitation and interphase precipitation of titanium carbide formed by cooling at 25°C per minute through transformation

a) laths

0.5 μm

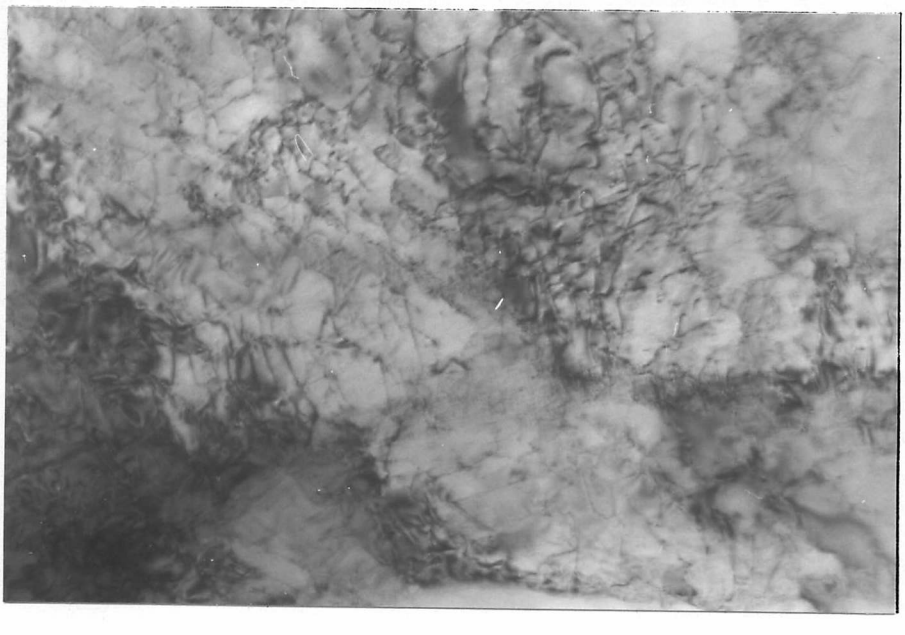

b) equiaxed grain

Figure 7.19: Mixed grain microstructure formed by air cooling

however, on cooling from the austenite greater concentrations of interstitial carbon could be retained than the furnace cooled or isothermally transformed specimens; consequently larger strain-ageing indices (21 and 33 MPa) and stress-induced ordering indices (1.4 and 2.9 MPa) were exhibited. Strain-age yield extensions of 3.06 and 2.13% were recorded. The continuous initial yielding can be attributed to the inhomogeneous microstructure.

The lath martensitic microstructures produced on iced-brine quenching have already been discussed in Section 3.4. Quenching from 1200° gave an average proof stress of 813 MPa, and from 1300° of 845 MPa. The lower strength of the former reflects the small volume fraction of titanium carbide calculated to be remaining undissolved at 1200°C and consequently unable to contribute to the strength on quenching. At 1300°, all the titanium carbide should be in solution. Due to the low ductility of the martensite and the limited number of specimens available, the strain-ageing behaviour was not fully characterised: a strain-ageing index of 83 MPa was determined after the standard prestrain of 1.4% but necking occurred immediately after the strain-age yield point invalidating the measurement. Using a prestrain of only 0.7% the strain-ageing index was 62 MPa but necking again occurred before the strain-age yield extension was complete, after 1%. Although this result is not directly comparable with the strain-ageing results of the other continuously cooled specimens, it is clear that large concentrations of interstitial carbon were retained by the iced-brine quenching.

7.6 Summary

1. Isothermally transformed specimens, sub-critically annealed at 830° within the two-phase ferrite plus titanium carbide field exhibited faster carbide coarsening behaviour and yield point development than the isothermally annealed specimens. However even in the 60 000 s treatments given, strength differences were maintained between specimens initially transformed at different temperatures, indicating that the starting structures were not entirely destroyed.

2. Reaustenitisation at 1000°C instead of the higher temperatures previously used resulted in only partial re-solution of the titanium carbides and consequent refinement of the austenite grain size. Air cooling from 1000°C produced a consistently fine ferrite grain structure of approximately 12 μm grain size with reproducible properties regardless of the starting structure. Initial and strain-ageing yield effects were very pronounced.

3. Very fine grained, heavily deformed specimens exhibited continuous initial yielding but when fully recrystallised to a uniform, 10 μm ferrite grain size gave very large initial and strain-ageing yield points.

4. The microstructures produced by continuous cooling were on the whole more inhomogeneous than those produced by isothermal transformation. Specimens transformed during cooling rates ranging from 5° to an estimated 30 000° per minute all exhibited continuous initial yielding and the discontinuous strain-ageing yielding behaviour became gradually more pronounced as the cooling rate was increased owing to the increasing concentrations of interstitial atoms remaining in solution.

CHAPTER EIGHT

GENERAL DISCUSSION

8.1 Microstructure

The principal objective of the present study was to explore the differences in microstructure which could be produced by direct isothermal transformation in a series of simple titanium steels, and to relate these to the mechanical properties. By quenching specimens after partial transformation from austenite at temperatures between 800° and 650°C, the development of the basically two-phase microstructure comprising ferrite and titanium carbide was followed in Alloys 1 (0.07C-0.07Ti) and 2 (0.07C-0.23Ti). Because of its lower titanium content, Alloy 1 contained a lower volume fraction of titanium carbide and a correspondingly higher carbon excess than Alloy 2. The austenite decomposition kinetics, as measured by the TTT curves, were found to be similar.

The morphologies of ferrite resulting from complete austenite transformation ranged from allotriomorphic equiaxed and elongated grains to colonies of plate- or lathlike grains separated by low angle boundaries. The equiaxed structures predominated at transformation temperatures of 700°C and above. Although described as equiaxed the grain shapes were by no means polygonal, the grain boundaries appearing jagged. It is postulated that the efficiency of grain boundary pinning by the stable titanium carbides tended to restrict any straightening of the grain

boundaries to minimise the area.

With the exception of the occasional mixed titanium nitrides and carbosulphides which had precipitated from the liquid or austenite, the ferrite grain interiors were optically featureless. The characteristics of the microstructure were therefore examined comprehensively by transmission electron microscopy. This technique had the limitation that investigations were confined to specimen volumes of only a few cubic microns which, by the jet electropolishing preparation method employed, were nearly always in the centre of the specimen and therefore not truly representative of the complete cross section. However, since isothermal conditions were reached throughout the specimen well before the TTT curve nose, little difference in transformation behaviour would be expected on the scale of the cross section. Indeed, no significant differences were found across the section using microhardness.

By employing a 200 kV electron microscope, in preference to the more usual 100 kV accelerating potential, the thicker regions of the foil up to 350 nm could be penetrated. The material volume examined was thereby increased and any foil surface effects reduced. This precaution was especially important in the examination of dislocation populations because the possibility of dislocation elimination or rearrangement caused by interaction with the foil surfaces was diminished.

A wide variety of different ferrite, precipitate and dislocation distributions was observed even within a single specimen. This would always be expected to a certain degree because the ferrite in different parts of the specimen would have formed at different times during the reaction. Precipitate-free proeutectoid ferrite may have formed at the very start of the reaction and carbon redistribution may have taken place. Care was taken to distinguish between real inhomogeneity in the specimen

and apparent inhomogeneity arising from the techniques employed. For example, sectioning through colonies of precipitate sheets could result in either rows of precipitates or a random dispersion being visible. Moreover, under certain diffraction conditions regions could appear to be precipitate-free because of lack of image contrast, and for the same reason a proportion of the dislocations could be rendered invisible. In each case, more information was obtained by tilting the foil. Bearing in mind the above effects, the microstructural characteristics were used to deduce the mechanisms by which the transformation had taken place.

At each isothermal transformation temperature the ferrite nucleated on the grain boundaries. The subsequent allotriomorphic growth of these nuclei delineated the boundaries at low transformation temperatures but was more blocky at the higher temperatures. The preponderance of observed macroscopically planar ferrite interfaces implied, but did not prove, that the ferrite was very frequently related crystallographically to one or both of the parent austenite grains, as discussed in a recent review by Howell & Honeycombe (1982) - it is possible that a planar interface may form solely to minimise the ferrite surface energy irrespective of any matching with the austenite. In the present work, both the Kurdjumov-Sachs and Nishiyama-Wassermann austenite/ferrite relationships were identified after partial transformation. These have 24 and 12 variants respectively and within each variant a range of several degrees of mismatch is possible, indicating that there is a high probability of achieving a close crystallographic relationship in these titanium steels.

The movement of the highly coherent, planar interfaces by the passage of more mobile ledges led to the formation of the sheets of identically orientated titanium carbides by the well-documented interphase ledge precipitation mechanism (eg Campbell & Honeycombe 1974). Curved sheets of

precipitates, also exhibiting a Baker-Nutting orientation with the ferrite matrix, were occasionally found in microstructures formed at high transformation temperatures. These provided evidence for incoherent austenite/ferrite interfaces at which it has been suggested regular precipitation can occur in conjunction with interface bowing or local ledge formation (Ricks & Howell 1983). For each mechanism the driving force for the interphase precipitation is provided by the very large decrease in titanium carbide solubility from tenths of a percent in austenite to parts per million in ferrite. The growth of the precipitate nuclei is made possible by the easy diffusion paths provided in the incoherent portions at the interface.

Although identified in all the isothermally transformed microstructures examined, interphase precipitation was not the only morphology of titanium carbide observed: precipitation on dislocations occurring either at the transformation front or from supersaturated ferrite, regions of random precipitation and precipitate-free regions were also found. Interphase precipitation tended to predominate at the higher transformation temperatures. In the lowest temperature, 650^{o} structure, interphase precipitation was never found in the plate-like grains. However in these heavily dislocated regions, detection of fine carbides may have been prevented by strain contrast.

The non-linear decrease in mean interphase sheet spacing with decreasing transformation temperature, plotted in Figure 3.21, is a commonly observed phenomenon arising from the increase in ledge nucleation rate at lower temperatures.

The use of a time-of-flight atom probe was essential for the accurate analysis of the titanium carbides as it permitted the identification of individual atoms including those of the lowest atomic numbers. For a

carbide formed at 800°C approximately 10 nm in diameter, the 2 nm probe hole was sufficiently small to exclude matrix atoms from the identification. In this way the iron content of the carbide was shown to be negligible. An average atomic titanium to carbon ratio of 0.95±0.25 was measured, in agreement with the common assumption that the atomic stoichiometric ratio for the carbide is unity.

The major uncertainties arising from the quantitative atom probe analyses were of a statistical nature, each particle only containing a few thousand ions and the number of particles which could be practically examined being severely limited.

The finding that carbon atoms in interstitial sites tended to be removed as multiple ions whereas those from the ionically bonded carbides were detected as single ions is postulated to arise from differences in binding energy. This observation provides additional evidence for the apparent presence of haloes of interstitial carbon atoms in the matrix surrounding the carbides, possibly attracted to the coherency strain fields. Such haloes have been noted before by Waugh (1978) in carbon desorption images but by that technique, the non-linearity of the ion trajectories leads to uncertainties about the original atom site within the specimen. In the current study the phenomenon was observed in Alloy 2 which contained a carbon excess; it would be informative to investigate carbides in a similar alloy without surplus carbon such as Alloy 3.

In all the isothermally transformed structures, strain fields were observed as image contrast around the fine titanium carbide precipitates when examined by bright field transmission electron microscopy. In Chapter 5 consideration of the interaction between these strain fields and those of dislocations, following the reasoning of Eshelby (1957) led to the suggestion that not only could dislocations be prevented from moving

through the crystal lattice by the repulsive pinning forces but also that in some cases dislocations could be attracted to the particles and trapped. Dislocations inherited from the austenite or generated during its transformation hence persisted in the ferrite and titanium carbide aggregate, even after prolonged (16 h) isothermal annealing.

To quantify the dislocation densities observed in the undeformed isothermally transformed microstructures, the line intersection method using electron micrographs proved suitable. Chapter 5 includes details of the special precautions taken in the specimen preparation and in the measurement technique. It was estimated that, despite the careful control of the diffraction conditions, the greatest inaccuracies arose from lack of dislocation visibility. Depending upon the reflection used, the corrected value of dislocation density could be as great as twice the observed value. The presence of residual contrast from nominally invisible dislocations meant that in practice the true value lay between the observed and "corrected" values.

Because of the requirements of suitable diffraction conditions and foil thickness, it was difficult to ensure that the sample of dislocation density measurement sites was truly representative of each isothermal heat treatment. This was especially true in the 650° microstructure which showed the widest range of ferrite morphologies and dislocation densities. For this reason a larger sample of measurements was used from the 650° specimens and the results were classified according to the grain morphology. It was not possible for this identification to be completely unambiguous but it appeared that the highest dislocation densities, up to $8 \times 10^{14}\ m^{-2}$ were associated with the colonies of parallel laths. Together with the absence of detectable interphase precipitation in these regions, this suggested that a shear transformation mechanism had

operated. The individual, elongated grains tended to have lower dislocation densities, between 10^{13} and 10^{14} m^{-2}, similar to those of the equiaxed grains. They were thought to have been formed by a diffusional ledge mechanism. The detection of planar interphase precipitate sheets in such grains supports this argument.

Complementing the TEM observations and dislocation density measurements, X-ray line broadening gave an average measure of the total content of local lattice strain. The relative contributions from each source cannot be distinguished but the method has the advantage of averaging over a large specimen volume (19 mm x 3 mm x 25 μm) and could thus be used more easily to follow trends between specimens. With decreasing isothermal transformation temperature, the increase in integral strain breadth from 0.46×10^{-6} in the 800° structure to 4.17×10^{-6} in the 650° specimen reflected the simultaneous increase in both the particle strain field contribution, a result of the finer precipitate dispersion, and the mean dislocation density.

The inhomogeneity of the ferrite grain structure, dislocation populations and precipitate distributions in the isothermally transformed specimens, particularly those transformed at the lowest temperature (650°) similarly prevented the separation and quantification of the different contributions to the material strength. The limited analysis possible revealed that the yield strength increase in Alloy 2 from 302 MPa in the 800° microstructure to 672 MPa in the 650° structure paralleled the refinement in the precipitate dispersions, with additional contributions from the increase in dislocation density and decrease in grain size. Changing the alloy composition showed that the strength was lowered overall when the content of titanium carbide precipitates was reduced.

8.2 Yielding behaviour

Tensile tests of the four alloys in the isothermally transformed condition showed that in the two alloys with the highest titanium to carbon ratios the stress-strain curve in the as-transformed condition and also after the 100°C strain-ageing treatment was always smooth at yield. However, in Alloys 1 and 2 which contained excess carbon over titanium carbide stoichiometry, the yielding behaviour of the as-transformed specimens depended on the transformation temperature: specimens transformed at 800° always exhibited discontinuous yielding with yield extensions of approximately 1 % whereas those transformed at lower temperatures showed smooth, continuous yielding. Moreover, after strain-ageing, all the specimens of Alloys 1 and 2 exhibited discontinuous yielding regardless of the original transformation temperature.

Dislocation immobilisation by carbon or nitrogen atoms plays a major role in the mechanisms of discontinuous yielding and consequently the distributions of these species were studied in detail. The four alloys each effectively contained enough titanium to remove all the nitrogen in the form of insoluble titanium nitride. The solubility of titanium carbide in ferrite is also sufficiently low for negligible levels of carbon to remain in solution when the titanium content exceeded a critical titanium to carbon ratio. For such compositions equilibrium concentrations of dissolved carbon and nitrogen were expected to be 2 at.ppm (0.5×10^{-4} wt%) at most and could possibly be one or two orders of magnitude less, such is the difficulty of measuring such low concentrations accurately. In consequence discontinuous yielding was absent.

The critical titanium to carbon ratio for eliminating discontinuous yielding was found in this study to lie between 3.1:1 and 5.1:1 by weight.

It is generally taken to be the titanium carbide stoichiometric weight ratio of four as found by Comstock (1943) investigating titanium steels in the normalised condition with and without annealing and by Meyer et al (1977) in cold-rolled titanium steels after box-annealing. However, this behaviour of titanium steels contrasts with that of the vanadium steels reported by Batte (1970). After isothermal heat treatments very similar to those of the study reported here, initial and strain-ageing yield points were shown even when there was twice the vanadium content required for vanadium carbide stoichiometry. Vanadium is a weaker carbide former than titanium and hence a less efficient scavenger for interstitials. It is inferred that sufficient dissolved carbon can remain in equilibrium with vanadium carbide to cause dislocation immobilisation.

It is evident from the large volume of literature that there are many variables which affect the yielding behaviour exhibited by steels, related not only to the material and its heat treatment, but also to the experimental procedure. In this study the testing conditions were optimised where possible for the observation of yield phenomena, as described in Chapter 4. However to achieve the rapid heat transfer rates required for isothermal transformation conditions, the specimens had to be heat treated without the protection of encapsulation. This raised the possibility of minor specimen distortions despite the care taken in handling. Hence it was thought that the primary reason for any variations in the initial yield point effects between nominally identical specimens was the otherwise undetectable misalignment resulting from this heat treatment route. It could also have contributed to the absence of distinct upper yield points in the majority of the specimens exhibiting discontinuous yielding. Straining would have removed any such distortion effects, ensuring alignment for the strain-ageing tests.

In those alloys with a carbon excess over the titanium carbide requirement, the sensitivity of the carbon distribution to the heat treatment posed potential difficulties in separating the effects of interstitials from those of the many other possible variables contributing to the yielding behaviour. This carbon excess, calculated to be 0.056 and 0.016 wt% in Alloys 1 and 2 respectively, would precipitate in part as cementite during the transformation of the austenite below the Ae_3 temperature particularly in Alloy 1. On cooling the extent of dislocation atmosphere formation by the remaining carbon depends on the cooling rate, because this affects the level of carbon supersaturation and the rate of carbon diffusion.

Comparison of specimens heat treated at 800° but given different subsequent cooling rates to room temperature indicated that only with iced-brine quenching were sufficient dislocations left unpinned to produce continuous yielding. At the other extreme during furnace cooling the carbon was removed from interstitial sites probably by precipitation as cementite or intermediate iron carbides.

Comparison of these specimens of Alloy 2 furnace cooled after isothermal transformation with similarly transformed specimens of Alloy 3, with no carbon surplus, gives greater insight into the mechanisms of yielding. All these microstructures contain fine dispersions of titanium carbides which will pin the dislocations. The complete absence of discontinuous yielding behaviour in Alloy 3 specimens therefore signifies that dislocation immobilisation by titanium carbide pinning alone is insufficient to produce yield points. None of the specimens mentioned above contained interstitial carbon, either segregated or free in the matrix, as evidenced by the lack of stress-induced ordering yield points: Alloy 3 contained no surplus carbon and that in the furnace cooled Alloy 2

would be present as precipitates with iron. It is suggested that at yield in either alloy, dislocation movement is provided by newly created dislocations rather than by the unpinning of existing dislocations. It is hence postulated that the discontinuous yielding behaviour of Alloy 2 is caused by segregated carbon raising the stress needed to activate potential dislocation sources.

In the case of the furnace cooled specimens carbon segregation is followed by condensation to form the iron-carbon precipitates; in specimens air cooled after transformation, carbon remaining as segregated interstitials would have the same effect. The mobility of the surplus carbon during cooling will enable it to segregate to low energy sites throughout the microstructure. For example, the time-of-flight atom probe analysis indicated that carbon was absent from the defect-free matrix of an isothermally transformed specimen given the standard air cool, and that carbon segregation to the strain fields of precipitates may have occurred. Similarly, it would be expected that carbon would segregate to other lattice defects such as grain boundary ledges, which are thought to be dislocation sources. In contrast, the negligible solubility of titanium carbide in ferrite would prevent its redistribution once formed during the transformation.

The presence of an initial yield point but no strain-ageing yield point is the type of yielding behaviour exhibited by many commercial pipe-line steels because they are cooled relatively slowly. Such steels only show discontinuous strain-age yielding behaviour if there is free nitrogen available, since iron-nitrogen compounds redissolve more readily than their iron-carbon equivalents. "Non-ageing" commercial steels are therefore produced using alloying additions such as aluminium, titanium or vanadium in quantities sufficient only to combine with the nitrogen (e.g.

Jones & Coombes 1953; Smaill, Keown & Erasmus 1976) In contrast, the fast air cool to ambient temperature, employed for the majority of heat treatments in this study was fast enough to retain carbon atoms in interstitial sites and hence be available for redistribution during ageing. At the same time, this cooling rate was slow enough to permit carbon segregation thus fulfilling one of the requirements for discontinuous yielding.

Local dislocation densities measured in the grain interiors varied from around $0.5 \times 10^{14} m^{-2}$ in the 800° as-transformed structure to as much as $8 \times 10^{14} m^{-2}$ in the 650° structure. A high dislocation density per se cannot be responsible for the absence of discontinuous yielding. This is well demonstrated by the pronounced discontinuous yielding behaviour of the strain-aged, and thereby more dislocated specimens. It is the density of mobile dislocations, ρ_m, which is important. The cooling rate used after heat treatment was demonstrated to permit carbon segregation to the lattice dislocations. Thus little difference in mobile dislocation density would be expected between specimens transformed at different temperatures and with different microstructures. This finding however does not necessarily conflict with the suggestion of other authors (e.g. Tither & Lavite 1975; Boyd 1976) that continuous yielding in acicular ferrites and martensites is caused by higher mobile dislocation densities than in polygonal ferrite since faster cooling rates and higher total dislocation densities in their steels compared with this study may prevent complete immobilisation.

Several investigators (e.g. Michalak 1965) have shown that the mobile dislocation density present during the deformation of steels is almost invariant as a function of strain. Nilsson, Lagneborg & Sandström (1975) have determined the dependency on strain-rate, $\dot{\epsilon}$, to be

$$\rho_m = 2.4 \times 10^{14} (\dot{\epsilon})^{0.4} m^{-2} \qquad \ldots 8.1$$

which predicts mobile dislocation densities of $6.9 \times 10^{12} m^{-2}$ during the $1.4 \times 10^{-4} s^{-1}$ strain-rate employed in all the tests of the current investigation. To produce strain-age yield points these dislocations would all have to be pinned. It was not possible to determine the total number of segregation sites nor the concentration of interstitial carbon atoms available except by inference from the strain-ageing yield point magnitudes. In Alloy 1 with the higher carbon excess the large strain-age yield points for all the transformation temperatures of structure indicated that there was more than sufficient interstitial carbon available to cover all the segregation sites. A lower concentration of available carbon in Alloy 2 may have been responsible for the smaller strain-age yield point observed in the 650° structure, although the magnitude of the strain-age yield point for the 800° structure in Alloy 2 was as great as for Alloy 1.

With increasing transformation temperature, there was a simultaneous tendency for the grain size to increase and discontinuous yielding to be developed. Since this is the opposite trend to that of the Hall-Petch grain size effect normally exhibited by yielding behaviour (e.g. Hutchison 1963; Figure 2.10), factors other than grain size must be dominating the behaviour in this system. However, the relatively large, 25 to 40 μm grain sizes encountered may have contributed to the diffuse nature of those initial yield points exhibited here.

During the recording of the yield extensions on the load-extension curve, Lüders bands were never observed on the gauge length. In general, when Lüders bands are pronounced, the discontinuous yielding is pronounced and plastic yielding is concentrated at the one propagation front. The

absence of Lüders bands is characteristic of the transition in behaviour from discontinuous to continuous yielding. It is taken to be associated with the progressive break-out of plastic yielding from nuclei throughout the gauge length. This situation will occur when the local stresses required to create new yield nuclei, for example by the activation of dislocation sources, are not greatly higher than those needed to propagate yielding at plastic zones already created.

In the present work the microstructural inhomogeneity observed in all specimens could produce this effect by providing variations in both the stress to initiate yielding and that for propagation. Plastic yielding could then take place at many sites in the specimen. One effect of an inhomogeneous microstructure will be the redistribution of the applied stress to create local stress concentrations. The applied macrostress required to activate dislocation sources and thus initiate yield will be lowered. The superposition of any residual stress gradients would also result in varying stresses experienced locally. The application of a 400° stress-relieving heat treatment was ineffective in restoring the initial yield point in a 650° structure. However with prolonged annealing at the higher temperature of 650°, an initial yield point was very gradually developed. Only after 100 h at 650°C was an initial yield extension of ~1% produced. Annealing for 330 s at 830° produced a similar effect. It is postulated that had residual stresses been the primary reason for the continuous initial yielding in the specimens transformed at the lower temperatures, then they should have been removed by dislocation rearrangement during the 400° stress-relief treatment. That more severe heat treatments were needed to restore the yield points implied that greater microstructural changes were required than stress-relief dislocation rearrangements. Indeed after these more severe annealing

treatments the dislocation densities in the 650° structures appeared to become more homogeneous and the titanium carbides were beginning to coarsen, allowing the dislocations to break away.

In inhomogeneous materials the stress to propagate yield will also vary from region to region. The local flow stress includes contributions from the grain size, precipitate dispersions and dislocation density as given in Equation 4.1 (Pickering & Gladman 1963). When a load is applied, the stress-strain behaviour at each part of the specimen will be governed by the local microstructure, whereas the measured load-extension behaviour is the macroscopic average. Thus a highly inhomogeneous microstructure will exhibit a continuous tensile curve even though local volumes may be of a structure which would show a yield point. With increasing homogeneity, the differences between the yield initiation and propagation stresses will begin to become apparent in the macroscopic behaviour.

The study by Butler & Wilson (1963) of temper rolled steel sheets is an extreme example of the masking of yield points. The temper rolling introduced alternate bands of deformed and undeformed material. These authors cite this gross inhomogeneity of microstructure and consequent ease of dislocation nucleation at the interfaces between the different regions as causing the continuous yielding behaviour in a steel which before temper rolling exhibited pronounced stretcher strains.

Aside from the prolonged annealing treatments of the isothermally transformed structures, the heat treatments most successful in promoting large initial yield points were:

i) reaustenitisation at a comparatively low temperature, 1000°C with air cooling; and

ii) recrystallisation after heavy cold working, with air cooling.

Each produced a finer grained, more uniform ferrite grain structure than

any of the isothermal transformation heat treatments.

It therefore appears that for the as-transformed specimens, a number of factors may be contributing to the decreasing tendency towards discontinuous initial yielding with decreasing isothermal transformation temperature. However one of the principal causes appeared to be the increasing inhomogeneity on a very local scale observed in the ferrite morphologies and in particular the dislocation densities and precipitate distributions.

CHAPTER NINE

CONCLUSIONS AND SUGGESTIONS FOR FURTHER WORK

The principal findings of the investigation can be summarised as follows:-

i) Microstructures comprising predominantly ferrite and dispersions of discrete titanium carbide particles are produced by the isothermal decomposition of austenite in the series of titanium-bearing steels examined.

ii) In all the alloys, transformation in the range 800° to 650°C is complete after 1000 s producing equiaxed ferrite grain structures and, at the lower transformation temperature, some elongated grains and colonies of heavily dislocated plate- or lathlike grains.

iii) Dislocation densities have been measured in the isothermally transformed microstructures and were found to lie between 10^{13} and $10^{15} m^{-2}$. X-ray line broadening has been used to quantify differences in total lattice microstrain and to follow changes occurring during annealing and during deformation.

iv) The scale and morphology of the parallel sheets of interphase

precipitates provide evidence for the mechanisms of diffusional transformation which can operate at the numerous low energy, highly coherent austenite/ferrite interfaces and the occasional high energy, incoherent interfaces. Mechanisms involving shear come into play at transformation temperatures below 700°C.

v) Dislocations formed during the transformation become trapped in the lattice by interaction with the precipitate strain fields. During plastic deformation, dislocation walls form around the sheets of interphase precipitates; dislocation bowing takes place rather than particle shearing.

vi) Yield strengths of up to 672 MPa and ultimate tensile strengths of up to 800 MPa are achievable in the isothermally transformed steels. The decrease in precipitate spacing and increase in dislocation density are the major factors producing greater strength with decreasing transformation temperature. Composition changes to increase the volume fraction of titanium carbides can produce only limited additional strength because of the restricted solubility of titanium carbide in austenite.

vii) Titanium carbide has negligible solubility in ferrite and consequently a high stability to annealing. Atom probe spectroscopy has shown the interphase precipitates to contain titanium and carbon atoms in almost equal proportions and insignificant quantities of any other species. Haloes of carbon atoms are apparent in the strained matrix surrounding the precipitates.

viii) Discontinuous tensile yielding behaviour in the as-transformed condition and after strain-ageing are entirely eliminated when the titanium content exceeds that required for titanium carbide stoichiometry.

ix) In those alloys with carbon levels above the titanium carbide requirement and for the isothermal heat treatments given, the cooling rates to room temperature allow the persistence of sufficient interstitially dissolved carbon to give rise to strain-ageing yield extensions.

x) Specimens exhibiting strain-ageing yield extensions do not necessarily show an initial yield point. Transformation at 650°C produces continuous initial yielding, whereas the 800°C structures exhibit discontinuous yielding. The possible contributions of carbon segregation, precipitate pinning, dislocation density, residual stresses and grain size are considered. It is concluded that the trend in yielding behaviour is primarily related to the greater inhomogeneity of the microstructure produced by transformation at lower temperatures.

* * * * *

Rather than use a commercial steel, this study employed simplified alloy compositions and isothermal heat treatment conditions to allow the transformation mechanisms and microstructural features to be analysed in detail and interrelated. This approach succeeded in that several transformation mechanisms could be shown to be operating, and competing, at

different temperatures, but the complexities of the resultant microstructures presented problems in trying to relate the structures quantitatively to the mechanical properties. In particular it proved difficult to separate the effects of the many different factors known to influence the yielding behaviour.

The proposals for further work therefore comprise direct extensions of the investigations reported here which would gain a deeper understanding of the behaviour encountered, and also ideas to widen the scope of the research primarily towards commercial applications.

The following suggestions are made:-

i) For a further insight into the effects of grain size on the strength and yielding behaviour, ferrite refinement could be achieved by employing finer austenite grain sizes prior to the isothermal decomposition reaction. Hot deformation of the austenite or alloy additions to create austenite grain boundary pinning could bring this about without preventing the solution of the titanium carbide.

ii) The capability of the atom probe to identify individual atoms could be utilised to examine the degree and nature of carbon segregation to dislocations and grain boundaries. Such a study would be time-consuming because of the difficulty in locating the relevant features, but might provide useful evidence in the consideration of the creation of mobile dislocations. It would also be interesting to determine the interface composition profile between a titanium carbide and the matrix in an alloy with no carbon excess with respect to titanium carbide stoichiometry, thus providing more

information about the carbon haloes reported in Chapter 6.

iii) A further means of exploring the distribution of interstitial species is with internal friction techniques by which the magnitudes of damping peaks, recorded as a function of temperature, can be used to estimate the concentrations of those unsegregated atoms which are in solid solution. Carbon which is segregated to low energy sites or present in compounds does not contribute to these Snoek peaks. The internal friction technique is an indirect means of determining carbon distributions. Absolute values of carbon concentrations are difficult to obtain, particularly at the levels encountered in these alloys, because of the sensitivity of the technique to differences in the ferrite microstructure.

iv) The study of the effects of isothermal transformation temperature on the yielding behaviour could be extended to other ternary alloys or alloys containing more than one carbide-forming element. The effects of differing equilibrium solubilities of the carbides could then be examined, and compositions closer to those of commercial steels might be employed.

v) In practice, the processing of high strength low alloy steels generally involves a combination of continuous cooling and deformation operations. An understanding of the distribution of both the alloy carbides and the remaining carbon in continuously cooled specimens would therefore be appropriate particularly in view of the sensitivity of the yielding behaviour to the carbon distribution.

vi) The employment of quench and temper heat treatment regimes would provide greater scope for the study of titanium carbide precipitation and growth mechanisms, and the interactions between dislocations and carbides. Extreme conditions of solute supersaturation would be expected in the quenched condition and could be instructive in examining the effects of dissolved species on the yielding behaviour.

* * * * *

From the outset the investigation was intended to be basic in character and limited to the behaviour of a family of simple steels; it was appreciated that the limited solubility of titanium carbide in austenite restricted the magnitude of the achievable dispersion strengthening contribution, and that in practice titanium would always be used in conjunction with other carbide-formers. Instead, the choice of composition served to isolate the characteristics of titanium, eliminating any effects from interactions between different carbide-forming elements thus enabling a more fundamental study of the microstructure to be made. In turn this led to a more confident approach to the determination of the factors influencing the incidence of discontinuous yielding behaviour than is possible in commercially processed steels. Simultaneously, the compositions and heat treatments employed were of more relevance to commercial HSLA steels than the much-studied mild steels and annealed iron. In this way it is hoped that the discoveries of this investigation can be used in the continuing improvement of high strength low alloy steels.

APPENDIX A

EXPERIMENTAL TECHNIQUES

A.1 Alloy preparation

All the alloys were melted under vacuum. The basic alloy used for these investigations was prepared by the British Steel Corporation and was received as 12.5 mm plate. The other alloys were produced as 2.5 kg melts in a Balzers vacuum induction furnace starting with Japanese electrolytic iron of composition given in Table A1, and chemically pure elements. The charge was held molten for 30 mins to allow solution of the alloying additions and to achieve homogenisation in the liquid by the stirring action of the induced eddy currents. The ingots were cast into chilled steel moulds and allowed to cool under argon before removal.

A.2 Homogenisation and working

To minimise any compositional differences between the lengths of rod ultimately produced, the outside edges of the rolled plate material were discarded. For the same reason the head, bottom and outside surfaces of the induction melted casts were removed and the remaining block sawn longitudinally into quarters. Subsequent hot rolling to 15 mm square bar broke down the as-cast microstructure thus helping to homogenise the material.

After removal of the oxide scale the bars of all the alloys were

sealed in quartz capsules under a reduced pressure of argon and homogenised for 72 h at 1300°C. The formation of coarse precipitates was discouraged by a rapid water quench from this temperature.

A sequence of hot rolling, hot swaging and cold drawing was then employed to reduce the bars to 5 mm diameter. Some of the rods were cold drawn further to 3 mm diameter. All the rods were cleaned and sealed under argon for a standardising treatment of 30 min at 1300°C followed by a water quench.

The alloys were analysed by wet chemical techniques after fabrication and homogenisation were complete. The results are given in Table A2.

A.3 Heat treatments

Metallographic studies were carried out using 15 mm lengths of the 3 mm diameter standardised rod. For ease of handling, a stainless steel wire was spot welded to each sample. A small horizontal tube furnace was used for reaustenitisation, and protection was provided by a constantly replenished argon atmosphere. Care was taken to avoid the entrance of air. The temperature was continually monitored with a Pt/Pt-Rh thermocouple positioned beside the specimens and was maintained at ±2°C.

For isothermal heat treatments the bath of molten tin was found to be accurate to ±1°C after 30 min equilibration. The specimen transfer from the furnace to the tin took one to two seconds. Once submerged, the specimens were agitated to improve the rate of heat transfer. For studies requiring the sudden arrest of the austenite to ferrite transformation the specimens were plunged into iced brine so that the remaining austenite was converted to martensite.

Similar heat treatment procedures were followed for the tensile specimens with additional precautions taken to minimise the introduction

of stresses. A double stainless steel handling wire was used, with the two arms spot welded to one shoulder in diametric positions. After the 1000 s treatments in the molten tin all the tensile specimens were allowed to cool to black heat in still air. Any adhering tin was then removed by brushing and the specimens were left to air cool to room temperature. To prepare the surface for electropolishing, the thin oxide skin was removed by careful abrasion with fine emery paper.

For longer heat treatments, the cleaned and polished tensile specimens were sealed in quartz capsules under a partial pressure of argon. To terminate these treatments, the capsules were lowered unbroken into stirred water, thus achieving a specimen cooling rate similar to an air cool.

A.4 Dilatometry

A Theta Industries high speed dilatometer employing induction heating and helium gas quenching was used. The specimens were nickel plated to prevent decarburisation. To allow direct comparison with the other heat treatment techniques, the specimens were 15 mm long, 3 mm diameter solid rods. Percentage transformations were calculated from plots of specimen length against temperature, assuming that the thermal expansion coefficients were constant for each phase.

A.5 Optical microscopy

Metallographic samples were taken from the gauge length and the undeformed shoulders of the tensile specimens, and from the 3 mm diameter rod specimens. The specimens were sectioned using a flood-lubricated silicon carbide slitting wheel and they were mounted in thermosetting plastic. The surface layers were removed in the conventional manner by

grinding, and progressively finer polishes were used culminating in $\frac{1}{4}\mu m$ diamond lapping compound.

To reveal prior austenite grain boundaries in martensitic structures an etch of saturated aqueous picric acid was used. The remaining samples were etched in 2% nitric acid in isopropyl alcohol. Photomicrographs were taken using a Carl-Zeiss Jena Neophot II microscope. Grain sizes are quoted as mean linear intercept values.

The volume fractions of ferrite and martensite in partially transformed samples were determined from tracings of the micrographs using a Quantimet quantitative image analyser; the average area fraction across the sections were measured with the exclusion of the outermost 200 μm which contained some surface nucleated ferrite.

A.6 Transmission electron microscopy

Discs 0.5 mm thick were cut transversely from tensile and rod specimens using a flood lubricated silicon carbide slitting wheel. For standard specimens, the discs were thinned to 0.05 mm by hand grinding. Thin foils were perforated in a 5% perchloric acid - 25% glycerol - 70% ethanol electrolyte using a twin-jet electropolishing unit at a potential of ~55 V at 15°C.

The electron microscopes used were a Philips EM300 operating at 100 kV and and a JEOL JEM 200A at 200 kV. For dislocation density measurement, extra precautions were taken during foil preparation to ensure that the dislocation populations were representative of the bulk specimens: the discs were cut 1 mm thick and were thinned chemically by immersion in 5% HF-15% 40volH_2O_2-bal H_2O. Thus any surface deformation

caused by the cutting process would be removed and without the introduction of dislocations. It should be noted, however, that although it is recognised that handgrinding is more likely to introduce dislocations than chemical thinning (e.g. Hirsch et al. 1977 p56), the linear dislocation arrays characteristic of such origins were rarely observed in foils prepared by either method. If present, these areas were avoided in the detailed microstructural investigations.

A.7 TEM foil thickness measurement

The expression used to calculate foil thickness, t, from the number of grain boundary fringes is

$$t = n_g \xi_g \qquad \ldots A1$$

where n_g is the number of extinction fringes for diffraction vector g and ξ_g is the extinction distance for the appropriate g and electron energy.

Values of extinction distances are given in Table A3 from Hirsch et al. (p510). It was ensured that diffraction was occurring in only one of the grains adjacent to the boundary to avoid the alterations in extinction distance caused by interference. The optimum number of extinction fringes was found to be six or seven: any less increased the percentage error in the measurement but with more, the extinction fringes became indistinct due to anomalous absorption (Edington 1975). Kikuchi lines were used to check the diffraction conditions because the extinction distance ξ_g is very sensitive to the deviation parameter.

The average foil thickness was 223 nm.

A.8 Calculation of observed TEM dislocation densities

The line intersection method, described by Hirsch et al. (p422), involves the superposition of a grid on micrographs of the dislocations.

The dislocation density is calculated using the expression

$$\rho_{obs} = \frac{2NM}{Lt} \qquad \ldots A2$$

where ρ_{obs} is the observed dislocation density

N is the number of dislocation intersections with grid

M is the magnification of the micrograph

L is the line length of grid on micrograph

t is the foil thickness

To minimise any dislocation orientation effects, a grid of concentric circles was used. Photographs with magnifications ranging from x9000 to x86 000 were selected according to the dislocation density. Several thousand dislocation intersections were counted for each heat treatment along line lengths corresponding to between 0.4 and 0.8 mm on the specimens.

A.9 Hardness measurements

Standard hardness measurements were made using a Vickers testing machine with a load of 10 kg. The specimens were mounted in thermosetting plastic and were given the standard metallographic preparation. A mean of five indentations was taken and the values are quoted as Vickers Pyramid Numbers.

Microhardness values were obtained using a Leitz microhardness tester fitted with a Vickers pyramid microindenter. Because microhardness is very sensitive to surface deformation, the specimens were chemically polished in 5%HF-15%H_2O-80% 40volH_2O_2 after the standard metallographic preparation. The indents were positioned in grain interiors to minimise the interference from grain boundaries.

For both types of hardness measurement the indents were separated by at least ten times the indent diameter.

A.10 Electropolishing of tensile specimens

The threaded ends of the tensile specimens were masked off with lacquer. The gauge length was electropolished using 5% perchloric acid in glacial acetic acid at 25 V and 1 mA mm^{-2} with the electrolyte temperature kept to $20^{o}C$.

To give an even removal of material, the specimen was rotated in the centre of a cylindrical stainless steel mesh cathode and the electrolyte was stirred in the opposite direction. The specimen was inverted half way through the polishing process.

A.11 Tensile testing

A 60 kN capacity screw-driven Mand tensile testing machine was employed and independent rapid response Bryans X-Y chart recorders with voltage back-off facilities were used to record the expanded load-time and load-specimen strain graphs. The specimen strain was measured from the mean output of two D.C. linear voltage-displacement transducers (LVDTs) mounted at opposite sides of the specimen in blocks clamped to the specimen holders. For each test the load, time and strain calibrations were verified.

The plastic strain of the specimen was measured as the deviation from the extrapolated linear loading line on each graph. For the load-time and load-crosshead displacement plots, the elastic loading line included the machine loading response and only at loads below 1.5 kN was any non-linearity detectable. For the majority of tests, yielding occurred at well above this load, and the plastic strains calculated from the two expanded graphs were thus equally accurate. In these tests, therefore, the strains were principally measured indirectly using the load-time

graphs, largely because of the unlimited equivalent strain range available but also because the method was independent of local temperature effects produced during the in-situ strain-age treatments and it was less susceptible to electrical interference.

The initial yielding behaviour of low strength specimens was monitored using the LVDT specimen strain output alone. In interrupted tests, when the elastic loading line could be redetermined, the strain in these specimens was measured using the load-time expanded graph once the range of the LVDTs was exceeded.

A.12 X-ray diffractometry

For all the X-ray diffraction work, a Philips diffractometer was employed with a PW 1730 X-ray generator operating at 50 kV and 35 mA. The divergence and scatter slits were set at 1° and the receiving slit at 0.2 mm throughout. To investigate the different phases present in samples, MoK_{α} was employed enabling a large number of different peaks to be scanned. CoK_{α} was more suitable for the studies of individual peak profiles because the longer wavelength results in the expansion of the diffraction spectrum.

The X-rays penetrate metals to only about 25 μm so diffraction studies are very sensitive to surface preparation. Consequently the surface layer of all the X-ray specimens was removed chemically using the 5%HF-15%40vol.H_2O_2 -bal.H_2O reagent. For the majority of the line broadening measurements the 211 ferrite peaks at $2\theta \simeq 99.7^{\circ}$ were selected because they had the best combination of intensity and angular resolution. For narrow peaks, 40 s counts were taken every $0.01^{\circ}(2\theta)$ and for broad peaks every 0.02°. Background counts were collected at 10° either side. The stepscan data were collected on punch tape and plotted by computer.

The peaks were then smoothed manually, the background subtracted and the α_1 and α_2 peaks separated by the Rachinger (1948) technique. The area under each peak and hence the integral breadth β was determined by a Quantimet image analysing computer, and the full width at half peak height $2w$ evaluated. The methods of data analysis and data tabulations are given in Appendix B.

A.13 Field ion microscope specimens

Field ion specimens were prepared from the gauge length of fractured tensile specimens by a three-stage electropolishing technique:

i) reduction from 3 mm to 0.5 mm diameter wire with 5% perchloric acid in acetic acid at ~50 V DC;

ii) necking of the wire, produced by coating the tip with lacquer and partially submerging the wire in 10% perchloric acid in acetic acid at ~25 V DC;

iii) failure at the neck giving a pointed specimen tip, using 2% perchloric acid in butoxyethanol at 15-20 V DC.

All stages were carried out at room temperature.

APPENDIX B

X-RAY LINE BROADENING ANALYSIS

In this appendix the methods of data analysis used for the X-ray line broadening investigations of Chapter 5 are described and the results of the calculations are tabulated.

The method adopted to correct the measured line profiles for instrumental broadening was that described by Langford (1979). In the analysis it is assumed that the measured, instrumental and diffraction profiles each approximate to a Voigt function which is a convolution of a Cauchy (Lorentzian) and a Gaussian curve.

For the analysis, the two parameters required from each peak profile are the full width at half peak, 2w, and the integral breadth β calculated from the integrated intensity and the peak height. The form factor $\phi = \frac{2w}{\beta}$ indicates the type of profile: if pure Cauchy, $\phi \simeq 0.64$; if pure Gaussian, $\phi \simeq 0.94$. Measured profiles generally have an intermediate form factor, instrumental and size broadening effects tending to give a more Cauchy profile and strain broadening a more Gaussian shape. Thus, by using a Voigt function, a more accurate answer is achieved than the simpler correction methods which take the curve shapes to be either pure Cauchy or pure Gaussian.

In practice, the form factor of the calibration peaks was 0.714, close to the pure Cauchy value as expected. The calculated form factors

for the corrected specimen diffraction peaks ranged between 0.68 and 0.87, thus justifying the use of the Voigt function.

There was no systematic variation of the form factor with heat treatment, though the value tended to be higher for 110 peaks than 211 peaks. Because both the dislocations and the semi-coherent precipitates have a crystallographic orientation with the matrix, the resultant X-ray line broadening will depend on the reflection employed and this could be causing the difference in form factor between the two reflections. Other crystallographic effects will result from the elastic anisotropy of iron, and also the residual axial <110> texture inevitably remaining despite the specimens having undergone a series of transformations since being cold drawn.

The Cauchy and Gaussian components β_C and β_G are derived for each peak profile using

$$\frac{\beta_C}{\beta} = a_0 + a_1\phi + a_2\phi^2 \qquad \ldots B1a$$

and

$$\frac{\beta_G}{\beta} = b_0 + b_{1/2}(\phi - \tfrac{2}{\pi})^{1/2} + b_1\phi + b_2\phi^2 \qquad \ldots B1b$$

where $a_0 = 2.0207$; $a_1 = -0.4803$; $a_2 = -1.7756$;

$b_0 = 0.6420$; $b_{1/2} = 1.4187$; $b_1 = -2.2043$; $b_2 = 1.8706$

Once separated, the components from the measured specimen peak profiles (subscript h) are corrected for instrumental broadening by subtracting those components of the calibration specimen profile (subscript g) as follows:

$$\beta_{fC} = \beta_{hC} - \beta_{gC} \qquad \ldots B2a$$

$$\beta^2_{fG} = \beta^2_{hG} - \beta^2_{gG} \qquad \ldots B2b$$

Recombination of the resultant components β_{fC} and β_{fG} produces the true widths of the specimen diffraction profile β_f and $2w_f$. The integral breadth β_f was then used to quantify the broadening produced by the microstructure. Tables B1 to 4 present the peak breadth data for the

measured specimen and instrumental peak profiles for the range of samples examined. The integral strain breadths ξ_{ε}^{2} and equivalent dislocation densities ρ calculated using Equation 5.2 are also tabulated.

electrolytic iron

element	concentration wt ppm
Oxygen	320
Tin	60
Arsenic	60
Phosphorus	40
Chromium	40
Sulphur	40
Carbon	30
Nitrogen	20
Copper	20
Zinc	20
Hydrogen	16
Germanium	10
Nickel	<50
Cobalt	<30
Aluminium	<20
Manganese	<20
Molybdenum	<20
Vanadium	<20
Zirconium	<20
Lead	<10
Silicon	<10
Titanium	<10
Chlorine	trace

Table A1: Principal impurities in starting material

alloy no.	analysis, wt%								
	C	Ti	Mn	Al	Si	Ni	S	P	N
1	0.070	0.067	0.34	-	<0.02	-	<0.002	0.002	0.003
2	0.073	0.227	0.40	0.04	<0.02	<0.02	0.017	0.006	0.007
3	0.10	0.52	0.36	-	-	-	-	-	<0.005
4	<0.02	0.38	0.27	-	-	-	-	-	0.006

Table A2: Analysis of experimental alloys investigated

g	extinction distance, nm	
	200 kV	100 kV
110	34.2	27.0
200	50.0	39.5
211	63.8	50.3
220	76.8	60.6
310	90.3	71.2

Table A3: Extinction distances in ferrite (from Hirsch et al. 1977 p510)

	211	110
$2w_g$	0.100	0.085
β_g	0.140	0.119
ϕ_g	0.714	0.714
β_{gc}	0.108	0.092
β_{gG}	0.058	0.050

Table B1: Data for instrumental profiles:
211 and 110 peaks from calibration specimens

(All measures of peak width in $^{\circ}2\theta$)

	211 peak				110 peak			
	650°	700°	750°	800°	650°	700°	750°	800°
$2w_h$	0.270	0.218	0.155	0.146	0.135	0.120	0.155	0.107
β_h	0.371	0.286	0.219	0.215	0.182	0.162	0.158	0.147
ϕ_h	0.728	0.760	0.708	0.679	0.742	0.741	0.728	0.728
β_{hC}	0.271	0.180	0.173	0.188	0.125	0.112	0.115	0.107
β_{hG}	0.170	0.156	0.087	0.064	0.091	0.080	0.072	0.067

a) As measured

	211 peak				110 peak			
	650°	700°	750°	800°	650°	700°	750°	800°
$2w_f$	0.215	0.163	0.087	0.062	0.083	0.066	0.058	0.046
β_f	0.278	0.194	0.112	0.092	0.098	0.076	0.068	0.053
ϕ_f	0.774	0.838	0.775	0.680	0.847	0.868	0.847	0.860
β_{fC}	0.163	0.072	0.065	0.080	0.033	0.020	0.023	0.016
β_{fG}	0.159	0.145	0.065	0.027	0.076	0.063	0.053	0.043
$\varepsilon^2_{f_6}$ $\times 10^{-6}$	4.174	2.033	0.677	0.457	3.018	1.815	1.453	0.883
ρ $\times 10^{14}\,m^{-2}$	8.3	4.1	1.4	0.91	6.0	3.6	2.9	1.8

b) After correction

Figure B2: Data for specimen peak profiles a) before and b) after correction for instrumental broadening: 211 and 110 peaks from specimens isothermally transformed in the range 650° to 800°C

	650° structure			800° structure				
% strain	0	1.3	5	0	1.3	5	7	9
$2w_h$	0.270	0.295	0.375	0.146	0.192	0.220	0.045	0.245
β_h	0.371	0.378	0.468	0.215	0.240	0.288	0.306	0.320
ϕ_h	0.728	0.780	0.801	0.679	0.800	0.764	0.801	0.766
β_{hC}	0.271	0.213	0.232	0.188	0.120	0.178	0.152	0.196
β_{hG}	0.170	0.226	0.305	0.064	0.156	0.160	0.199	0.179

a) As measured

	650° structure			800° structure				
% strain	0	1.3	5	0	1.3	5	7	9
$2w_f$	0.215	0.305	0.327	0.062	0.140	0.166	0.194	0.192
β_f	0.278	0.291	0.384	0.092	0.152	0.197	0.220	0.230
ϕ_f	0.774	0.841	0.852	0.680	0.919	0.843	0.886	0.835
β_{fC}	0.163	0.105	0.124	0.080	0.012	0.070	0.044	0.088
β_{fG}	0.159	0.219	0.300	0.027	0.145	0.149	0.190	0.170
$\varepsilon^2_{f\times10^{-6}}$	4.174	4.573	7.963	0.457	1.248	2.096	2.614	2.857
$\rho_{\times10^{14}m^{-2}}$	8.3	9.1	15.9	0.91	2.5	4.2	5.2	5.7

b) After correction

Table B3: Data for specimen peak profiles a) before and b) after correction for instrumental broadening: 211 peaks from specimens isothermally transformed at 650° and 800° and plastically strained

	1000 s 650°	1000 s + 60 000 s 650°	1000 s 800°	1000 s + 60 000 s 800°
$2w_h$	0.270	0.220	0.146	0.135
β_h	0.371	0.300	0.215	0.195
ϕ_h	0.728	0.733	0.679	0.692
β_{hC}	0.271	0.214	0.188	0.163
β_{hG}	0.170	0.142	0.064	0.068

a) As measured

	1000 s 650°	1000 s + 60 000 s 650°	1000 s 800°	1000 s + 60 000 s 800°
$2w_f$	0.215	0.163	0.062	0.056
β_f	0.278	0.205	0.092	0.076
ϕ_f	0.774	0.795	0.680	0.730
β_{fC}	0.163	0.106	0.080	0.055
β_{fG}	0.159	0.129	0.027	0.034
$\varepsilon^2_{F\times10^{-6}}$	4.174	2.270	0.457	0.312
$\rho_{\times10^{14}m^{-2}}$	8.3	4.5	0.91	0.62

b) After correction

Table B4: Data for specimen peak profiles a) before and b) after correction for instrumental broadening: 211 peaks from specimens heat treated at 650° and 800°C

REFERENCES

AARONSON H I 1962
in "Decomposition of austenite by diffusional processes", p387
Interscience Publishers, New York

AARONSON H I 1980
Scripta Met. 14, p825

AINSLEY M H, COCKS G J and MILLER D R 1979
Metal Science 13, p20

ANDREN H-O and NORDEN H 1979
Scand. J. Metallurgy 8, p147

ARONSON B 1969
in Procs. Symp. on "Steel strengthening mechanisms" Zurich
1979, p77. Climax Molybdenum Co., London

BAIRD J D 1963
Iron and Steel 36, pp186, 326, 368, 400, 450

BAIRD J D 1971
Metallurgical Reviews 16, p1 (Review 149)

BAIRD J D and PRESTON R R 1973
in Procs. "Processing and properties of low carbon steels"
Pittsburgh (Ed. J M Gray), p1 Metallurgical Soc. of AIME

BAKER T N 1978
Sci. Prog., Oxf. 65, p493

BAKER R G and NUTTING J 1959
ISI Special Report No 64, p1

BALLIGER N K and GLADMAN T 1978
British Steel Corporation Publn. SH/PT/8262/-/78/A

BALLIGER N K and HONEYCOMBE R W K 1980a
Metal Science 14, p121

BALLIGER N K and HONEYCOMBE R W K 1980b
Met. Trans. 11a, p421

BATTE A D 1970
PhD Thesis, University of Cambridge

BATTE A D and HONEYCOMBE R W K 1973
Metal Science 7, p160

BHADESHIA H K D 1980
Scripta Met. 14, p821

BHADESHIA H K D 1981
Acta Met. 29, p1117

BOYD J D 1976
Met. Trans. 7A, p1577

BRENNER S S and MILLER M K 1980
in Procs. 27th International Field Emission Symposium,
Tokyo, Japan (Eds. Y Yashiro and N Igata)

BRINDLEY B J and WORTHINGTON P J 1970
Metallurgical Reviews 15, p101 (Review 145)

BROOKS H 1952
in "Metal Interfaces", p20. A.S.M., Metals Park, Ohio

BROWN L M and HAM R K 1971
in "Strengthening methods in crystals"
(Eds. A Kelly and R B Nicholson), p9. Elsevier, Amsterdam

BUTLER R D and WILSON D V 1963
J. Iron Steel Inst. 201, p16

CAMPBELL K and HONEYCOMBE R W K 1974
Metal Science 8, p197

COMSTOCK G F 1943
Trans. AIMME 15, p521

COTTRELL A H and BILBY B A 1949
Proc. Phys. Soc. A62, p49

COTTRELL A H and LEAK G M 1952
J. Iron Steel Inst. 172, p301

DALBY W E 1913
Proc. Roy. Soc. A88, p281

DAVENPORT A T and HONEYCOMBE R W K 1971
Proc. Roy. Soc. Lond. A322, p191

DAVIES R G 1979
Met. Trans. 10A, p1549

DINGLEY D J and McLEAN D 1967
Acta Met. 15, p885

DUNLOP G L and HONEYCOMBE R W K 1975
Phil. Mag. 32.1, p61

DUNLOP G L and TURNER P J 1975
Metal Science 9, p370

EDINGTON J W 1975
Monograph 3: "Interpretation of transmission electron micrographs" MacMillan, London

EDWARDS C A, PHILLIPS D L and JONES H N 1940
J. Iron Steel Inst. 142, p199

EMBURY J D, EVENSON J D and FILIPOVIC A 1977
in Proc "Fundamental aspects of structural alloy design", Seattle, 1975 (Eds. R I Jaffee and B A Wilcox), p67. Plenum Press

ESHELBY J D 1957
Proc. Roy. Soc. A241, p376

FREEMAN S 1971a
PhD Thesis, University of Cambridge

FREEMAN S 1971b
ISI Report 145, p152

FREEMAN S and HONEYCOMBE R W K 1977
Metal Science 11, p59

GEROLD V 1979
in "Dislocations in solids, Vol. 4" (Ed. F R N Nabarro), p219 North-Holland, Amsterdam

GLADMAN T, DULIEU D and McIVOR I D 1977
in Procs. "Microalloying 75" Washington D C 1975, p25 Union Carbide, New York

GLADMAN T and McIVOR I D 1972
Scand. J. Metallurgy 1, p247

GOLDSCHMIDT H J 1967
"Interstitial Alloys", p172. Butterworths, London

GOODENOW R H and HELD J F 1970
Met. Trans. 1, p2507

HAHN G T 1962
Acta Met. 10, p127

HALL E O 1970
"Yield point phenomena in metals and alloys" MacMillan, London

HANSEN SS and PRADHAN R R 1981
in Proc. Conf. Met. Soc. AIME, Chicago 1981 (Eds. R A Kot and B L Bramfitt), p113

HAYNES F J and BAKER T N 1981
Metals Technology 8, p413

HEHEMANN R F, KINSMAN K R and AARONSON H I 1972
Met. Trans. 3, p1077

HEIKKINEN V K 1973
Scand. J. Metall. 109, p112

HIRSCH P B, HOWIE A, NICHOLSON R B, PASHLEY D W and WHELAN M J 1977
"Electron microscopy of thin crystals"
Robert E Krieger, New York

HONEYCOMBE R W K 1976
Met. Trans. 7A, p915

HONEYCOMBE R W K 1979
Scand. J. Metallurgy 8, p21

HOWELL P R and HONEYCOMBE R W K 1982
in Procs. Internat. Conf. on "Solid-solid phase transformations" Pittsburgh 1981 (Eds. H I Aaronson et al.), p399.
TMS-AIME, New York

HUTCHINSON M M 1963
Phil. Mag. 8, p121

IRVINE K J, PICKERING F B and GLADMAN T 1967
J. Iron Steel Inst. 205, p161

JACK D H and JACK K H 1973
Mat. Sci. and Eng. 11, p1

JOHNSTON W G 1962
J. Applied Physics 33.9, p2716

JOHNSTON W G and GILMAN J J 1959
J. Applied Physics 30.2, p129

JONES A, HUDD R C and KALE M N 1970
British Steel Corporation Report No. 1881A

JONES W R D and COOMBES G 1953
J. Iron Steel Inst. 174, p9

KEH A S and WEISSMANN S 1963
in "Electron microscopy and the strength of crystals"
(Eds. G Thomas and J Washburn), Interscience, New York

KIESSLING R and LANGE N 1966
ISI Publication 100, pp137, 145

KINSMAN K R, EICHEN E and AARONSON H I 1975
Met. Trans. 6A, p303

KLUG H P and ALEXANDER L E 1974
"X-ray diffraction procedures" 2nd Edition
John Wiley, New York

KURDJUMOV G V and SACHS G 1930
Z. Phys. 64, p325

LAGNEBORG R and SANDSTRÖM R 1975
Metal Science 9, p226

LANGFORD J I 1979
in Procs. Symp. on "Accuracy of powder diffraction"
Gaithersburg, Maryland (Eds. S Block and C R Hubbard), p255
NBS Special Publication 567

LAW N C, HOWELL P R and EDMONDS D V 1979
Metal Science 13, p507

LESLIE W C 1972
Met. Trans. 3, p5

LESLIE W C and SOBER R J 1967
Trans. ASM 60, p99

LI J C M, and CHOU Y T 1970
Met. Trans. 1, p1145

LOW J R and GENSAMER M 1944
Trans. AIMME 158, p207

MEYER L, HEISTERKAMP F and MÜSCHENBORN W 1977
in Procs. "Microalloying 75" Washington D C 1975, p130
Union Carbide, New York

MICHALAK J T 1965
Acta Met. 13, p213

MIRKIN L I 1964
"Handbook of X-ray analysis of polycrystalline materials",
p585

MORRISON W B 1980
Scand. J. Metallurgy 9, p83

NILSSON S, LAGNEBORG R and SANDSTRÖM R 1975
Metal Science 9, p223

NISHIYAMA Z 1934
Sci. Rep. Res. Inst. Tohoku Univ. 23, p637

OKAMOTO A and TAKAHASHI M 1981
in Procs. Conf. Met. Soc. AIME Chicago 1981 (Eds. R A Kot and B L Bramfitt), p427. TMS-AIME New York

OWEN W S and CARISELLA J V 1978
in Procs. 2nd Int. Conf. on "The mechanical behaviour of materials" 1976, p15. ASM, Metals Park Ohio

PEARSON W B (1967)
"Handbook of lattice spacings and structures of materials", p631. Pergamon Press

PETCH N J 1964
Acta Met. 12, p59

PICKERING F B 1976
"The basis of quantitative metallography"
Inst. Metall. Technicians Monograph No. 1

PICKERING F B 1977
in Procs. "Microalloying 75" Washington D C 1975, p3
Union Carbide, New York

PICKERING F B and GLADMAN T 1963
ISI Spec. Rep. 81, p10

PUSSEGODA L N and ERASMUS L A 1977
in Procs. 6th Australasian Conf. on "The mechanics of structures and materials", New Zealand 1977, p445

RACHINGER W A 1948
J. Sci. Instrum. 25, p254

RAO B V N and RASHID M S 1981
General Motors Research Publication GMR-3576

RASHID M S 1975
Met. Trans. 6A, p1265

RASHID M S 1976
Met. Trans. 7A, p497

RASHID M S 1978
SAE Trans. 86.2, p835

RASHID M S 1981
Ann. Rev. Mater. Sci. 11, p245

RASHID M S and RAO B V N 1982
Met. Trans. 13A, p1679

RICKS R A and HOWELL P R 1983
Acta Met. 31, p853

RICKS R A, HOWELL P R and HONEYCOMBE R W K 1979
Met. Trans. 10A, p1049

RONAY M 1981
Met. Trans. 12A, p1951

SANDSTROM R and LAGNEBORG R 1974
Scand. J. Met. 3, p205

SCHWARTZ D M 1968
PhD Thesis, University of Cambridge

SHAFFER P T B 1964
High Temperature Materials Index. Plenum Press

SMAILL J S, KEOWN S R and ERASMUS L A 1976
Metals Technology 3, p194

SMITH E 1966
Acta Met. 14, p583

SPEICH G R and LESLIE W C 1972
Met. Trans. 3, p1043

SPEICH G R and MILLER R L 1981
in Procs. Conf. Met. Soc. AIME, Chicago 1981 (Eds. R A Kot and B L Bramfitt), p279. TMS-AIME, New York

STAKER M R and HOLT D L 1972
Acta Met. 20.1, p569

STORMS E K 1967
in "The refractory carbides", p6
Academic Press, New York

STUART H and RIDLEY N 1970
J. Iron Steel Inst. 208, p1087

TEKIN E and KELLY P M 1965
J. Iron Steel Inst. 203, p715

THELNING K-E 1975
"Steel and its heat treatment" Bofors Handbook, pp184-188
Butterworths, London

THOMAS G and RAO B V N 1977
"Martensitic transformations", Kiev, USSR
(Reported by Law et al., 1979)

THOMAS W R and LEAK G M 1955
J. Iron Steel Inst. 180, p155

TITCHENER A L and DAVIES G J 1965
Phil. Mag. 11, p1225

TITHER G and LAVITE M 1975
J. of Metals 27, p15 (September)

WASSERMANN G 1933
Arch. Eisenhuttenwes. 16, p647

WAUGH A R 1978
J. Phys. E: Sci. Instrum. 11, p49

WAUGH A R and SOUTHON M J 1979
Surface Science 89, p718

WILLIAMSON G K and SMALLMAN R E 1956
Phil. Mag. 1, p34

WILSON D V 1967
Metal Science 1, p40

WILSON D V 1968
Acta Met. 16, p743

WILSON D V and RUSSELL B 1959
Acta Met. 7, p628

YOULE A 1972
PhD Thesis, University of Cambridge

YOULE A, RALPH B, FREEMAN S and HONEYCOMBE R W K 1974
Metallography 7, p333